Hydrological Responses to Wetland Changes in the Yangtze River Basin

Ziying Guo

Submitted in fulfilment of the requirements for the Degree of

Doctor of Philosophy

School of Social & Environmental Sustainability

College of Social Sciences

University of Glasgow

June 2025

Abstract

As the most productive ecosystems in the world, wetlands play a vital role in carbon cycling, climate change mitigation, socio-economic development, and natural disaster protection. The Yangtze River Basin (YRB) contains 40% of the national wetlands and the most frequent floods in China. In recent decades, the abundant wetland resources in the YRB have experienced substantial changes due to the climate change and human activities, significantly affecting the flood risk. Due to the lack of a long-term time series wetland dataset with comprehensive categories for the YRB, the effects of wetland variations on flood risk, as well as improved assessments of past and future flood risk incorporating wetland dynamics, remain underexplored. Moreover, wetland-related flood risk mitigation efforts in the YRB are less widely adopted. It is crucial to address these gaps for enhancing the sustainable wetland management and flood risk mitigation in the YRB.

This thesis aims to achieve three primary objectives: 1) to establish a long-term time series wetland classification dataset with the comprehensive categories in the YRB and analyze driving forces of their variations; 2) to investigate the long-term wetland effects on the flood risk in the YRB based on an improved GIS-based multi-index flood risk assessment model incorporating wetlands input; and 3) to predict the future flood risk with wetland effects in the middle-lower YRB under climate change and socio-economic scenarios.

The Long-term Wetland Classification Dataset for YRB (LTWCD_YRB) with nine wetland categories from 1984 to 2021 was created by using the Random Forest machine learning classifier on the Google Earth Engine platform with 30m resolution Landsat images. The LTWCD_YRB revealed that: 1) the total wetland area of the YRB in 2021 was larger than that in 1984, with a constant increase in human-made wetlands and fluctuating natural wetlands; 2) aquaculture ponds expanded the most by 4,987 km^2, while inland marshes in the source region exhibited the most fluctuations; and 3) seasonal changes in wetlands were prominent in the Poyang Lake Basin, Dongting and Honghu Lake Basin, and YRB source

region; and 4) human activities were found to be more dominant than natural driving forces in affecting wetlands. The LTWCD_YRB offers a consistent agreement of wetland area variations with the other satellite-based wetland datasets in the YRB.

To investigate the long-term effects of wetland variations on flood risks in the YRB, this thesis developed an improved GIS-based multi-index flood risk assessment model incorporating the wetland input obtained from the LTWCD_YRB. The findings indicated that: 1) wetlands in the Taihu Lake Basin, Wanjiang Plain, Poyang Lake Basin, and Dongting and Honghu Lake Basin could mitigate flood risks, while wetlands in the Sichuan Basin have aggravated but limited impacts on flood risks; and 2) Precipitation in the Taihu Lake Basin and Poyang Lake Basin, runoff and vegetation cover in the Wanjiang Plain, GDP in the Taihu Lake Basin, population density in the Taihu lake Basin, Dongting and Honghu Lake Basin, and the Sichuan Basin are dominant flood risk indicators under wetland effects. The wetland-related suggestions to mitigate flood risks including maximizing stormwater storage capacity of wetlands and increasing vegetation coverage in urbanized and precipitated regions

The flood risk prediction of the middle-lower YRB applied the improved flood risk model to assess the flood risk from 2021 to 2100 under the Shared Socioeconomic Pathways (SSP) 2 - Representative Concentration Pathways (RCP) 4.5 and SSP5-RCP8.5 scenarios. The results indicated that: 1) the high and very high flood risk areas will totally cover 38% and 40% of the total study area under the SSP2-4.5 and SSP5-8.5 scenarios by 2100, respectively; 2) the overall flood risk of the MLYRB was predicted to become severer by 2100 under both scenarios; and 3) there would be a prominent northward expansion of the high and very high flood risk areas in Jiangxi, Hunan and the southern part of the Taihu Lake Basin in Jiangsu.

In summary, this thesis provides the data support for the long-term wetland variations in the YRB, develops an improved flood risk model to investigate the long-term wetland effects on the flood risk and predicts the future flood risk incorporating wetland dynamics in the YRB. The efforts of thesis contribute to the sustainable wetland conservation and flood risk mitigation in the YRB, aligning with the United Nations Sustainable Development Goals.

Table of contents

List of tables

List of figures

List of supplementary materials

Acknowledgments

During these four and a half years journey of my PhD study, I would like to express my greatest gratitude to my first supervisor Dr John Xiaogang Shi. He gives me the opportunity to pursue my PhD degree at University of Glasgow and is the most important person in my academic journey. He always encouraged and supported me to persevere through difficulties and challenges, never giving up on me. I also extend the heartfelt thanks to my second supervisor Prof Qunshan Zhao for his contributions and support in my academic development.

I owe a deep debt of gratitude to my parents and partner. They give me the unconditional support and love, which sustained me throughout my PhD journey. I'm also thankful for my colleagues and friends Keke Zhou, Dianyu Feng, Dingfan Zhang, and Niantang Liu, for their selfless help in my research.

I am thankful for the support provided by the academic, technical, and administrative staff at the School of Social & Environmental Sustainability, whose assistance was crucial to my work.

I would like to thank my examiners and viva convenor for the time taken to review my thesis and for their forthcoming feedback.

Over these years of PhD study, I encountered many difficulties and challenges, but my passion for research kept me going. I want to thank myself for my courage and perseverance. No matter what path I choose in the future, these years of study will always be the most valuable experiences in my life.

Author's declaration

I declare that I am the sole author of the work contained within this thesis, except where explicit reference is made to the contribution of others, and that it is of my own composition. No part of this work has been submitted for any other degree at the University of Glasgow or any other institution.

Chapters 4, 5, and 6 are presented as reformatted versions of research papers that have been published or submitted to academic journals. In accordance with the requirements from 'Alternative Format Thesis' guidelines, these chapters collectively represent a coherent and interrelated body of work.

The work in Chapter 4 of this thesis has been published as follows:

Guo, Z., Zhao, Q., & Shi, X. (2024). A long-term (1984–2021) wetland classification dataset for the Yangtze River Basin from continuous Landsat image collections. *Total Environment Advances*, 11, 200111. https://doi.org/10.1016/j.teadva.2024.200111

As the first author and corresponding author of this paper, I confirm that Chapter 4 was jointly authored with Qunshan Zhao and Xiaogang Shi, and my contribution to this paper accounts for 90%.

The work in Chapter 5 of this thesis has been published as follows:

Guo, Z., Shi, X., Zhang, D., & Zhao, Q. (2025). Effects of Long-Term Wetland Variations on Flood Risk Assessments in the Yangtze River Basin. *Environmental Impact Assessment Review.* 116, 108123. https://doi.org/10.1016/j.eiar.2025.108123.

As the first author and corresponding author of this paper, I confirm that Chapter 5 was jointly authored with Xiaogang Shi, Dingfan Zhang, and Qunshan Zhao, and my contribution to this paper accounts for 90%.

The work in Chapter 6 of this thesis has been submitted to the journal:

Guo, Z., Shi, X., & Zhao, Q. (2025). Future flood risk assessments in the Middle-Lower Yangtze River Basin under climate and socio-economic scenarios.

As the first author and corresponding author of this paper, I confirm that Chapter 6 was jointly authored with Xiaogang Shi and Qunshan Zhao, and my contribution to this paper accounts for 90%.

Printed Name: Ziying Guo

Date: 12/06/2025

Abbreviations

AHP	Analytic Hierarchy Process
ANN	Artificial Neural Network
CART	Classification and Regression Tree
CAS_Wetlands	National Wetland Mapping in China
CLCD	China Land Cover Dataset
CMIP	Coupled Model Intercomparison Project
CO	Site Contamination
DHB	Dongting and Honghu Lake Basin
DW	Dynamic World
EFZ	Ecological Function Zones
EM-DAT	Emergency Events Database
ESRI_GLC	Esri World Cover
ETM+	Enhanced Thematic Mapper-plus
ΔFR	Flood Risk Difference
FROM-GLC	Finer Resolution Global Land-cover Map
GCM	General Circulation Models
GDP	Gross Domestic Product
GEE	Google Earth Engine
GHG	Greenhouse Gas
GIS	Geographical Information System
GLC_FCS	Global Land-cover Product with Fine Classification System
GlobeLand	Global Land Cover Dataset
GPS	Global Positioning System
GPU	Graphics Processing Unit
GSW	Global Surface Water
GYRPP	Great Yangtze River Protection Program
HDD	Hard Disk Driver

HSWDC	High Spatial-Temporal Water Body Dataset in China
IPCC	Intergovernmental Panel on Climate Change
ISWDC	Inland Surface Water Dataset in China
LTWCD_YRB	Long-Term Wetland Classification Dataset for YRB
LULC	Land Use and Land Cover
MCI	Momentary Conditional Independence
MLC	Maximum Likelihood Classifier
MLYRB	Middle and Lower Reaches of the YRB
NB	Naïve Bayes
NbS	Nature-based Solutions
NDMA	National Disaster Management Authority
NDSI	Normalized Difference Snow Index
NDVI	Normalized Difference Vegetation Index
NDWI	Normalized Difference Water Index
NRSCC	National Remote Sensing Center of China
OLI	Operational Land Imager
PC	Peter and Clark
PD	Population Density
PLB	Poyang Lake Basin
PR	Cumulative Max-three Day Precipitation
RCP	Representative Concentration Pathways
RF	Random Forest
RU	Runoff and Vegetation Cover Factor
SAR	Synthetic Aperture Radar
SB	Sichuan Basin
SDG	Sustainable Development Goal
SSP	Shared Socioeconomic Pathways
SVM	Support Vector Machines
TGD	Three Gorges Dam

TLB	Taihu Lake Basin
TM	Thematic Mapper
UAV	Unmanned Aerial Vehicles
USD	United States Dollar
WHO	World Health Organization
WP	Wanjiang Plain
YRB	Yangtze River Basin

Chapter 1 Introduction

1.1 The importance of wetlands

Wetlands are aquatic systems or landscapes characterized by a seasonal or permanent water table throughout the year, positioned in the transition zone between aquatic and terrestrial ecosystems (McCauley et al., 2015; Mitsch, 2015). They are among the most productive ecosystems, providing a wide array of services that play crucial roles in ecology, environments, economies, and societies, especially under changing climate conditions (Greb et al., 2009; Karmakar, et al., 2023; Sharma, et al., 2021). Wetland ecosystem services play a vital role that can simultaneously benefit the economy and environment, including aquaculture, erosion control, sediment transport, groundwater recharge, flow regulation, waste assimilation, and the provision of natural products (Jisha and Puthur, 2021; Nayak and Bhushan, 2022). They support the environmental health and economic development, contributing to nature-based solutions and achieving Sustainable Development Goals (SDGs) (Karmakar et al., 2023; Xu et al., 2019a). Ecologically, wetlands provide a natural cycle for supporting the wide range of biotas, such as well-managed rice paddies, estuaries, and coastal fish farms, and species involved in decomposition, pests, and disease regulations (Ronco et al., 2020). They are also critical habitats for migratory waterbirds that rely on wetlands worldwide for breeding and feeding (Karmakar et al., 2023). Wetlands can support hydrological connectivity with other landscapes, linking freshwater ecosystems through groundwater, nitrogen, and sulfur cycles, thus helping to aggregate impacts at catchment scales (Cunillera-Montcusí et al., 2022). In the climate system, wetlands serve as a natural source of blue carbon, acting as a carbon sink that sequesters carbon for millennia, then releasing it to the atmosphere as CO_2 to energize the hydro-climatic changes in their catchments (Mcleod et al., 2011). Given their ecological services, wetlands are vital to human livelihoods, particularly for coastal communities (Karmakar et al., 2023).

This section will explore the critical roles of wetlands in carbon cycling and climate change

mitigation, economic value, disaster protection, the preservation of Indigenous communities, and human livelihoods.

1.1.1 Carbon cycling and climate change mitigation

Wetland ecosystems generate substantial amounts of organic matter in semi-decomposed forms, which store carbon by absorbing it from the atmosphere through photosynthesis, aggregating organic matter in anoxic soil, and storing plant biomass while releasing methane due to reduced decomposition rates (Kayranli et al., 2010; Rogers et al., 2019). This process of carbon capture and stabilization as a carbon sink or pool is known as carbon sequestration (Kayranli et al., 2010; Rogers et al., 2019). Poulter et al. (2021) estimated the global wetland carbon stock range between 520 and 710 Pg. Carbon sequestration in wetlands involves several functions: respiration of the aerobic zone, methane formation by microbes, sedimentation, and biodegradation (Kayranli et al., 2010). Wetlands with a higher water table tend to store more carbon in the soil, creating anaerobic soil conditions that contribute to carbon-rich wetlands (Karmakar et al., 2023).

Compared to freshwater wetlands, the production rate of methane in coastal wetlands is lower due to the inhibition of methane by salinity (Karmakar et al., 2023). Coastal wetlands, such as tidal salt marshes, mangrove forests, and seagrass meadows, play an important role in mitigating climate change by reducing Greenhouse Gas (GHG) emissions and serving as significant blue carbon reservoirs (Gallego-Sala et al., 2018). The 2006 Intergovernmental Panel on Climate Change (IPCC) guidelines for National Greenhouse Gas Inventories highlight the potential for blue carbon storage in wetlands as a valuable component of climate change mitigation and adaptation strategies (IPCC, 2006).

1.1.2 Economic values

Freshwater wetlands contain over 40% of the biosphere's species, serving as crucial nursery environments for numerous freshwater fish species of great economic importance (Nayak and Bhushan, 2022). Beyond their role as habitats, wetlands have diverse economic value, including human habitation, agriculture, energy generation, wildlife conservation, resource

gathering, tourism, and recreation, as well as the production of cash crops (Gallego-Sala et al., 2018). The global value of wetland ecosystem services is 26.4 trillion United States dollars (USD) annually, contributing 20% of the global value of ecosystem services, encompassing benefits such as flood management, storm attenuation, and recreation (Thorslund et al., 2017).

The economic value of wetlands varies by different wetland types. Meta-regression analyses have shown that urban and marine wetlands in coastal developing countries hold higher economic value than other wetland types (Chaikumbung et al., 2016; Díaz-Pinzón et al., 2022). In China, however, the annual total ecosystem service value provided by lake and marsh wetlands was calculated to be very high, which is 55% of the total service value of the natural grassland ecosystem (USD 2.55×10^{10} and USD 5.63×10^{10} , respectively) (Zhang et al., 2014). Values of marsh ecosystem services were concentrated in Heilongjiang, Qinghai, and Inner Mongolia. The value of lakes was concentrated in the Tibet autonomous region, Heilongjiang, and Qinghai (Zhang et al., 2014). Coastal wetland ecosystem services provided by 35 national nature reserves in China are estimated to be USD 3.3×10^{10} per year (Li et al., 2020). Wetlands that provide water regulation and support biodiversity are generally more valuable than those used for recreation, and conserving wetlands yields greater economic benefits than converting wetlands for tourism development (Chaikumbung et al., 2016).

1.1.3 Natural disaster protection

The frequency and intensity of natural disasters, such as floods, droughts, and storms, have significantly increased worldwide in recent years, resulting in loss of life, infrastructure damage, and economic loss (Bouwer, 2011; IPCC, 2012). The annual cost of damage caused by natural disasters in the United States has exceeded USD 100 billion over the past decade, and over 11,000 people died due to floods and landslides in India in 2021 alone (Karmakar et al., 2023). Wetlands play a critical role in protecting against natural disasters under a changing climate by mitigating impacts on human populations and the environment. In the United States, coastal wetlands of New York and New Jersey reduced flood levels by up to 30% during Hurricane Sandy in 2012 (Temmerman et al., 2013). Similarly, mangrove forests in

Indonesia and Thailand acted as natural barriers against storm surges by absorbing and dissipating wave energy to protect coastal communities from the devastating impacts of the 2004 Indian Ocean Tsunami (Barbier et al., 2011). For the high flood risk regions in the northeast Haor region of Bangladesh, lakes in the middle and lower reaches of the Yangtze River Basin (YRB), and the Rocuant-Andalién coastal wetlands of Chile, wetlands are the key factor in local flood risk mitigation (Cui et al., 2013; Kamal et al., 2018; Rojas et al., 2022). Wetlands also act as natural water storage systems, mitigating drought impacts by releasing stored water into rivers and streams, thereby maintaining water levels and supporting downstream ecosystems (Karmakar et al., 2023). Wetlands have been found to provide 25% of the national water resources in South Africa (Mander et al., 2015).

1.1.4 Preservation of Indigenous communities

Besides the ecological and economic importance, wetlands hold strong cultural significance, particularly for Indigenous communities. The livelihoods of Indigenous communities are deeply connected to ecosystem services provided by wetlands. For example, the Baka people of Cameroon rely on wetlands for hunting, gathering, and traditional medicine (Sunderland et al., 2014). Consequently, the loss of wetlands can have the significant socio-economic impacts on Indigenous cultures and livelihoods. A notable example is the Mekong Delta in Vietnam, where wetland degradation has led to flooding and water insecurity for local communities (Quan et al., 2018). The situation is similar in India, where rising sea levels and wetland contamination caused by climate change and human activities have threatened mangroves in West Bengal and the Loktak Lake regions, with significant resources for local fishing communities (Karmakar et al., 2023). Conversely, wetland restoration in the Murray-Darling Basin in Australia has provided employment opportunities for local Indigenous communities while enhancing water quality and preserving culturally significant sites (Kingsford, 2000).

1.1.5 Human livelihoods

Human livelihoods encompass the capacities, socio-economic resources, and activities necessary for supporting a way of life. Wetlands offer diverse services that are vital to

people's daily lives, especially those of coastal residents (Barbier, 2019). The contributions of wetlands to livelihoods depend on the interaction between their ecological functions and society (McCartney et al., 2015). Many communities living near wetlands rely solely on natural resources for daily sustenance, particularly coastal fishing communities (Gopal, 2013). Wetlands also enhance human well-being by providing groundwater storage for drinking, filtration, and the retention of toxins (Sharma and Naik, 2024). However, the wetland degradation has led to severe crises in rural, urban, and suburban livelihoods (Adhya and Banerjee, 2022). This has led to the reduced incomes and increased poverty among communities that rely on wetlands (Kundu et al., 2024). Additionally, wetland degradation negatively affects human health and traditional ways of life; degraded wetlands can become breeding grounds for disease-carrying parasites, such as those causing schistosomiasis and malaria (Karmakar et al., 2023).

1.2 The status of global wetlands

As stated in Section 1.1, wetlands are among the most productive ecosystems on the planet, playing irreplaceable roles in global climate regulation, carbon and hydrological cycling, ecosystem diversity, and human welfare. Nevertheless, global threats to wetlands persist. Due to the combined effects of human activities and natural factors, wetland loss and degradation threaten wetland sustainability against the climate change (Asselen et al., 2013; Xu et al., 2019a). Field studies have confirmed that the global wetland area has declined, with the quality of remaining wetlands simultaneously deteriorating (Davidson, 2014; Gardner et al., 2015; Finlayson et al., 2018). In regions with available data, approximately 87% of global wetlands have been degraded since 1700, with more than 50% occurring in the middle 20th and early 21st centuries (Davidson, 2014; Dugan, 1993; Fluet-Chouinard et al., 2023; OECD, 1996).

The degradation of most inland wetlands is driven by destructive factors such as agriculture, aquaculture, industry, urbanization, water use, and pollution (Asselen et al., 2013; Ballut-Dajud et al., 2022; Finlayson et al., 2018; Secretariat, 2010; Vörösmarty et al., 2010).

Globally, 25% of wetland loss is attributed to agricultural development, followed by 17% from urbanization, 11% from aquaculture, 8% from industry, and other contributing factors (Ballut-Dajud et al., 2022). Rivers and lakes are the wetland categories most affected by the land occupation, with 87% and 80% of their area affected, respectively (Xu et al., 2019a). Water resources management is another major driving factor of inland wetland degradation, as many rivers worldwide are strictly controlled by dams to meet the growing demand for hydropower and irrigation (Gardner and Finlayson, 1999). Globally, 37% of the world's 227 largest rivers are seriously affected by dams, particularly in developing countries, such as the YRB in China, the La Plata Basin in South America, and the Tigris and Euphrates River Basins in the Middle East (Millennium Ecosystem Assessment, 2005). Natural and anthropogenic factors such as climate change, extreme weather, and natural disasters contribute significantly to wetland loss and degradation (IPCC 2021).

Coastal wetland is the most vulnerable category to climate change, with 41% affected by climate-related factors, particularly mangrove, which is the most impacted coastal wetland category. Lake wetlands (24%) and marsh wetlands (23%) follow in terms of vulnerability (Ballut-Dajud et al., 2022; Xu et al., 2019a). Blankespoor et al. (2014) quantified that 68% of coastal wetlands in 86 developing countries and territories was at risk given a future 1 m sea-level rise, with potential economic losses exceeding USD 703 million annually. Regarding spatial distribution, Oceania is the most vulnerable continent, with 42% of its wetlands affected by climate change and extreme weather (Xu et al., 2019a).

According to the Ramsar Convention, the world's important wetlands were designated reserves (Kim, 2010; Smardon et al., 2009). Today, there are 2303 Wetlands of International Importance (Ramsar Sites) across 169 countries around the world, covering 229 million hectares, accounting for 19% of the global wetland area (Davidson et al., 2018; Finlayson et al., 2018). However, many Ramsar Sites are currently experiencing degradation and facing significant threats.

Among the 20 Asian Ramsar Sites monitored by the National Remote Sensing Center of China (NRSCC) in 2014, the total wetland areas and landscape integrity declined, primarily due to the insufficient water supply and climate change (NRSCC, 2014). The Sanjiang Plain, China's largest natural marsh wetland region, serves as a representative Ramsar Site in Asia. (Kui et al., 2008). However, the area of wetlands had decreased by 79.4% (about 2.99 million hectares) from 1994 to 2015 (Xu et al., 2019a). The primary cause of wetland loss in this region was land encroachment by agricultural development, while wetland degradation was driven by reduced water supply (NRSCC, 2014). Lake Urmia, one of the world's largest permanent high salinity lakes, was shrunk by 40% between 2001 and 2013 — almost half of its flooded wetlands have been converted to artificial and barren land (NRSCC, 2014). In South Asia, many Ramsar Sites are located in the Mekong River Basin. In recent years, wetlands in the Mekong River Basin have been threatened by human activities, such as agricultural development, urbanization, and industrialization. The construction of dams and reservoirs is the significant factor contributing to wetland degradation in the Mekong River Basin (Mitsch and Gosselink, 2015).

In Europe, NRSCC has found that 34% of seasonal marshes and 12% of reservoirs listed as Ramsar Sites have degraded into non-wetlands (NRSCC, 2014). The Danube and Volga Deltas, both large and inland, contain many of the world's important inland wetlands on the Ramsar List. The Danube Delta has degraded due to drainage and related human activities such as agriculture, gravel mining, and dumping (Coleman et al., 2008). In the Volga Delta, wetlands are now affected by the dam construction, disrupting natural river hydrology, along with a decline in the Caspian Sea water level (Mitsch and Gosselink, 2015). Lake Sevan, one of the largest alpine freshwater lakes in the world, faces significant threats due to excessive groundwater extraction, despite efforts to artificially replenish the lake (Babayan and Adamovich, 2023). The Wadden Sea is the representative coastal wetland of Ramsar Sites in Europe. However, it has been cultivated by local residents (Lotze et al., 2005).

The total wetland area of 30 Ramsar Sites in Africa has decreased to just 2000 hectares, all

with severe ecosystem degradation. Approximately 20% of inland flooded wetlands and 17% of rivers have degraded into non-wetland and other degraded wetland categories (Xu et al., 2019a). Drought and drainage for irrigation have caused an 89% reduction in seasonal herbaceous swamps in Lake Chad (NRSCC, 2014). The Democratic Republic of Congo has the largest areas of Ramsar Sites in the world, playing a vital role in the conservation of rare and endangered species of plants and animals. However, the civil war and illegal human activities in the country have severely affected these wetlands and related flora, highlighting the need for international efforts to protect them (Ramsar, 2024). The Okavango Delta System in Botswana is one of the largest Ramsar wetlands in the world. Unfortunately, it faces many threats from natural burning and intercepting water resources upstream, tourism development, and overuse of raw materials (Shinn, 2016). Coastal Ramsar Sites in West Africa, predominantly mangroves, are also threatened by desertification, over-exploitation, and conversion to rice agriculture (Almar et al., 2023).

Monitoring by the NRSCC found that two major Ramsar Sites in Oceania declined by 80,000 hectares, with 90% of seasonal marshes transitioning to forest shrubs between 2001 and 2013, marking the highest disturbance degradation index among the continents (NRSCC, 2014). The number of wetland ecosystems in Kakadu National Park in Australia has declined, with wetlands changing to bare lands or artificial lands (Bangalang et al., 2022). Mangroves in Shoalwater and Corio Bays in eastern Queensland are threatened by pollution, erosion, pests, and recreation (Chamberlain et al., 2021). The Whangamarino peatland on New Zealand's North Island faces threats from reduced river flooding and silt deposition caused by agricultural development, increased fire frequency, and alien species invasions (Pronger et al., 2014).

Everglades National Park is the largest Ramsar Site in the United States. It has lost half of its original area due to agricultural activities to its north and urban development to its east and west (Mitsch and Gosselink, 2015). Fortunately, restoration efforts to improve water flow have been recently implemented positively (NRSCC, 2014). San Francisco Bay is recognized

as one of the most important estuaries in North America and one of the most urbanized wetlands in the United States. However, 95% of its tidal wetlands have been destroyed, primarily for climate change, agricultural development, and salt industry (Parker et al., 2011). At present, upstream hydraulic mining is a significant threat due to its impact on sediment deposition and erosion (Mitsch et al., 2015).

In South America, the total wetland area of 20 Ramsar Sites decreased by 0.26 million hectares by 2013, with most losses occurring in marshes and lakes (NRSCC, 2014). Pantanal, one of the largest wetland regions in the world, contains a number of South America's Ramsar Sites (Junk and de Cunha, 2005). Many factors threatened it such as the development of the upper Paraguay River for agriculture, water pollution caused by mining, and the invasion of exotic species (Boin et al., 2019). Additionally, illegal wildlife trafficking and cocaine smuggling make wetland management in this region be difficult and expensive (Mitsch and Gosselink, 2015).

Currently, about one-third of the global Ramsar wetland sites have been artificially reconstructed (Xu et al., 2019a). In China, wetland conservation is transitional, with large-scale restoration and reconstruction projects being implemented in recent years. As a result, 42% of inland wetlands and 38% of coastal wetlands in China have been artificially reconstructed or altered, much higher than the global average (Xu et al., 2019a). Nevertheless, wetland loss and degradation have led to a dramatic reduction in the value of ecosystem services. Between 1997 and 2011, the degradation of marsh wetlands caused economic losses equivalent to 1.4 times China's Gross Domestic Product (GDP) in 2011 (Gardner et al., 2015). But this economic loss is only part of the issue, as it also contributes significantly to carbon emissions, leading to the release of 0.2-1.5 Pg per year; approximately 6–18% annual anthropogenic emissions (Karmakar et al., 2023).

The current patterns of global wetland loss and degradation as well as its negative impacts lead to a future scenario far from optimistic. Integrated management approaches to wetland

protection are essential to ensure the sustainable use of wetland resources and to mitigate the effects of climate change and other human activities. However, wetlands continue to face significant threats due to the lack of management planning and regulations on wetland protection and restoration. Therefore, the next section focuses on challenges in wetland management.

1.3 Challenges in wetland management

Section 1.2 discusses the Ramsar Convention as a milestone in wetland conservation and management by establishing wetland protected areas (Zheng et al., 2012). It enshrines the principle of the necessity to understand past and present wetland status, human use, current and future impacts, and ways to achieve sustainable wetland use (Chatterjee et al., 2008). To address threats faced by global wetlands, an effective wetland management plan plays an indispensable role in wetland conservation (Chatterjee et al., 2008). After 1950s, wetland management has evolved into a stand-alone science to protect wetlands as the wildlife habitat (Mitsch and Gosselink, 2015; Smardon and Faust, 2006). However, wetlands in less developed countries still face significant threats due to the lack of management planning and regulations on wetland protection and restoration, especially in Asia and Africa (Mitsch and Gosselink, 2015). In Africa, nearly 50% of wetland sites do not have management plans. The situation in Asia is also not optimistic — 45% of wetland sites in Asia lack management plans (Xu et al., 2019a).

Monitoring is the first step in the wetland management and conservation process (Chatterjee et al., 2008). Each country should establish a long-term wetland dynamic monitoring system to monitor and analyze the wetland status, particularly the large-scale wetlands of international importance by using global remote sensing resources (NRSCC, 2014). The establishment of monitoring stations, the advanced monitoring technology, the construction and open access of monitoring databases are essential for the effective wetland monitoring (Demarquet et al., 2023). Remote sensing has been confirmed as an effective technology for monitoring wetlands, which can regularly monitor the spatial and temporal distribution and

dynamic change in large-scale wetlands in an accurate, objective, and effective way based on both satellite images and field observations (Bartsch et al., 2009; Mao et al., 2020; Niu et al., 2011; Zheng et al., 2015). Remote sensing technology should be continuously improved in the data resolution and updating speed when organizations and researchers use it for wetland monitoring.

With the support of wetland monitoring, various integrated wetland restoration strategies aim to enhance resilience to climate change and help ensure the sustainable use of wetland resources. Wetland restoration is the restoration and reconstruction of degraded or disappeared wetlands through the ecological technology (Xu et al., 2019a). Restoration strategies can be divided into different categories: Maintaining and enhancing hydrologic processes, improving water quality, restoring wetland vegetation, facilitating transformation of wetland communities, adjusting wetland systems, and creating new wetlands (Johnson and Havranek, 2013; Karmakar et al., 2023; Perry et al., 2015). Besides, the long-term wetland monitoring can provide the data support for establishing wetland protected areas, natural reserves, and wetland parks (Zheng et al., 2012).

Although the implementation of wetland management processes has led to effective outcomes in many regions, challenges still exist. Managing coastal wetlands and alpine wetlands is typically challenging (Li et al., 2018; Zhao et al., 2020). Coastal wetlands have experienced the most serious degradation in the 20th century — world coastal wetlands have lost more than 50% of their area due to accelerating climate change (Li et al., 2018). The efforts of coastal wetlands restoration can be found in different regions around the world, with examples of the salt marshes in the Yangtze Estuary in China, the marshes and shellfish aquaculture management at San Francisco Bay and the Mississippi River Delta in the United States, and the implementation of 'build with nature' by nourishing the coast in the Netherlands (Li et al., 2018). However, challenges remain for coastal wetland management and restoration. For example, coastal wetlands are highly dynamic, sometimes within days. As a result, it is relatively challenging to map them remotely with the high levels of accuracy and consistency

due to the substantial altered reflectance and energy backscatter properties (Gallant, 2015). Besides, coastal wetland restoration relates to site-specific biomorphic interactions, especially in tidal zones. It is necessary to consider interactions between the ecosystem and the physical environment (Li et al., 2018). Additionally, land reclamation is often inevitable to maintain the income for coastal residents and support the local economic development, making the coastal wetland restoration difficult to implement (Liu et al., 2020). Therefore, community participation and technological support need to be strengthened to develop the restoration framework that balances economic development and coastal wetland protection (De Oliveira et al., 2024; Liu et al., 2020).

Apart from coastal wetlands, alpine wetlands are typically vulnerable to climate change, and the wetland management process is challenging (Zhao et al., 2020). For instance, the revegetation of wetlands in the Intermountain West of the United States faces limited budgets and personnel, difficult water access, invasive plants, drought, and climate change (Henry et al., 2024). Managers cannot always find the specific plant materials for wetland revegetation, due to poor access and technical knowledge (Henry et al., 2024). Additionally, alpine wetlands in the eastern edge of the Qinghai-Tibet Plateau of China have been severely disrupted due to the dramatic climate change and the interference of human activities (Zhang et al., 2025). The local wetland management remains incomplete because of the lack of fundamental monitoring data support and the restorability assessment for alpine wetlands (Zhang et al., 2024b). Alpine wetlands are typically monitored using remote sensing methods to capture their dynamics, given the complex surface coverage and frequent spatial distribution changes (Zhang et al., 2017; Zhao et al., 2024). Therefore, increasing funding and human resources for developing the alpine wetland monitoring, along with collaborations with more researchers and stakeholders, are essential to address challenges faced in the alpine wetland management.

The lacked or limited monitoring data has become a major challenge for the wetland management. Therefore, given the importance and the threated status of wetlands worldwide,

as discussed in Sections 1.1 and 1.2, the long-term time series wetland monitoring is essential to fill data gaps and to support the development or validation of the effective wetland management strategies, particularly for vulnerable and dynamic wetlands.

1.4 The negative impacts of floods

Floods are defined as the overflowing of normal water bodies and streams, as well as the accretion of water over areas that are generally not inundated in the IPCC Special Report on Managing the Risks of Extreme Events and Disasters to Advance Climate Change Adaptation (SREX) (IPCC, 2012). Different mechanisms produce various types of floods, including river (fluvial) floods, flash floods, urban floods, pluvial floods, sewer floods, coastal floods, and glacial lake outburst floods (IPCC, 2012). As the most common and costly type of natural disaster in the world, floods are responsible for 44% of global natural disasters and severely lead to a variety of negative impacts across space and time (Petit-Boix et al., 2017; WMO, 2021; Wu et al., 2020).

The direct economic loss caused by floods is one of the major tangible social impacts and has shown an increasing trend globally over the past 20 years (Bubeck et al., 2017; Tanoue et al., 2020; Willner et al., 2018). According to the two most well-known natural disaster databases in the world (Emergency Events Database [EM-DAT] and NatCatService) the flood event with the highest economic loss in the last 35 years was the Chao Phraya River Flood in Thailand in 2011, accounting up to USD 40 billion in losses (Bubeck et al., 2017). The economic loss of the YRB flood event in China in 1998 was the second (USD 30 billion) and the third highest (USD 16 billion) in EM-DAT and NatCatService, respectively (Bubeck et al., 2017). The difference between two databases relate to the difficulties and uncertainties associated with collecting the data of disaster loss and different data collection methods (Gall et al., 2009; Guha-Sapir & Below, 2002). Between 1980 and 2015, 62% of global flood losses occurred in Asia, which was much higher than other continents, followed by Europe (19%) and the Americas (15%) (Bubeck et al., 2017). In recent decades, the global trend of economic loss brought by floods was increasing in most regions, which was predominantly

associated with the accumulation of population and economic assets in flood-prone regions (Barredo, 2009; Bouwer, 2011).

The loss of human life is another major direct social impact due to flood disasters (Jonkman, 2005). According to the EM-DAT, a single flood event causes thousands of deaths (Bubeck et al., 2017). The largest number of fatalities between 1980 and 2016 was caused by a single flood event that occurred in Venezuela in 1999, with the death of 30,000 in mudslides on the steep slope of the Sierra de Avila (Wieczorek et al., 2001). Large flood events occurring in China in 1980, 1996, and 1998 killed 12,631 people (Bubeck et al., 2017). Similar to the geographical distribution of global economic loss, the human life loss of floods was the highest in Asia (67%) since 1980 (UNISDR, 2011). Besides, floods can cause many disaster-related injuries and diseases with both direct and indirect consequences during the flood event (e.g., injuries caused by cuts, falls, being struck by fast-moving objects in flood water, exposure to toxins, communicable diseases), and delayed physical or mental issues (Alderman et al., 2012). The World Health Organization (WHO) has noted that a higher risk of communicable disease always occurs immediately following floods when the population is displaced, infrastructure is damaged, and water supply systems are polluted (Jafari et al., 2011). Additionally, in some flood-prone regions, such as Bangladesh, and some parts of Africa and Australia, floods inundate agricultural land and destroy crops, resulting the severe food shortages and malnutrition in rural areas and very high concentration urban neighborhoods (Douglas, 2009; Smith et al., 2016).

Floods not only affect the economy and human health but also have serious impacts on the environment, generally including water pollution, erosion, and deposition, and impacts on the survival of organisms, possibly affecting biodiversity (Baral, 2013; Carrivick et al., 2011; Goodwell et al., 2014; Hrdinka et al., 2012; Milani, et al., 2020; Zhang et al., 2024a). For example, heavy metals, organic chemicals, and fecal coliform bacteria were detected in the floodwater and were widely dispersed after Hurricane Katrina in 2005 (Dortch et al., 2008; Foulds et al., 2014).

To address those losses brought by flood events, the research related with floods is essential. For any given climate conditions, characteristics and variations of wetlands play significant roles in the flood generation (Wu et al., 2020). As described in Section 1.1.3, protecting against flood disasters is one of the most important ecosystem services of wetlands (Gulbin et al., 2019). However, wetland effects on floods are various among different regions worldwide. For example, the low-lying floodplain wetlands made the northeastern Bangladesh to be typically vulnerable to flash floods (Kamal et al., 2018). In contrast, The water storage capacity of lakes in the middle-lower YRB reduces the local flood risk (Cui et al., 2013). Rocuant-Andalién coastal wetlands of Chile mitigated the impacts of flood disasters, but this ability was diminished due to the reduction of wetland areas caused by urbanization (Rojas et al., 2022).

1.5 How wetlands influence flood risk

The mechanisms of how wetlands mitigate the flood risk generally include water storage capacity, slowing water flow, increasing water infiltration, and sediment trapping and erosion control.

Wetlands act as natural water retention systems, temporarily storing the excess water during high-precipitation events or river flood peaks. Depressional wetlands, floodplain marshes, lakes, and riparian wetlands across the watershed can store large volumes of water. This storage capacity reduces the immediate hydraulic load on river channels, helping to reduce the downstream flood peaks and mitigating flood risk (Acreman and Holden, 2013). Besides, after storm events, wetlands gradually release the stored water through surface outflow, subsurface seepage, and evapotranspiration. This delay release ensures that water returns to the river system slowly after the critical flood peak period has passed and reduces the long-term inundation pressure on the downstream infrastructures (Ferreira et al., 2023).

Wetlands can slow water flow due to the increased hydraulic roughness generated by the vegetation coverage, which reduces the velocity of surface water and flood waves (Ballet et

al., 2011; Lane and Milledge, 2013). The flood flow velocity is 29% faster in sloughs compared to the more densely vegetated wetlands in the Everglades wetlands, USA (Harvey et al., 2009). Additionally, vegetation change from wet meadow to shrubs and trees can double the size and depth of the inundated area for the exact size of the flood. Particularly, wooded wetlands reduce flood peaks and increase peak water transit time (Thomas and Nisbet, 2007).

Besides, wetlands enhance the infiltration capacity to mitigate floods by allowing water to percolate into underlying soils and aquifers. The percolation contributes to groundwater recharge**,** effectively transferring water from surface floodwaters into subsurface aquifers, which reduces water volume on the surface during precipitation events, thereby reducing the immediate flood hazards (Kebede et al., 2024; Simon et al., 2023). The Sponge City in Jinan of China is a representative example of applying this wetland-based mechanism for the groundwater recharge and flood mitigation. It uses urban wetlands as the temporary stormwater storage space and facilitates groundwater recharge by allowing stormwater to infiltrate through wetland systems. (Yin et al., 2021).

Moreover, wetlands effectively trap sediments transported by runoff or river flow, as the reduced water velocity promotes sediment deposition. Therefore, wetlands can reduce the channel aggradation by keeping the excessive sediment out of the main channel (Blackwell & Pilgrim, 2011). At the same time, sediment trapping in wetlands contributes to maintain the wetland surface, typically the coastal wetlands. For example, sediment trapping of coastal marshes and tidal flats helps maintain wetland elevation, and attenuate waves and storm surges, thereby reducing the flood risk (Reed et al., 2018). Furthermore, sediment trapping in wetlands provides erosion control benefits by retaining eroded materials within floodplains, which reduces bank instability and contributes to the mitigation of local flood risk (Hupp et al., 2009). In the Nenjiang River Basin, sediment-trapping wetland solutions have helped stabilize floodplains and reduce flood risk over time (Wu et al., 2023).

Given that floods have caused massive socio-economic and environmental losses worldwide, and wetlands play a key role in influencing the flood risk under different conditions, it is crucial to investigate the effects of wetlands on flood risk across different regions of a basin to effectively address and reduce the flood risk.

1.6 Improvements in flood risk assessments

According to the IPCC report, flood risk is projected to continue increasing throughout the 21st century due to intensified climate change and human activities (IPCC, 2021). Flood risk mitigation has been a global issue for governments and communities. Flood risk mitigation activities are dedicated efforts to reduce flood hazards, as well as flood exposure and vulnerability (Kron et al., 2019). Generally, flood risk mitigation approaches can be divided into two broad categories: structural and nonstructural (Rajkhowa and Sarma, 2021). Structural approaches are permanent solutions or facilities to mitigate floods, such as soil conversion, surface land restructuring, runoff delay, rise of infiltration, downstream discharge, flood attenuation, groundwater control, and construction of dams. However, these approaches contain a number of disadvantages, including lowering of floodplain fertility, morphological changes, negative ecological impacts, and land subsidence (Rajkhowa and Sarma, 2021). In recent years, non-structural approaches, such as flood risk assessment, flood forecasting, regulations and policies for flood-proofing, and the improvement of flood awareness and education have gradually become the dominant approaches (Chen et al., 2018). Flood risk assessment is the crucial aspect of risk management, with the aims to identify high flood risk areas and to provide the important references for developing planning, disaster prevention, and disaster mitigation scheduling (Disse et al., 2020; Elshorbagy et al., 2017; Li et al., 2023). The development and application of the flood risk assessment vary across different countries. The flood risk mitigation in Europe and United States generally focuses on the nature-based non-structural approaches and strategies (Alexander et al., 2016; Fournier et al., 2016; Hegger et al., 2016). The application of flood risk assessments has been well established in these countries. Several flood risk guidance and assessments with the more complex probabilistic methods have been introduced to improve the resilience of flood risk (Lewis et al., 2024).

Therefore, improvements in flood risk assessments are discussed in the context of flood-prone countries in Asia with the rapid urbanization.

Countries in South Asia suffer floods that result in massive damages every year, particularly in Bangladesh and India, which have been confronted for decades with flooding risk (Abbas et al., 2016; Ahmed et al., 2022). Bangladesh has learned lessons from the past flood disasters and has developed a relatively effective framework of flood mitigation policy and disaster control. After floods occurred in 1987 and 1988, all the structures with strategic importance for flood mitigation were built above the 100-year flood elevation and with the temporary shelter in flood-prone regions (Abbas et al., 2016). Besides, local policymakers developed policies to effectively manage land and water, to reduce river loads for the infrastructure protection (such as embankments), and the easy conveyance to the Bay of Bengal through the improved river system capacity (Samuels et al., 2006). Strengthening the flood forecasting and early warning systems has garnered encouraging results (Pal et al., 2011). However, flood risk assessments are still limited in the flood mitigation in Bangladesh, typically in the coastal areas (Ahmed et al., 2022; Islam et al., 2019). The over-reliance and poor maintenance of structure-based flood controls, such as embankments and polders, have led to internal drainage problems, waterlogging, and siltation (Brammer, 2014). Most of flood risk assessments conducted the single flood vulnerability indicator such as only the digital elevation model or land cover criteria, which ignored several essential indicators (Bhuiyan and Dutta, 2012; Bhuiyan and Al Baky, 2014). In recent years, studies related with the flood risk assessment in Bangladesh has been improved to consider the roles of urbanization, river distribution, and the local medical services in the flood risk. Ahmed et al. (2022) developed the flood risk assessment in the Kurigram district of Bangladesh with the much more comprehensive categories, which incorporated river density, population density, and health facilities.

In India, 12% of its land is prone to flooding (Gol, 2009). With the support of federal governments, flood forecasting centers and meteorological departments have effectively

saved many lives (Abbas et al., 2016). The National Policy on Disaster Management implemented technology-based mitigation measures for flooding, the timely forecasting and communication, efficient mechanisms for risk assessment, and the response and recovery operation to floods (GoI, 2009). Flood hazard maps of India at the state and district levels have been in place since 1997 to help achieve flood mitigation goals, which was the first step to assess flood risk (BMTPC, 2010). However, the weakness and inaction of several flood-related authorities become a challenge for flood risk mitigation in India. For instance, establishing river basin authorities for supporting the flood risk monitoring and assessment lacked a legislative and policy focus for many years (GoI, 2011). Following this, the National Disaster Management Authority in India was established. As a result, the flood risk assessment framework started to be strengthened (Abbas et al., 2016). Currently, the multi-criteria flood risk assessments with the comprehensive hazard, vulnerability, and exposure indicators have been developed in flood-prone cities, suburban regions, and basins in India (Bhere and Reddy, 2025; Pathan et al., 2022; Vegad et al., 2024).

Floods have become commonplace in basins of the large rivers of China, such as the Yangtze River, the Yellow River, and the Huai River (Kundzewicz et al., 2019). Increasing attention has been paid to further upgrading the flood risk reduction measures in China following a series of destructive flood disasters. Generally, flood risk mitigation in China relies on the structural approaches. For example, China moved quickly to build large-scale water conservancy projects on the YRB and its tributaries after the large flood disaster in 1998, including the Three Gorges, Xiluodu, Wudongde, Banqiao, and other hydroelectric power generation stations (Jia et al., 2022; Zhang et al., 2020a). The total adjusted storage capacity of the Yangtze River and its tributary reservoir groups exceeded 80 billion m^3 (Duan et al., 2016). Tributaries and lakes in the YRB were further reinforced after 1998, constituting a robust line of defense against flood disasters, mitigating flood risks in the YRB (Jia et al., 2022). Besides, the large reservoirs, embanked bends, water transfer projects, and flood storage detention areas had been constructed in the Yellow River Basin and Huai River Basin as well, which played an important role in reducing the risks of flood disasters (Tang et al.,

2020a; Feng et al., 2024). However, structural approaches of flood control have started to face several problems under climate change. Monsoon regions in China are characterized by their annual precipitation, which is mainly concentrated in the rainy season. Therefore, the inter-annual variability between monsoons caused greater challenges to flood-control facilities because of their inconvenience to daily life and economic activity during the dry season (Jia et al., 2022). In addition, the fragmentation, locality, and discontinuity brought problems for local governments when constructing dikes in those basins with the complicated water networks (Jia et al., 2022). For instance, 39,000 km of non-compliant dikes remain in the YRB, which is 46% of the total dike length (Zhang et al., 2020b).

For the non-structural flood mitigation approach, the improved flood risk assessments with comprehensive indicators have developed in China (Guo, 2017; Peng et al., 2024; Yu et al., 2023). Given the basis of these flood risk assessments, nature-based and eco-friendly solutions have been implemented in the high flood risk regions. Taking Dongting Lake as an example, the reclamation of farmlands into lakes increased lake area by 800 km^2 (Jia et al., 2022). To mitigate urban floods, the concept of 'Sponge Cities' has become a national policy of China since 2014 (Chan et al., 2018). It acted in various ways to increase the water storage capacity of wetlands, improve drainage systems to collect much more rainwater, and use filtration and absorption of rain to reduce the surface runoff, thus mitigating flood risk (Chan et al., 2018). Urbanization in China has increased rapidly, from 33.4% in 1998 to 60.6% in 2019 (National Bureau of Statistics, 2024). The rapid urbanization has brought massive challenges to flood risk mitigation in the economic developed regions of China, such as the Yangtze River Delta, the Pearl River Basin, Zhengzhou, and Chongqing (Chen et al., 2015; Guoyi et al., 2023; Li et al., 2013; Li et al., 2024; Yin et al., 2015). The urban heat-island effect makes water vapor evaporate more strongly and densely, increasing the probability of precipitation and flood risk. High-rise buildings can slow down the water movement and vapor speed, and thus extend the period when precipitation falls, increasing the vulnerability to floods of such regions (Chan et al., 2021; Jia et al., 2022; Shao et al., 2020). As a result, both vulnerability and exposure dimensions of flood risk in China have changed, necessitating

the inclusion of more flood-related indicators associated with urbanization to address rapid socio-economic growth and urban sprawl (Ding et al., 2022). Besides, urbanization changes the Land Use and Land Cover (LULC), leading to the expansion of urban construction lands, the loss of arable lands, wetlands, and woodlands, which reduces the water-seepage capacity and the flood control function of original lands, especially wetlands (Du et al., 2015; Gulbin et al., 2019; Luo and Zhang, 2022). Therefore, incorporating wetland distribution in the flood risk assessment is essential in regions with the rapid urbanization.

To sum up, in flood prone regions experiencing rapid urbanization and intensive wetland distribution, the indicators influencing flood risk have become increasingly complex. Therefore, improving the effectiveness of flood risk assessments that incorporate comprehensive indicators, such as wetland dynamics, LULC, and urbanization-related factors, is more crucial than relying solely on traditional structural approaches to mitigate flood risk.

1.7 The status of wetlands and floods in the Yangtze River Basin

The Yangtze River is the longest river in China and the third longest in the world (6,300 km) (Zhang et al., 2020a; Zheng et al., 2021). It drains 1.8 million km^2 of land, and the drainage area represents 18.8% of China's total terrestrial area (Zheng et al., 2021). There are a large number of lakes and tributaries in the YRB, forming the complex water system (Lai et al., 2013; Cai et al., 2016). Lakes account for approximately 22,000 km^2, which are generally distributed in the middle and lower reaches of the YRB (Zheng et al., 2021). Poyang Lake is the largest among them, and controls the inflow of five tributaries, while Dongting Lake is the second largest and receives four tributaries (Cheng et al., 2001). These lakes play a significant role in regulating floods in the middle and lower reaches of the YRB (Cheng et al., 2001). There are more than 7000 tributaries of the Yangtze River with different drainage areas. For instance, eight tributaries drain an area of more than 80,000 km^2: Yalong River, Minjiang River, Jialing River, Hanjiang River, Wujiang River, Yuanshui River, Xiangjiang River, and Ganjiang River (Cheng et al., 2001). These tributaries also have the eight most significant

average annual flows of more than 1,500 m^3 per second (Cheng et al., 2001). Apart from lakes and rivers in mid-lower reaches of the YRB, a large area of inland marshes that primarily distributes in the YRB source region of the Qinghai-Tibetan Plateau, is a significant alpine wetland ecosystem (Zhao et al., 2020). Additionally, Chongming Island of the YRB estuary encompasses broad natural coastal wetlands, including coastal marshes and tidal flats, covering approximately 847.5 km^2, about 212 km^2 of which are above sea level (Huang et al., 2008; Mao et al., 2020). The Chongming Island coastal wetland ecosystem plays an important role in maintaining both ecosystem health and ecological security of the island, such as protecting the island coastal hazards, providing habitats for invertebrates, fish, and waterfowl, purifying the coastal environment, as well as tourism resources and aquatic products for residents (Cui et al., 2015; Peng et al., 2021).

Although the abundant wetlands resources across the YRB account for 40% of the national wetlands, they have been significantly affected by both climate change and anthropogenic activities, thus experiencing dramatic losses in recent decades (Finlayson et al., 2018; Mao et al., 2020). During the first 15 years of this century, wetlands shrank substantially of the YRB, more than half of lakes experienced the significant decreasing trend (Cai et al., 2016). For the lost wetlands, 47.7% were converted to agriculture, 14.5% to grasslands, and 13.8% to urban areas (Xu et al., 2019b). The middle and lower reaches of the YRB are not only the largest complex wetland ecosystem and the most abundant wetland resource in China, but also one of the most developed regions in eastern China with both rapid economic growth and high population density (Huang et al., 2008; Li et al., 2014; Ma et al., 2023; Mao et al., 2018). As a result, wetlands in the middle and lower reaches of the YRB are facing severe anthropogenic damage (Mao et al., 2018). The area of wetlands in the middle reaches of the YRB has decreased by 70% from the 1950s to the 2000s (Ma et al., 2023). Between 1930 and 2000, the area of Dongting Lake declined by 2433 km^2, and Jianghan Plain Lake declined by 4368 km^2 (Du et al., 2011). In contrast, a number of artificial wetlands, such as aquacultural ponds and reservoirs, expanded in the middle-lower YRB because of the aquacultural development (Meng et al., 2023; Zhu et al., 2022). From 1950 to 2001, about 532 km^2 of native wetlands in

Chongming Island were cultivated for agricultural production (Huang et al., 2008). Almost all the high, middle, and low tidal marshes in Chongming Island have been reclaimed in the past few decades (Huang et al., 2008). Alpine wetlands in the source region of the YRB are more vulnerable to climate change than wetlands in other regions, with declining marshes and expanded lakes (Jiping et al., 2011; Zhang et al., 2011; Zhang et al., 2024b). A large area of marsh is threatened by inundation due to the rise of lake water levels caused by recent climate change (Xue et al., 2018). As mentioned in Section 1.3, monitoring is the essential first step for the wetland conservation and management. Therefore, the long-term monitoring of the various wetland categories in the YRB is crucial for guiding the subsequent wetland conservation and management.

The YRB is a flood-prone region that experienced severe flood disasters (Jia et al., 2022; Zhang et al., 2020a). The YRB experienced seven massive floods in 1860, 1870, 1931, 1935, 1964, 1998, and 2010. Each caused a large number of casualties and socio-economic losses (Kundzewicz et al., 2019; Peng et al., 2020). Generally, floods in the YRB were caused by heavy precipitation and have become very common since 1860 (Cheng et al., 2001). The spatial distribution of flood risk is uneven across the YRB (Yu et al., 2023). Flood risk has been investigated to be relatively high in the middle-lower of the YRB because of the heavy precipitation (Peng and Li, 2021). Due to short-term rainfall, most of the central mountainous areas of the YRB are medium-level flood risk zones. The low-risk areas of flood disaster in the YRB are generally concentrated in the upstream, due to the low rainfall and the relatively light impacts of typhoons and tides in western regions dominated by plateau topography (Yu et al., 2023; Zhang et al., 2020a). The major rainstorm regions with the high flood risk in the YRB including the western part of Sichuan, the Dongting Lake Basin, most areas of Jiangxi including the Poyang Lake Basin, and several YRB downstream cities in the Taihu Lake Basin, which are affected by both upstream flow and tidal influences (Cheng et al., 2001; Jia et al., 2022; Yu et al., 2009). The spatial distribution of flood-prone regions in the YRB illustrates that the high flood risk areas are generally concentrated in the major lake basins, with the abundant wetlands. As a result, the wetland effects on the flood risk cannot be

ignored in the YRB.

The entire YRB is covered by the Yangtze River Economic Belt (YREB), which is the strongest socio-economic area in China, including three national level urban agglomerations: The Yangtze River Delta, the Middle Reaches of the Yangtze River, and the Chengdu-Chongqing city cluster (Peng et al., 2020). As a result, the highest level of urbanization contributed to more than 40% of the national population and GDP in the YRB (Xu et al., 2025). However, the rapid socio-economic growth and the extensive human activities have led to several adverse environmental effects in the YRB (Jin et al., 2019). Nearly 80% of the major lakes in the YRB have been affected by human activities, and water-related disasters have become more frequent and severe, typically in the middle-lower YRB, which experiences the higher precipitation and denser water networks (Peng et al., 2020; Xu et al., 2018). Therefore, assessing and mitigating water-related disasters, such as floods, is of great importance in the YRB, where anthropogenic activities are becoming increasingly complex.

Given the frequent flooding, the abundant wetland resources, and the rapid socio-economic development in the YRB, this basin can be served as the globally representative case for developing the sustainable flood risk management strategies. Due to the lack of a long-term time series wetland dataset with comprehensive categories for the YRB, however, significant research gaps still remain in the flood risk assessments without incorporating wetland dynamics, and long-term effects of wetland changes on flood risk. These gaps pose the substantial challenges to the development of the sustainable flood risk management in the YRB.

1.8 Research aims and objectives

This thesis aims to monitor the long-term variations of different wetland categories, and to analyze wetland effects on floods by assessing the flood risk incorporating wetlands in the YRB. It can provide the valuable insights to support the local sustainable wetland

conversation and the effective flood risk mitigation. The study is structured around a series of objectives and questions:

Objective 1 (Chapter 4): To analyze wetland dynamics in the YRB by establishing a long-term time series wetland classification dataset with the comprehensive wetland categories from 1984 to 2021. Research questions include:

- How do different wetland categories in the YRB vary over time and across spatial areas?
- Which driving force has the most significant impact on the long-term wetland variations of the YRB? Natural driving forces ort human activities?

Objective 2 (Chapter 5): To investigate the long-term wetland effects on the flood risk in the YRB based on an improved flood risk assessment model incorporating the wetlands input. Research questions include:

- How do long-term wetland variations influence flood risks in the YRB?
- Which flood risk factor is most dominant under wetland effects in the YRB?
- What wetland-related approaches are suitable to mitigate flood risk in different flood-prone regions of the YRB?

Objective 3 (Chapter 6): To predict the flood indices and flood risk by the end of the 21st century under different climatic and socio-economic scenarios in the Middle-lower YRB (MLYRB) by applying the improved flood risk model. Research questions include:

- How will flood hazard, vulnerability, exposure, and integrated flood risk change across spatial and temporal dimensions in the future of the MLYRB?
- What strategies are necessary for the future flood risk prevention in the MLYRB?

1.9 Thesis structure

This thesis comprises eight chapters. Chapter 1 introduces the background information, including the importance and status of global wetlands, challenges of wetland management, the relationship between wetlands and floods, the improvement in flood risk assessments, and

the status of wetlands and floods in the YRB. Additionally, Chapter 1 states the research gap, research aim, and objectives for this study.

Chapter 2 situates this study in the literature and other studies done in the field. It reviews the past wetland-related datasets covering the YRB, wetland effects on the YRB floods, and the extant flood risk assessments of the YRB. Chapter 3 provides an overview of the methodology to generate the results of this thesis.

Chapters 4, 5, and 6 present the comprehensive version of the three papers. Chapter 4 constructs a long-term wetland classification dataset of the YRB from continuous Landsat image collections. It presents how different wetland categories vary in the YRB from 1984 to 2021 and their corresponding driving factors. Chapter 5 analyses the long-term effects of wetland variations on the flood risk of the YRB and the dominant flood risk indicators under wetland effects. Chapter 6 predicts the future flood risk in the MLYRB by 2100. Chapters 5 and 6 provide the wetland-related suggestions to mitigate the flood risk in the YRB.

Chapter 7 discusses implications, contributions, limitations, and uncertainties of this thesis. Finally, Chapter 8 summarizes results from three papers and makes the overall conclusion of this thesis, as well as looking ahead to future work. Supplementary materials of this thesis are arranged as appendices before references.

Chapter 2 Literature review

2.1 Wetland-related datasets covering the Yangtze River Basin

To quantify and analyze the spatiotemporal dynamics of wetlands, several global and regional wetland-related datasets have been developed using remote-sensed data in previous studies (Che et al., 2015; Li et al., 2020; Lu et al., 2019; Mao et al., 2020; Pekel et a., 2016; Yang and Huang, 2021). These datasets could provide necessary information for decision-makers in the wetland restoration and management processes, aiming to reduce the related challenges caused by wetland information gaps (Wang et al., 2018).

From a global perspective, the Global Surface Water (GSW) dataset, produced by Pekel et al. (2016), is the most comprehensive long-term time series dataset for waterbody worldwide. It quantifies long-term changes in global surface water over the past 37 years, monthly and annually (the updated data is from 1984 to 2021) at 30m resolution by using the entire multi-temporal Landsat 5 Thematic Mapper (TM), Landsat 7 Enhanced Thematic Mapper-plus (ETM+), Landsat 8 Operational Land Imager (OLI) orthorectified, and top-of-atmosphere reflectance and brightness temperature images (L1T) (Pekel et al., 2016). With advances in remote sensing technology, the GLH-Water dataset, derived from very high-resolution optical satellite imagery, mapped global surface waterbodies at a 0.3 m resolution from 2011 to 2022. (Li et al., 2024). The GSW dataset investigated that approximately 90,000 km^2 of the global permanent surface waterbodies disappeared over the past 37 years, with the significant changes in geographical distributions (Pekel et al., 2016). The GLH-water dataset detected the more accurate variations in small water bodies based on the GSW dataset (Li et al., 2024).

Several wetland-related datasets have been developed in China. The Inland Surface Water Dataset in China (ISWDC) demonstrates water bodies larger than 0.0625 km^2 between 2000 and 2016 with 250m spatial resolution, derived from the MODIS MOD09Q1 surface reflectance archive images (Lu et al., 2019). The ISWDC shows a good consistency and

similar change dynamics with the GSWE results. For lake groups in the central Tibetan Plateau in 2015, the comparison between the two datasets indicates a close pattern. However, for the Poyang Lake Basin, the under-extracted surface water and over-extracted surface water of the ISWDC still exist when compared with the GSWE (Lu et al., 2019). Afterwards, the High Spatial-Temporal Water Body Dataset in China (HSWDC) developed by Li et al. (2020) maps the dynamics of the surface water body in China from 2016 to 2018 with a higher monthly spatio-temporal resolution (10m) than both the ISWDC and GSWE by using the cloud-based Google Earth Engine (GEE) platform and Sentinel-1 imageries, the overall accuracy reaches 93% (Li et al., 2020). The HSWDC develops an extraction method for the Sentinel-1 Synthetic Aperture Radar (SAR) data based on a large number of land cover samples (Li et al., 2020). The SAR data has the advantage of being unaffected by clouds. Thus, they can monitor surface water regularly (Aries et al., 2018; Santoro et al., 2014). With the release and application of the GEE platform, it is possible to carry out monitoring and mapping of water bodies on a large scale with the high resolution, so that removing the limitation of research scale and data processing in the past (Kaplan and Avdan, 2018; Slinski et al., 2019; Xing et al., 2018). Taking Dongting Lake as an example, the water area detected by the HSWDC is larger than that of the GSW, primarily due to the higher spatial resolution. Especially in winter, when water storage decreased, the area of some small waterbodies becomes too small for the GSW to detect (Li et al., 2020). Besides, the HSWDC shows higher consistency with water levels from 2016 to 2018 compared to the GSW (Li et al., 2020). Li et al. (2020) further classified the wetlands of Dongting Lake into permanent waters, seasonal marshes, mudflats, and rice fields using the water occurrence information from the HSWDC. The classification result is generally consistent with the result in the corresponding year of Chen et al. (2016), except the difference between rice fields of Li et al. (2020) and agricultural lands (including dry crop lands) of Chen et al. (2016). The HSWDC has the advantage of detecting and extracting waterbodies accurately during freezing months with the help of the SAR data. For example, compared to the ISWDC, the HSWDC can map a more comprehensive water surface of Selinco Lake, located on the Tibetan Plateau, even during freezing months (Li et al., 2020).

In addition to surface water datasets, several global and national land cover datasets with 30m or 10m resolution include wetland or water categories. At the global level, the Global Land Cover Dataset (GlobeLand30) (Chen et al., 2015), the Finer Resolution Global Land-cover Map (FROM-GLC10) (Gong et al., 2019), the Global Land-cover Product with Fine Classification System (GLC_FCS30) (Zhang et al., 2021), the Esri World Cover (ESRI_GLC10) (Karra et al., 2021), and the Dynamic World (DW10) (Brown et al., 2022) all contain only two categories related to wetlands, including permanent water bodies and herbaceous wetlands. Among these datasets, GlobalLand30 and ESRI_GLC10 misrepresent the real land cover situation, where many independent aquaculture ponds and paddy fields are incorrectly mapped. GLC_FCS30 underestimates water bodies, as most of ponds are not indicated as water in the mapping results (Li et al., 2023). For the national perspective of China, the China Land Cover Dataset (CLCD) , which provides the annual 30m resolution land cover data from 1990 to 2019, is a representative dataset with long-term time series national land cover (Yang and Huang, 2021). However, the CLCD faces the challenge of capturing short-term fluctuations in water and wetlands. Therefore, it shows a smaller area of water and wetlands in Poyang Lake than the monthly GSW dataset (Yang and Huang, 2021). In recent years, some high-resolution national land cover datasets have been developed, such as Hi-ULCM, which provides 2m resolution data for 42 major cities of China (Huang et al., 2020), and SinoLC-1, the first 1m resolution national-scale land cover map of China (Li et al., 2023). Similar to global land cover datasets, all of these national land cover datasets include only general categories for water and wetland, without distinguishing subcategories.

The national wetland mapping of China (CAS_Wetlands), developed by Mao et al. (2020), is the most comprehensive wetland dataset in China, encompassing a wide range of wetland categories. The application of the hybrid object-based hierarchical classification approach (HOHC) and the wetland classification system to Landsat 8 OLI data produces a 30m resolution wetland map of China in 2015, with an overall classification accuracy of 95% (Mao et al., 2020). According to the Ramsar definition of wetlands, it includes marsh, fen,

peatland, and water, whether natural or artificial, permanent or temporary, and whether water is static or flowing, fresh, brackish or salty, and include marine water with the depth of which at low tide does not exceed 6 m (Gong et al., 2010). The wetland classification system of the CAS_Wetlands is referred from the Ramsar definition of wetlands and the unprecedented amount of field samples in the wetland mapping history of China, as well as considering the applicability of moderate resolution images and its practical use for ecosystem management of a developed remote sensing wetland classification system (Mao et al., 2020). Therefore, the creation of a new designed wetland classification system is one of the most important novelties of the CAS_Wetlands, which contains three broad categories and fourteen sub-categories (Mao et al., 2020). The CAS_Wetlands gives the result of the total wetland area of 451,084 ± 2014 km^2 of China in 2015, of which 70.5% are inland wetlands. Among 14 wetland categories, inland marshes have an area of 152,429 ± 373 km^2, which accounts for 34% of the total wetlands, while coastal swamps have the smallest coverage (259 ± 15 km^2) (Mao et al., 2020).

Due to its comprehensive wetland classification system, the CAS_Wetlands dataset of Mao et al. (2020) reports a larger national wetland area in 2015 compared to other datasets, such as the CLCD (Yang and Huang, 2021), the China National Land Cover Database (ChinaCover) (Mao et al., 2018), and the earlier wetland-related datasets covered the YRB from Gong et al. (2010), Niu et al. (2009), and Niu et al. (2012). Overall, the CAS_Wetlands provides a significant wetland data reference and the wetland classification system to establish a continuous long-term time series wetland dataset in the YRB.

Given that no existing wetland classification dataset meets the requirements for comprehensive wetland categories and a long-term study period covering the YRB, there is a research gap in establishing a long-term time series wetland classification dataset for the YRB.

2.2 Wetland effects on floods in the Yangtze River Basin

According to Section 1.6, there are abundant wetland resources covering the YRB. The Sichuan Basin and most areas in the YRB middle and lower reaches are the typical flood-prone regions of the YRB (Jia et al., 2022; Li et al., 2014; Mat et al., 2023; Zhang et al., 2020). Cui et al. (2013) and Yu et al. (2009) both confirmed that lake shrinkage and degradation in the YRB middle and lower reaches have led to the rise of lakebed level and the reduction in water storage capacity, especially in the Poyang Lake Basin and the Dongting Lake Basin, which are key driving factors of floods in the long term (Cui et al., 2013; Yu et al., 2009). For example, during the latest severe flood disaster that occurred in the YRB in 2020, the five provinces of Hubei, Anhui, Jiangxi, Hunan, and Jiangsu were most severely affected by floods due to the vast rivers and lakes (Jia et al., 2022). The continuous rainstorm process exceeded the limited carrying capacity of these wetlands, resulting in a high flood risk when the water levels of lakes and rivers exceeded their alarm levels (Jia et al., 2022). Not only lakes and rivers, but also the water level in reservoirs, affect the flood risk in severe flood disasters. For example, the water level reached 22.59m of the Hukou Reservoir in Poyang Lake, 35.94m of the Chenglingji Reservoir in Dongting Lake, and 160.17m of the Three Gorges Reservoir during the flood disaster in 1998, which were all the highest water level in the history of reservoirs (Jia et al., 2022).

Several studies have examined the effects of wetlands on floods in flood-prone regions of the YRB. Taihu Lake, the third-largest freshwater lake in China, is located in the YRB downstream (Xu and Chen, 2023). The Taihu Lake Basin is one of the most developed regions in China, characterized by the highest level of urbanization and the densely populated area (Xu and Chen, 2023). Hence, compared with other major freshwater lakes in the YRB, the Taihu Lake Basin faces far more complex socio-economic and environmental problems (Liang et al., 2011). It has been confirmed that the trend of increased floodwater in the Taihu Lake Basin has accelerated faster than in other flood-prone regions, which is heavily influenced by lake shrinkage due to rapid urbanization and aquaculture development (Cai et al., 2013; Xu and Chen, 2023).

The Poyang Lake Basin is situated in the middle and lower reaches of the Yangtze River Basin. Poyang Lake is the largest freshwater lake in China, which creates extensive floodplains that adjoin the main lake (Feng et al., 2012; Li et al., 2019; Wu et al., 2022). The Poyang Lake Basin is a region with the frequent and extensive precipitation affected by both the south-east and south-west monsoons. The average annual cumulative precipitation frequency is 192 days, and the annual average precipitation is 1638 mm (Liu et al., 2021). Xu et al. (2023) monitored the long-term land-use change in the Poyang Lake Basin from 1986 to 2020. The results showed that the categories of wetlands in Poyang Lake underwent significant changes from 1986 to 2020. Mudflats and paddy fields showed an increasing trend, while the water area decreased (Xu et al., 2023). The analysis of the long-term and short-term flood risk in the Poyang Lake Basin reveals that flood-prone areas are primarily located near rivers and lakes, with the majority of these areas concentrated in the northern part of the basin (Wu et al., 2022).

Dongting Lake is the second largest freshwater lake in China, which is located in the YRB middle reaches. The Dongting and Honghu Lake Basin is a typical wetland region that frequently experiences severe flooding due to subtropical monsoons, with the flood risk typically high in its northern and central regions (Wang et al., 2011). As one of the most important eco-areas in the world, wetlands in the Dongting Lake Basin play the significant role in flood storage and regulation in the south-central area of the YRB (Wang et al., 2011). Hence, the dynamics of wetlands in the Dongting and Honghu Lake Basin have been studied by several researchers. Xing et al. (2018) and Huth et al. (2020) both monitored monthly surface water dynamics of Dongting Lake in 2016. The results indicated that the surface water area varied the most in April and August, the difference between maximum and minimum areas of wetlands in 2016 reached 1301 km^2 (Xing et al., 2018; Huth et al., 2020). The annual average water flow and water level dynamics of the Dongting Lake wetland ecosystem are 37% and 36%, respectively (Wang et al., 2022). Regarding the long-term variation of Dongting Lake wetlands, Guo et al. (2022) reported that the wetland area expanded by 66.43 km^2 during the wet season and shrank by 132.86 km^2 during the dry season between 2001 and

2020.

Although there's no single large freshwater lake in the Wanjiang Plain, a dense group of freshwater lakes is distributed along both banks of the Yangtze River, forming the Wanjiang Lake group in the middle and lower reaches of the YRB (Dong et al., 2022). In the Wanjiang Plain, annual precipitation and river runoff are concentrated between May and October. Lake shrinkage has been confirmed to increase flood risk by contributing to elevated warning water levels during this period, typically in Chaohu Lake, one of the five largest freshwater lakes in China and a flood-prone region with complex natural conditions (Sun et al., 2016; Dong et al., 2022). Apart from flood-prone regions in the YRB middle and lower reaches, the flood risk in the Sichuan Basin has been analyzed as well. The Sichuan Basin has low flood storage potential due to its extensive river and cropland areas, as well as the limited lake coverage. As a result, it has a relatively low capacity to mitigate flooding (Fu et al., 2013; Liu et al., 2017).

To sum up, previous studies illustrate that wetland variations play a significant role in the flood risk of different flood prone regions across the YRB. However, investigations into the long-term effects of wetlands on flood risk across the entire YRB based on the comprehensive wetland data are still lacking.

2.3 Assessing the past and future flood risks in the Yangtze River Basin

To evaluate and discuss the flood risk, and to improve the public's flood risk awareness as well as mitigating flood risks in the YRB under climate change, it is essential to conduct the integrated flood risk assessment that incorporating various flood risk factors with spatial and temporal dynamics (Wu et al., 2022; Zhang et al., 2020). Hence, several studies around the world focused on the flood risk assessment at the local, regional, and national scale. Examples include the Wadi Nu'man Basin of Saudi Arabia (Abdelkarim and Gaber, 2019), the YRB of China (Zhang et al., 2020), coastal regions of China (Sajjad, et al., 2020), urban regions in Sri Lanka (Weerasinghe et al., 2018), the United Arab Emirates (Abuzwidah et al., 2024), and

European countries (Thaler and Hartmann, 2016).

As a significant flood-prone region, the YRB has received an increasing attention in the flood risk assessment research. A number of flood risk assessments have been conducted across the YRB, focusing on typical lake basins such as the Poyang Lake Basin (Wu et al., 2022) and the Dongting Lake Basin (Wang et al., 2011), as well as flood-prone urban regions like Chongqing (Cai et al., 2021) and Wuhan (Fang et al., 2019). Zhang et al. (2020) conducted a large-scale flood risk assessment of the entire YRB for the years 1998, 2008, and 2016, which experienced major flood events. The flood risk assessment studies in the YRB focused not only on the past events. Peng and Li (2021) predicted the future flood risk until 2050 under the Coupled Model Intercomparison Project (CMIP6) shared socioeconomic pathways (SSP) and representative concentration pathway (RCP) climate change scenarios of the Yangtze River Economic Belt.

According to the United Nations Office for Disaster Risk Reduction, flood risk is identified as the product of hazard, vulnerability, and exposure (McGlade et al., 2019). Flood hazard usually refers to natural events or trends related to climate and their natural influences, while flood exposure refers to risk elements affected by floods, typically referring to human, buildings, property, and economic activities exposed in unfavored places and settings (Dou et al., 2018; Zou et al., 2013). Flood vulnerability is a more complex index than hazard and exposure, and it is the main construct in the flood risk assessment (Balica and Wright, 2010; Nasiri et al., 2016). The general concept of vulnerability refers to a condition shaped by physical, social, economic, and environmental factors that increase people's susceptibility to the impacts of hazards. It reflects the interaction among exposure, susceptibility, and resilience within each community during a hazardous event (Balica and Wright, 2010; UNDP, 2004). Therefore, the flood risk assessment is a multi-criteria analysis project that integrates the results of flood hazard, vulnerability, and exposure (Wu et al., 2022).

A number of approaches have been applied for the flood risk assessment, such as historical

disaster statistical method (Halgamuge and Nirmalathas, 2017; Youssef et al., 2015), scenario simulation analysis for future flood risk predictions (Alfieri et al., 2015; Cai et al., 2021; Gangrade et al., 2019), index system method (Christie et al., 2018), Set Pair Analysis (SPA) combined with variable fuzzy sets (VFS) model (Su et al., 2010; Zhang et al., 2011; Zou et al., 2013), deep learning mechanisms (Lai et al., 2011; Li et al., 2008; Yosri et al., 2024), and the GIS-based approach (Cai et al., 2021; Gigović et al., 2017a; Zhang et al., 2020). Each of these methods contains both advantages and disadvantages in the application of the flood risk assessment (Table 2).

Table 2.1: Advantages and disadvantages of the major flood risk assessment approaches.

Approaches	**Advantages**	**Disadvantages**
Historical disaster statistical method	Provides essential information for the long time series assessment. Refers to the disaster databases which have been categorized and contained enough details. (Zhang et al., 2020).	The limitation of data availability. The requirement of high amount of data. Differences in the ways of data recording. Most data collections are based on cities. Thus, it is hard to get the detailed spatial distribution of flood risks (Zhang et al., 2020).
Multi-Index analysis	Multiple indicators of flood risks can be considered comprehensively, and the contribution of each indicator can be analyzed accurately (Zhang et al., 2020).	The selection of assessment indicators varies depending on regional characteristics (Zhang et al., 2020).

Scenario simulation analysis	Make predictions for future flood risk assessment under different climate change scenarios (Gangrade et al., 2019).	The results are affected by analytic tools and the simulated data. Thus, the assessment accuracy contains uncertainties (Cai et al., 2019).
SPA-VFS model	Simple operation, easy computation, clear physical meaning as well as reasonable results. The model has been applied more frequently in multi-attribute assessment fields (Zou et al., 2013).	Uncertainties in the complicated flood disaster risk system under the fuzzy environment (Zou et al., 2013).
Deep learning mechanism	Complete information processing of networks through the interaction of neural cells with the high fault tolerance (Li et al., 2008; Lai et al., 2011).	The low generalization ability and reliability because it is easy to fall into over learning and local minimum dilemma during its learning process (Zou et al., 2013).
GIS-based approach	Handle the large amount of flood risk spatial data. Visualized results of flood risk spatial distribution maps. Analyze the flood risk in the large scale. The investigation process is rapid (Zhang et al., 2020).	Cannot be used alone, need to be applied with other flood risk assessment approaches (Zhang et al., 2020).

From Table 2.1, integrating the multi-index analysis with the GIS-based approach offers

advantages in handling large-scale datasets and incorporating comprehensive indicators into flood risk assessments with the greater accuracy. Therefore, given the large spatial scale and multiple indicators of the YRB flood risk assessment, the multi-index system method combined with the GIS-based approach is the most suitable selection to evaluate flood risks in the YRB. The GIS-based spatial multi-index approach has been widely applied in flood risk assessments of different basins worldwide, such as the Wadi Nu'man Basin in Saudi Arabia (Abdelkarim et al., 2019), the Tapi River Basin in India (Ramkar and Yadav, 2021), the Taihu Lake Basin (Yu et al., 2012), the Dongting Lake Basin (Wang et al., 2011), the Poyang Lake Basin (Wu et al., 2022), the Lijiang River Basin (Ziwei et al., 2023), and the entire YRB in China (Zhang et al., 2020). This approach has also been applied in the flood risk prediction worldwide by integrating the scenario simulation analysis, such as the Yangtze River Economic Belt of China (Peng and Li, 2021), the Pearl River Delta of China (Chen et al., 2021a), the Petite Nation River watershed, southern Quebec, Canada (Oubennaceur et al., 2021), and the United Arab Emirates (Abuzwidah et al., 2024).

Among the previous studies assessing the past and future multi-criteria flood risk covering the YRB, none incorporated the long-term variations of wetlands as one of indicators into the flood risk model. Instead, most included only river or drainage density, which represents a single wetland category. Given the diverse effects of different wetland categories on flood risk in the YRB, as discussed in Section 2.2, an improved multi-criteria flood risk assessment model needs to be developed with wetland inputs.

Chapter 3 Research methodology

This chapter provides a general overview of research methods used in the thesis, which are used to address the research questions and achieve the research objectives identified in Chapter 1. Detailed descriptions of these methods are described in Chapters 4, 5, and 6, correspondingly.

3.1 Machine learning algorithm

Machine learning is the technology for developing computer algorithms that emulate human intelligence (El Naqa and Murphy, 2015). The inception of machine learning can be traced to the 17th century, followed by the development of the perceptron as one of the early neural network architectures in 1958 (El Naqa and Murphy, 2015; Ifrah, 2000). Google Earth Engine (GEE) is a cloud-based geo-computation open source platform for machine learning algorithms, offering a high volume of Earth Observational Data such as Landsat and Sentinel Data (Gorelick et al., 2017). In recent years, the combination of machine learning algorithms and GEE has gained popularity in various satellite data applications, including LULC classification, deforestation, drought monitoring, crop monitoring, hydrology, land cover mapping, and environmental protection (Belgiu and Drăguţ, 2016; Pokhariya et al., 2023). Machine learning can be categorized into supervised, unsupervised, and semi-supervised algorithms based on the nature of data labeling (Singh et al., 2016). Supervised machine learning algorithms are commonly used as the classifier for LULC classification (Belgiu and Drăguţ, 2016; Singh et al., 2016). There are several supervised machine learning classifiers, including parameter classifiers like Maximum Likelihood Classifier (MLC) (Liu et al., 2011) and Naïve Bayes (NB) (Singh et al., 2016), and non-parametric classifiers, such as Random Forest (RF) (Belgiu and Drăguţ, 2016), Support Vector Machines (SVM) (Mountrakis et al., 2011), Classification and Regression Tree (CART) (Razi and Athappilly, 2005), and Artificial Neural Network (ANN) (Mas and Flores, 2008). MCL and NB deliver excellent and fast results when training unimodal data, but they have limitations when dealing with multimodal input datasets that involve interactions (Liu et al., 2011; Singh et al., 2016). CART, SVM, RF, and ANN have become more popular than parameter classifiers for classifying remotely

sensed data due to the advantage of requiring no assumptions regarding frequency distribution (Belgiu and Drăguţ, 2016).

SVM is well-known in the field of machine learning and has been successfully applied to a wide range of remote sensing image classifications with the high accuracy (Castillo et al., 2008; Chowdhury, 2024; Ghosh and Joshi, 2014; Huang and Zhang, 2010). It utilizes classification and regression to identify the optimal hyperplane that separates the data based on a given sample (Chowdhury, 2024). ANN is a supervised classifier belonging to the deep learning algorithm. It contains a large number of hidden layers compared to traditional algorithms (Alshari et al., 2023). Generally, ANN is effective in remote sensing image classification, but neural networks are less sensitive to noisy sample data than other algorithms (Sidike et al., 2018; Waqas et al., 2023). CART models employ tree-building algorithms, which comprise a set of split conditions that enable classifications (Razi and Athappilly, 2005). The noticeable advantage of decision-tree-based models, such as CART, is that they are scalable to large regions than neural networks (Razi and Athappilly, 2005). The RF classifier is an ensemble classifier that utilizes a set of CARTs to generate multiple predictors, aggregating the plurality of votes derived from these predictors to make a final decision (Chowdhury, 2024). RF has been widely used in remote sensing studies currently due to its high classification accuracy (Belgiu and Drăguţ, 2016; Chowdhury, 2024; Ge et al., 2020; Pokhariya et al., 2023). Chapter 4 of this thesis compares the wetland classification accuracy among CART, SVM, and RF in the representative regions of the YRB and finds that RF achieves the highest classification accuracy across all the representative regions, which is selected as the algorithm for the long-term wetland classification in the YRB. The detailed comparison process is presented in Section 4.2.4, Chapter 4.

3.2 GIS-based multi-criteria flood risk assessment model

Geographical Information System (GIS) is a computer-based technology designed to capture, store, manipulate, analyze, and display diverse sets of spatial or georeferenced data (Huabin

et al., 2005). Nowadays, the risk analysis of natural disasters is unimaginable without the support of GIS (Gigović et al., 2017a). Natural disasters are multidimensional phenomena with a spatial dimension, making GIS very applicable for analyzing landslide hazards, flood risks, and the potential suitability for infrastructure construction and urban planning due to its powerful geostatistical tools to manage the large volume of spatial data (Abuzwidah et al., 2024; Bathrellos et al., 2012; Cai et al., 2021; Huabin et al., 2005).

To address the shortcomings of GIS in the decision-making process involving multiple criteria, it is necessary to integrate tools for multi-criteria decision-making with GIS (Gigović et al., 2017a). Multi-criteria analysis is a framework for ranking or scoring the overall performance of decision options across multiple objectives from various scientific fields (Wang et al., 2011). The input of the multi-criteria analysis model is a set of grouped, standardized, and weighted maps with spatial representation of the criteria. The output is one or more composite index maps (Wang et al., 2011). In recent decades, the application of multi-criteria or multi-index GIS-based models has been successful in various assessments, as it enables greater flexibility and accuracy in decision-making (Gigović et al., 2017b; Malczewski, 2006; Rahmati et al., 2016; Wang et al., 2011; Zhang et al., 2020). Approaches to determine the indicator's weight include objective and subjective methods, such as Technique for Order of Preference by Similarity to Ideal Solution (TOPSIS) and Simple Additive Weighting (SAW) (Meshram, et al., 2020), the analytic hierarchy process (AHP) and fuzzy AHP (Roy et al., 2021a;Yang et al., 2013), the entropy weight method (Khosravi, et al., 2016), and principal component analysis (Nandi et al., 2016). Several studies show that the analytic hierarchy process (AHP) is the most popular method with the high accuracy and cost-effectiveness (Abuzwidah et al., 2024; Gigović et al., 2017a; Lyu et al., 2018; Ramkar and Yadav, 2021; Zhang et al., 2020; Ziwei et al., 2023). AHP is a flexible and practical multi-criteria decision-making method that quickly qualifies qualitative problems using simple principles and a rigorous mathematical basis (Zhang et al., 2020; Ziwei et al., 2023), proposed by Saaty (1977). An improved GIS-based multi-index flood risk assessment model incorporating wetlands is developed in Chapter 5 and applied in Chapter 6

of this thesis, along with a detailed explanation of the framework. The model investigates the long-term wetland effects on the flood risk from 1984 to 2021 and predicts the future flood risk incorporating wetland effects under climatic and socio-economic scenarios by 2100 in the YRB.

3.3 Causality inference algorithm

Causal inference is the process of determining whether a specific relationship between variables is directly causal rather than merely correlational (Guo et al., 2020). It involves analyzing the effects of actions, interventions, or natural occurrences on outcomes (Nogueira et al., 2022). The application of causal inference is significant across various scientific domains, including statistics, computer science, education, public policy, economics, and earth and environmental science (Massmann et al., 2021; Nogueira et al., 2022; Runge et al., 2023). A robust method for inferring causality was first developed in the early 20th century by mitigating confounding influences through randomized experiments, which is the Neyman-Rubin potential-outcome framework (Rubin, 2005; Pearl, 2010). This framework introduces the concept of potential outcomes from different treatment states within the same unit (Pearl, 2010). Nowadays, with the development of computational power, causal effects can be quantified by combining domain knowledge, machine learning models, and observational or interventional datasets (Runge et al., 2019a; Runge et al., 2023). Several causal discovery algorithms have been developed, including the Peter Clark (PC) algorithm (Spirtes and Glymour, 1991), the linear non-Gaussian model (LiNGAM) (Shimizu et al., 2006), the Convergent Cross Mapping (CCM) (Sugihara et al., 2012), and the Peter Clark Momentary Conditional Independence (PCMCI) algorithm (Runge et al., 2019b).

In this thesis, the PCMCI algorithm is used to determine the causal relations between the YRB flood risk indicators and the flood risk area under wetland effects. The PC algorithm was applied to analyze the probability of power outage caused by natural disasters in the research of Chen et al. (2024). The PCMCI algorithm is further developed by combining the PC algorithm with the Momentary Conditional Independence (MCI) test (Runge, 2018).

Further details about using the PCMCI algorithm are provided in Section 5.2.3, Chapter 5.

Chapter 4 A long-term (1984-2021) wetland classification dataset for the Yangtze River Basin from continuous Landsat image collections

Highlights:

- We create a long-term wetland classification dataset in the Yangtze River Basin.
- The total wetland area is larger in 2021 compared with the starting year of 1984.
- Man-made wetlands increase constantly but natural wetlands fluctuate over years.
- The change of aquaculture ponds and inland marsh are the largest.
- Human activities are more dominant than natural driving forces of wetland changes.

This chapter is a reformatted version of a manuscript published in the *Total Environment Advances*, which is available at https://doi.org/10.1016/j.teadva.2024.200111. The LTWCD_YRB classification maps of YRB downstream, middle stream and upstream with 30m resolution between 1984 and 2021 are available in the figshare repository in the Geotiff format: https://doi.org/10.6084/m9.figshare.21859920.v1. They are provided in the ESPG:4326 (WGS_1984) spatial reference system. The maps can be visualized in ArcGIS, QGIS, or other similar software. JavaScript codes on the GEE platform to process Landsat images, implement machine learning method and generate wetland classification maps are available: https://doi.org/10.6084/m9.figshare.21859854.v1.

4.1 Introduction

Wetlands are among the most productive ecosystems that serve as the transition between land and water with a variety of ecological and economic benefits (Liang et al., 2020). However, in recent decades, wetlands worldwide have experienced dramatic loss and degradation caused by climate change and human activities (Asselen et al., 2013). The extensive wetlands across the Yangtze River Basin (YRB) in China have been particularly affected, experiencing a striking loss (Mao et al., 2020; Xu et al., 2019b), which accounts for nearly 40% of the national wetlands (Finlayson et al., 2018). The variation of wetlands in the YRB is complex due to several driving forces including climate change, rapid urbanization along the Yangtze River Economic Belt, dam construction, and agricultural and livestock activities (Xu et al., 2019b; Zheng et al., 2020). According to the latest wetland classification system and spatial distribution map in China, wetlands along the YRB include nearly all types of wetlands in China (Mao et al., 2020). Different reaches of the YRB are covered with various categories of wetlands: Swamps and marshes distributed at the source and estuary regions of the YRB, and waterbody wetlands mostly centralized at middle-lower reaches (Mao et al., 2020). Overall, wetlands remained stable at the source of YRB, expanded at the middle reaches, and shrank at the lower reaches of YRB in the first 15 years of the 21st century (Xu et al., 2019b). Wetlands management and protection have become a significant issue in the initiative of Yangtze River Conservation proposed by the Chinese government in 2016 (Zheng et al., 2020). The study on the long-term historical variations of all the wetland categories will provide evidence-informed policymaking for stakeholders to formulate more definite wetland conservation policies in the YRB. However, there are currently no comprehensive wetland datasets in the YRB to support this research.

Several wetland-related datasets have been generated in previous studies (e.g., Pekel et al., 2016; Lu et al., 2019; Li et al., 2020; Mao et al., 2020). The Chinese Academy of Science Wetland (CAS_Wetland) Dataset contains the most comprehensive wetland categories in China at the 30m spatial resolution by using the Landsat 8 Operational Land Imager (OLI)

(Mao et al., 2020). In this classification system, wetlands are grouped into three broad categories and 14 sub-categories: 1) Inland wetland (Inland swamp, Inland marsh, lake, river); 2) Coastal wetland (coastal swamp, coastal marsh, lagoon, estuary water, tidal flat, shallow marine water); and 3) Human-made wetland: (reservoir/pond, channel, salt pan, aquaculture pond) (Mao et al., 2020). The limitation of this dataset is that it only demonstrates wetlands information in 2015 instead of a longer period. The same issue occurred in the High Spatial-temporal Water Body Dataset in China (HSWDC) launched in 2016, even though it has a higher spatial resolution at 10m (Li et al., 2020). The representative National waterbody datasets with longer time series covered the YRB, including the Landsat-derived annual land cover product of China (CLCD) (1980-2019)，the time series of Inland Surface Water Dataset in China (ISWDC) (2000-2016) (Yang and Huang, 2021; Lu et al., 2019), and the Global Surface Water Explorer (GSWE) maximum water extent map (1984-2021), generated by using Landsat 5, 7, and 8 images in the YRB (Pekel et al., 2016).

The overall limitation of the above datasets (except the CAS_Wetland dataset) is that the wetland data is just a by-product that needs to be derived from the whole dataset. Most importantly, there is no detailed wetland classification in these datasets. The CAS_Wetland dataset contains comprehensive wetland categories but only demonstrates wetlands information in one year. Therefore, the scarcity of long-term time series of wetland distribution and classification datasets in the YRB has resulted in severe limitations on the specific policymaking and implementation for the YRB wetlands conservation. Meanwhile, such deficiency in the dataset has generated a barrier to evaluating the long-term variations in different categories of YRB wetlands for their habitat health, carbon storage, greenhouse gas emission, and ecosystem service capacity (Mei et al., 2016; Xu et al., 2008; Zhou and Xia, 2020).

To support evidence-informed policymaking for wetland management and protection in the YRB, this study aims to explore annual and seasonal variations of various wetland categories by creating a long-term time series (1984-2021) wetland classification dataset with

comprehensive wetland categories for the YRB. Additionally, this study identifies potential driving forces of variations in different wetland categories by analyzing their spatial shifts across the YRB in the representative regions.

4.2 Materials and Methods

4.2.1 Study area

The Yangtze River (YR) (Figure 4.1) is the third longest river in the world and the longest one in China, stretching over 6,300 km. The YRB is located between 24°27' to 35° 54' N and 93°33' to 122°19' E, with a long and narrow shape running from west to east and a shorter extent from north to south (Zheng et al., 2021). The topography of the YRB is high in the west and low in the east. The river originates in the Tanggula Mountains of the Tibetan Plateau, with the flowing direction from the west to the east of the country and finally flows to the East China Sea at Chongming Island near Shanghai (Zhang et al., 2020). The YRB covers 11 provinces, autonomous regions, and municipalities including Qinghai, Tibet, Sichuan, Yunnan, Chongqing, Hubei, Hunan, Jiangxi, Anhui, Jiangsu, and Shanghai, with a population of approximately 440 million (nearly one-third of China's population). The YRB covers 18.75% of China's total area, which reaching 1.8 million km^2 (Zhang et al., 2020). Wetlands account for 40% of the national wetlands in China, with hundreds of tributaries and lakes (Finlayson et al., 2018).

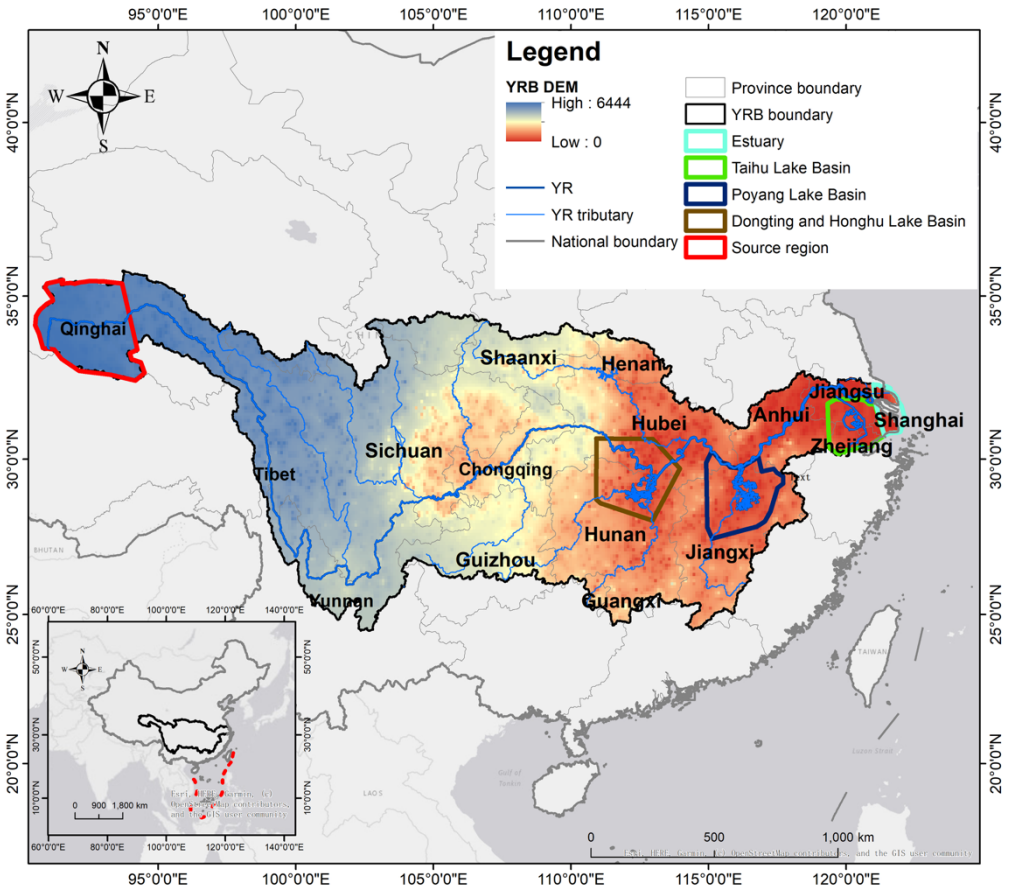

Figure 4.1: The location, hydrographical and topographical information of the Yangtze River Basin.

4.2.2 Data

Regarding muti-spectral remote sensing images, the surface reflectance products were derived from Landsat 5 Thematic Mapper (TM) (1984-1999), Landsat 7 Enhanced Thematic Mapper Plus (ETM+) (2000-2013) and Landsat 8 Operational Land Imager (OLI) (2014-2021) images, all with a 30m resolution from January 1984 to December 2021. The selected spectral bands were 2, 3, 4, 5, 6, and 7 (Gorelick et al., 2017). The starting year of 1984 was selected because it marked the proposal of the Yangtze River Economic Belt, an economic region with the Yangtze River as its axis, covering more than 40 cities, which led to increased impacts on the wetlands due to rapid economic growth (Zhou et al., 2020). The corresponding Normalized Difference Vegetation Index (NDVI), Normalized Difference Water Index (NDWI), and Normalized Difference Snow Index (NDSI) were selected as the datasets for

this research. The satellite image interpretation represents the current situation of each wetland type after atmospheric correction (surface reflectance products have been atmospherically corrected on the Google Earth Engine), cloud filtering, mean compositing (to obtain the average image from the image collection and image cropping (Dang et al., 2020).

4.2.3 Wetland classification system

The Ramsar Convention on Wetlands defines the traditional global wetland classification system as "... areas of marsh, fen, peatland, and water, whether natural or artificial, permanent or temporary, and whether water is flowing, fresh, brackish or salty, including areas of marine water the depth of which at low tide does not exceed 6 m" (Ramsar Convention Bureau 2001). The latest and most comprehensive wetlands classification system in China, known as CAS_Wetlands, refers to the Ramsar definition and the wetland mapping history of China (Mao et al., 2020). This remote sensing wetland classification system incorporates the advantages of moderate-resolution images, providing high acceptability and efficient, practical use for ecosystem management (Mao et al., 2020). The YRB study region covers extremely complex geographic and hydrological conditions, thus contributing to a wide range of wetland categories (Cui et al., 2018). There are two broad categories and nine sub-categories of wetlands referring to the CAS_Wetland in the YRB (Table 4.1) (Mao et al., 2020). Paddy fields and floodplains are excluded from this wetland classification system. Paddy fields are more appropriate to be defined as farmland, while floodplains are not considered an individual wetland category because they are defined as either inland marshes or rivers during the wet season (Mao et al., 2020).

Table 4.1: The wetland classification system adopted in this study (Mao et al., 2020).

Category	Sub-category	Description
Natural wetland	Inland marsh	Natural wetland with dominant herbaceous vegetation in inland areas.
	Lake	Natural polygon waterbody with flowing water.
	River	Natural linear waterbody with flowing water.
	Coastal marsh	Natural wetland with dominant herbaceous vegetation in coastal areas.
	Estuary water	Natural waterbody with flowing water from the boundary of inland areas to coastline.
	Tidal flat	The inter-tidal flat with no or very low vegetation coverage.
Human made wetland	Reservoir	Artificial polygon waterbody with standing water generating with obvious dam.
	Aquaculture pond	Polygon waterbody used for aquaculture.
	Canal	Artificial linear waterbody with flowing water and straight boundary.

4.2.4 Machine learning classifiers selection

Google Earth Engine (GEE) is a representative cloud-based geo-computation platform for machine learning algorithms, offering a centralized and standard framework of Earth Observation data (Gorelick et al., 2017). GEE has been leveraged in several remote sensing studies (Mayer et al., 2021, Tassi et al., 2020), and this study will use the GEE platform for collecting samples and training models.

Machine learning classifiers can be broadly categorized into supervised parametric classifiers, such as the Maximum Likelihood Classifier (MLC) and Naïve Bayes, and non-parametric classifiers, including Random Forest (RF), Support Vector Machines (SVM), Classification and Regression Tree (CART), and Artificial Neural Network (ANN) (Belgiu and Drăgut,

2016; Liu et al., 2011; Mas and Flores, 2007). Non-parametric classifiers are preferred for classifying remote sensing data because they do not impose assumptions on data distribution (Belgiu and Drăgut, 2016). On the other hand, parametric classifiers have limitations regarding normal data distribution and are not suitable for this study with multi-modal input data (Liu et al., 2011).

Several previous studies have compared RF with other machine learning classifiers in terms of classification accuracy, training time, and training stability when study regions or training samples change (Chan and Paelinckx, 2008; Gislason et al., 2006; Vetrivel et al., 2015). RF has been shown to outperform Binary Hierarchical Classifier (BHC), Linear Discriminant Analysis (LDA), and ANN in terms of classification accuracy (Chan and Paelinckx, 2008; Ham et al., 2005; Shang and Chisholm, 2014). Although Ghosh and Joshi (2014) stated that SVM classification performs slightly better than RF in Object-based Image Analysis (OBIA), RF is less sensitive to feature selection, making it more user-friendly (Li et al., 2015; Vetrivel et al., 2015). Additionally, RF is computationally efficient, capable of handling high-dimensional and multicollinear data, reducing the risk of overfitting, and ensuring robust results regardless of the training data quality (Belgiu and Drăgut，2016; Hemmerling et al., 2021; Mei et al., 2016; Rodriguez-Galiano et al., 2012). In summary, RF achieves better classification results compared to other machine learning classifiers, especially with hyper-spectral or multi-source data, and it is faster and more stable than SVM and other ensemble classifiers (Belgiu and Drăgut，2016).

Therefore, RF is widely used in complex remote sensing image classification involving large-scale, multiple categories, and multiple features (Li et al., 2015; Rodriguez-Galiano et al., 2012; Talukdar et al., 2020). Corcoran et al., (2013) evaluated that wetland classification in northern Minnesota achieved the best results based on the RF classifier with input Landsat TM data. Considering the large spatial scale of the YRB, and the time cost of training and testing the monthly satellite images in the whole 37 years of 18 divided region patches, the deep learning algorithms are not considered in this study due to the disadvantages of

time-consuming when training of deep learning models (Jamali et al., 2021). In the selected representative regions among the YRB, the comparison results of classification accuracy for RF, SVM, and CART were shown in Table 4.2, and RF is selected as the classifier for this study because of its highest classification accuracy.

Table 4.2: The classification accuracy of three machine learning classifiers in 5 representative regions along the YRB.

Machine learning classifier	**Accuracy**				
	Estuary	TLB	PLB	DLB	Source
RF	95.80%	90.50%	90.30%	92.90%	93.70%
SVM	92.30%	89.80%	85.40%	92.70%	81.80%
CART	92.80%	86.30%	88.00%	90.10%	89.50%

RF consists of a large number of decision trees generated randomly and automatically (Belgiu and Drăgu, 2016). Each decision tree is independently produced without any pruning and each node is split using a number of features defined by users (Belgiu and Drăgut, 2016; Olofsson et al., 2014). The final classification result is determined by averaging the class assignment probabilities generated by all the decision trees in the ensemble. When evaluating a new unlabelled input data, it is assessed against all the decision trees, and each tree contributes its vote for a class membership. The class with the highest number of votes is ultimately selected as the final classification result (Belgiu and Drăgut，2016). The training dataset is divided into two parts: 80% for bootstrap sampling for each decision tree and 20% for testing to evaluate the RF model (Cui et al., 2018). The computing time required to establish the RF classification model is:

$$T\sqrt{MNlog(N)} \tag{4.1}$$

Where T is the number of trees, M is the number of variables used in each split, and N is the

number of training samples (Belgiu and Drăgut，2016). *T* is a configurable parameter in RF and affects the classification accuracy. In this study, the number of trees was 30 for training each image patch.

4.2.5 Machine learning structure

The machine learning method is divided into 1) Landsat and sample labeling datasets; 2) Input data preparation; and 3) Model training and accuracy assessment (Figure 4.2).

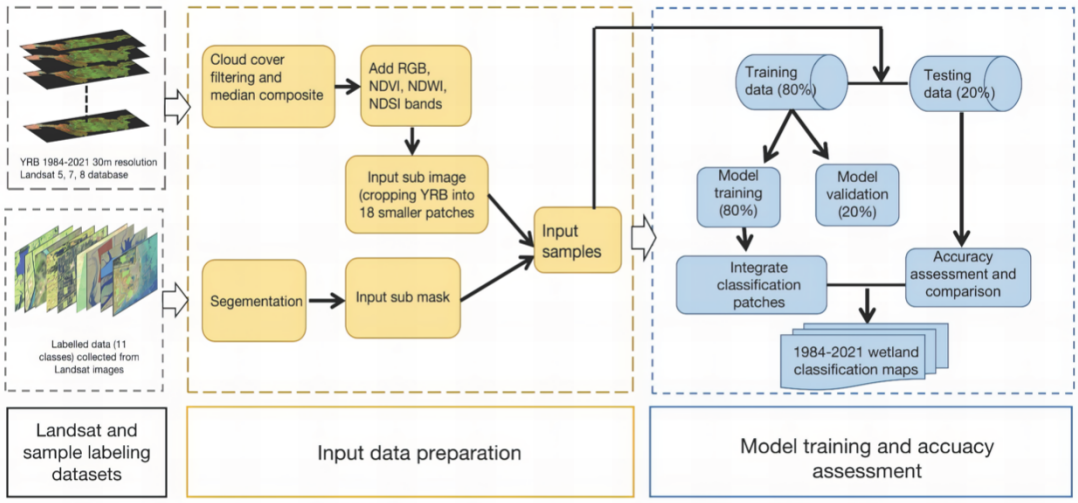

Figure 4.2: The structure of machine learning method for wetland classification.

4.2.5.1 Landsat and sample labelling datasets

Sample labeling for training and testing generally proceeds on Landsat images by the visual distinguishing combined with references from the published literature and datasets (e.g. the CAS_Wetland dataset, and the China Land Cover dataset from the Resource and Environment Science and Data Center) (Mao et al., 2020, Yang and Huang, 2021). We also used the GEE platform to calculate different indices of the classification features, including NDVI, NDWI and NDSI, which characterize vegetation canopy, water bodies and snow coverage, respectively (Feng et al., 2022). The formulas are shown as below:

$$NDVI = (NIR - RED)/(NIR + RED) \tag{4.2}$$

$$NDWI = (GREEN - NIR)/(GREEN + NIR) \tag{4.3}$$

$$NDSI = (GREEN - SWIR)/(GREEN + SWIR) \quad (4.4)$$

NIR, SWIR, RED and GREEN are reflectance values from the near-infrared, short-wave infrared, red and green bands of the Landsat imagery, respectively (Feng et al., 2022). The examples with nine different wetland categories and labelled samples are shown in Figure 4.3. For the wetland categories with clear boundaries, such as lake, river, reservoir, canal, and aquaculture pond, samples need to be labelled along the boundary; the wetland categories without the boundary like the inland marsh, tidal flat, estuary water, and coastal marsh, just drawing squares for samples on Landsat images.

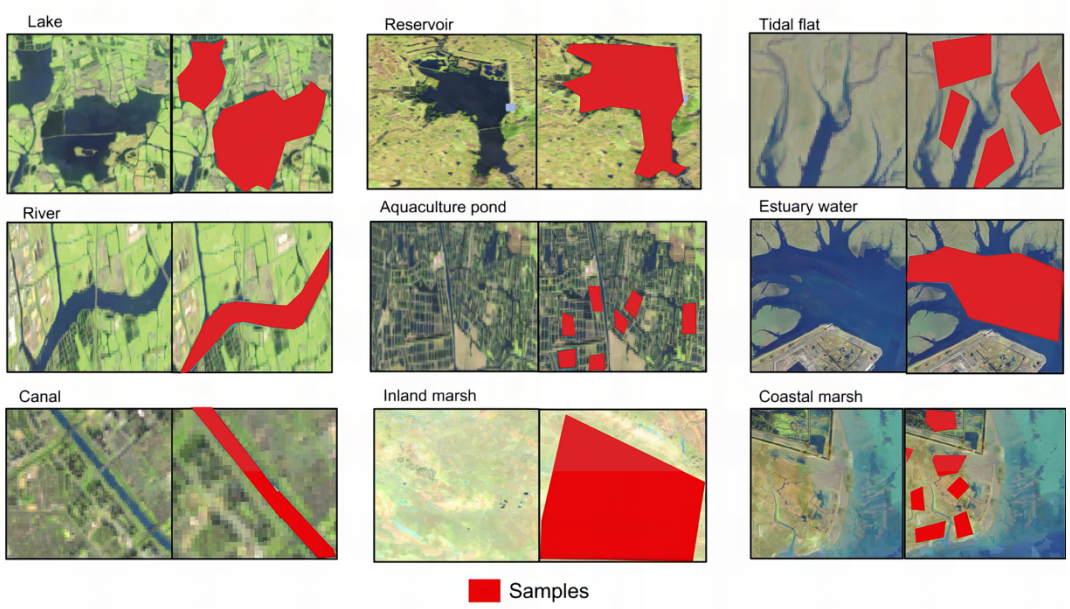

Figure 4.3: The example of sample zoning and labeling on the Landsat 8 RGB composite images of wetland categories.

4.2.5.2 Input data preparation

The preparation of input data involved several steps. Firstly, Landsat imagery of the YRB was cropped into 18 sub-images following cloud cover filtering and mean compositing. Concurrently, corresponding sub-masks of labelled samples were generated through segmentation. Then, the labelled samples were utilized for RF classification, which was

allocated 80% for training and validation. the remaining 20% for testing. Once the model training was finalized, the classification maps of the sub-images were integrated to obtain the final wetland classification maps for the YRB.

4.2.5.3 Validation

Several wetland classification studies have used the existing datasets as reference sources for validation to substitute for ground-truth field data, especially in the large-scale wetland classification. For example, Martínez et al. (2021) assessed the classification accuracy of all the coastal wetlands in Estonia by measuring the agreement between classified values derived from previous studies and the training samples used in their analyses. Huo and Niu (2024) validated the wetland map of the Yellow River Basin by comparing it with the existing products including the CAS_Wetlands (Mao et al., 2020). Amani et al. (2019) used the visual comparison against previous wetland classification maps to assess the wetland classification accuracy for entire Canada. Moreover, due to the 37-year temporal span of the LTWCD_YRB, no corresponding long-term reference dataset with the consistent wetland categories is available for validation. Therefore, the LTWCD_YRB wetland classification dataset is validated through the visual comparison with the validation samples for each wetland category derived from the 30m resolution CAS_Wetlands dataset developed by Mao et al. (2020). The CAS_Wetlands is the only existing wetland dataset with the same spatial resolution and consistent classification system as the LTWCD_YRB.

The CAS_Wetlands dataset contains the precise ground-truth field data in the single year of 2015 derived from field investigations and public databases associated with the national projects funded by the Ministry of Science and Technology of China (Mao et al., 2020). There are totally 5022 ground-truth field validation samples representing all the wetland categories, with their locations recorded using the Global Positioning System (GPS) with the positional error of less than 2 m. In addition, the unmanned aerial vehicles (UAVs) equipped with real-time kinematic GPS and supported by the high-resolution satellite images were used to validate wetlands that were inaccessible on the ground. The overall accuracy of the

CAS_Wetlands dataset reached 95%. Given its rigorous validation process and high accuracy, the CAS_Wetlands dataset is considered as the suitable reference for validating the LTWCD_YRB. The validated samples were randomly selected from all the samples of the LTWCD_YRB in 2015 and visually compared with the corresponding wetland categories in the CAS_Wetlands. In addition, a confusion matrix was generated to assess the classification accuracy of the LTWCD_YRB based on this indirect validation method, including the overall accuracy, producer's accuracy, and user's accuracy.

In this study, confusion matrices were constructed in the GEE platform to evaluate the classification accuracy. The confusion matrix is a commonly used method for assessing accuracy in land use and land cover (LULC) studies (Feng et al., 2022). It summarizes the number of samples correctly and incorrectly classified for each class, thereby quantifying the agreement and differences between the classification result and the reference LULC of the study region (Olofsson et al., 2014). The matrix provides quantitative accuracy metrics, including the overall accuracy (OA), producer's accuracy (PA), user's accuracy (UA), and Kappa coefficient. The OA is a metric for the general evaluation, which is calculated through the sum of all the correctly classified sites divided by the total of number of reference site, but it only provides the basic accuracy information for the map user and producer (Nehzak, et al., 2022). The PA and UA are used to measure the quality of the classification for each wetland category from the perspectives of map producer and map user, respectively. The PA is the map accuracy from the point of view of the map producer. It reflects the probability that the real features on the ground of a given class are correctly classified on the map, therefore indicating how well the actual wetlands are captured. The PA is calculated as the number of validated samples classified accurately divided by the total number of validated samples for that class. The UA is the accuracy from the point of view of a map user. It reflects the probability that a given class on the map truly belongs to that class on the ground, indicating the reliability of the classified wetlands. The UA is calculated by taking the total number of the correct classifications for a particular class divided by the total classified samples for that class. At last, the Kappa coefficient was applied to assess the difference between the observed

wetland classification accuracy and that expected by random chance (Tselka et al., 2023)

4.3 Results

4.3.1 Classification accuracy

The validation results were demonstrated in Table 4.3. It indicates that the LTWCD_YRB dataset achieves the overall accuracy of 85%. The natural wetland categories demonstrated higher classification accuracy in terms of both UA and PA compared to the human-made wetland categories. Among all the wetland categories, estuary water attained the highest UA at 98%, followed closely by lakes at 95%, which means these two categories demonstrated the highest agreement between the classification result and the actual wetland class. In contrast, the UA of canals and aquaculture ponds was relatively lower at 61% and 67%, respectively. This can be attributed to the smaller area occupied by these wetland categories compared to others, as well as the tendency for canals to be confused with lakes and aquaculture ponds with other water bodies.

Table 4.3: Wetland category accuracy of the LTWCD_YRB.

Category	**Sub-category**	**Sample testing number**	**PA**	**UA**
Natural wetland	Lake	8362	98%	95%
	River	15762	81%	75%
	Inland marsh	2331	86%	70%
	Coastal marsh	407	93%	89%
	Tidal flat	2035	85%	82%
	Estuary water	629	99%	98%
	Total	29526	90%	85%
Human-made wetland	Reservoir	9398	92%	87%
	Aquaculture pond	6364	79%	67%
	Canal	4588	94%	61%
	Total	20350	88%	72%

Summary	49876	Overall accuracy	Kappa coefficient
		85%	0.84

Figure 4.4 illustrates the validation samples derived from the LTWCD_YRB and CAS_Wetlands datasets, together with the corresponding classification results in representative regions. This figure confirms that wetland categories with lower classification accuracy in Table 4.3, such as canals, aquaculture ponds, inland marshes, and tidal flats, exhibit the greater sample inconsistency between the LTWCD_YRB and CAS_Wetlands datasets than other wetland categories, particularly in the coastal regions of Shanghai.

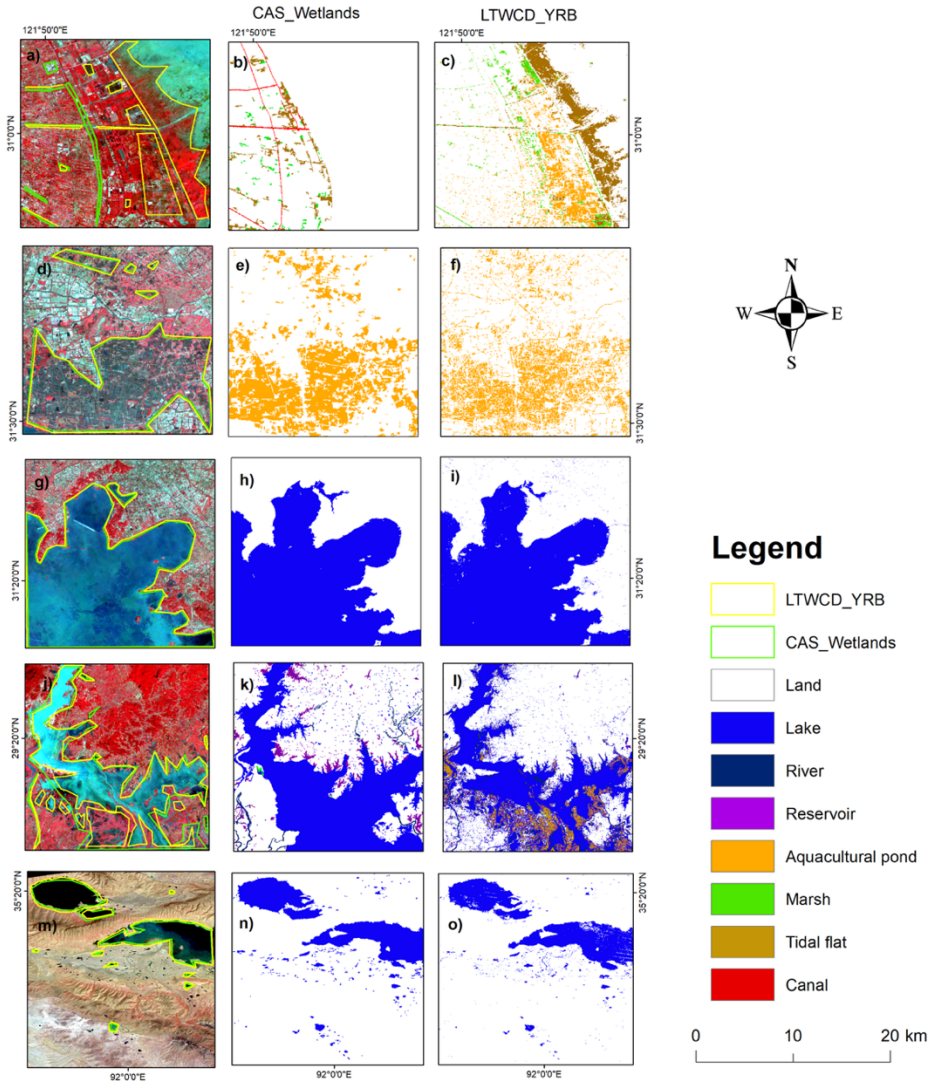

Figure 4.4. The comparison of typical subsets between the LTWCD_YRB and

CAS_Wetlands. a)-c): Coastal wetlands in Shanghai; d)-f): aquacultural ponds near Yangcheng Lake in the TLB; g)-i): a part of Taihu Lake; j)-l): wetlands in the PLB; and m)-o): alpine lakes in the YRB source region.

4.3.2 Classification results

Table 4.4 presents the annual average change of the nine wetland categories in the YRB between 1984 and 2021. Comparing the area in 1984 with 2021, the aquaculture pond experienced the most significant expansion and increased by a total of 4987 km^2 across the YRB. The highest expansion rate occurred from 2000 to 2010, with an increase rate of 199.5 km^2 per year. The area of inland marsh also increased by 2284 km^2, although it exhibited with a fluctuation trend. Particularly, in the 2010-2021 period, the inland marsh shrunk by 8630 km^2 at a decrease rate of 784.5 km^2 per year. Lake and estuary water are the only two wetland categories with a smaller area in 2021 than those in 1984, with lake area decreasing more. Human-made wetlands in the YRB exhibited a consistently increasing trend from 1984 to 2021 (161.7 km^2 per year), while natural wetland areas displayed more extensive fluctuations (as shown in Figure 4.5). Overall, the total wetland area in the YRB was larger in 2021 compared to 1984, with the most substantial variation from 2000 to 2010.

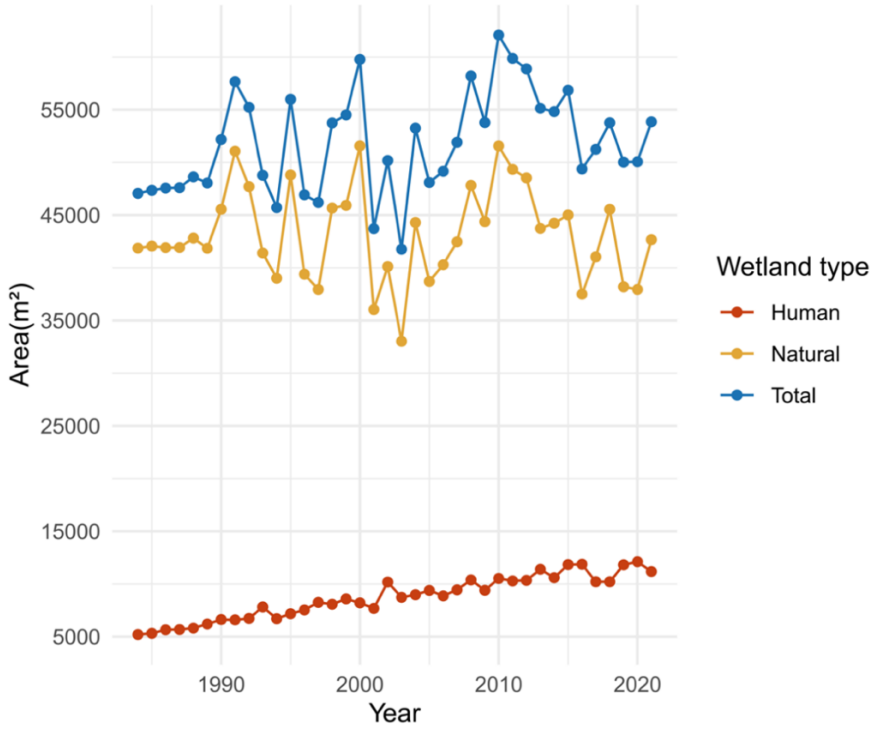

Figure 4.5: The long-term variations of natural, human, and total wetland areas in the YRB between 1984 and 2021.

Table 4.4: Decaded wetland changes in the YRB between 1984 and 2021.

Classes	**Area in 1984**	**Area in 2021**	**Area change (km^2)**			
	(km^2)	**(km^2)**	1984-1990	1990-2000	2000-2010	2010-2021
Lake	16819	15685	-1238	+2540	-3912	+1476
River	11792	11981	+1656	-1045	+49	-471
Canal	240	277	+59	-26	-82	+86
Aquaculture pond	1275	6262	+1180	+1575	+1995	+237
Reservoir	3682	4640	+189	+35	+436	+339
Coastal marsh	219	314	+41	-46	+1	+99
Inland marsh	9361	11645	+3148	+6073	+1693	-8360
Tidal flat	410	533	+252	-26	-381	+278
Estuary water	3256	2156	-173	-31	-267	-278

Figures 4.6-4.10 show the mapping of classification results and spatial variations in the five representative regions across the YRB between 1984 and 2021. Each region includes the starting year (1984), the ending year (2021), and two more representative years (2001 and 2011) of classification results. All other figures for the rest years are available in the Figshare repository. The YRB estuary region (Figure 4.6) is located near the East China Sea. This region primarily consists of coastal wetlands such as coastal marsh, tidal flats, and estuary water. The figure reveals notable changes over time. In the Yaowang Harbor area, the aquaculture pond expanded, displacing the tidal flat in 2011 and 2021, which was caused by the development of local fish farming industries and related infrastructures. Additionally, the tidal flat and coastal marsh on the Dongtan Nature Reserve of Chongming Island exhibited a shrinking trend, while they expanded on the reclaimed Changxing and Hengsha Islands. Moreover, the disappearance of coastal wetlands along the Yangtze River Delta (YRD) is significant in 2011 and 2021, indicating substantial changes in the region's wetland composition. Natural driving forces including sea-level rise and slower rate of sedimentation play significant roles in the coastal wetlands degradation of Chongming Island and the YRD.

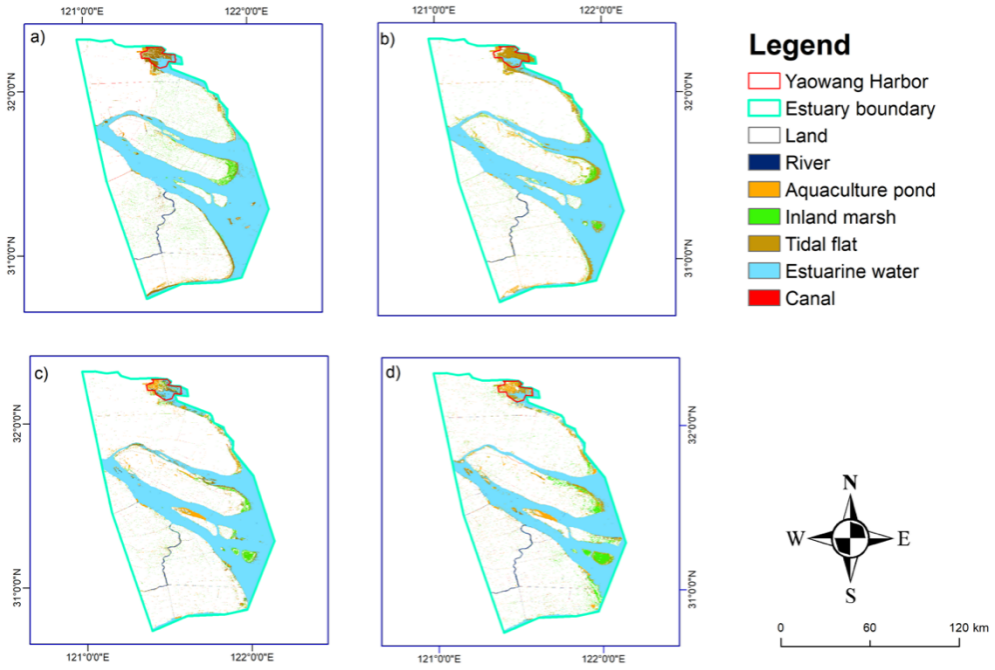

Figure 4.6: The wetland classification of a) 1984 b) 2001 c) 2011, and d) 2021 at the YRB estuary.

The TLB is in the YRB downstream, as shown in Figure 4.7. The major variation of Taihu Lake is shown on the southeast corner. Among the wetland categories, the aquaculture pond exhibits the most distinct variation. It is primarily distributed around the eastern corner of Taihu Lake and the northern area of Yangcheng Lake, as well as other smaller lakes within the TLB. Notably, there was a significant expansion of the aquaculture pond between 2001 and 2011. However, by 2021, the area covered by the aquaculture pond had contracted brought by the implication of fish farming banned in the Taihu Lake and local standardized management.

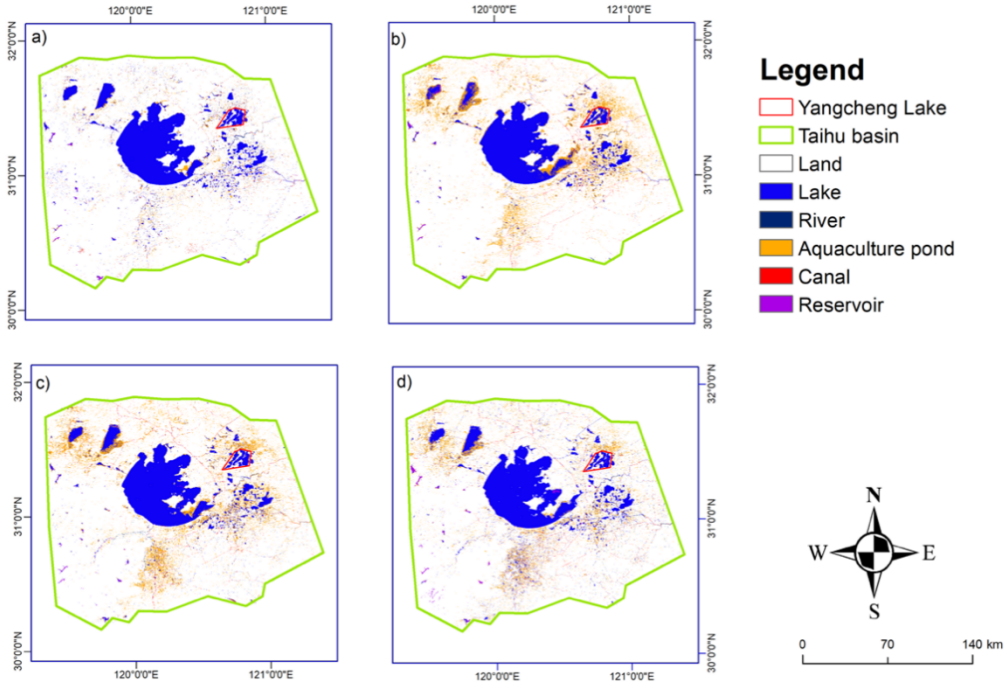

Figure 4.7: The wetland classification of a) 1984, b) 2001, c) 2011, and d) 2021 at the Taihu Lake Basin.

The PLB and DHB are the two central water-body systems of the YRB midstream (Figures 4.8 and 4.9). In the PLB case, the area of Poyang Lake experienced a decrease between 1984 and 2011. This decrease was primarily attributed to the expansion of aquaculture ponds and flats within the basin. However, by 2021, the lake area showed signs of recovery. Regarding the DHB, significant shrinkage of the lake area occurred between 1984 and 2021. This shrinkage can be attributed to the expansion of the inland marsh and aquaculture pond within and around the lake. However, in contrast to Dongting Lake, Honghu Lake located in the northeast of the DHB exhibited continuous expansion over the study period, accompanied by

an increase in the aquaculture pond surrounding it.

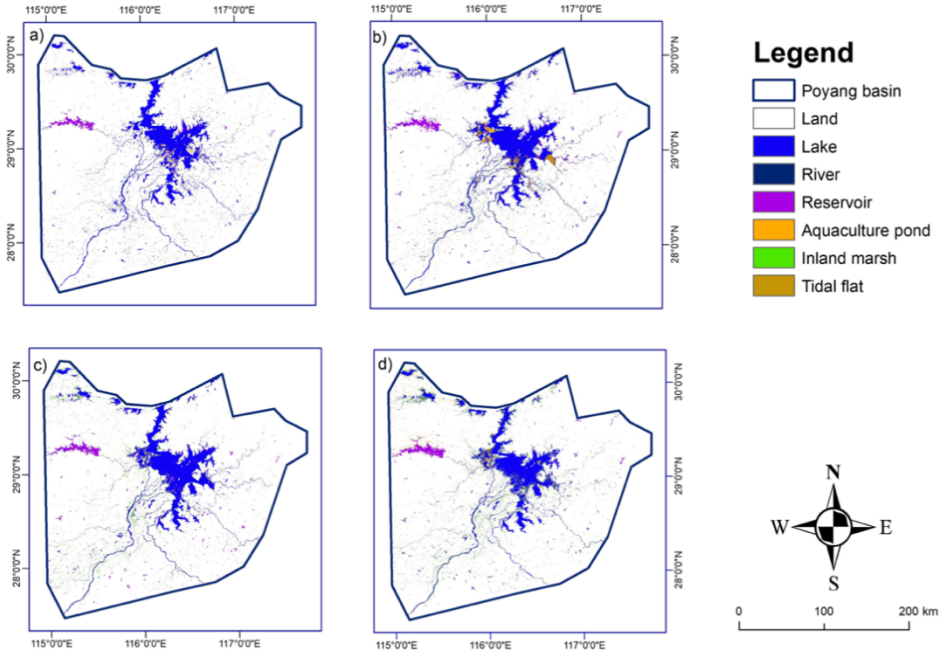

Figure 4.8: The wetland classification of a) 1984 b) 2001 c) 2010, and d) 2021 at the Poyang Lake Basin.

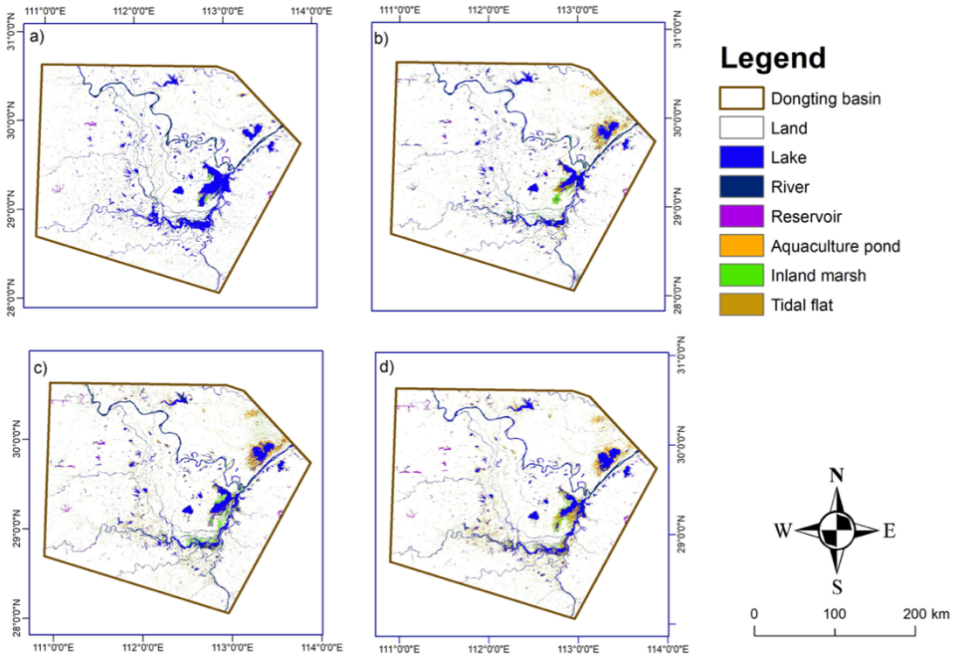

Figure 4.9: The wetland classification of a) 1984, b) 2001, c) 2011, and d) 2021 at the Dongting Lake and Honghu Lake Basin.

Figure 4.10 represents the SR of the YRB. In this region, the inland marsh area exhibited continuous shrinkage and variable spatial distribution in the study period. In contrast, lakes and rivers in the source region maintain a relatively stable presence without significant variations because of the less vulnerability to climate change compared with the inland marsh.

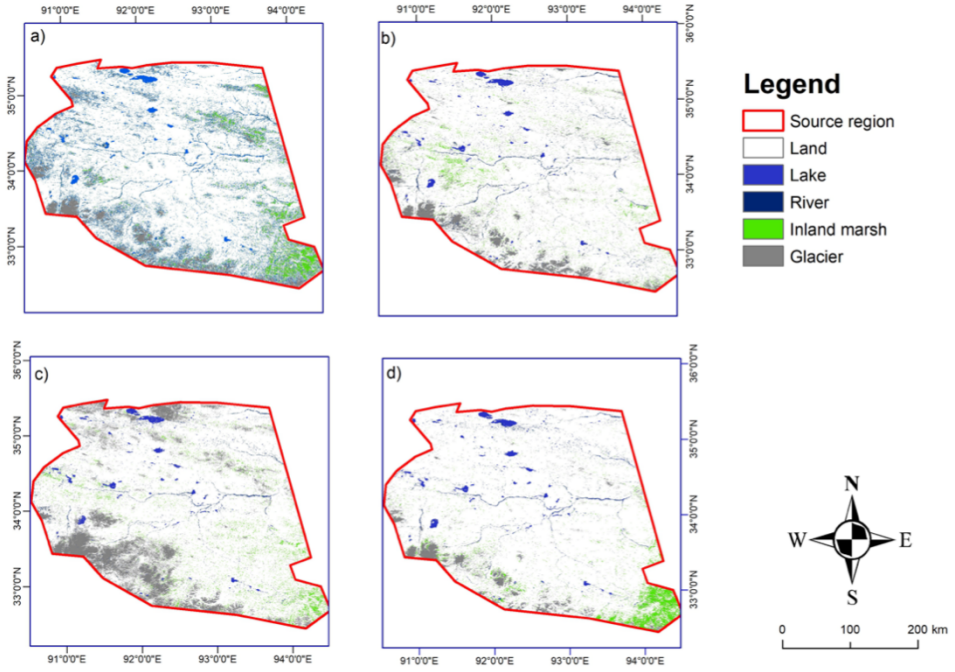

Figure 4.10: The wetland classification of a)1984, b)2001, c) 2011, and d) 2021 at the YRB source region.

4.3.3 Seasonal variations of wetlands

Figures 4.11 to 4.15 showcase the seasonal change of wetlands in the YRB estuary between 1984 and 2021. Wetlands exhibit much more prominent seasonal variations in PLB, DHB, and SR compared to the estuary and TLB. All the wetland categories stayed in the relatively constant area from January to December in the estuary and TLB. In PLB, the lake area expands to 4128 km^2 in July, which is 2538 km^2 larger than that in winter. In contrast, tidal flats and inland marsh both shrink in summer months. A similar pattern is observed in the DHB, the lake area reaches the peak value in August, and the area of tidal flats keeps a low value during the wet months (from May to September). The area of inland marsh in DHB expands in April, November, and December but contracts in August and September. While unlike the constant value of aquaculture ponds in the PLB, the area of aquaculture ponds in

DHB reduces continuously from March to December, which means local aquaculture ponds are more affected by dry and wet seasons. The most significant seasonal change of wetlands occurring along the YRB is inland marshes in the source region, with the peak value in September and much lower values in winter months. These findings highlight the various seasonal dynamics of wetlands for different regions along the YRB, experiencing distinct patterns of expansion, shrinkage, and stability throughout the year.

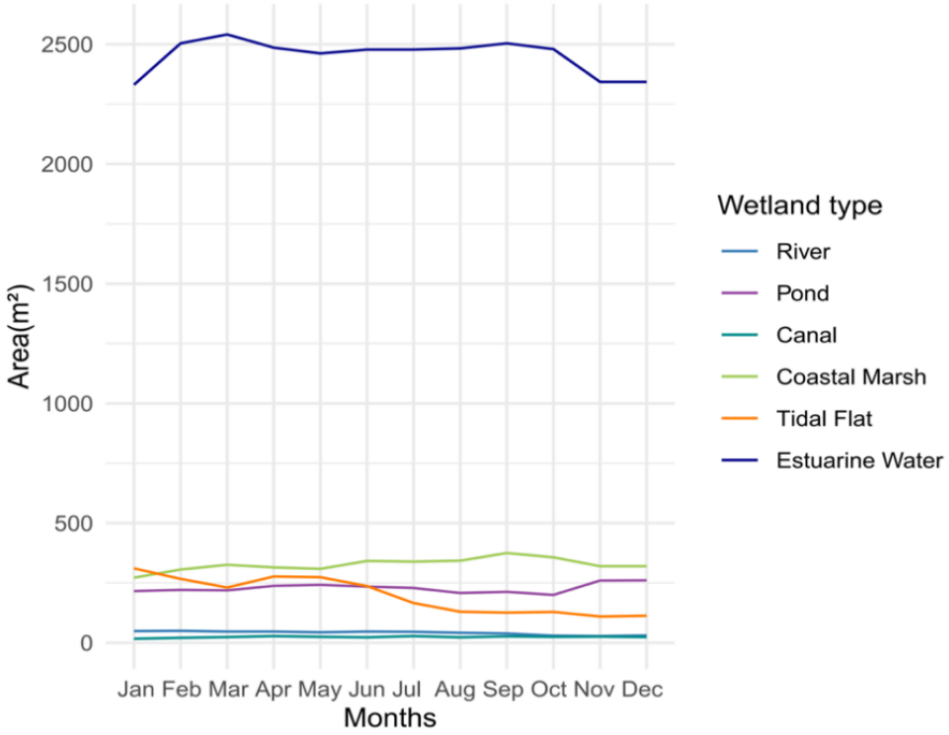

Figure 4.11: Long-term mean monthly areas of various wetland categories in the YRB estuary between 1984 and 2021.

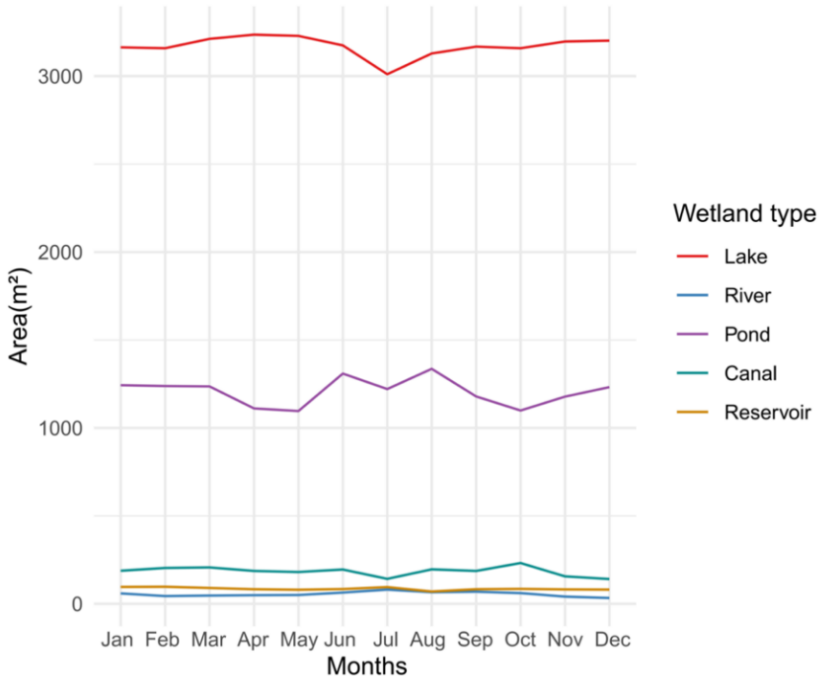

Figure 4.12: Long-term mean monthly areas of various wetland categories in the Taihu Lake Basin between 1984 and 2021.

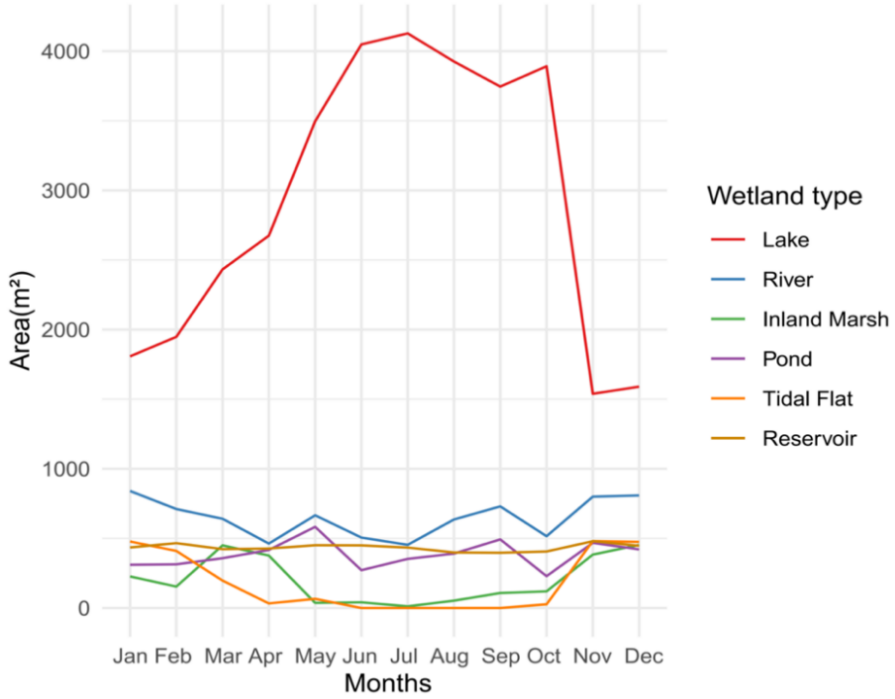

Figure 4.13: Long-term mean monthly areas of various wetland categories in the Poyang Lake Basin between 1984 and 2021.

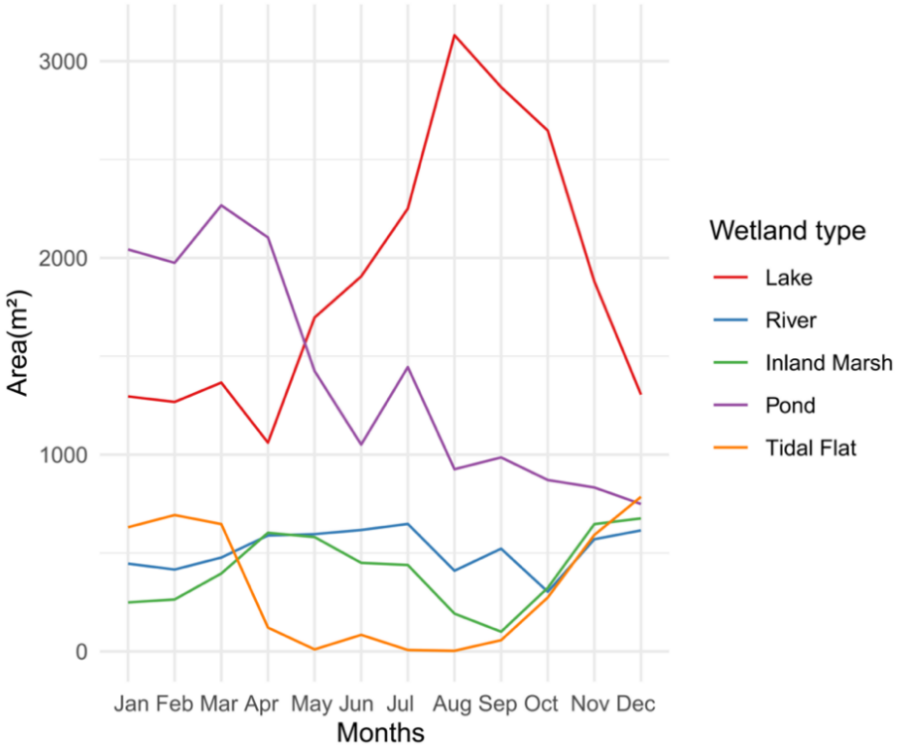

Figure 4.14: Long-term mean monthly areas of various wetland categories in the Dongting and Honghu Lake Basin between 1984 and 2021.

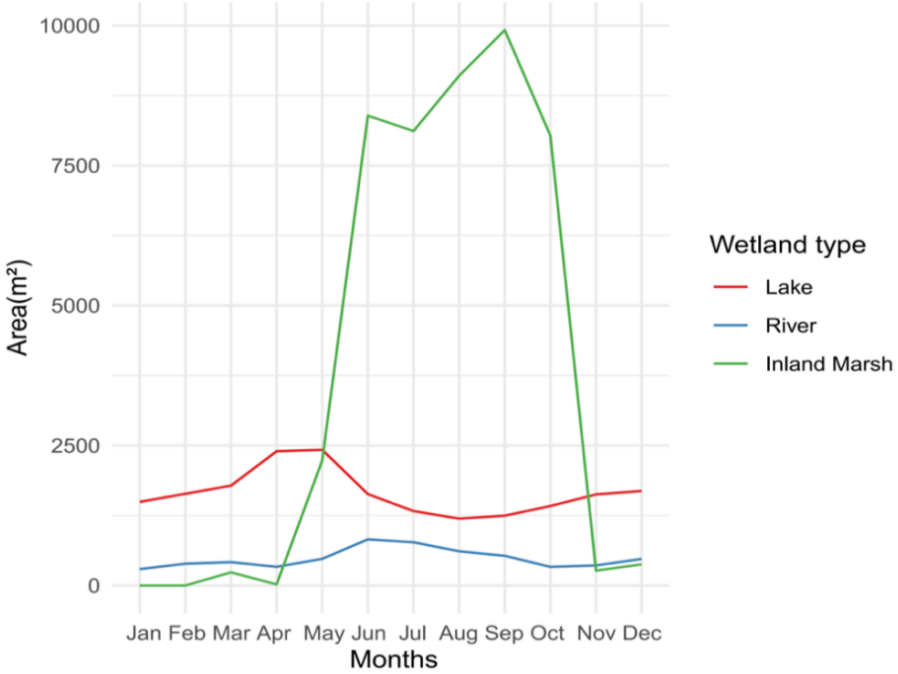

Figure 4.15: Long-term mean monthly areas of various wetland categories in the YRB source region between 1984 and 2021.

4.3.4 Natural and human activity drivers' division of wetland variations

Table 4.5 summarizes the attribution of wetland categories with significant changes to natural and anthropogenic drivers in the Estuary, TLB, PLB, DHB, and SR of the YRB from 1984 to 2021. In the estuary region, tidal flats experienced the most significant changes, shrinking by 52 km^2 and 47 km^2 due to natural factors (sea-level rise) and human activities (urbanization and fish farming) in the Dongtan Natural Reserve and Yaowang Harbor, respectively. In the TLB, the development of fish farming led to the expansion of 2475 km^2 of aquaculture ponds and the corresponding 655 km^2 reduction of lake areas. Soil erosion and flooding caused the expansion of 479 km^2 of inland marsh and 93 km^2 of tidal flats in the PLB. Urbanization and fish farming are the main human activities in the PLB, resulting in a reduction of 32 km^2 in lake area and an increase of 438 km^2 in aquaculture ponds. The DHB exhibited a similar situation to the PLB, with the expansion of 159 km^2 of inland marshes and 193 km^2 of tidal flats attributed to natural driving forces; human activities led to a shrinkage of 678 km^2 in lake areas and an expansion of 945 km^2 in aquaculture ponds. The total area influenced by human activities in these three regions exceeds that affected by natural drivers. In the SR region, the shrinkage of 2284 km^2 inland marshes was mainly attributed to changes in precipitation and temperature, with no significant wetland changes caused by human activities. Overall, human activities have a more dominant influence than natural factors on wetland changes in the YRB, although the exact influence varies in different regions of YRB. Human activities caused a total of 5270 km^2 of wetland changes, while natural driving forces affected 3260 km^2. Detailed analyses of each driving force and their impacts on the corresponding wetland categories are discussed in Section 4.4.1.

Table 4.5: Natural and human activity driving factors division of wetland categories with significant changes in the five representative regions of the YRB between 1984 and 2021.

	Natural driving forces (Sea level rise, soil erosion, flooding, temperature and precipitation change)	**Human activities (Urbanization, fish farming, sand dredging)**
Estuary Region	Tidal flats -52km^2 (Dongtan Natural Reserve of Chongming Island)	Tidal flats -47km^2 (Yaowang Harbor)
Taihu Lake Basin	-	Aquaculture ponds +2475km^2 Lake -655km^2
Poyang Lake Basin	Inland marshes +479km^2 Tidal flats +93km^2	Lake -32km^2 Aquaculture pond +438km^2
Dongting Lake Basin	Inland marshes +159km^2 Tidal flats +193km^2	Lake -678km^2 Aquaculture pond +945km^2
Source Region	Inland marshes: -2284km^2	-

4.4 Discussion

4.4.1 Wetland variation drivers

Urbanization is one of the most non-negligible factors of wetland variations in the YRB estuary (Mao et al., 2018). After 2000, the YRD, recognized as China's most economically advanced region, witnessed a noticeable reduction in marshes and tidal flats along its coastal areas (Mao et al., 2018). This phenomenon can be attributed to the rapid expansion of urbanized areas within the YRD (Mao et al., 2018). Urban build-up land was not the only type of urbanization that destroyed coastal wetlands, the expansion of industrial and transportation lands including roads and harbors indirectly caused the loss of coastal wetlands as well (Mao et al., 2018). The disappearance of tidal flats in the Yaowang Harbor between 2001-2021 in Figure 4.5 reflects this finding, the tidal flats shrank by nearly half, from 91km^2 to 44km^2.

Sea level rise is another major driver for the long-term variations of coastal wetlands in the YRB estuary due to its low elevation across the estuary region. (Chen et al., 2018). Over the past three decades, both Jiangsu Province and Shanghai Municipality have witnessed a sea level rise (Chen et al., 2018). According to the SPRC (Source-Pathway-Receptor-Consequence) model, the vulnerability of coastal wetlands in the YRB estuary to sea level rise is expected to continue rising in the coming decade (Cui et al., 2015). Furthermore, the construction of the Three Gorges Reservoir and the completion of the South to North Transfer projects have resulted in decreased sediment discharge into the YRB estuary, leading to a slower rate of sedimentation and subsequent reduction of coastal mud flats (Chen et al., 2018). Song and Wang (2014) discovered that the YRD and Dongtan Natural Reserve of Chongming Island both experienced an ‘erosion - deposition - erosion’ pattern in 1980-1990, 1991-2001, and 2002-2012 (Song and Wang, 2014). This pattern corresponds to the variations in tidal flats of the YRD and Dongtan Natural Reserve, as shown in Figure 4.5. The area of tidal flats increased from 264km^2 to 357km^2 in 1985 and 2021 and then reduced to 130km^2 in 2011.

The expansion of aquaculture pond areas in the TLB is mainly caused by the rapid development of aquaculture farming (Cai et al., 2013). This driving force resulted in the expansion of 2475 km^2 of aquaculture ponds in the TLB, directly contributing to the overall increase in human-made wetlands within the YRB between 1984 and 2021. Wild capture fisheries reached the environmental carrying capacity limit in the 1990s, leading the Chinese government to encourage aquaculture production since then (Cai et al., 2013). The lakeside regions of the TLB and Yangcheng Lake are the key inland aquaculture pond regions due to their ideal geography. Consequently, a large number of cages were observed aggregating in the lakeside regions of the TLB (Cai et al., 2013).

In 2007, following cyanobacteria blooms in Taihu Lake, the government began addressing the environmental issues associated with pond culture in lakes. As a result, more than half of the cages in Taihu Lake and Yangcheng Lake were cleared by 2008, and pond culture in lakes was subsequently banned (Cai et al., 2013). This is why there are almost no ponds in the southeast corner of Taihu Lake in 2021, and the area of ponds in the TLB decreased significantly after 2011, continuously reducing from a peak of 3225 km^2 in 2011 to 2885 km^2 in 2021. Currently, the majority of aquaculture ponds in the TLB are concentrated to the north of Yangcheng Lake and have transitioned towards more intensive and standardized practices, moving away from the uncontrolled expansion as in the past (Duan et al., 2020). According to Liu et al. (2020), the area of Taihu Lake has increased from 1984 to 2018, with the eastern part of Taihu Lake being the main impact area. As shown in Figure 4.6, the southeast corner of TLB expanded in 2021 compared with that in 1984. However, this lake region is also affected by aquaculture pond coverage and degradation. Therefore, the lake area of TLB has experienced shrinkage from 1984 to 2021, decreasing from 2912km^2 to 2257km^2.

For the wetlands of the PLB and DHB, the long-term annual variations are primarily driven by several factors, including increased soil erosion in the upper reaches of the YRB, flooding events, and human activities (Mei et al., 2016). Although precipitation from April to October between 2003 and 2012 was lower compared to that from 1960 to 2002 in the PLB, it does

not directly indicate that climate change is responsible for the changes in annual changes in wetland areas (Cui et al., 2013; Mei et al., 2016). Compared with precipitation, soil erosion in the upper reaches of the YRB and tributaries contains more significant implications on annual variations of wetland area in the YRB middle and lower reaches, especially for natural water bodies like Poyang and Dongting Lakes (Cui *et al.,* 2013; Deng et al., 2019). Soil erosion can increase the sediment load in lakes, leading to a reduction in the lake area with the expansion of marshes and flats. In the PLB and DHB, both of marshes and flats areas expanded in the long-term time series. The area of inland marsh increased 479km^2 in the PLB and 159km^2 in the DHB from 1984 to 2021; tidal flats expanded 93 km^2 and 193km^2 in the PLB and DHB in the same time period, respectively. Some experts argue that the increase in soil erosion in the YRB was primarily attributed to human activities rather than climate change (Wei et al., 2011).

Human activities such as fish farming, urbanization along the lakeside, and sand dredging have contributed to the lake shrinkage of 32 km^2 in PLB and 678 km^2 in DHB, as well as the expansion of aquaculture ponds with 438 km^2 and 945 km^2 in the PLB and the DHB, respectively between 1984 and 2021 (as shown in Figures 4.7 and 4.8) (Cui et al., 2013; Mei et al., 2016; Xie et al., 2017). After 2015, fish farming and sand dredging started to be managed and banned by the government, respectively (Met *et al.,* 2016). Consequently, this led to the reduction of 475 km^2 of aquaculture pond area around Hong Lake (northeast of Dongting Lake) and the reduction of 406 km^2 of aquaculture pond in the PLB in 2021 compared with the largest area in 2015. Additionally, severe flooding occurred in the YRB in 1998, 2008, and 2016, which brought impacts on water body changes in two aspects. Firstly, flooding increased the lake area and number; secondly, the large number of sediments in the lakes resulted in the shrinkage of lake water storage capacity and extracted water bodies by raising lakebed levels (Cui et al., 2013; Zhang et al., 2020). Flooding is a significant driving factor behind the seasonal wetland change in PLB and DHB, affecting floodplains and seasonal lakes (Li et al., 2019). Both PLB and DHB, with complex floodplains and interconnected seasonal lakes, were coupled with the main lake during the wet summer

months but became isolated in winter (Li et al., 2019). Meanwhile, the wetland area with plant coverage, such as inland marshes, is reduced during the flooding seasons. The area of inland marsh reached the lowest value in July (12 km^2) and September (100 km^2) of the PLB and DHB, respectively, as shown in Figures 4.12 and 4.13.

The annual wetland degradation in the source region of the YRB is primarily indicated by the shrinkage of inland marsh, which reduced to 7333 km^2 in 2021 from 9617 km^2 in the 1980s. Climate change is identified as the main driving force behind this degradation due to the high vulnerability of wetlands in alpine areas to changes in temperature and precipitation (Xue et al., 2018). Previous studies have confirmed that both annual temperatures and precipitation have increased in the source region of the YRB, and future projections suggest that climate warming on the Qinghai-Tibetan Plateau will continue and potentially intensify in the future (Guo et al., 2016; Xue et al., 2018). Regarding seasonal changes in wetlands in the source region, rising temperatures during summer leads to a reduction in water levels of lakes, with the lowest lake area recorded at 1193 km^2 in August. Simultaneously, plant coverage replaces snow coverage, explaining the observed expansion of inland marshes between May and September, with the highest value reaching 9919 km^2 in September, as shown in Figure 4.14 (Xue et al., 2018).

4.4.2 Comparison with other wetland datasets

In this study, the LTWCD_YRB was generated from continuous Landsat images collections with comprehensive wetland categories. Due to the absence of a dataset offering comparable wetland classifications and time series specifically for the YRB, the LTWCD_YRB was compared with the YRB wetland classification dataset from 2008, as well as several other datasets that cover different regions of the YRB and various years between 1987 and 2021 (Table 4.6).

The comparison between the LTWCD_YRB with the whole YRB wetland classification in 2008 demonstrated almost the same natural wetland area (Yan et al., 2013). However, the

human-made wetland area appears smaller in the LTWCD_YRB because Yan et al. (2013) included paddy fields and artificial farms, which are not considered as part of the wetland categories in the LTWCD_YRB. Instead, the LTWCD_YRB has included aquaculture ponds rather than artificial farms.

In terms of the wetland area in the YRB estuary, the total wetland area in 1980 and 2015 from Chen et al. (2018) is comparable to the corresponding years in the LTWCD_YRB. However, due to differences in the zoning of the YRB estuary boundaries, Chen et al. (2018) included more human-made wetlands in the TLB but fewer tidal flats along the coastal line. Consequently, Chen et al. (2018) reported a larger area of human-made wetlands, but fewer natural wetlands compared to the LTWCD_YRB.

The wetland area in the YRB lower stream (LYRB) of LTWCD_YRB is compared with multiple datasets because few past datasets cover this region with completed wetland categories (Table 4.6). Lake and aquaculture ponds are the two representative wetland categories belonging to the natural and human-made wetlands in the LYRB, respectively. Cui et al (2013) demonstrated similar wetland area in 1990, 2000, and 2008 with the LTWCD_YRB and confirmed that the lake area in the LYRB decreased more rapidly from the period of 1990-2000 than that from 2000 to 2008 (Cui et al., 2013). For aquaculture ponds, the study region of the compared dataset focuses on Jiangsu province, which partially overlaps with the LYRB, as there is a lack of suitable aquaculture pond data specifically for the LYRB. And the continuous expansion of the aquaculture pond area from 1988 to 2018 was confirmed.

The trend of wetland changes in the YRB midstream (MYRB) from 2000 to 2019 (Liu et al., 2022) is consistent with the LTWCD_YRB, which decreased until 2009, a rebound to the highest value in 2015, and finally reduced in 2019 (Liu et al., 2022) (Table 4.6). In the YRB source region, the total areas of wetlands and three main wetland categories (lake, river, and inland marsh) in the LTWCD_YRB closely align with the findings of Zhang et al. (2011).

Zoning differentiation of the research area is the main reason for the differences in wetland areas between the LTWCD_YRB and the compared datasets.

Table 4.6: Comparison of wetland areas between the LTWCD_YRB and other satellite datasets.

Research report	Research period	Research region	Data source	Wetland area		
				Natural	Human-made	Total
Yan et al., 2013	2008	YRB	Landsat 8 OLI, 30m	47,784	33,003	80,787
LTWCD_YRB	1984-2021	YRB	Landsat 5 TM, 7 ETM, 8OLI, 30m	47,817 (2008)	10,384 (2008)	58,201 (2008)
Chen et al., 2018	1980	YRB	Landsat 5 TM,	473	167	640
	2015	Estuary	7 ETM, 8 OLI, 30m	411	699	1,110
LTWCD_YRB	1984-2021	YRB Estuary	Landsat 5 TM, 7 ETM, 8 OLI, 30m	511(1984) 712(2015)	115(1984) 302(2015)	626 (1984) 1,014 (2015)
Cui et al., 2013	1990	LYRB	Landsat 5 TM,	5,716 (Lake)	-	-
	2000		7 ETM, 30m	5,015 (Lake)	-	-
	2008			4,946 (Lake)	-	-
LTWCD_YRB	1984-2021	LYRB	Landsat 5 TM,	5,657 (Lake 1990)	-	-
			7 ETM, 8 OLI,	5,035 (Lake 2000)	-	-
			30m	4,929 (Lake 2008)	-	-
Duan et al., 2020	1988	Jiangsu	Landsat 5 TM, 8	-	660 (Aquaculture pond)	-
	1993	Province	OLI, TIRS, 30m	-	1,121(Aquaculture pond)	-
	1998			-	1,834(Aquaculture pond)	-
	2003			-	3,005(Aquaculture pond)	-

	2008			-	3,107(Aquaculture pond)	-
	2013			-	3,853(Aquaculture pond)	-
	2018			-	4,098(Aquaculture pond)	-
LTWCD_YRB	1984-2021	LYRB	Landsat 5 TM,	-	832 (1988)	-
			7 ETM, 8 OLI,	-	1,403 (1993)	-
			30m	-	1,594 (1998)	-
				-	2,460 (2003)	-
				-	3,067 (2008)	-
				-	3,406 (2013)	-
				-	3,776 (2018)	-
Liu et al., 2022	2000	MYRB	Landsat 5 TM,	-	-	10,335
	2006		7 ETM, 8 OLI,	-	-	7,182
	2009		30m	-	-	7,231
	2015			-	-	11,143
	2019			-	-	8,290
LTWCD_YRB	1984-2021	MYRB	Landsat 5 TM,	-	-	11,191 (2000)
			7 ETM, 8 OLI,	-	-	10,427 (2006)
			30m	-	-	10,027 (2009)
				-	-	12,804 (2015)
				-	-	12,057 (2019)
Zhang et al.,	2000	YRB Source	Landsat 5 TM,	964 (lake)	-	10,445
2011			30m	4,289 (River)	-	
				5,192 (Inland marsh)	-	

LTWCD_YRB	1984-2021	YRB Source	Landsat 5 TM, 7 ETM, 8 OLI, 30m	1,492(Lake 2000) 3354(River 2000) 5235(Inland marsh 2000)	- - -	10,081 (2000)

4.4.3 Advantages and limitations

Researchers and policymakers can use the LTWCD_YRB to analyze both spatial and temporal changes for multiple wetland categories along the YRB based on different regions, seasons, and period of interest. Additionally, the wetland classification results can be used to assess the ecological and environmental impacts of natural and human activities such as climate change, urbanization, agriculture, aquaculture, and other driving forces on the YRB wetlands, supporting evidence-informed decision-making for sustainable wetland management. Moreover, the LTWCD_YRB can be instrumental in monitoring the implementation of wetland conservation policies and assessing their effectiveness. By comparing the wetland classification results with policy objectives, researchers, policymakers and stakeholders can determine whether conservation efforts are achieving the desired outcomes and make necessary adjustments. Furthermore, the seasonal change patterns of wetlands in different regions of the YRB can provide insights into the hydrological processes and ecological dynamics of the wetlands and inform water resource management strategies. Overall, the long-term time series of the wetland classification dataset is a valuable tool for researchers, policymakers, and stakeholders to better understand the YRB wetlands and support sustainable management practices.

The validation process of the LTWCD_YRB dataset has several limitations. This study validated the wetland classification accuracy using an existing wetland dataset from Mao et al. (2020) rather than field-based ground truth data. As indicated in the literature review, the use of existing datasets as the indirect validation has become a common practice in the large-scale wetland classification research, because of the practical challenges to obtain the comprehensive field-based ground truth data for large-scale wetlands. However, it may impose uncertainties on the reliability and interpretation of the indirect validation process. Given that the CAS_Wetlands dataset only covers the year of 2015, the classification accuracy assessments for other years of the LTWCD_YRB may contain uncertainties. Besides, some small, narrow, and temporary wetlands may be underrepresented by the CAS_Wetlands. Thus, the validation dataset may fail to capture the wetland features that are

correctly identified by the classification, thus potentially leading to the biased accuracy assessment.

Additionally, the classification accuracy of some human-made wetland categories (e.g., canals and aquaculture ponds) with small areas is relatively low. These categories can be challenging to accurately classify due to the difficulty in collecting precise samples from the Landsat imagery and the inherent size limitations of the samples. Improving the classification accuracy of small-scale human-made wetland categories would require more precise sampling techniques and potentially higher-resolution satellite imagery. This could involve ground truth data collection, field surveys, or utilizing other data sources such as high-resolution Unmanned Aerial Vehicles (UAV) imagery. Incorporating additional ancillary data and advanced classification algorithms could also help enhance the accuracy of these specific wetland classifications.

4.5 Conclusions

In this study, the LTWCD_YRB dataset was generated from continuous Landsat images with completed wetland categories, utilizing the RF machine learning method on the GEE platform. A thorough investigation of the LTWCD_YRB dataset yielded several significant findings: 1) The total wetland area of the YRB in 2021 was larger than that in 1984, with a consistent increase in human-made wetlands and fluctuating natural wetland areas. Anthropogenic driving forces have a greater impact on the expansion of wetland areas compared to natural driving forces; 2) The aquaculture pond was the wetland category that expanded the most in 2021 compared with that in 1984 due to urbanization and fish industry development. Key regions affected include the YRB estuary, TLB, and DHB. Conversely, inland marsh was the category with the most fluctuations between 1984 and 2021, particularly in the YRB SR; 3) Seasonal changes in wetland areas were prominent in the PLB, DHB, and SR, driven by variations of floodplains and inland marsh vegetation coverage. The LTWCD_YRB demonstrated a consistent agreement of wetland area variations with the other satellite-based wetland datasets of the YRB. It would provide a valuable time series for evaluating historical

wetland changes, developing future wetland conservation strategies, and analyzing the interactions between natural and human-made driving forces in the YRB.

Chapter 5 Effects of long-term wetland variations on flood risk assessments in the Yangtze River Basin

Highlights:

- We analyze flood risks with long-term wetland effects by using the GIS-based model.
- Wetland expansion leads to flood risk reduction in years with normal rainfall.
- Causal relation analysis is a useful way to find dominant flood risk indicators.
- Precipitation is the dominant indicator in all the five flood prone regions.
- We give wetland-related suggestions for flood risk mitigation.

This chapter is a reformed version of a manuscript published in the *Environmental Impact Assessment Review*, which is available at https://doi.org/10.1016/j.eiar.2025.108123.

5.1 Introduction

In recent decades, global climate change has brought inevitable consequences, such as sea level rise, global warming, seasonal irregularities, droughts, and floods (Rajkhowa and Sarma, 2021). Among these extreme events, floods have been responsible for 44% of global natural disasters (WMO, 2021). The annual deaths and economic losses caused by the floods reached 1254 people and US$2.5 billion, respectively (Petit-Boix et al., 2017). From 1998 to 2017, floods have affected two billion people across the world (Wu et al., 2020). In the Yangtze River Basin (YRB) of China, flooding is the most frequent natural disaster with enormous socio-economic damages (Xia and Chen, 2020). The YRB has experienced a high proportion of flood occurrences, including seven massive floods since 1860. The disastrous flood in 1998 led to heavy casualties, and ecological and economic losses (Zhang et al., 2020; Zhang et al., 2023).

According to the latest wetland classification system from Mao et al. (2020), wetlands include various categories, including Inland marsh, inland swamp, lake, river, tidal flats, reservoir, canal, and aquaculture pond. As a critical component in the hydrological cycle, the wetlands offer numerous ecological and economic advantages, including contributing to the global carbon cycle, purifying water, mitigating floods, boosting fish production, and sustaining biodiversity (Liang et al., 2020; Xing et al., 2015). Flood control is one of the most important ecosystem services of wetlands under climate change (Gulbin et al., 2019). Numerous cases of high flood-risk regions around the world have proved that wetland variations brought large implications on flood resilience, such as the northeast Haor region of Bangladesh, lakes in the middle and lower reaches of the YRB, and Rocuant-Andalién coastal wetlands of Chile (Cui et al., 2013; Kamal et al., 2018; Rojas et al., 2022). To reduce the negative results brought by flood disasters, the development of nature-based solutions regarding wetlands land use and land cover (LULC) in the long-term process has attracted increased awareness (Schanze 2017; Thorslund et al., 2017; Wu et al., 2022). The effectiveness of wetland-related solutions has been confirmed by several studies (Fournier et al., 2016; Qin et al., 2024; Van and Temmerman, 2019; Wu et al., 2020), including

developing river restoration projects like the riverside corridor restoration in European countries (Fournier et al., 2016), improving hydrological resilience to flood risk by wetlands protection and restoration of the Nenjiang River Basin in Northeast China (Van and Temmerman, 2019), protecting wetlands from transferring to built-up areas in the Guangdong-Hong Kong-Macao Greater Bay Area (Qin et al., 2024), and mitigating coastal floods by restoring and creating tidal wetlands in flood-exposed coastal cities around the world (Wu et al., 2020).

The YRB covers 40% of the national wetland area in China with complex variations due to various driving forces (e.g., climate change, rapid urbanization along the Yangtze River Economic Belt, dam construction, and agricultural and livestock activities) (Finlayson et al., 2018; Xu et al., 2019b; Zheng et al., 2020). According to the characteristics of wetlands, the influence on floods depends on the categories and locations of wetlands (Acreman and Holden, 2013). Although the YRB has abundant wetland resources, wetland-based flood risk mitigation approaches are less prevalent compared to structural approaches, such as large-scale water conservancy projects like the Three Gorges Dam (Jia et al., 2022). To align with the ecological civilization development goals outlined in the national strategy for the Great Yangtze River Protection Program (GYRPP) launched in 2016 (Sheng et al., 2022), it is valuable to develop wetland-based approaches to enhance flood resilience and protect wetland resources in the YRB. Analyzing the effects of long-term wetland variations on flood risk assessments in the YRB flood prone regions is the basis for policymakers to develop feasible wetland-based flood risk management practices.

The area of middle and lower reaches of the YRB (MLYRB) is only half of the total YRB, but it contains the largest and one of the most abundant wetland ecosystems in China (Li et al., 2014; Yu et al., 2009). Also, the MLYRB is more easily to suffer from large-scale floods (Jia et al., 2022). Hence, the selection of flood prone regions gives more focus on the MLYRB in this study. Taihu Lake, Poyang Lake, and Dongting Lake are all significant water bodies to accommodate floods in the YRB (Yu et al., 2009). However, soil erosion in the upper reaches and frequent human activities altered their wetland function to floods in the basins of these

water bodies (Ma et al., 2023). Hence, it is valuable to investigate the effects brought by wetlands on flood risks of the Taihu Lake Basin (TLB), Poyang Lake Basin (PLB), and Dongting and Honghu Lake Basin (DHB). The Wanjiang Plain (WP) is selected as a study area due to its extensive alluvial floodplain. It also features a dense cluster of small lakes on both sides of the Yangtze River. These characteristics distinguish the WP from other basins (Dong et al., 2022). The only flood prone region selected in the YRB upstream is the Sichuan Basin (SB). It has been confirmed with the highest flood risk in the province of Sichuan because of the complex landform, lower altitude compared with surrounding mountainous areas, large precipitation, and dense population (Guo et al., 2023; Liu et al., 2017). Hence, five major flood prone regions were selected for this study, including the TLB, WP, PLB, DHB, and SB.

The World Meteorological Organization (WMO) defines risks as the potential loss of lives, property damages, disrupted economic activities, caused by a specific hazard within a given area and reference period (WMO, 1999). In recent years, flood risk has become increasingly complex due to emerging challenges associated with flood disasters. Flood risk factors are various because of different socio-economic conditions and ecological environments (Zhang et al., 2020). In this study, flood risk is defined based on the Intergovernmental Panel on Climate Change (IPCC) report, which encompasses hazards, systemic vulnerability, and exposure of human and natural systems (IPCC, 2014). Assessing the integrated flood risk with various flood risk indicators is the most effective way to evaluate and discuss the flood risk, as well as improving the public awareness of flood risk mitigations in the YRB (Wu et al., 2022; Zhang et al., 2020). There have been several studies for flood risk assessments covering the YRB: some of them focusing on typical lake basins like the PLB and DHB (Wu et al., 2022; Wang et al., 2011), some focusing on typical cities like Chongqing and Wuhan (Cai et al., 2021; Fang et al., 2019), Peng and Li (2021) and Zhang et al. (2020) both assess the flood risk for the entire YRB. For the study period of these flood risk assessments, most of them assess one or a few years, except Wu et al. (2022) that incorporates both short-term and long-term flood risk assessments. A number of methods have been applied for the flood risk

assessment, such as the historical disaster statistical method (Halgamuge and Nirmalathas, 2017; Youssef et al., 2015), scenario simulation analysis for future flood risk predictions (Alfieri et al., 2015; Cai et al., 2021; Gangrade et al., 2019), index system method (Christie et al., 2018), Set Pair Analysis (SPA) combined with variable fuzzy sets (VFS) model (Su et al., 2010; Zhang et al., 2011; Zou et al., 2013), machine learning method like the Artificial Neural Network (ANN) (Li et al., 2008), and the multi-criteria decision making GIS-based approach (Cai et al., 2021; Lyu et al., 2023; Peng et al., 2024; Zhang et al., 2020; Ziwei et al., 2023).

Among various flood risk assessment methods, the multi-index GIS-based approach is widely used and recognized as an effective method for identifying flood risks. It offers advantages in analyzing the large-scale spatial data and comprehensively considering all aspects of flood risk indicators (Zhang et al., 2020). Cai et al. (2021) applied the multi-index GIS-based model with 11 indicators to assess the flood risk in Chongqing, in which the river density was considered as an exposure indicator. Similarly, Ziwei et al. (2023) and Zhang et al. (2020) used the river network density as an indicator to make the flood risk assessment in the Lijiang River Basin and the YRB. Peng et al. (2024) included the river distribution as an indicator in the model to assess flood risks in Beijing. In Lyu et al. (2023), the drainage condition was selected as a flood risk indicator in the multi-index GIS-based models to assess the flood risk in Lanzhou. Wetlands are abundant and encompass various categories in the YRB, their spatial dynamics lead to complex effects on the flood risks (Acreman and Holden, 2013). In previous studies, however, wetlands were not well represented in the flood risk assessment model and the river or drainage indicator is the only wetland category that has been included. Therefore, there is a research gap that exists in incorporating the wetland effects as a flood risk indicator into the multi-index GIS-based model.

Through the literature review of flood risk assessment studies, no prior research has been found to adopt the comprehensive wetland data as a model input to assess the flood risk of all the flood prone regions in the YRB. As a result, investigating the spatial and temporal long-term wetland effects on flood risks in the YRB remains a significant research gap.

Therefore, the novelty of this study lies in analyzing the long-term annual wetland effects on flood risks from 1985 to 2021 in the YRB by using an improved multi-index GIS-based model that incorporating the wetland input. Moreover, this improved multi-index GIS-based model can be applied to assess the flood risk in flood prone regions of other basins worldwide with abundant wetland resources. To address this, this study incorporates the Long-Term Wetland Classification Dataset for the YRB (LTWCD_YRB) from Guo et al. (2024) as a flood risk indicator, to develop the long-term flood risk assessment with wetland implications. The research objectives of this study include: 1) To improve the flood risk assessment model by incorporating the effects of wetland variations, and to investigate how long-term wetland changes affect flood risk assessments in the YRB; 2) To examine the causal relationships among flood risk indicators and identify the dominant indicators for each flood prone region under wetland effects; 3) To provide useful suggestions for policymakers on the wetland-related flood risk management.

5.2 Materials and methods

5.2.1 Study area

The YRB (Figure 5.1) is located between 24°27’ to 35° 54’ N and 93°33’ to 122°19’ E, covering 18.75% of China’s total area, with the area of 1.8 million km^2 (Zhang et al., 2020). Wetlands in the YRB account for 40% of the national wetlands in China, with hundreds of tributaries and lakes (Cui et al., 2018; Xue et al., 2018). Under implications of topography, subtropical monsoon climate, and annual precipitation, the flood prone regions are unevenly distributed in the YRB (Zhang et al., 2020).

The major flood prone regions are labelled in Figure 5.1, including the TLB, WP, PLB, DHB, and SB. The TLB is situated in the Yangtze River Delta, one of the most rapidly developing regions in China, and encompasses Taihu Lake, the third-largest freshwater lake in the country (Peng et al., 2018). The WP is located within the MLYRB, spanning 416 km of Yangtze River on the plain, with several lakes on both sides of Yangtze River (Dong et al., 2022). The PLB and DHB are situated in the midstream of the YRB, encompassing the first

and second largest freshwater lakes in China respectively. These basins feature extensive floodplains that adjoin their main lakes (Li et al., 2019; Wang et al., 2022; Wu et al., 2022). The SB, located in the central-eastern part of Sichuan province and the upper reaches of the YRB, including numerous tributaries, is one of the most densely populated areas in China (Guo et al., 2023; Liu et al., 2017).

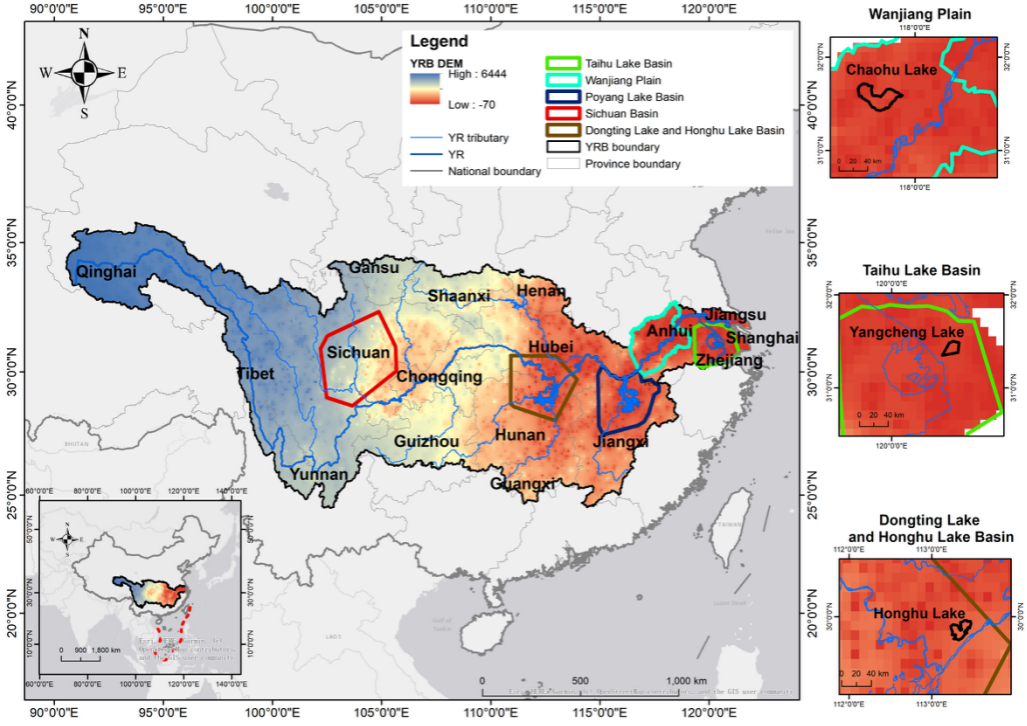

Figure 5.1: The location, hydrographical and topographical information of the Yangtze River Basin and five flood prone regions.

5.2.2 GIS-based spatial multi-index model

This study used a GIS-based spatial multi-index model to assess the flood risk in the YRB. The model includes two parts: a multi-index system and an analysis procedure in ArcGIS.

5.2.2.1 The multi-index flood risk system

The multi-index system consists of the index layers including the hazard index (H), vulnerability index (V), and exposure index (E), with 13 flood risk indicators for representing these index layers, as described in Zhang et al. (2020). The weight of each indicator is evaluated by the Analytic Hierarchy Process (AHP) method, which was firstly proposed by

Saaty (1977). The AHP method is considered as the practical technique in the multi-index flood risk assessment, which produces rapid, reliable, and cost-effective performances by subdividing the flood risk into specific factors tailored to different zones (Cai et al., 2021; Roy et al., 2021a). It has been widely employed in flood risk assessments and successfully applied in a GIS environment to generate flood risk maps in the YRB in our research group (Zhang et al., 2020). Firstly, the flood risk assessment framework was established with a hierarchical structure based on the flood formation mechanism and relationships between indicators. As shown in Figure 5.2, the assessment structure is consisted with the object layer, the index layer, and the indicator layer. Secondly, the judgement matrix [aij] in Eq. (5.1) between each indicator was used to determine the relative importance of factor ai to factor aj from experts' questionnaire (Zhang et al., 2020).

$$aij = \begin{bmatrix} a_{11} & a_{12} \cdots & a_{1m} \\ a_{21} & a_{22} \cdots & a_{2m} \\ \vdots & \vdots \ddots & \vdots \\ a_{m1} & a_{m2} \cdots & a_{mm} \end{bmatrix} \tag{5.1}$$

Besides, the weight of each indicator in the matrix should meet the following condition, which means that the sum of weight from all the indicators should be 1.

$$\begin{cases} \sum a_{ij} = 1 \\ a_{ij} = 1/a_{ji} \end{cases} (i, j = 1, 2, \cdots, n) \tag{5.2}$$

In this study, weights of all the indicators are divided into positive and negative. A positive weight means that this indicator can aggravative the flood risk, whereas negative weights would reduce the flood risk. The consistency check of the judgment matrix is the third step of the AHP. It can be calculated by Eq. (5.3):

$$\mathrm{CR} = \frac{CI}{RI} \tag{5.3}$$

CR is the consistency ratio, $CI=(\lambda_{max}-n)/(n-1)$ and λ_{max} is the largest eigenvalue of the judgment matrix. *RI* is the average random consistency index. The test will be passed if CR is less than 0.1, otherwise the matrix needs to be reconstructed (Lyu et al., 2018). The weight of

each indicator is shown in Table 5.1.The relative importance of each index is obtained by adding weights of corresponding indicators. Thirdly, the YRB flood risk can be calculated by the following equation:

$$YRBFR = H \times W_H + V \times W_V + E \times W_E \quad (5.4)$$

YRBFR is Yangtze River Basin Flood Risk; W_H, W_V, and W_E are the weights of hazard index, vulnerability index, and exposure index, respectively.

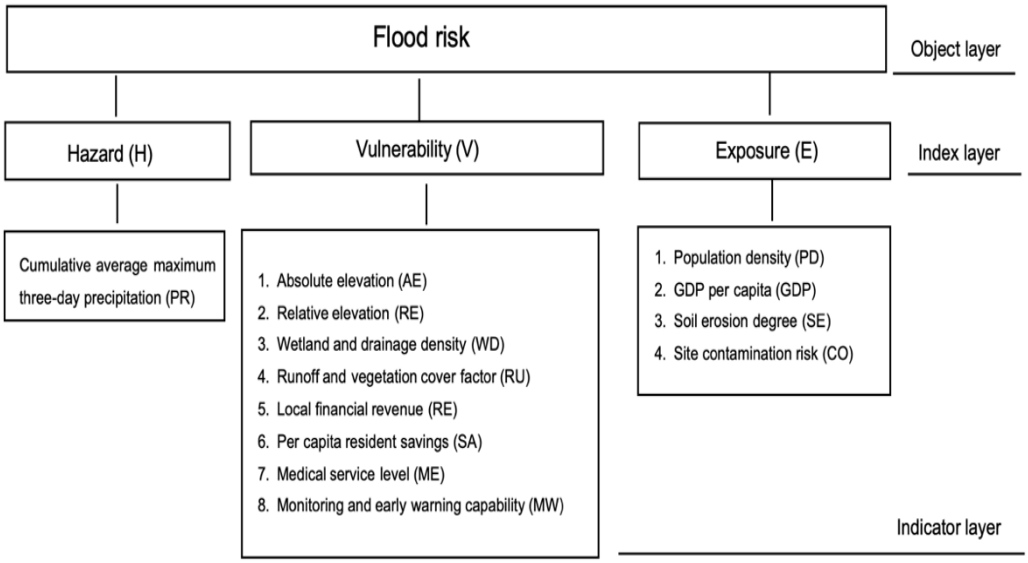

Figure 5.2: The improved flood risk assessment model by incorporating the effects of wetland variations.

Table 5.1: Weights and data source of flood risk indicators of the improved flood risk assessment model

Indicator layer	Weight of the indicator layer	Data source
Cumulative average maximum 3-day precipitation	+0.469	National Meteorological Information Center (China Surface Climate Data Day Value Data Set) (V3.0)
Absolute elevation	-0.053	Resource and Environment Data Cloud Platform
Relative elevation	-0.061	Calculated from absolute elevation data
Wetland and drainage density	+0.039	The Long-Term Wetland Classification Dataset for YRB (LTWCD_YRB) (Guo et al., 2024)
Runoff and vegetation cover factor	+0.041	Resource and Environment Data Cloud Platform (Liu et al., 2014)
Local financial revenue	-0.028	China City Statistical Yearbook (http://www.chinayearbooks.com)
Per capita resident saving	-0.025	China City Statistical Yearbook (http://www.chinayearbooks.com)
Medical service level	-0.027	China City Statistical Yearbook (http://www.chinayearbooks.com)
Monitoring and early warning capability	-0.047	National Meteorological Information Center (China Surface Climate Data Day Value Data Set) (National, 2019)
Population density	+0.046	Resource and Environment Data Cloud Platform (Xu, 2020)
GDP per capita	+0.066	Resource and Environment Data Cloud Platform (Liu et al., 2005)
Soil erosion degree	+0.068	Resource and Environment Data Cloud Platform (Wang et al., 2016)
Site contamination risk	+0.030	Resource and Environment Data Cloud Platform (Liu et al., 2014)

The selection of flood risk indicators is referred from Zhang et al. (2020) due to the same study region of the YRB, considering the principles of objectivity, operability, and easy spatialization, which has been theoretically based on their relevance to the past floods in the literature. Flood risks were assessed based on the following two model scenarios: one is through the general flood risk model from Zhang et al. (2020) generated with the flood risk indicators in the YRB, and the other is the improved flood risk assessment by incorporating the effects of wetland variations. In the improved YRBFR scenario as shown in Figure 5.2, the drainage density in the vulnerability layer was replaced by the wetland and drainage density derived from the LTWCD_YRB data. In the original YRBFR, drainage density is defined as the density of main and tributary streams. The improved indicator derived from LTWCD_YRB covers comprehensive wetland categories with river networks in the YRB. The total area difference for each level of flood risks between these two models (ΔFR) could explain how long-term wetland variations would affect flood risks. The uncertainty resulting from the indicator replacement is discussed in Section 5.4.1.

5.2.2.2 GIS analysis procedures

5.2.2.2.1 Data collection and processing

All the indicators' data collected has been rasterized before being input into the model, to reflect further details of the flood risk spatial distribution. The primary data sources of flood risk indicators are shown in Table 5.1. ArcGIS has been used to extract required elements from the collected real geographic and socio-economic data. All conversion processes and data processing of each index were completed in ArcGIS.

Hazard Index

Flood hazard is directly related with precipitation intensity, which associated with both of frequency and amount of precipitation. Hence, the maximum precipitation for cumulative three days of each year from 1985 to 2021 in the YRB is selected as the hazard indicator. The point data from the daily meteorological dataset of China National Surface Weather Station (V3.0) can be converted to raster data by using the Kriging interpolation method (Zhang et al.,

2020) in the ArcGIS.

Vulnerability Index

For vulnerability, we choose absolute elevation, relative elevation, wetland density, runoff and vegetation cover factor, local financial revenue, per capita resident saving, medical service level, and monitoring capability as assessment indicators. Absolute and relative elevation indicate the height and slope, respectively, which are topographic impacts on flooding. The standard deviation of 25 grid elevations around the centre grid was calculated as the terrain change, then obtaining the terrain standard difference level map by using the Focal Statistics tool. The wetland density refers to the ratio of wetland area and drainage area to the basin area. Runoff and vegetation cover factor is the velocity coefficient of the land. This study assigns values to the vegetation cover factor for each LULC class based on the LULC classification map, creating a new vegetation cover factor map. The local financial revenue, per capita resident savings, and medical service level indicators reflect the self-rescue ability of communities and residents facing the flood disaster. These data are rasterized to each grid by connecting with the vector data at the city level. Monitoring and early warning capability is defined as the hydrometeorological station density in this study, with the purpose to prevent and reduce disaster losses in advance.

Exposure Index

The exposure aspect contains population density, GDP per capita, soil erosion degree, and site contamination risk. The influence of flood risk on people and constructions is examined by population density and GDP. Soil types affect flood risk formation, the severe soil erosion can aggravate flood disasters. Site contamination risk determines the polluted level of lands and waterbodies after floods. Similarly to the vegetation cover factor, the site contamination map is generated from the LULC data through value reassignment.

5.2.2.2.2 Data normalization and classification

In this analysis, 13 flood risk indicators for the YRB are expressed in different units. In this

case, data normalization is necessary to enable comparison. The normalization shown in equation (5.5) as below:

$$i_{ij} = \frac{i_{actual} - i_{min}}{i_{max} - i_{min}} \quad (5.5)$$

The data normalization has been done by the Raster Data Calculator tool in ArcGIS. The value after normalization is between 0 to 1. When the value is closer to 1, the flood risk is higher.

The integrated flood risk is classified into 5 levels: Very low, low, medium, high, and very high by using the 'classified tool' in the Layer Properties of ArcGIS. With the purpose to make the comparison of the flood risk spatial distribution with and without wetlands, the classification interval standard of the integrated flood risk with and without wetland density should keep consistently. Hence, the classification interval of flood risk assessment results with and without wetlands need to be adjusted manually in the ArcGIS. With the reasonable standard by considering both years with the minimum and maximum flooding, levels of flood risk are defined as very low (0-0.09), low (0.09-0.17), medium (0.17-0.25), high (0.25-0.35), and very high (0.35-1.0).

5.2.3 Causal relationship based on the PCMCI algorithm

Causal inference plays the significant role to address many open problems with relevant environmental, social and economic implications, which are inherently causal (Runge et al., 2023). This study utilizes the PCMCI algorithm (Runge et al., 2019b), which is based on the Python package called TIGRAMITE (Runge et al., 2019b) to detect the strength of the causal relationship between the ΔFR and flood risk indicators in the 36-year time series. PCMCI has been applied in detecting the time-lagged causal discovery from observational discrete or continuous time series data like the climate change data and producing high-quality result graphs (Runge, 2018). PCMCI is a two-step approach that combines the PC algorithm (named after its inventors Peter and Clark) and the Momentary Conditional Independence (MCI) test, to assess the causal structure and to accommodate nonlinear functional dependencies of discrete or continuous variables (Krich et al., 2020; Runge, 2018). The first step is PC

algorithm, which is established to identify pseudo-links between variables $X_t^j \in \{X_t^1, \ldots, X_t^n\}$ and their respective sets of causal parent nodes $\hat{\mathscr{p}}(\mathrm{X_t^j})$ (Runge et al., 2019b). In this study, X_t^j represents all the variables including ΔFR and flood risk indicators. $\hat{\mathscr{p}}(\mathrm{X_t^j})$ means the causal parents (lagged adjacency) for variables. After three interactions, PC algorithm adaptively converges to relevant conditions that include the causal parents with the high probability. The second step is the MCI test, to test whether there's a relationship of Eq.(5.6) between time-shifted parents of $\mathrm{X_{t-\tau}^i}$ and the parents of $\mathrm{X_t^j}$ (Runge et al., 2019b).

$$\mathrm{MCI}: \mathrm{X_{t-\tau}^i} \not\perp \mathrm{X_t^j} \,|\hat{\mathscr{p}}(\mathrm{X_t^j})\backslash\{\mathrm{X_{t-\tau}^i}\}, \hat{\mathscr{p}}(\mathrm{X_{t-\tau}^i}) \tag{5.6}$$

The MCI test is the most significant difference between the original PC algorithm and PCMCI. The additional conditions on the parents $\hat{\mathscr{p}}(\mathrm{X_{t-\tau}^i})$ in MCI leading to autocorrelations, so that controlling false positive rates at the expected level (Runge, 2018; Runge et al., 2019b). While detecting the causal network structure is the main goal of PCMCI, the MCI test can provide a well-interpretable notion of a normalized causal strength (Runge et al., 2019b). Hence, the causal link strength in the PCMCI framework is given by the partial correlation value (ParCorr) of the MCI test, which is between -1 and 1 (Krich et al., 2020).

5.3 Results

5.3.1 Comparison of flood risk assessments between two model scenarios

The flood risk assessments based on the improved model incorporating the wetland indicator produced reasonable results when compared with those from the flood risk assessment model without the wetland indicator. Figures 5.3 to 5.7 present the comparisons of flood risk spatial distribution between those two models in the selected years, while the corresponding area changes are detailed in Tables 5.2 to 5.6.

5.3.1.1 Taihu Lake Basin

Figures 5.3a, 5.3b and Table 5.2 demonstrate the area with the very high flood risk level expanded 819 km^2 with wetland effects in the eastern TLB in 1991, which was the year with

the highest flood risk. The TLB was confirmed to experience the large flood disaster caused by the heavy precipitation in 1991, filling up inlets and outlet channels and lakes, as well as lake reclamation (Sun and Mao, 2008). As a result, the combination of high precipitation and small wetland areas diminished water storage capacity, contributing to the higher flood risk in 1991. In 2005, the overall flood risk level in the TLB was much lower than that in 1991 and the highest level is medium (Figures 5.3c, 5.3d and Table 5.2). Comparing Figure 5.3d with Figure 5.3c, the medium-level flood risk shrank the area of 771 km^2 after adding the effects of wetlands around Yangcheng Lake and north of Taihu Lake in 2005. At the same time, the area of very low flood risk expanded 321 km^2 with wetland impacts, mainly concentrated in the southeast corner and southern region of the TLB. The differences in flood risk with wetland effects between these years are primarily attributed to the significant increase in wetland area in 2005, reached 5,168 km^2 (Guo et al., 2024), due to the expansion of aquaculture ponds around Taihu Lake and Yangcheng Lake (Figures 5.8a and 5.8b). The local government started to encourage aquaculture production in these regions due to their ideal geography since 1990s, and reached the peak after 2000 (Cai et al., 2013; Liu and Zhang, 2017). Consequently, the area of aquaculture pond was much larger in 2005, thus playing the important role as a sink to reduce the flood risk.

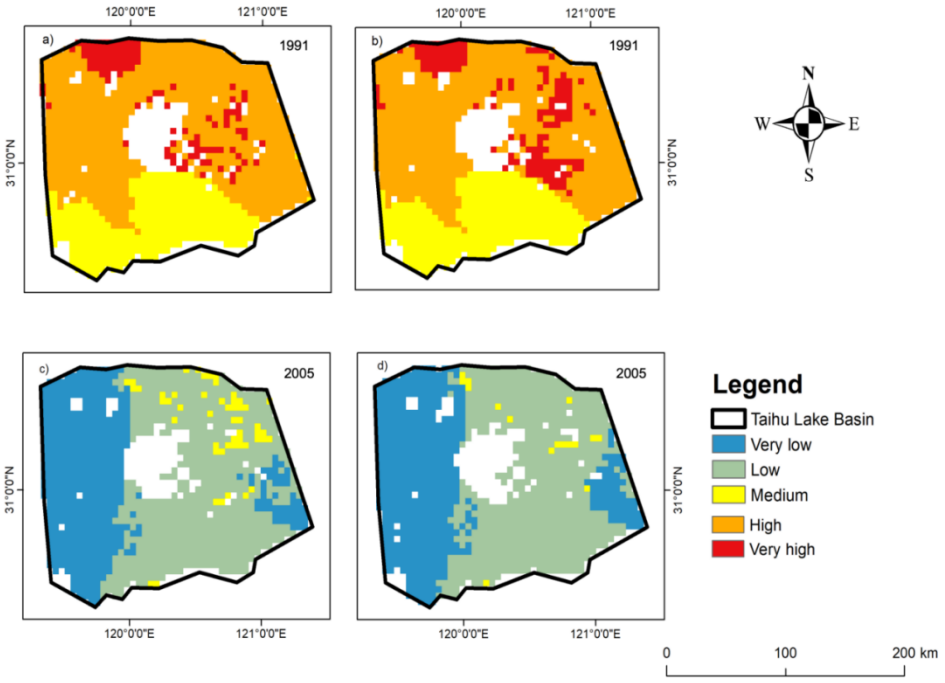

Figure 5.3: Flood risk spatial distribution maps in a) 1991 and c) 2005 without wetlands; b)

1991 and d) 2005 with wetland effects of the Taihu Lake Basin.

Table 5.2: The flood risk assessment area (km^2) in 1991 and 2005 of the Taihu Lake Basin.

	1991	1991 with wetland effects	2005	2005 with wetland effects
Very low	0	0	10778	11099
Low	0	0	14249	14699
Medium	7126	7049	1114	343
High	16457	15715	0	0
Very high	2375	3194	0	0

5.3.1.2 Wanjiang Plain

The comparison between flood risk results of two models in the WP in 2003 and 2010 are demonstrated in Table 5.3 and Figure 5.4. It showcases that the very high flood risk area expanded 6,069 km^2 with wetland effects in the year of 2003 with the high precipitation, mainly around Chaohu Lake; the high flood risk region expanded in the central area of the WP with an area of 577 km^2 in 2003. The Chaohu Lake Basin is a flood prone area located in the central part of Anhui Province, the area around Chaohu Lake contains typically low flood disaster resilience because of the low-lying terrain (Sun et al., 2016). In Figures 5.4c and 5.4d, the spatial distribution of very-high flood-risk areas demonstrates the significant shrinkage from 16,027 km^2 to 15,194 km^2 in the southwestern part of the Chaohu Lake Basin with wetlands implications in 2010, which is the area with the relatively higher flood disaster resilience than other regions when the local precipitation reduced (Sun et al., 2016). However, because of the weak flood disaster resilience around Chaohu Lake, the high flood risk area still expanded with the wetland effects in 2010. Although the central WP is vulnerable to flood risk because of the low-lying terrain, its isolated lakes have been shown to act as natural sinks, storing stormwater under normal conditions (Acreman and Holden, 2013). However, the agricultural development in the WP, especially around Chaohu Lake since the 1970s, led to significant wetland reclamation, shrinking lakes and tidal flats, and converting them into farmland (Dong et al., 2022). Between 2000 and 2010, approximately 58 km^2 of lakes were

converted to farmland and construction land (Dong et al., 2022). Consequently, the ability to capture and hold rainfall became weak in the floodplain, thus promoting the high flood risk surrounding Chaohu Lake (Acreman and Holden, 2013). Comparing wetland distribution in 2003 and 2010 (Figures 5.8c and 5.8d), the expansion of aquaculture ponds in the eastern corner and central WP near the Yangtze River in 2010 contributed to the increased very low flood risk area in the eastern corner and the reduced high flood risk area in the WP central region near the Yangtze River in Figures 5.4c and 5.4d.

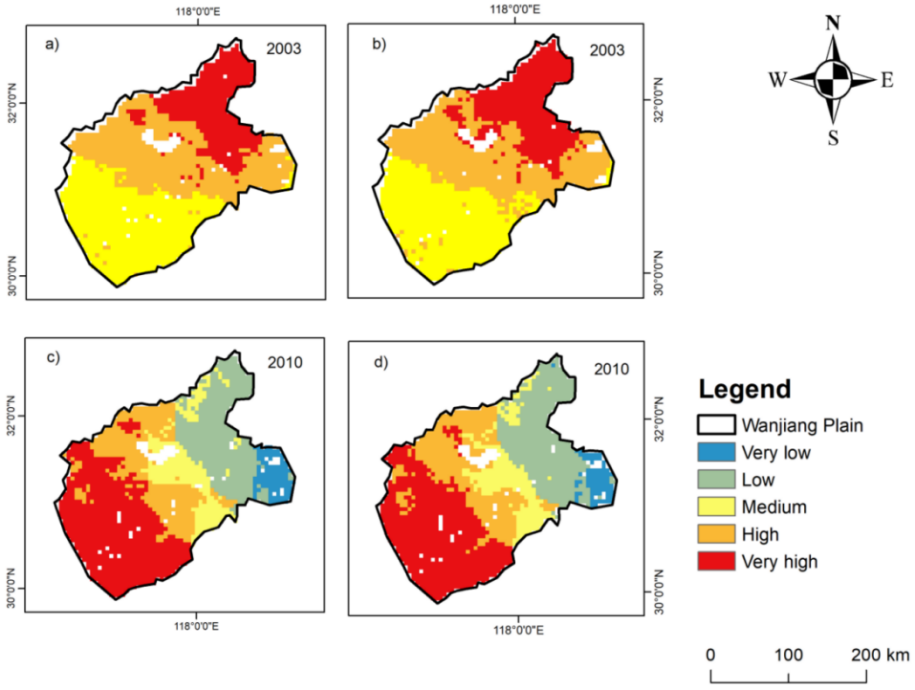

Figure 5.4: Flood risk spatial distribution maps in a) 2003 and c) 2010 without wetlands; b) 2003 and d) 2010 with wetland effects of the Wanjiang Plain.

Table 5.3: The flood risk assessment area (km^2) in 2003 and 2010 of the Wanjiang Plain.

	2003	2003 with wetland effects	2010	2010 with wetland effects
Very low	0	0	2158	2265
Low	0	0	9723	9916
Medium	16049	10557	5364	5320
High	15664	15087	8890	9467
Very high	9510	15579	16027	15194

5.3.1.3 Poyang Lake Basin

PLB experienced severe flooding in 1994, more than half of the PLB (26,308 km^2 and 29,093 km^2 out of 54,618 km^2 in Table 5.4) was covered by the very high flood risk level spreading outward from Poyang Lake as the centre (Figures 5.5a and 5.5b). The year of 1994 is an extremely wet year with the very large precipitation, thus coupling all the wetlands to become floodplains. The interconnected seasonal lakes surrounding Poyang Lake, which typically retain water, contributed to this increased flood risk due to their lower water storage capacity compared to permanent lakes (Li et al., 2019). Although lakes generally play a critical role in stormwater storage and control in the PLB, the limited capacity of seasonal lakes led to a 2,585 km^2 expansion in the very high flood risk area in 1994 under heavy precipitation conditions (Li et al., 2019; Shankman et al., 2009). In contrast, comparing Figures 5.6d and 5.6c, the area of very high flood risk decreased by 1,642 km^2 in 2006 after accounting for wetlands. This reduction was primarily observed in the southwestern region of the PLB, where the expansion of water bodies (Figure 5.8f) increased flooding water storage capacity. Wu et al. (2022) confirmed that the areas with consistently very-high flood risk are concentrated near Poyang Lake and Ganjiang River (southwest of Poyang Lake), aligning with the spatial flood risk distributions as shown in Figure 5.5 both models.

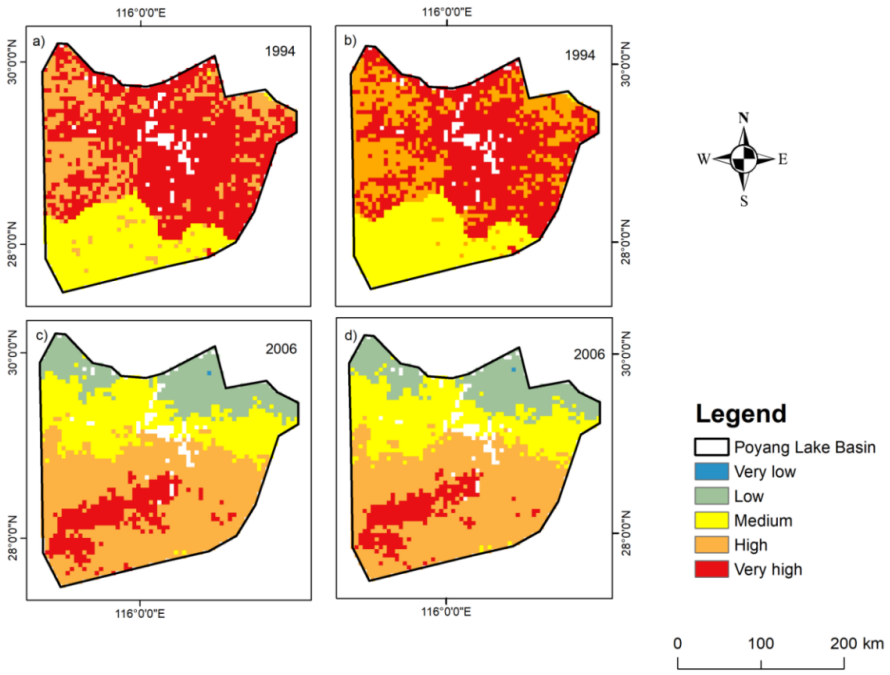

Figure 5.5: Flood risk spatial distribution maps in a)1994 and c) 2006 without wetlands; b)

1994 and d) 2006 with wetland effects of the Poyang Lake Basin.

Table 5.4: The flood risk assessment area (km^2) in 1994 and 2006 of the Poyang Lake Basin.

	1994	1994 with wetland effects	2006	2006 with wetland effects
Very low	0	0	22	22
Low	0	0	2824	3437
Medium	12969	12469	15938	15763
High	15341	13056	20492	21696
Very high	26308	29093	15675	14033

5.3.1.4 Dongting and Honghu Lake Basin

In a similar situation to the PLB, the highest flood risk regions in the DHB distribute around Dongting Lake as the center, and generally locate near rivers and lakes, has been confirmed by results of the GIS-based flood risk assessment in DHB from Wang et al. (2011). In 1998, Figure 6a demonstrates that the highest flood risk area is generally distributed in the north-eastern, and south-western corner of the DHB, as well as the south of Dongting Lake. The very high flood risk area decreased to the high flood risk level with wetlands implications in the southern region of Dongting Lake in Figure 5.6b. Table 5.6 supports this finding, showing a reduction of 587 km² in very high flood risk areas, alongside an increase of 610 km² in high flood risk areas in 1998 due to wetland effects. In 2009, Figures 5.6c, 5.6d, and Table 5.5 illustrate a significant expansion of high flood risk areas in the northeastern corner of the DHB around Dongting Lake, increasing by 6,898 km², with 65 km² transitioning to very high flood risk levels with wetlands input. As one of the most eco-areas, Dongting Lake plays a similar role in flood storage as Poyang Lake (Wang et al., 2011). Hence, The larger size of Dongting Lake in 1998 (Figure 5.8g) compared to 2009 (Figure 5.8h) contributed to more effective flood risk mitigation. Besides the large expansion of high flood risk area after adding wetlands in the DHB, the small area of very high flood risk observed in 2009 (Figure 6d) corresponds to regions of lake shrinkage and aquaculture pond expansion around Honghu Lake, northeast of Dongting Lake (Figure 5.8h). This suggests that the aquaculture ponds

around Honghu Lake could not compensate for the lost flood storage capacity caused by lake shrinkage.

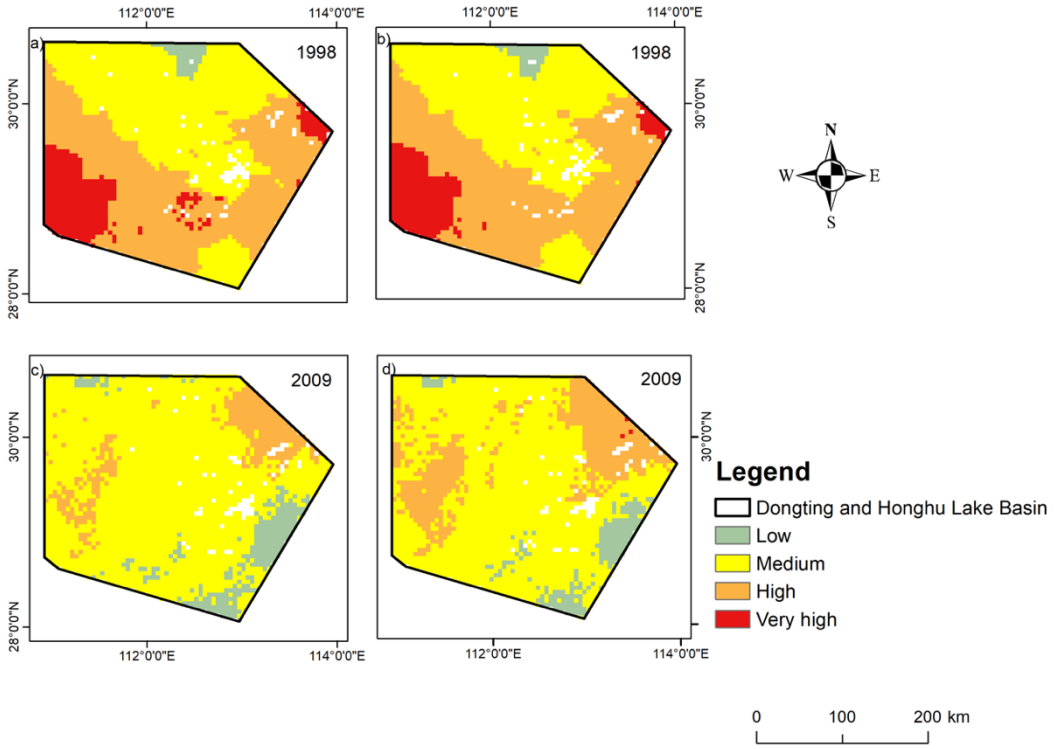

Figure 5.6: Flood risk spatial distribution maps in a) 1998 and c) 2009 without wetlands; b)1998 and d) 2009 with wetland effects of the Dongting and Honghu Lake Basin.

Table 5.5: The flood risk assessment area (km^2) in 1998 and 2009 of the Dongting and Honghu Lake Basin.

	1998	1998 with wetland effects	2009	2009 with wetland effects
Very low	0	0	0	0
Low	1262	1318	5810	4482
Medium	27048	26969	49808	44173
High	26808	27418	7268	14166
Very high	7572	6985	0	65

5.3.1.5 Sichuan Basin

Compared with other regions, the impact on the flood risk area distribution brought by wetlands is relatively smaller in the SB, mainly because of the much smaller area of wetlands

in this region. According to Figure 5.7 and Table 5.6, the high flood risk level area reduced 780 km^2 but expanded 195 km^2 in the centre of the SB after adding wetlands in 1998 and 2020, respectively. Besides, the very high flood risk level experienced a slight expansion with an area of 78 km^2 due to wetland effects in 2020. The wetland area in SB is limited, and the main wetland category is river, which restricts its capacity to function as a stormwater sink (Acreman and Holden 2013; Fu et al., 2013). Hence, downstream in the main rivers and river confluences of the SB, usually suffers serious flooding (Fu et al., 2013). At the same time, the shrinkage of wetlands in 1998 and their expansion in 2020 in the central SB resulted in a decrease in high flood risk in 1998 and an increase in 2020. Inland swamp is another major wetland category distributed in the YRB upstream (Fu et al., 2013). Figures 5.8i and 5.8j show that inland swamps are generally distributed in the western part of SB, which is close to the YRB source region. Although inland swamps contain limited impacts on the reduction of floods in the SB, the flood regulation and storage function of inland swamps are embodied in the upstream floods and slow down flood peak advance (Fu et al., 2013). This process reduces flood hazards downstream, which may explain some of the flood risk reduction associated with wetland effects in the SB (Fu et al., 2013).

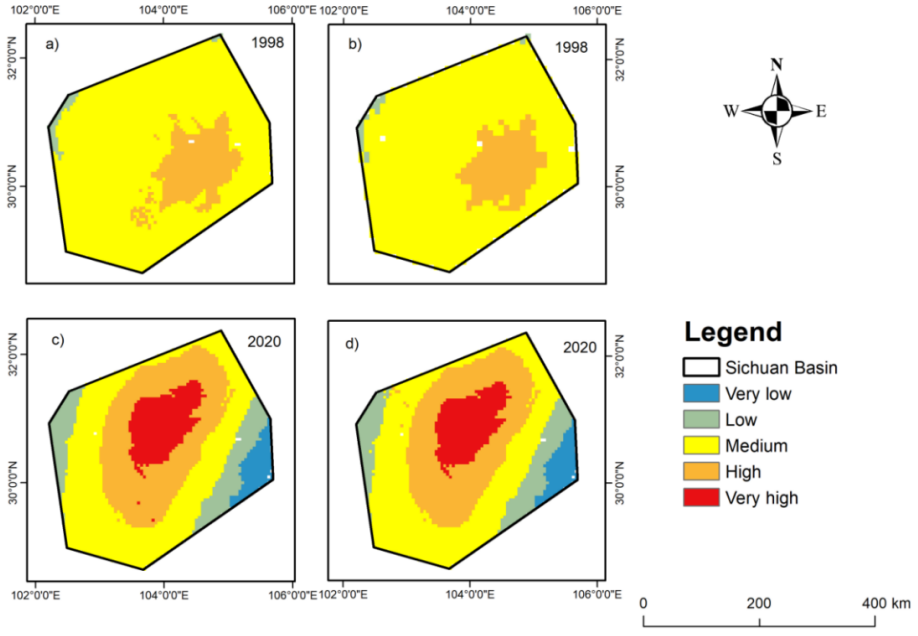

Figure 5.7: Flood risk spatial distribution maps in a) 1998 and c) 2020 without wetlands; b) 1998 and d) 2020 with wetland effects of the Sichuan Basin.

Table 5.6: The flood risk assessment area (km^2) in 1998 and 2020 of the Sichuan Basin.

	1998	1998 with wetland effects	2020	2020 with wetland effects
Very low	0	0	4238	4259
Low	1448	1229	11545	11437
Medium	79172	80171	39370	39305
High	14226	13446	28927	29122
Very high	0	0	10723	10680

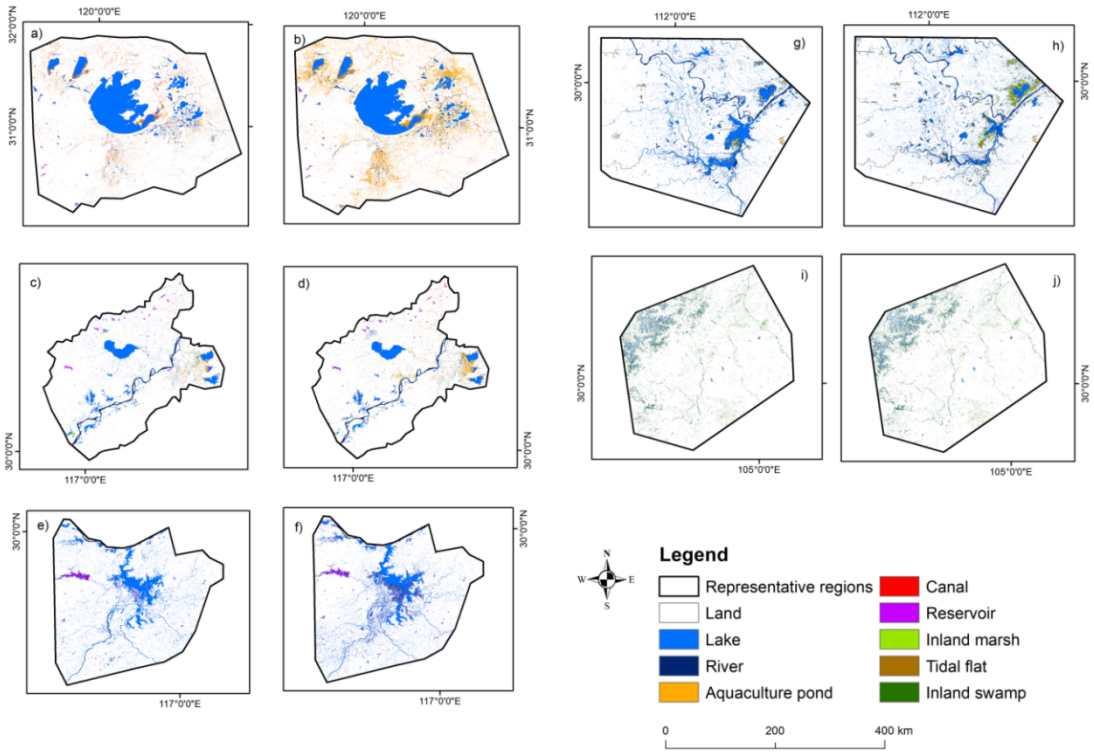

Figure 5.8: Spatial distribution maps of wetland categories in corresponding years of the Taihu Lake Basin: a) 1991 and b) 2005; Wanjiang Plain: c) 2003 and d) 2010; Poyang Lake Basin: e) 1994 and f) 2006; Dongting and Honghu Lake Basin: g) 1998 and h) 2009; Sichuan Basin: i)1998 and j) 2020.

5.3.2 Annual flood risk variations with wetland effects

Figures 5.9 demonstrates the ΔFR of each flood risk level from 1985 to 2021 in the five flood prone regions, derived from the improved flood risk assessment model. It also includes the

corresponding wetland area from the LTWCD_YRB dataset (Guo et al., 2024) and the cumulative maximum three-day precipitation.

The wetland area in the TLB exhibited a growing trend, reaching its peak in 2005. Prior to this peak, the relatively limited wetland area contributed to a reduction in low and very low flood risk areas, while simultaneously increasing the extent of high and very high flood risk areas, particularly for the years with high precipitation. For instance, in 1991 and 1998, high precipitation coupled with insufficient wetland area resulted in an increase of very high and high flood risk areas by 2.2% and 4.3%, respectively. Conversely, the very low flood risk area experienced a significant decline, with a reduction of 14.3% in 1998. When the wetland area expanded to the maximum value in 2005, both the very low and low flood risk areas increased 1.3% and 0.6%, respectively. Notably, the very high and high ΔFR areas were zero, indicating that sufficiently large wetland areas will not affect the high and very high flood risk zones when the precipitation level is low. In years with both relatively large wetland areas and high precipitation, such as 2015 and 2019, the very high and high flood risk areas under wetland effects reduced 2.9% and 3.4%, respectively. This demonstrates the significant role of expanded wetlands, particularly aquaculture ponds and lakes, in stormwater storage and flood risk mitigation.

In the WP, the wetland area increased continuously with fluctuations between 1985 and 2021. The area of each flood risk level showed the minimal variation under wetland effects before 1998 due to the relatively low precipitation. In this period, the notable ΔFR occurred in 1991, 1996, and 1998. The shrinkage of wetland area and the increase of precipitation caused the decrease of 1.1% low flood risk area in 1991 and the increase of 0.8% very high flood risk area in 1996, while the high flood risk area expanded 5.8% in 1998. Afterwards, the ΔFR for the very high flood risk area peaked at 14.7%, driven by wetland shrinkage. Concurrently, the medium flood risk area decreased 13.3% in 2003 with wetland effects, while no ΔFR was observed for low and very low flood risk levels due to extremely high precipitation. After 2005, the wetland area started to increase continuously, mitigating the flood risk. Typical

years with the large wetland area include 2013, 2016, 2017, and 2020. The ΔFR area for the very high level decreased 2.6%, 2.9% and 0.3% in 2013, 2017, and 2020, respectively. The area of very low and low ΔFR increased 7.2% and 1.5% in 2013 and 2017, respectively. Despite the large wetland area, the very high ΔFR area in 2006 increased 0.4% under the high precipitation. It means that wetlands in the WP lose the flood storage capacity under extreme precipitation conditions.

Wetlands in the PLB fluctuated throughout the period from 1985 to 2021, peaked in 1998, the year marked by the extreme precipitation and severe flood disaster. Similar to the condition in the WP, wetlands in the PLB transformed into floodplains during this extremely rainy year, losing their capacity to store stormwater despite the large wetland area. In other years, wetlands in the PLB generally play an important role in mitigating flood risks. For example, when the precipitation decreased in 1999 and 2016, the large wetland area contributed reductions in very high ΔFR areas by 6.3% and 4.3%, respectively. Meanwhile, it led to a 0.1% increase in very low ΔFR areas in 1999 and an 8.7% increase in low ΔFR areas in 2016. Oppositely, in years with the relatively smaller wetland area, such as 1994, 1995, and 2011, wetlands contributed to expansions of the very high ΔFR area by 5.1%, 4.5%, and 0.6%, respectively.

The variation of high and very high flood risk area caused by wetlands in the DHB primarily occurred during the following two periods with high precipitation: 1996-1998, 2007-2021. In the rest of years, the high and very high ΔFR kept zero, indicating that changes in wetland areas did not affect these flood risk levels. Similar to wetlands in the TLB, WP, and PLB, wetlands in the DHB generally served as flood water storage, mitigating flood risks. Wetlands expansion in 1998 and 2015 reduced the very high and high flood risk area by 0.9% and 0.5%, respectively, while increasing low flood risk areas by 0.09% in 1998 and 0.24% in 2015. Conversely, the largest increase in very high ΔFR (2.2%) occurred in 2011, a year with the high precipitation but relatively small wetland areas.

Figure 5.9e shows that both the wetland area and its variation in the SB remained small from

1985 to 2021. When the wetland areas expanded, the high and very high ΔFR increased as well. For instance, the wetland expansion in 1996 and 2020 led to a 0.4% increase in the very high flood risk area and a 0.3% increase in the high flood risk area, respectively. Unlike the other four flood-prone regions, which contain numerous lakes and ponds, river is the main wetland category covering most areas of the SB (Figures 8i and 8j). Therefore, due to the smaller water storage capacity of rivers and their lower elevation in the SB, the expansion of river areas driven by the large precipitation in the upstream, resulted in the increased flood risk under the wetland effects in the downstream areas and river confluences of the SB (Fu et al., 2013). Conversely, the wetland reduction in 1998 and 2011 decreased the high flood risk area by 1.4% and 0.4%, respectively. Comparing 1998 and 2011, wetland areas were similarly low, but the higher precipitation in 1998 made the high flood risk area be more sensitive to wetland effects than in 2011. Additionally, the low and very low flood risk areas showed greater variations in 2011 compared to 1998.

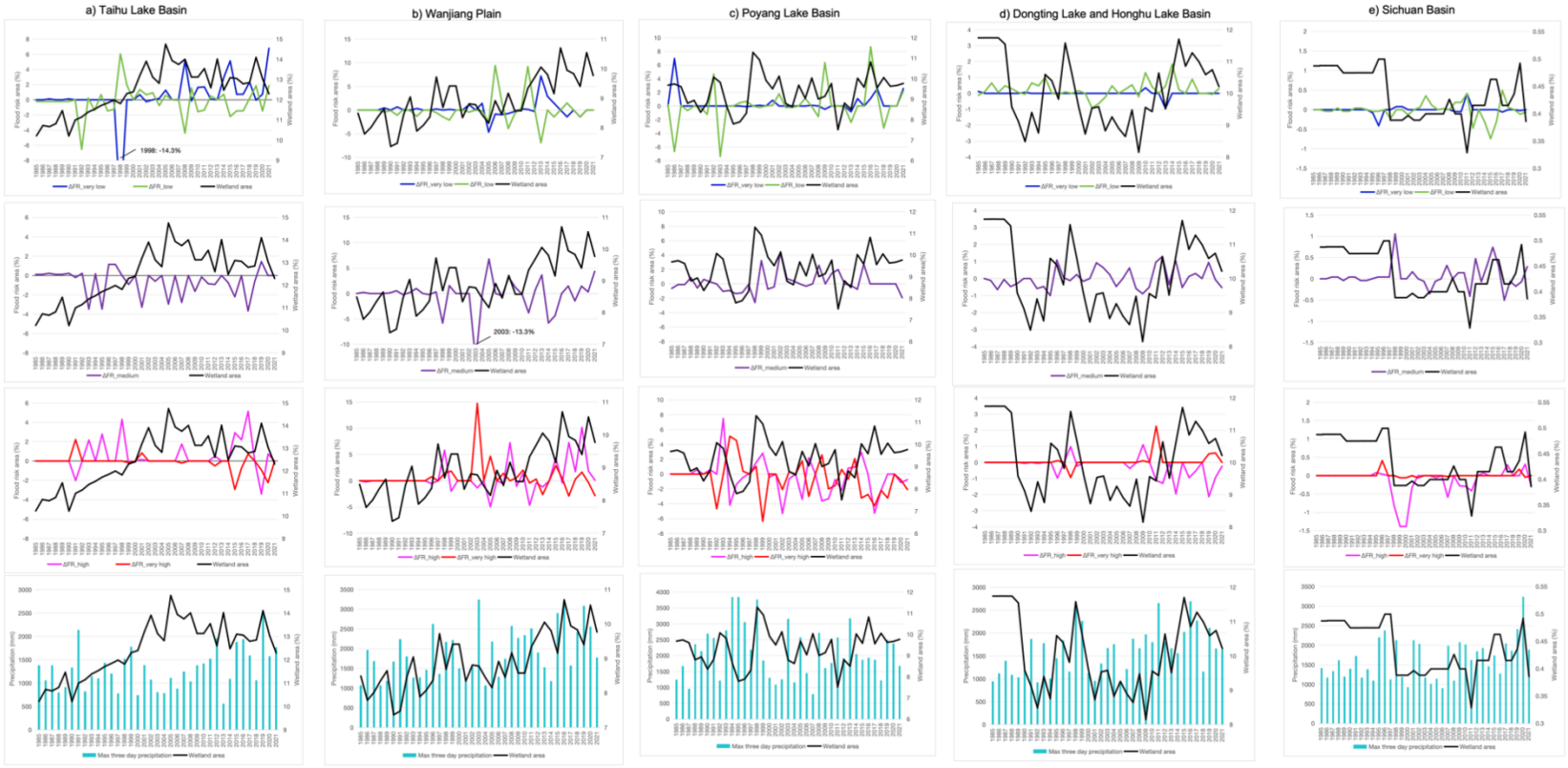

Figure 5.9: Annual ΔFR of very low, low, medium, high, very high food risk levels, the corresponding wetland area and the cumulative maximum three-day precipitation in the a) Taihu Lake Basin; b) Wanjiang Plain; c) Poyang Lake Basin; d) Dongting and Honghu Lake Basin; and e) Sichuan Basin from 1985 to 2021.

5.3.3 Causal relationships between each flood risk indicator and ΔFR

The causal relationship between the indicators and ΔFR of all five levels are examined based on the PCMCI algorithm. Their causal relation strength are numbers on the arrow. The results of ΔFR_{low} and ΔFR_{medium} are demonstrated in Appendices 5.1 and 5.2, respectively. Indicators that contain the causal relationship with ΔFR_{low} and ΔFR_{medium} are very limited. Additionally, *p*-values for the causal relation results of ΔFR_{low} and ΔFR_{medium} are all higher than 0.05 throughout the statistical significance test (one side t-test), indicating the lack of the statistical significance. Hence, this study focuses on causal relation results of dominant flood risk indicators with $\Delta FR_{very\ low}$, ΔFR_{high}, and $\Delta FR_{very\ high}$, with values equal to or greater than 0.44 (Figures 5.10-5.12). The corresponding *p*-values of them are lower than 0.05, confirming their statistical significance. Among all the indicators, cumulative maximum three-day precipitation (PR) is the only indicator that has the causal relationship with one of ΔFR levels (ΔFR_{high}) in all the five flood-prone regions.

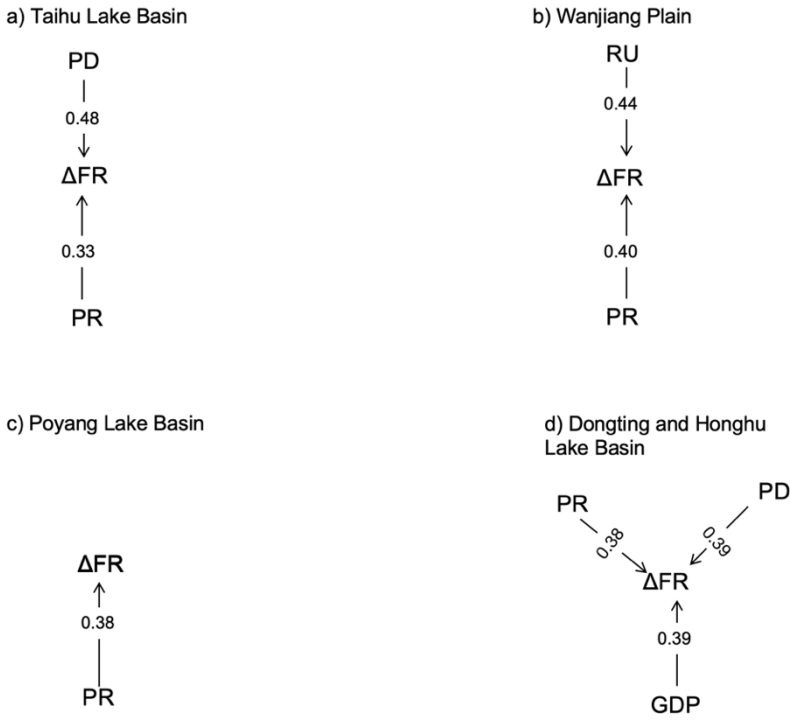

Figure 5.10: The causal relationships between the $\Delta FR_{very\ low}$ and indicators in the a) Taihu Lake Basin; b) Wanjiang Plain; c) Poyang Lake Basin; and d) Dongting and Honghu Lake Basin. No indicator exhibits a causal relationship with $\Delta FR_{very\ low}$ in the Sichuan Basin.

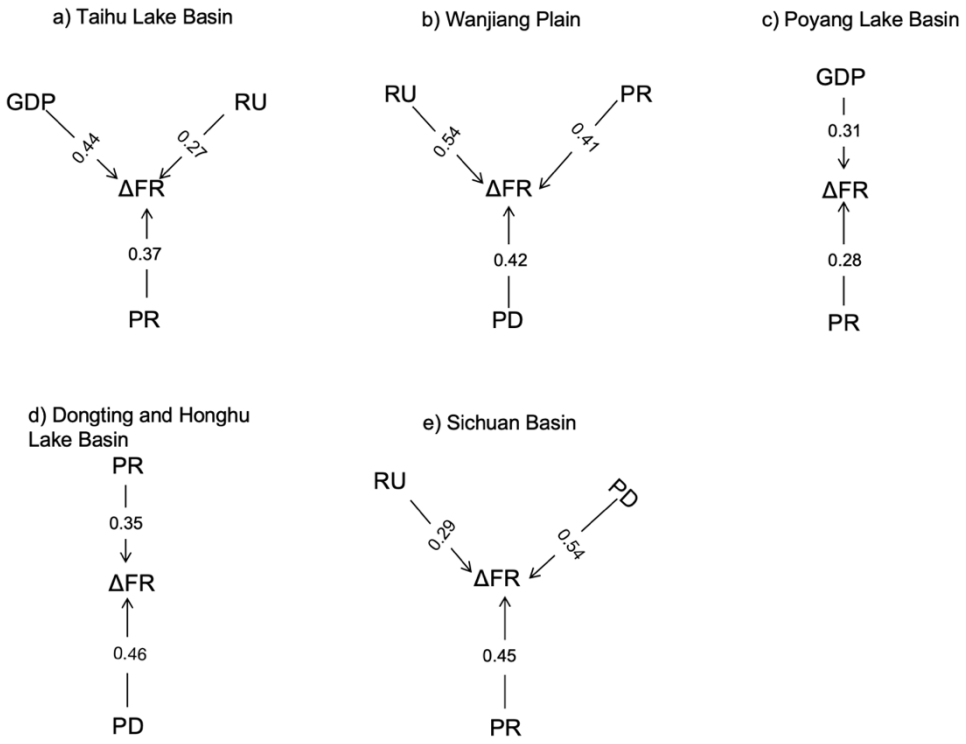

Figure 5.11: The causal relationships between the ΔFR_{high} and flood risk indicators in the a)Taihu Lake Basin; b) Wanjiang Plain; c) Poyang Lake Basin; d) Dongting and Honghu Lake Basin; and e) Sichuan Basin.

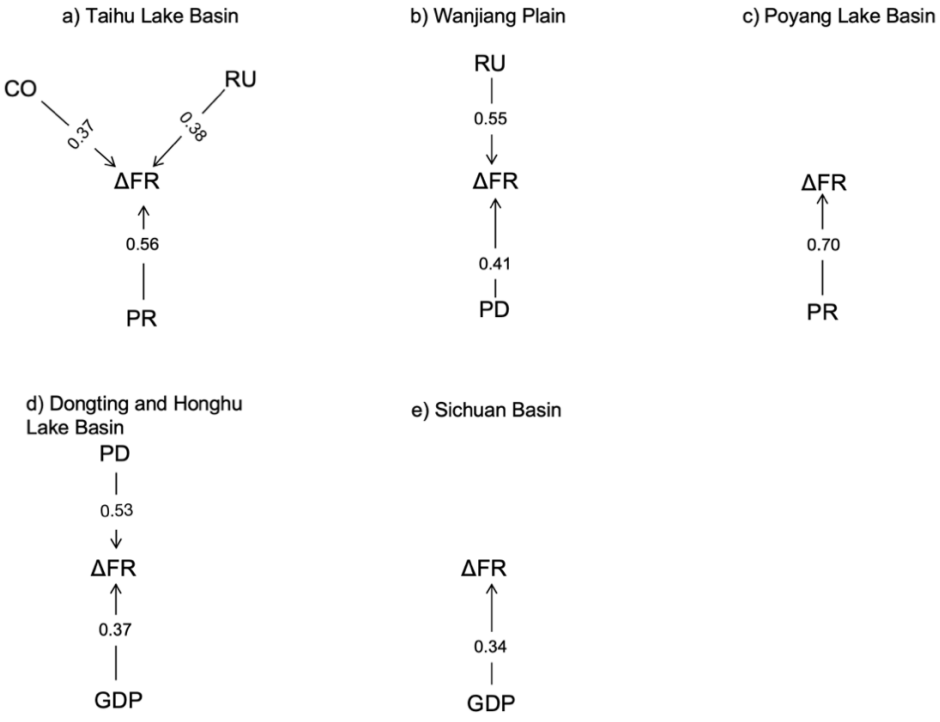

Figure 5.12: The causal relationships between the $\Delta FR_{very\ high}$ and flood risk indicators in the a) Taihu Lake Basin; b) Wanjiang Plain; c) Poyang Lake Basin; d) Dongting and Honghu Lake Basin; and e) Sichuan Basin.

In the TLB, population density (PD), GDP per capita (GDP), and PR display dominant causal relationships with $\Delta FR_{very\ low}$ (0.48), ΔFR_{high} (0.44) and $\Delta FR_{very\ high}$ (0.56), respectively. Among these indicators, the strength of the causal relation between PR and $\Delta FR_{very\ high}$ is the largest, with the highest statistical significance (the lowest *p*-value 1.9×10^{-11}), which means PR is the most significant ΔFR indicator in the TLB. The TLB is a region with the large area of wetlands and the extreme precipitation in rainy seasons caused by the subtropical monsoon climate, which makes the flood risk to be typically sensitive to precipitation (Liang et al., 2011). In addition, the TLB is the most economically developed region in the YRB, characterized by the rapid urbanization, the large PD, and the high GDP (Sun et al., 2023; Xu and Chen, 2023). As key flood exposure indicators, the high GDP and the large PD have driven rapid industrialization and urbanization, which have significantly increased pressure on flood risk (Sun et al., 2023; Xu and Chen, 2023). Consequently, it is reasonable that PD and GDP are dominant indicators of the $\Delta FR_{very\ low}$ and ΔFR_{high} in the TLB.

In the WP, RU is the indicator with the dominant causal relation with $\Delta FR_{very\ low}$ (0.44), ΔFR_{high} (0.54) and $\Delta FR_{very\ high}$ (0.55). Due to the large-scale wetland reclamation for the cultivation and urban construction in the WP, the local LULC has converted forestlands and shrubs to urban lands with the less vegetation coverage and the higher RU (Dong et al., 2022). Because of the special terrain in the WP, wetlands are concentrated along streams and the Yangtze River in the WP (Dong et al., 2022). As a result, the higher RU in this region more readily increases the water level of the Yangtze River compared to other areas, thereby exacerbating the flood risk.

In the PLB, PR is the only dominant causal indicator, it shows the strength of causal relation of 0.7 with the $\Delta FR_{very\ high}$. Hence, precipitation is the dominant flood risk indicator in the PLB, primarily due to the extreme annual precipitation driven by both of south-east and

south-west monsoons, as well as the more extensive floodplains compared to other regions (Liu et al., 2021; Wu et al., 2022).

In the DHB, population density (PD) is the only indicator that has the causal relation with ΔFR_{high}, and it is most important factor that affects $\Delta FR_{very\ high}$ (with the causal strength of 0.53). In recent years, urbanization has accelerated significantly in the DHB, the urbanization rate reached 54.8% in 2019 (Xiong et al., 2022). The hotspots cities are mainly located in the flood prone regions of the DHB around Dongting Lake (Xiong et al., 2022). As a result, the large PD in this region will typically cause the high and very high flood risk.

Similarly, PD in the SB is the dominant factor as well, the causal relationship with ΔFR_{high} is 0.54. The SB is one of the most densely populated regions in China (Liu et al., 2017). Human activities are concentrated in the east-central low mountain area, which has been the densely populated area throughout the history of China and also a high flood risk zone (Liu et al., 2017). The relative study has confirmed the strong correlation between human activities and floods in the SB (Liu et al., 2017).

Precipitation, runoff and vegetation cover factor, GDP, and population density are the dominant indicators not only in the YRB, but also in other flood prone basins of China and worldwide. Precipitation is the most common and dominant flood risk indicator in the major wetland basins such as the Yellow River Basin and Lijiang River Basin of China, Tapi River Basin in India, and Lancang-Mekong River Basin which spans over multiple Southeast Asian countries (Ramkar & Yadav, 2021; Sun et al., 2024; Ziwei et al., 2023). Vegetation cover changes caused by the rapid urbanization in the Teunom watershed of Indonesia, and the watershed north of Charlotte in the United States are the most dominant indicator of local flood risk (Banjara et al., 2024; Sugianto et al., 2022). GDP and population density are the two key factors that contain strong positive correlations with several flood disasters among a number of cities in China, India, and other rapidly urbanizing countries (Wang et al., 2021).

5.3.4 Model validation

Historical statements and data regarding the flood spatial distribution over these five flood prone regions in the YRB are used to verify the accuracy of the improved flood risk model in this study. In 1991, the levels of high and very high flood risks covered most areas of the TLB (Figure 5.3b). It is consistent with the major TLB flood disaster occurred in 1991 because of the heavy precipitation and the decline in the capacity of flood water storage and drainage of wetlands (Sun and Mao, 2008). Through the flood spatial distribution data, Yu et al. (2012) confirmed that most of flooded areas in 1991 were distributed on the eastern side of Taihu Lake, as shown in Figure 3b. As a number of drainage projects and aquacultural ponds were constructed in 2005, the overall flood risk became relatively low, thus improving the local flood control (Cai et al., 2013; Zhang et al., 2019). These changes in 2005 can be demonstrated by the flood risk distribution map in Figure 3d that shows the flood risk levels of very low, low, and medium in the TLB , and the overall decreasing trend of the very high flood risk area under wetland effects as illustrated in Figure 9a.

The lake wetland dynamics analysis of the WP provided by Dong et al. (2022) indicates that the high flood risk area in the WP area was generally distributed in regions with a high density of lake wetlands, such as the northeastern WP around Chaohu Lake, and the southern corner of the WP, which is covered by a number of lakes. These regions lost 120 km^2 of lake wetlands due to the agricultural development after 2000, leading to an increase in the flood risk (Dong et al., 2022). This situation is similar to the expansion of high and very high flood risk areas around Chaohu Lake in 2003 and 2010 after the inclusion of wetland input (Figure 5.4) and verifies the general increase of the high flood risk area with wetland effects after 2000 in Figure 5.9b.

The flood risk spatial distribution maps of the PLB, generated in this study using the improved model, can be verified by previous flood risk assessments of this region. Previous research has shown that the higher flood risk areas were distributed around Poyang Lake, while the areas with the lower flood risk were found in the surrounding regions during 2000-2020 (Wu et al., 2022; Zhu et al., 2024), In 1994, an extreme precipitation event resulted in widespread very high flood risk across the PLB, primarily due to the relatively low

stormwater storage capacity of the interconnected seasonal lakes surrounding Poyang Lake (Li et al., 2019). This finding is consistent with the flood risk distribution as shown in Figure 5b. Under normal conditions, lakes in the PLB serve as stormwater storage areas, allowing the low and medium flood risk areas to recover, and accounting for 35.5% of the PLB area (Zhu et al., 2024). The flood risk assessment results for 2006 (Table 5.4) further validate this finding by comparing their flood risk areas with Zhu et al. (2024). The low and medium flood risk areas of this study account for 34.9% of the PLB area, which is generally consistent with the findings of Zhu et al. (2024).

The flood risk spatial distribution of the DHB based on the improved model in this study (Figures 6b and 6d) is consistent with findings of Wang et al. (2011). Most of the Dongting Lake region is at the medium flood risk level, while the high and very high flood risk areas are primarily distributed in the northeastern, central, and southwestern parts of the DHB. The expansion of the high and very high flood risk area around Honghu Lake after incorporating wetland area as a model input was also found by Liu et al. (2013). Our study confirmed the flood risk had increased in the Honghu Lake region over the last 50 years due to the interacting effects of wetland dynamics caused by the lake reclamation and aquacultural development under heavy precipitation conditions.

For the SB, results in Figure 5.7 are supported by the risk assessment of flood disaster in Sichuan province from Guo et al. (2023). This indicates that flood risk is higher in the central and northeastern parts of the SB, but lower in the western region. According to Fu et al. (2013), wetlands have limited impacts on flood risk in the SB because wetlands upstream in the YRB are primarily distributed in the source region, where the probability of heavy precipitation is low. Consequently, the smaller spatial distribution changes after adding wetlands input (Figure 5.7), along with the limited long-term variations of ΔFR in the SB (Figure 5.9e), compared with the other basins, can be verified.

5.4 Discussion

5.4.1Uncertainties of this study

The flood risk assessment in this study includes the entire YRB, making data collection for flood risk indicators more complex than if the model was for a specific flood-prone region or administrative area. For example, some socio-economic indicators used in the model developed of this study, such as local financial revenue, per capita resident savings, and medical service level, were obtained from the statistical yearbook and represented total or average values for an entire administrative area. These data lack the detailed information inside the administrative area and thus cannot reflect the spatial distribution information. However, the rasterization process applied in this study helps overcome this limitation by breaking down administrative boundaries and enabling the spatial distribution of flood risk across the entire study region, thereby reducing this uncertainty. Besides, the flood risk assessments at regional or macro-scales require the detailed topographical information, different characteristics of flood disasters, and both of direct and indirect socio-economic losses in the study region (De Moel et al., 2015; Zhang et al., 2020). Consequently, given the complexities involved in modeling the large and dynamic region, indicators in the flood risk assessment model in this study may not comprehensively cover all flood risk driving factors in the YRB.

Zhang et al. (2020) defined the drainage density as the ratio of main and tributary streams to the area. However, in the improved flood risk assessment model, the replacement includes not only mainstreams and tributaries but also other water bodies, such as lakes, aquaculture ponds, and reservoirs. In our study, the weight of the substituted indicator was kept constant due to its minor impact on the flood risk assessment results, given its relatively low assigned weight (3.9%). It may introduce potential uncertainties in the model results because of the absence of a new AHP questionnaire. To justify this uncertainty, a sensitivity analysis for the replaced indicator in the flood risk assessment model was conducted. Sensitivity analysis is used to assess the extent to which an output is influenced by variations in a specific input (Chen et al., 2013). Therefore, it can be applied to determine whether the flood risk result is sensitive to weight dynamics of wetland density. The weight range used in the sensitivity test is set between 2% and 20% (the equal weight of the 13 flood risk indicators is 7.7%). As shown in Figure 5.13a, the results indicate that the changes in the weight of wetland and drainage

density can only result in minor variations in the flood risk assessment within the model. The largest change in the annual average flood risk areas of the five flood risk levels was 0.2%, 1.2%, 4.2%, 4.6%, and 1.9% in the TLB, WP, PLB, DHB, and SB, respectively (Figure 5.13b).The uncertainty is relatively higher in the PLB and DHB regions compared to the TLB, WP, and SB regions, due to the more abundant wetlands in those areas. Overall, the flood risk results in this study are not sensitive to weight variations of wetland density. This result is supported by the sensitivity test of the flood risk assessment in Chongqing, which shows that changes in the weight of river network density led to a little modification in the flood risk (Cai et al., 2021).

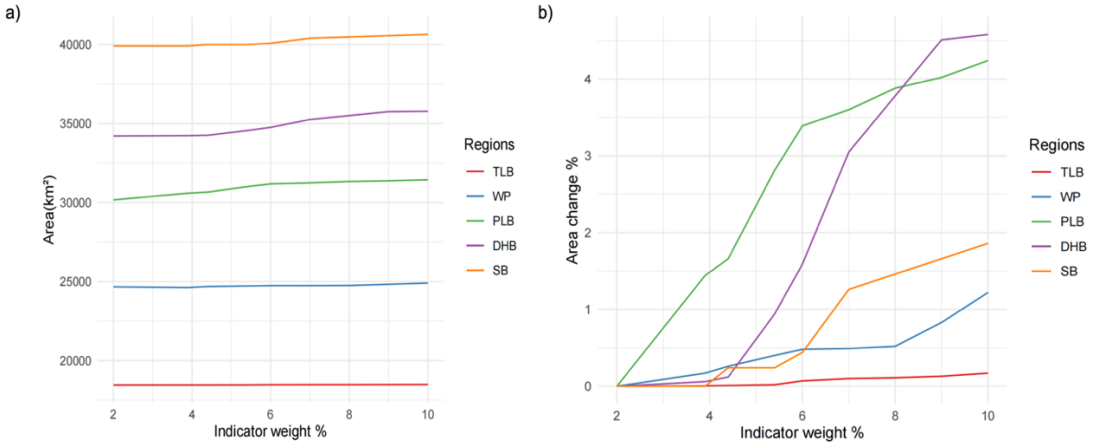

Figure 5.13: The sensitivity test for wetland density in the wetland-related–flood risk assessment model. The X-axis indicates the weight of the wetland density; the Y-axis of a) indicates the corresponding flood risk area, b) indicates the changes in the flood risk areas.

Beyond that, the use of fixed weights for particular indicators across the entire YRB over the long term may introduce uncertainties to the flood risk assessment results. The weights of some indicators should be spatially or temporally dynamic. For example, indicators related to economic development, such as GDP per capita, population density, local financial revenue, per capita resident savings, and medical service level, may carry greater importance in regions experiencing rapid economic growth. The TLB area, regarded as the region with the most

developed economy and the greatest urbanization in China (Xu and Chen, 2023), may require higher weights for relevant flood risk indicators than other flood-prone regions. In addition, some indicators may exhibit temporal dynamics. For instance, the weight of precipitation should be higher in years when severe flood disasters occurred (e.g., 1998, 2008, and 2016) (Zhang et al., 2020). Therefore, incorporating indicator weight dynamics into the AHP process should be a key consideration in the model assumption for the large-scale long-term flood risk assessment in future studies.

The flood risk assessment at large regional scales will generate different results under variable climate scenarios (Shared Socioeconomic Pathways (SSP) and Representative Concentration Pathways (RCP)), despite using the same flood risk indicators in the model (Chen et al., 2021b). It has been estimated that flood risks are higher under the SSP5-RCP8.5 than other scenarios using the same multi-index flood risk model. This is primarily due to the larger projected precipitation, GDP, and population density under the high emission scenario (Bai et al., 2019; Chen et al., 2021b; Peng and Li, 2021). The model of this study focuses solely on the YRB flood risk assessment by using the historical data without considering the impacts of different climate scenarios. Therefore, the future research should evaluate the YRB flood risk under different climate scenarios, to explore climate change effects on flood risk dynamics in this region.

5.4.2 Relevance of existing flood management frameworks

The Three Gorges Dam (TGD), located in the YRB midstream, is one of the largest dams in the world (Guo et al., 2012) and plays a significant role in flood control within the YRB (Hao et al., 2019). Since its operation began in 2003, the TGD's impact on floodplains in the YRB middle and lower reaches (including the DHB, PLB, WP, and TLB in this study) has been evident (Sun et al., 2020). The general decreasing trend in the high or very high annual flood risk area under wetland effects after 2003 in the TLB, WP, PLB, and DHB (Figure 5.9), supports the TGD's role in mitigating flood risk. Taking the WP as an example, the very high flood risk area under wetland effects decreased continuously with some small fluctuations from +14.7% to -2.8% from 2003 to 2021. The TGD additionally contributes to a reduction in

the sediment transport in the Yangtze River, thus decreasing the river discharge (Guo et al., 2012). Therefore, changes in river discharge and water level of the Yangtze River affect the water storage capacity of lakes downstream by changing the blocking force of the river on outflows from lakes (Hu et al., 2007). As a result, the very high flood risk area generally increased in years with the extreme precipitation, due to the reduction of stormwater capacity of major lakes such as Dongting Lake, Poyang Lake, and Taihu Lake. For example, as demonstrated in Figure 5.9, the very high flood risk area affected by wetlands in the TLB in 1991 and the DHB in 2011 both increased 2.2%, corresponding to over 2000mm maximum three-day precipitation and the relatively small wetland areas. Additionally, $\Delta FR_{very\ high}$ in the PLB increased 5.1% in 1994, associated with an extreme maximum three-day precipitation of 3847mm.

In addition to the TGD, land use changes in the YRB plays a significant role in the flood risk change. Results of this study show that the vegetation cover change is the dominant indicator of flood risk under wetland effects in the WP, with the causal relation strength of 0.55, which is higher than other indicators. From an optimistic perspective, both of spatial and temporal results of this study confirm that wetlands in the YRB flood prone regions contain the ability to mitigate the flood risk during years with large wetland areas and normal precipitation, except for the SB, which has a limited number of lakes. For instance, in the TLB (2020), the WP (2013), the PLB (1999 and 2016), the DHB (2019), wetland areas were all relatively large. In these years, the high or very high flood risk areas affected by wetlands decreased significantly, with the $\Delta FR_{very\ high}$ of -2.2%, -2.6%, -6.3%, -4.3%, and ΔFR_{high} of -2.1%. This validated the effectiveness of land use management frameworks in China, such as the “Grain for Green Program” (Delang and Yuan, 2015) and “Returning Farmland to Lakes” (Ma et al., 2021) policies, in recovering flood storage capacity and expanding flood retention areas by preserving forests and wetlands in the YRB (Liu et al., 2024; Shen et al., 2023).

5.4.3 Wetland-related management suggestions to mitigate flood risks

This study provides some wetland-related management suggestions by considering flood risk spatial distribution results and dominant indicators of the flood risk assessment with wetland effects in the YRB flood prone regions.

In the TLB, flood risk distribution maps show that the very high flood risk area expanded due to heavy precipitation in the eastern TLB by using the improved flood risk model. Therefore, the reasonable allocation and management of aquaculture ponds, and the control of lake reclamation around Yangcheng Lake, and the southeast region of Taihu Lake are important. For example, the thorough groundwater drainage system of aquaculture ponds can be constructed to reduce flood risks and increase flood resilience in seasons of heavy precipitation. The protection of the Chaohu Lake Basin in the WP is significant because of the concentration of high and very high flood risk areas in this region, as indicated by the improved flood risk assessment model. Hence, it is essential to uphold the ban on lake reclamation caused by agricultural development in this area.

Results from the improved flood risk assessment model indicate that the flood risk around Poyang Lake is typically high when considering wetland effects. In this case, the lake reclamation caused by human activities such as urbanization and sand dredging around Poyang Lake should be controlled. This will ensure that Poyang Lake maintains its large stormwater storage capacity in extreme years with high precipitation. In the DHB, the high and very high flood risk areas were distributed around Dongting Lake and exhibited significant changes with wetland effects. Hence, similar to Poyang Lake, lake reclamation and human activities of Dongting Lake should be regulated to mitigate flood risks associated with wetland dynamics. Besides, the improved flood risk model finds that aquaculture ponds around Honghu Lake lead to a higher flood risk. Therefore, aquaculture ponds need to be reasonably managed to minimize the impacts on the water capacity of Honghu Lake, thus mitigating the flood risk of this region. The area of aquacultural ponds surrounding Honghu Lake expanded 766 km^2 from 2016 to 2021 (Han et al., 2023). Figure 5.9d shows that the year of 2016 had the lowest overall values of $\Delta FR_{very\ high}$ and ΔFR_{high} from 2016 to 2021. Therefore, the 766 km^2 of aquaculture ponds, accounting for 28% of the total aquaculture pond area in

2021, could potentially be restored to lake systems if necessary. In the SB, the expansion of high flood risk areas under wetland effects were distributed in the western region. To address the limited capacity for stormwater storage due to the scarcity of lakes and ponds in the SB, constructing additional artificial ponds and reservoirs in the western SB could improve the stormwater storage capacity of water bodies, thereby reducing pressure on rivers during periods of heavy precipitation.

Precipitation, vegetation coverage, GDP, and population density are dominant indicators contributing to the higher flood risk under wetland influences of the YRB. Hence, regions with the high precipitation, population density, and GDP per capita should be reasonably managed to mitigate flood risks affected by wetlands. The policy of returning farmland to lakes has expanded Dongting Lake by approximately 800 km², contributing to a reduction in flood-related losses from USD 39.46 billion in 1998 to USD 27.68 billion in 2020 (Jia et al., 2022). First of all, maximizing the floodwater storage capacity becomes a key issue for local managers to mitigate the flood risk. In addition to preserving the area of natural wetlands, constructing artificial ponds and lakes is an effective approach. However, in densely populated and economically developed urban areas, space for artificial water bodies may be limited. Therefore, the development of a 'Sponge City' (Sun et al., 2023) is a recommended approach for reducing flood risks in the TLB— a flood prone region characterized by the dense population and rapid urbanization (Xu and Chen, 2023). The Sponge City Approach has successfully reduced the flood losses of 35%-50% in the Sishui River Basin in Zhengzhou, compared to regions without such interventions (Peng et al., 2022). This strategy involves collecting and managing rainwater through the sunken green spaces, permeable ground materials, and extensive drainage systems (Guan et al., 2021). Similar to the TLB, the 'Sponge City' approach is recommended in the PLB to mitigate the high flood risk resulting from the extensive precipitation (Sun et al., 2023). The factor of runoff and vegetation cover is the dominant indicator influencing flood risk under wetland effects in the WP. Hence, the LULC in the WP area plays a significant role in mitigating flood risk under wetland influences. Generally, vegetation-covered land contains a lower runoff factor than non-vegetated waterbodies and urban areas (Zhang et al., 2020). Given the significant role of

vegetation retention in flood risk mitigation, as demonstrated in the Nenjiang River Basin (Wu et al., 2023a), restoring vegetation-covered wetlands in high flood risk areas of the WP could be an effective strategy for reducing flood risks associated with the wetland dynamics.

5.5 Conclusions

This research analyzes the effects of long-term wetland variations on flood risk assessments across the five flood prone regions in the YRB, by using the improved GIS-based spatial multi-index flood risk assessment model. The dominant indicators of flood risks under wetland effects are identified, alone with the practical suggestions for wetland-based flood risk management.

The results highlight that the wetland expansion in the TLB, WP, PLB, and DHB contributes to the decrease of high and very high flood risk area and the increase of very low and low flood risk area between 1985 and 2021, except some typical years with extreme high precipitation in the WP and PLB. While the wetland expansion in the SB has aggravated but limited impacts on the flood risk because of the unique wetland category of streams and the small area of wetlands. For the spatial distribution of flood risks with wetland effects, the eastern TLB demonstrates stormwater storage potential. Chaohu Lake and its surrounding areas are regions with high and very high flood risk under wetland effects in the WP. In the PLB, high and very high flood risk areas cover more than half of the region. the weak stormwater storage capacity of seasonal lakes surrounding Poyang Lake increases flood risks during years of heavy precipitation. The northeastern and southwestern regions of the DHB, including Honghu Lake, are the highly flood prone regions with wetland effects.

Each flood prone region contains different dominant flood risk indicators under wetland effects: Precipitation in the TLB and PLB, runoff and vegetation cover in the WP, GDP in the TLB, and population density in the TLB, DHB and the SB. Suggestions for improving the flood resilience include reasonably managing local wetlands, maximizing stormwater storage capacity in urban regions, controlling lake reclamation, increasing vegetation coverage, and prioritizing flood risk managements in highly precipitated and densely populated regions.

Chapter 6 Future flood risk assessments in the Middle-Lower Yangtze River Basin under climate and socio-economic scenarios

Highlights:

- We predict flood risks by applying a multi-index GIS-based model.
- Flood risk areas above the medium level will account for 40% of the MLYRB by 2100.
- There will be a northward expansion of the high and very high flood risk area.
- Jiangxi, Hunan, and Jiangsu should be prioritized to prevent the future flood risk.

This chapter is a reformed version of a manuscript submitted to *Natural Hazards*.

6.1 Introduction

Climate change has increased the frequency and intensity of floods and other natural weather-related events around the world (IPCC, 2021). By 2030, floods and other natural hazards can lead to significant economic losses, with total estimates reaching up to 415 billion USD annually worldwide (Mahmoodi et al., 2023). Therefore, numerous studies have focused on assessing the impacts of climate change on flood risks worldwide (Chen et al., 2021a; Dottori et al., 2020, Wing et al., 2022). Dottori et al. (2020) predicted that the economic losses of river flooding in Europe would be more than six times by the end of this century compared to the present at the 3°C global warming scenario if no mitigation and adaptation measures were implemented. Wing et al. (2022) showed a 26.4% increase in flood risk in the United States between 2020 and 2050 under the moderate climate change scenario. Chen et al. (2021a) projected that the area of the highest flood risk level would increase by 8.7% and 19.8% in the Pearl River Delta of China under the scenarios of Representative Concentration Pathway (RCP) 4.5 and RCP 8.5, respectively. In addition to the traditional RCP climate change scenarios, Shared Socioeconomic Pathways (SSP) scenarios were used to represent five different trends of the socio-economic development and human activities (Riahi et al., 2017). Several studies illustrated that the future prediction of flood risk must account for both climate change and human activities (IPCC, 2021; Li et al., 2020; Luo et al., 2023; Nguyen et al., 2022; Yosri et al., 2024; Zhou et al., 2019). Therefore, the combination of SSP and RCP scenarios needs to be considered in future flood risk assessments for understanding potential future climate change and its impact on society, to provide comprehensive flood mitigation and response strategies (Peng and Li, 2021).

The middle and lower reaches of the YRB (MLYRB) are the largest and one of the most abundant wetland ecosystems in China, with numerous lakes that play an important role in flood storage (Ma et al., 2023). However, the dramatically increased human activities have led to the serve shrinkage of lake wetlands in the MLYRB since the last century (Ma et al., 2023). Land use changes driven by wetland dynamics significantly affect flood regulation services in the MLYRB (Shen et al., 2023). Moreover, the annual plum rain season in the

MLYRB leads to the persistently high water levels in Dongting Lake, Poyang Lake, and Taihu Lake, making the MLYRB particularly vulnerable to large-scale flooding (Jia et al., 2022). As a result, the MLYRB is the region with the most severe flood disasters in China (Liu et al., 2023a). The food event occurred in the summer of 1998 caused the loss of 4150 people and 166 billion RMB (Liu et al., 2023a). Besides, the MLYRB is comprised by one of the most important economic zones in China: The Yangtze River Economic Belt (Pei et al., 2017). Therefore, due to significant land use changes in the MLYRB caused by the rapid urbanization, cities occupy large number of lands near wetlands, making them increasingly vulnerable to severe floods (Jia et al., 2022). As a critical region, it is essential to understand how future flood risks in the MLYRB will be influenced by both natural and socio-economic factors (Liu et al., 2023a; Ma et al., 2023). Given that, the flood prediction and management of Yangtze River mainly focuses in on the MLYRB (Jia et al., 2022).

The comprehensive prediction of future flood risk is based on the combination of simulated hazard components from climatic projections, as well as predicted vulnerability and exposure indicators under future climate scenarios (Liu et al., 2025a). At present, there are various methods for projecting the disaster risk, such as artificial intelligence based approaches including classic machine learning models (e.g., support vector machine, random forest, and multi-layer perceptron) (Chen et al., 2021b), and deep learning models (e.g., convolutional neural network and hierarchal deep neural network) (Liu et al., 2025b; Yosri et al., 2024), and multi-index decision analysis with the GIS technology (Abuzwidah et al., 2024; Peng et al., 2024). Among these methods, the GIS-based multi-index model with the fuzzy Analytic Hierarchy Process (AHP) was selected for the flood risk assessment in the MLYRB. The AHP approach offers the advantage of effectively addressing uncertainties in decision-making processes involved in quantitative assessments (Peng and Li, 2021). Besides, the integrated flood risk assessment by using the multi-index model enables a comprehensive consideration of various natural and socio-economic factors, such as land use changes, GDP per capita, resident savings, and the coping capacity of populations, in a large-scale study area with the complex topography and socio-economic conditions (Liu et al., 2025a; Zhang et al., 2020).

Several studies have assessed flood risk related with the MLYRB by using the GIS-based multi-index model, such as the flood risk of the Poyang Lake Basin (Wu et al. (2022), the Dongting Lake Basin (Wang et al., 2011), and the flood risk assessments and predictions of the entire YRB (Guo et al., 2025; Peng and Li, 2021; Zhang et al., 2020). Among these literatures, Peng and Li (2021) was the only one that generated the flood risk prediction under future climate scenarios and socioeconomic pathways covering the MLYRB. However, their flood risk predictions lacked certain flood vulnerability and exposure indicators that incorporated the comprehensive socio-economic factors, such as wetland density (not only river density), runoff and vegetation cover factor, site contamination risk, soil erosion degree, monitoring and early warning systems, and etc. These indicators have been confirmed to be the essential factors for a multi-index flood risk assessment (Guo et al., 2025; Zhang et al., 2020). Moreover, the study period from 2020 to 2050 was relatively short, limiting the ability to analyze long-term trends in flood risks under future climate change after 2050. Therefore, a research gap exists in generating long-term scientific flood risk predictions for the MLYRB. It includes the need for comprehensive flood risk indicators and the detailed analysis of flood vulnerability and exposure under climate change and socio-economic scenarios. Addressing this gap can help prevent flood disasters, reduce socio-economic loss, and promote the sustainable development of the MLYRB.

The overarching goal of this research is to investigate the flood risk dynamics and predict the flood risk under future climate change scenarios in the MLYRB by the end of this century. Therefore, the research objectives of this study are: 1) To predict the spatial distribution of flood hazard, vulnerability, exposure, and overall integrated flood risk in the MLYRB based on a GIS-based multi-index flood risk model with comprehensive indicators under different future scenarios by 2100; 2) To analyze the temporal changes of predicted integrated flood risk areas and the areas of flood hazard, vulnerability, and exposure; 3) To provide suggestions on future flood risk management based on the prediction results of integrated flood risks.

In this paper, we applied the improved multi-index flood risk assessment model to predict flood hazard, vulnerability, exposure, and integrated flood risk in the MLYRB by the end of this century under the moderate and high emission climatic scenarios. In Section 6.2, the study area, climatic scenarios, data sources, and flowchart of the flood risk prediction are described. In Section 6.3, the historical and predicted results for flood hazard, vulnerability, exposure, and the integrated flood risk in the MLYRB under the SSP2-4.5 and SSP5-8.5 scenarios are described and analyzed from both of spatial and temporal perspectives. In Section 6.4, the results are further compared with the findings from other related flood risk prediction studies. Additionally, the uncertainties in this study and suggestions for future flood risk mitigations are discussed in Section 6.4. Finally, conclusions are summarized in Section 6.5.

6.2 Data and methods

6.2.1 Study area

The MLYRB (Figure 6.1) is located between 105° 30’ to 122° 30’E and 23° 45’ to 34° 15’N, which covers the area of approximately 8 × 105 km2 along the foreland tectonic belt of the Dabie Mountain Orogen (Ma et al., 2023). It includes 9 sub-basins of the YRB from the Three Gorges to the Yangtze River Estuary (Guan et al., 2019). The Taihu Lake Basin, Poyang Lake Basin, as well as Dongting Lake and Honghu Lake Basin are the three major sub-basins in the MLYRB. The region belongs to a typical subtropical monsoon climate, with the annual average temperature of 13°C and the annual mean precipitation of 1,100 mm (Yuan et al., 2021). Because of the East Asian subtropical monsoon, the high temperature and abundant precipitation are always concentrated in summer (Pei et al., 2017). Both large annual precipitation and high frequency of extreme precipitation events could lead to a higher flood risk (Ran et al., 2022).

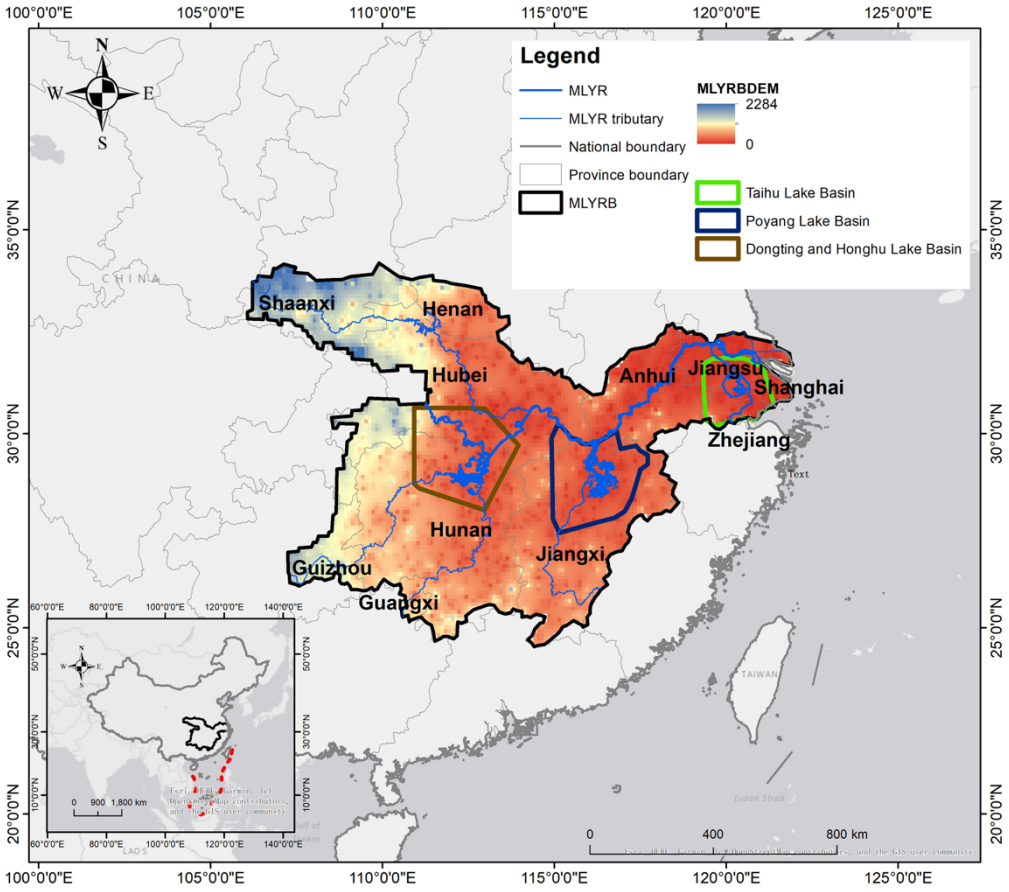

Figure 6.1: The location, hydrographical and topographical information of the Middle and Lower Reaches of Yangtze River Basin (MLYRB), and three important basins including the Taihu Lake Basin, Poyang Lake Basin, and Dongting and Honghu Lake Basin.

The MLYRB encompasses 11 provinces and municipality including Shanghai, Jiangsu, Anhui, Zhejiang, Jiangxi, Henan, Hubei, Hunan, and a small part of Guangxi, Shaanxi, and Guizhou. Among these provinces and municipality, Shanghai, Jiangsu, and Zhejiang are the most developed areas in the East China, characterized by the rapid urbanization due to the high population density, developed agricultural bases, and strong socio-economic development (Ma et al., 2023; Zhang et al., 2020).

6.2.2 Data

The data sources for both projected years from the 2040s to 2100s (2021- 2100) and the base line period of the 2020s (2001-2020) of flood risk assessment indicators were demonstrated in Table 6.1. The projected cumulative maximum three-day precipitation data at a 1 km

resolution, corrected for bias, were utilized in this study. These data cover four future periods: the 2040s (2021–2040), 2060s (2041–2060), 2080s (2061–2080), and 2100s (2081–2100), under the SSP2-4.5 and SSP5-8.5 climate scenarios. The data were derived from 46 General Circulation Models (GCMs) of the Coupled Model Intercomparison Project (CMIP) 6 database (O'Neill et al., 2017). GCMs are a class of reliable computer-driven models for understanding and projecting climate change (Chen et al., 2021b; Yue et al., 2021). According to the most complete spatial and temporal capability evaluation of the 46 GCMs from CMIP6 in China by Lu et al. (2022), MRI-ESM2-0 had been confirmed as the best precipitation simulation model for the YRB, with the least overestimation of the observed maximum precipitation among all the GCMs (Lu et al., 2022). The relative bias (PBIAS) of the MRI-ESM2-0 over the YRB (10.2%) is lower than other GCMs and the Multi-model Ensemble Mean (MEM) of all the ten best-performing models for precipitation projection (with the PBIAS of 21%) (Lu et al., 2022). Several studies have confirmed that the MRI-ESM2-0 model performs reasonably well in replicating observed extreme precipitation in the subtropical humid zone of East China, covering the MLYRB (Jiang et al., 2023; Shiru et al., 2022; Song et al., 2023; Yazdandoost et al., 2021). Hence, the predicted precipitation data based on the MRI-ESM2-0 model were selected for this study.

Table 6.1: Data sources of flood risk indicators.

No.	Indicators	Data source of base line years (2020s)	Data source of prediction (2040s-2100s)
1	Cumulative average maximum 3-day precipitation	National Meteorological Information Center (China Surface Climate Data Day Value Data Set) (National, 2019)	CMIP6 database (https://esgf-node.llnl.gov/search/cmip6/)
2	Absolute elevation	Resource and Environment Data Cloud Platform (Jarvis, 2008)	Resource and Environment Data Cloud Platform (Jarvis, 2008)
3	Relative elevation	Calculated from absolute elevation data	Calculated from absolute elevation data
4	Wetland and drainage density	The Long-Term Wetland Classification Dataset for YRB (LTWCD_YRB) (Guo et al., 2024)	The projection of wetland in the MLYRB under future emission scenario (Ma et al., 2023)
5	Runoff and vegetation cover factor	Resource and Environment Data Cloud Platform (Liu et al., 2014)	1km gridded LULC dataset of China under SSP-RCP scenarios (Luo et al., 2022)
6	Local and financial revenue	China City Statistical Yearbook (http://www.chinayearbooks.com)	China City Statistical Yearbook (http://www.chinayearbooks.com)
7	Per capita resident saving	China City Statistical Yearbook (http://www.chinayearbooks.com)	China City Statistical Yearbook (http://www.chinayearbooks.com)
8	Medical service level	China City Statistical Yearbook (http://www.chinayearbooks.com)	China City Statistical Yearbook (http://www.chinayearbooks.com)
9	Monitoring and early warning capability	National Meteorological Information Center (China Surface Climate Data Day Value Data Set) (National, 2019)	National Meteorological Information Center (China Surface Climate Data Day Value Data Set) (National, 2019)
10	Population density	Resource and Environment Data Cloud Platform (Xu, 2017)	Provincial and gridded population projection for China under shared socioeconomic pathways (Chen et al., 2020).
11	GDP per capita	Resource and Environment Data Cloud Platform (Liu et al., 2005)	Global gridded GDP dataset under the historical and future scenarios from (Wang and Sun, 2022)

12	Soil erosion degree	Resource and Environment Data Cloud Platform (Wang et al., 2016)	Resource and Environment Data Cloud Platform (Wang et al., 2016)
13	Site contamination risk	Resource and Environment Data Cloud Platform (Liu et al., 2014)	1km gridded LULC dataset of China under SSP-RCP scenarios (Luo et al., 2022)

The predicted GDP and population data were obtained from the global gridded GDP dataset (Wang and Sun, 2022) and the provincial gridded population projection dataset for China (Chen et al., 2020), respectively. The GDP projection data from the Global gridded GDP dataset were estimated for SSP 1-5 in the unit of Purchasing Power Parity international dollars, with the spatial resolution of 1km (Wang and Sun, 2022; Xu et al., 2024). The population projection data were calculated based on age, sex, and education of each province in China under various SSP scenarios and downscaled to the spatial resolution of 1km, referring from the RCP urban grid and historical grid (Chen et al., 2020; Xu et al., 2024). The data of runoff and vegetation cover factor, and site contamination risk were derived from the 1km gridded Land Use and Land Cover (LULC) dataset of China under SSP-RCP scenarios by using the approach to integrate the Global Change Analysis Model and Future Land Use Simulation model (Luo et al., 2022). The wetland projected data in the MLYRB under the scenarios of SSP2-4.5 and SSP5-8.5 in 2040s, 2060s, 2080s, and 2100s was based on the machine learning method of Adaptive Boosting tree (AdaBoost) algorithm (Ma et al., 2023).

Precipitation, GDP per capita, population density, runoff and vegetation cover factor, site contamination risk, and wetland density were the indicators those contain variations and were predicted based on the projected data in 2040s, 2060s, 2080s, and 2100s under the SSP2-4.5 and SSP5-8.5 scenarios. The rest of the indicators have been confirmed to exhibit minimal long-term variations in the MLYRB (Guo et al., 2024b; Zhang et al., 2020). Hence, they were assumed to remain unchanged in the flood risk prediction and were based on the historical data in 2020s.

6.2.3 Climatic scenarios

CMIP has become a central element of national and international climate change assessment to study the past, present and future climate changes globally (Eyring et al., 2016). At present, CMIP 6 is the latest phase to provide a multi-model ensemble to capture a range of climate change trajectories, with advantages of increasing the reliable reflection of future climate status by the higher spatial resolution and the fewer uncertainties because of the more complicated physical process (Eyring et al., 2019; Mondal et al., 2021; Xu et al., 2019b).

CMIP 6 has proposed a new projection scenario, namely the combination of different RCPs and SSPs. SSP1 to SSP5 represent five distinct societal development pathways: SSP1 focuses on sustainability; SSP2 reflects moderate development following historical trends; SSP3 depicts a fragmented world concerned with security and competitiveness; SSP4 highlights growing inequality in economics and politics; and SSP5 envisions rapid economic growth fueled by fossil-intensive energy use (O'Neill et al., 2017). When combined with the RCP scenarios, the new scenarios including SSP1-2.6, SSP2-4.5, SSP3-7.0, and SSP5-8.5. In this study, SSP2-4.5 and SSP5-8.5 were selected as future scenarios for the flood risk prediction, representing moderate and high-emission pathways, respectively. For the SSP2-4.5 scenario, global and national institutions work towards but make the slow progress in achieving sustainable development goals. For the SSP5-8.5 scenario, fossil fuel resources are exploited all around the world (Riahi et al., 2017). In China, flood risk is always projected under the SSP2-4.5 and SSP5-8.5 scenarios, which align more closely with China's projected future emissions and socio-economic development trends (Liu et al., 2023a).

6.2.4 Future flood risk simulation

According to Figure 6.2, the spatial distribution maps and the temporal change of average areas in the 2040s, 2060s, 2080s, and 2100s of flood hazard, vulnerability, exposure, and the integrated flood risk under the SSP2-4.5 and SSP5-8.5 scenarios in the MLYRB can be predicted by applying the improved multi-index flood risk system. The model had been used to assess the flood risk with the long-term wetland effects of the YRB between 1985 and 2021 (Guo et al., 2025).

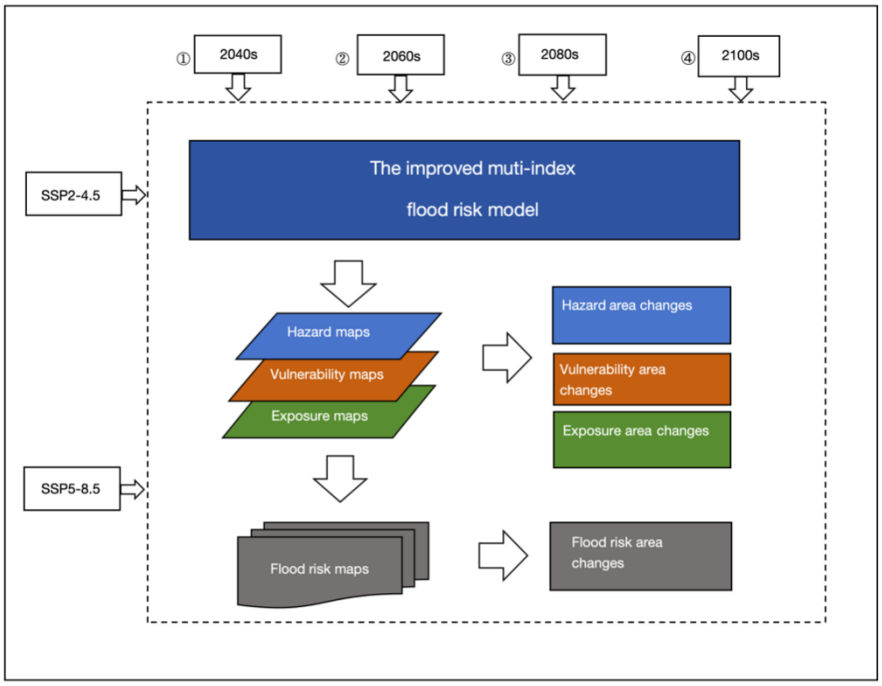

Figure 6.2: The flowchart for predicting the spatial and temporal changes of flood hazard, vulnerability, exposure, and the integrated risk under the SSP2-4.5 and SSP5-8.5 scenarios in the MLYRB. ①-④ represents four time periods of the prediction in this study: 2040s (2021-2040), 2060s (2041-2060), 2080s (2061-2080), and 2100s (2081-2100).

A comprehensive multi-index flood risk assessment system is based on three indices identified by the United Nations Office for Disaster Risk Reduction: Hazard, vulnerability, and exposure (Liu et al., 2023b; Nguyen et al., 2021). Hazard often refers to climate and its influence, precipitation is the main factor of flood hazard (Nguyen et al., 2024). Exposure refers to the presence of at-risk elements in a flood zone, such as population, infrastructure, property, and economic activity. In contrast, the level of vulnerability to floods is defined as the potential influence that flooding contains on an exposed object, which depends on the characteristics of the community that make it susceptible to damage during the flood, like socio-economic indicators (Nguyen et al., 2024). In this study, the flood hazard (H), vulnerability (V), exposure (E) are calculated as the weighted sum of corresponding indicators, with each indicator multiplied by its assigned weight. The weights of indicators and indices, determined by using the AHP method, were presented in Table 6.2. Afterwards, the integrated flood risk can be mapped by the following equation:

$$FR = H \times W_H + V \times W_V + E \times W_E \quad (6.1)$$

The area dynamics of flood hazard, vulnerability, exposure, and overall flood risk during these four periods were calculated based on the mapped results of the corresponding indices and flood risk assessments. To compare flood indices and flood risk across the four time periods under two scenarios, the classification results for five levels (very low, low, medium, high, and very high) of flood indicators, hazard, vulnerability, exposure, and risk were demonstrated in Table 6.3. The classification standards across all scenarios and time periods need to be consistent to enable comparison. Therefore, the classification interval of flood indicators, flood indices, and the integrated flood risk need to be manually adjusted in ArcGIS by considering the minimum and the maximum values.

Table 6.2: The flood risk assessment model structure and weights of flood risk indicators.

	Index layer	Weight of the index layer	Indicator layer	Weight of the indicator layer
Integrated flood risk (FR)	Hazard (H)	+0.469	Cumulative average maximum 3-day precipitation (H)	+0.469
	Vulnerability (V)	+0.322	Absolute elevation (V1)	-0.053
			Relative elevation (V2)	-0.061
			Wetland and drainage density (V3)	+0.039
			Runoff and vegetation cover factor (V4)	+0.041
			Local financial revenue (V5)	-0.028
			Per capita resident saving (V6)	-0.025
			Medical service level (V7)	-0.027
			Monitoring and early warning capability (V8)	-0.047
	Exposure (E)	+0.209	Population density (E1)	+0.046
			GDP per capita (E2)	+0.066
			Soil erosion degree (E3)	+0.068
			Site contamination risk (E4)	+0.030

Table 6.3: The classification standard.

	Very low	Low	Medium	High	Very high
Runoff and vegetation cover factor	0-0.2	0.2-0.4	0.4-0.6	0.6-0.8	0.8-1.0
GDP per capita (yuan/km^2)	<27	27-480	480-3,840	3,840-125,408	>125,408
Population density (people/km^2)	<50	50-60	60-237	237-5,000	>5,000
Site contamination risk	0-0.2	0.2-0.4	0.4-0.6	0.6-0.8	0.8-1.0
Hazard	0-0.22	0.22-0.39	0.39-0.54	0.54-0.68	0.68-1.0
Vulnerability	0-0.25	0.25-0.37	0.37-0.55	0.55-0.61	0.61-1.0
Exposure	0-0.18	0.18-0.25	0.25-0.31	0.31-0.49	0.49-1.0
Flood risk	0-0.15	0.15-0.27	0.27-0.38	0.38-0.52	0.52-1.0

6.3 Results

6.3.1 Spatial distribution pattern of flood risk in the historical period

Figure 6.3 illustrated the spatial distribution pattern of integrated flood risk and its associated indices, including hazard, vulnerability, and exposure in the historical period (2020s). As presented in Figure 6.3a, 22% and 12% of the MLYRB were covered by the high and very high flood hazard levels in 2020s. These areas were mainly concentrated in the flood prone regions with high precipitation, including the Wanjiang Plain, Poyang Lake Basin, as well as Dongting and Honghu Lake Basin. Figure 6.3b illustrated that the areas surrounding Poyang Lake and Dongting Lake were much more vulnerable to floods than the other regions of the MLYRB. In the flood exposure map (Figure 6.3c), the regions with the very high flood exposure were generally concentrated in the eastern MLYRB, typically in Jiangsu and Shanghai, where both population density and GDP per capita were notably high. The integrated flood risk map (Figure 6.3d) in the historical period showed that 33% of the MLYRB was located in the high and very high flood risk areas, with 3% falling into the very high category. These high and very high flood risk zones were primarily distributed in Anhui, Jiangxi, Hubei, Hunan, and some parts of Jiangsu surrounding Taihu Lake.

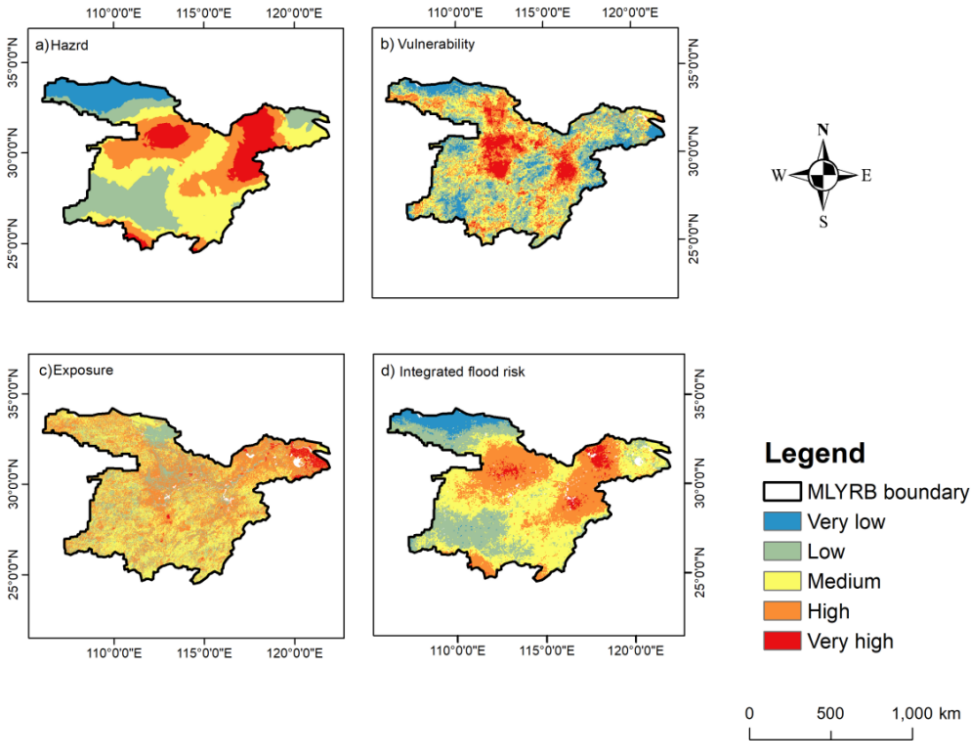

Figure 6.3: The spatial distribution of MLYRB flood risk indices in the historical period (2020s): a) hazard; b) vulnerability; c) exposure; and d) integrated flood risk.

6.3.2 Spatial distribution pattern of future flood risk

Figures 6.4 to 6.7 displayed the spatial distribution maps of the predicted flood hazard, vulnerability, exposure, integrated risk. Appendices 6.1 to 6.5 demonstrated indicators with the significant changes under the SSP2-4.5 and SSP5-8.5 scenarios of the MLYRB in 2040s, 2060s, 2080s, and 2100s. Results from Figure 6.4 demonstrated that the areas with the high and very-high flood hazard level generally located in Hunan, Jiangxi, and the southern part of Jiangsu. It showed that there would be an overall northward movement of the high and very high level flood hazard regions in the MLYRB by the end of this century, typically in the Taihu Lake Basin under the SSP5-8.5. It was attributed to the northward shift in the intensity of the East Asian Summer Monsoon rainfall (Huang et al., 2019; Katzenberger and Levermann, 2024).

The spatial distribution maps of flood vulnerability prediction in the MLYRB under the scenarios of SSP2-4.5 and SSP5-8.5 were illustrated in Figure 6.5. Wetlands density and runoff vegetation cover factor were the main indicators with significant variations to predict the flood vulnerability. Overall, the regions with very high flood vulnerability were estimated to distribute in the Poyang Lake Basin, and Dongting and Honghu Lake Basin, due to the concentration of wetlands and the surrounding urban areas with the high runoff vegetation cover factor (Ma et al., 2023; Shen et al., 2023). The predicted results were similar to the vulnerability results in 1998, 2008, 2016, and 2020 as shown in Zhang et al. (2020) and Jia et al. (2022). These studies showed that areas with high flood vulnerability in the MLYRB were generally located in Hunan, Hubei, Jiangxi, and Anhui, covering the major lake basins.

The spatial distribution results of flood exposure prediction in the MLYRB under the scenarios of SSP2-4.5 and SSP5-8.5 were demonstrated in Figure 6.6. The central and eastern parts of the MLYRB were projected to contain the high and very high flood exposure, typically in Shanghai and the areas around Taihu Lake in Jiangsu. The GDP per capita,

population density, and site contamination risk were the main flood exposure indicators. Appendices 6.3 and 6.4 illustrated that the central and eastern regions of the MLYRB were projected to contain the higher GDP per capita and population density than those in the western region. For the site contamination risk (Appendix 6.5), the high and very high contamination regions were projected to distribute in water bodies, typically in Taihu Lake. According to the spatial changes in the population projection of China, it indicated that the high population density areas were primarily concentrated in the southeast coast region, the central part of Jiangsu and Henan (Sang et al., 2024). Besides, Peng and Li (2021) confirmed that the YRB eastern region, including Shanghai, Jiangsu, and Zhejiang was much more densely populated than other regions. accounted for more than 50% of the GDP in the entire Yangtze River Economic Belt because of the unbalanced economic development and the rapid urbanization.

The integrated flood risk assessment predictions were derived by superimposing the layers obtained from the flood hazard, vulnerability and exposure predictions. The flood risk results were closely related to the hazard results due to the significant weight. Generally, the projected flood risks presented a spatial pattern of the low level in the west and high level in the east of the MLYRB. Figure 6.7 clearly demonstrated the high and very high flood risk areas were predicted to distribute in Jiangxi, Hunan, and the southern part of Jiangsu, covering the three main lake basins (Taihu Lake Basin, Poyang Lake Basin, and Dongting and Honghu Lake Basin) of the MLYRB. Besides, a significant expansion of the high and very high flood risk areas was predicted in Jiangxi, Hunan and Jiangsu. The northward expansion was particularly prominent in the southern region of the Taihu Lake Basin, driven by the northward shift of the rain belt.

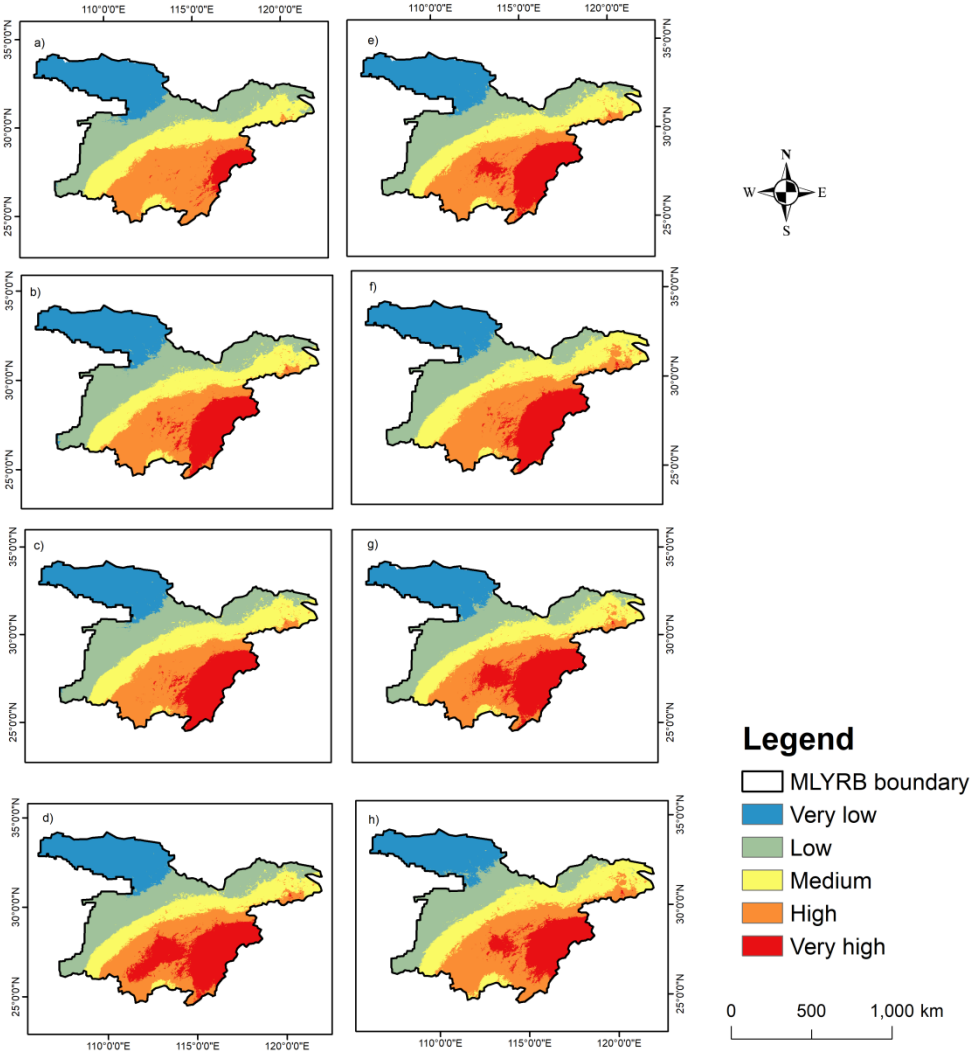

Figure 6.4: The spatial distribution maps of flood hazard level in the MLYRB under the SSP2-4.5 scenario in a) 2040s; b) 2060s; c) 2080s; and d) 2100s; under the SSP5-8.5 scenario in e) 2040s; f) 2060s; g) 2080s; and h) 2100s.

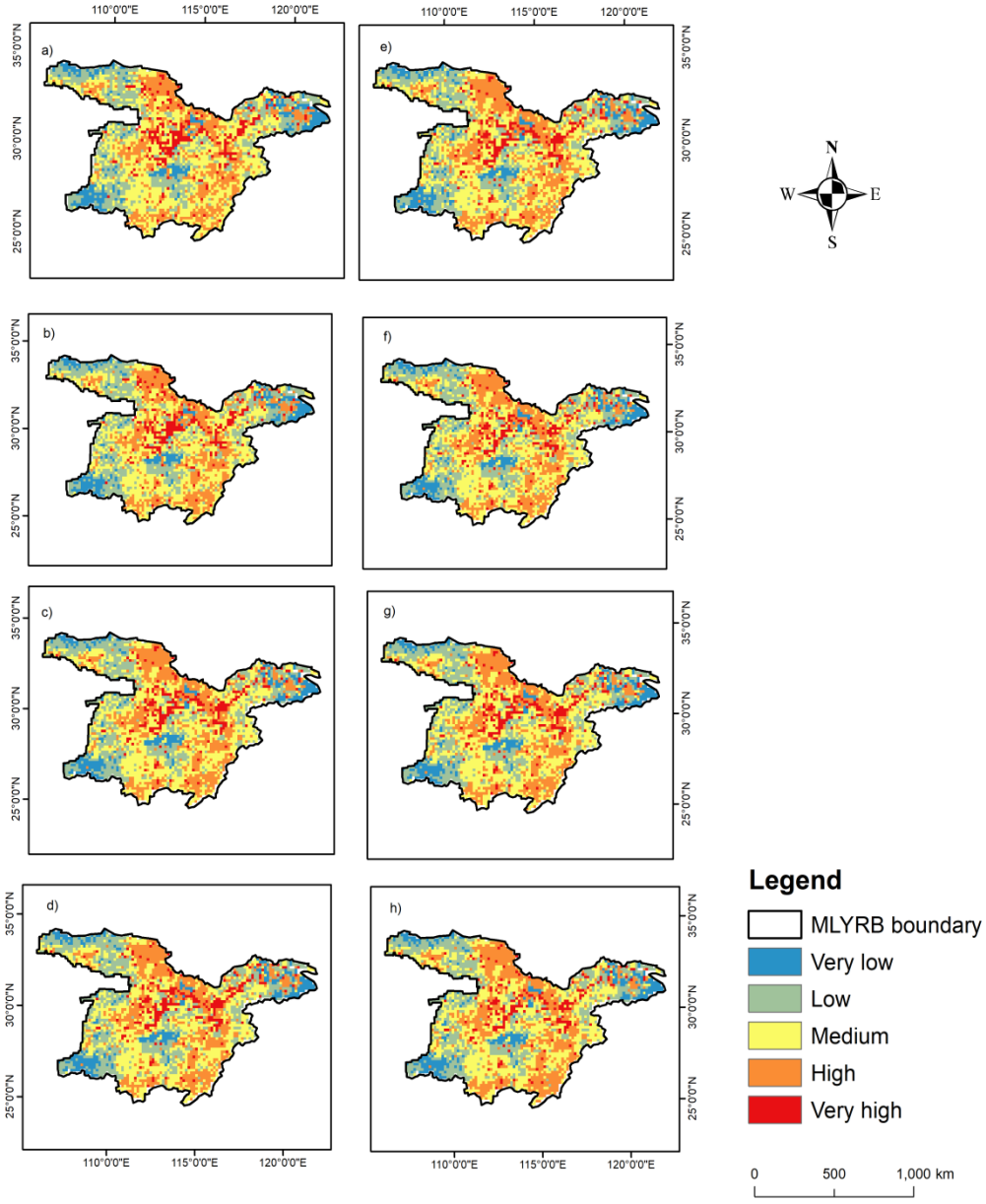

Figure 6.5: The spatial distribution maps of flood vulnerability level in the MLYRB under the SSP2-4.5 scenario in a) 2040s; b) 2060s; c) 2080s; and d) 2100s, under the SSP5-8.5 scenario in e) 2040s; f) 2060s; g) 2080s; and h) 2100s.

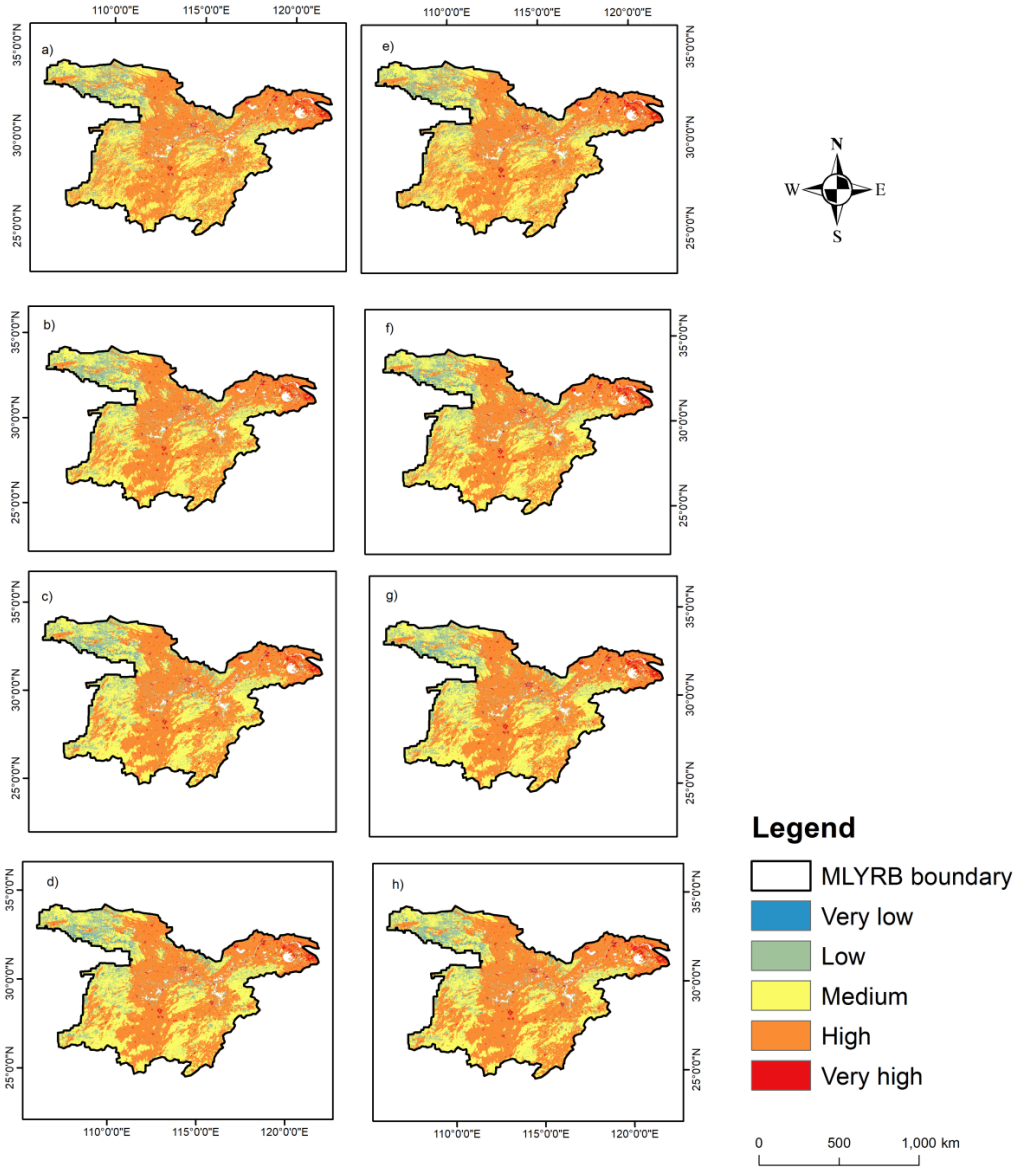

Figure 6.6: The spatial distribution maps of flood exposure level in the MLYRB under the SSP2-4.5 scenario in a) 2040s; b) 2060s; c) 2080s; and d) 2100s, under the SSP5-8.5 scenario in e) 2040s; f) 2060s; g) 2080s; and h) 2100s.

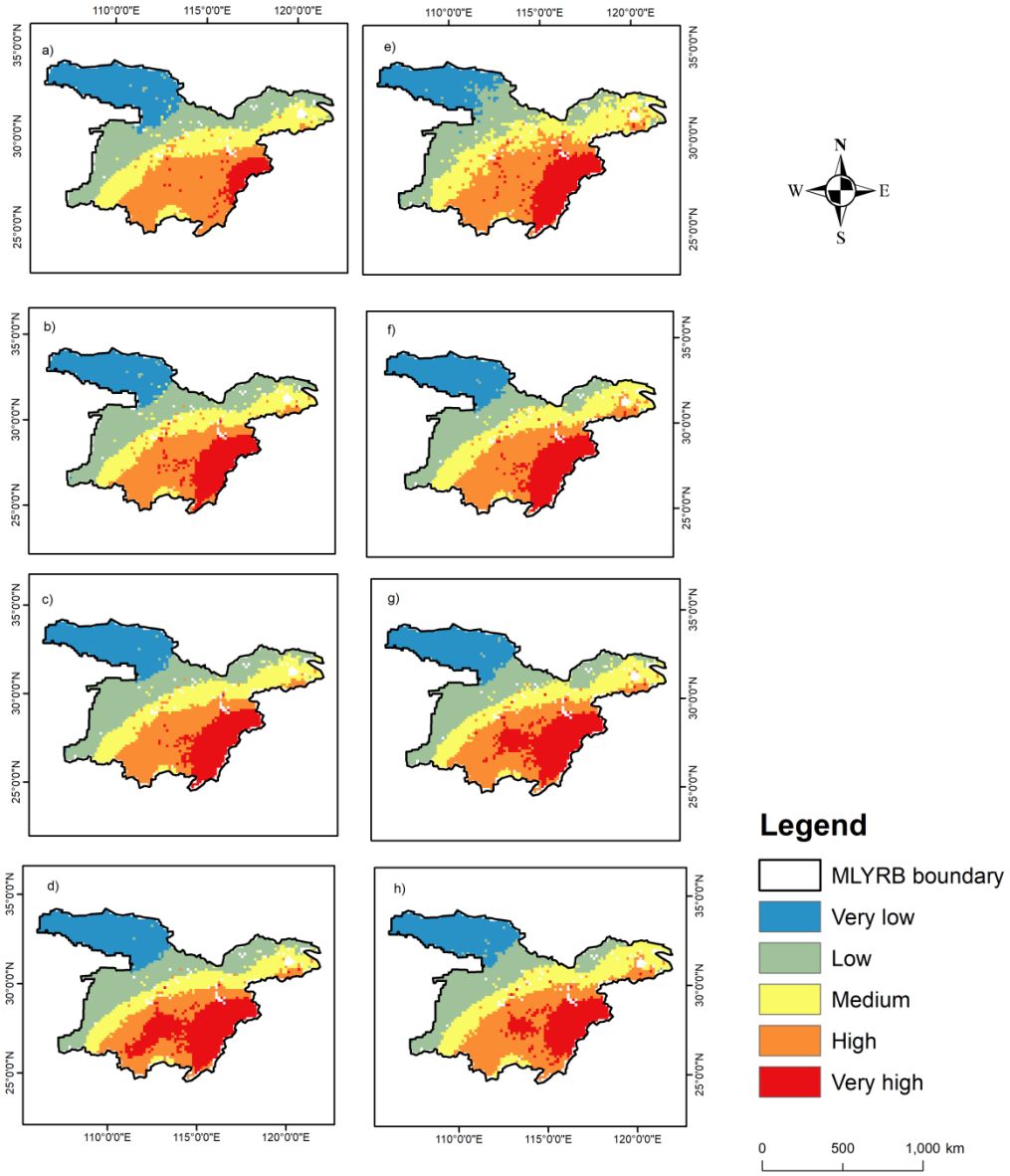

Figure 6.7: The spatial distribution maps of flood risk level in the MLYRB under the SSP2-4.5 scenario in a) 2040s; b) 2060s; c) 2080s; and d) 2100s, under the SSP5-8.5 scenario in e) 2040s; f) 2060s; g) 2080s; and h) 2100s.

6.3.3 Temporal changes in future flood risk areas

Figure 6.8 illustrated that the low and very low flood hazard areas both contained the decreasing trend. The total proportion of areas with the high and very high hazard would continuously increase from 30% to 39% under the SSP2-4.5 scenario and from 36% to 39%

under the SSP5-8.5 scenario from 2040s to 2100s. However, the very high flood hazard area under the SSP5-8.5 scenario was projected to decrease 3% (16%-13%) of the total MLYRB area from 2080s to 2100s. The extreme precipitation was considered as the most significant driving force, making floods to become one of the most costly and dangerous natural hazards around the world (Huang et al., 2021). Pei et al. (2017) found that historically, the frequency and intensity of extreme daily precipitation in the MLYRB generally increased from 1961 to 2012. And it has been confirmed that there would be a general increase of extreme precipitation frequency and intensity in the YRB by the end of the twenty-first century under all the climate change scenarios (Wu et al., 2023b; Xu et al., 2023; Yue et al., 2021). From 2040s to 2100s, the area with very-high hazard level was predicted to be larger under the climate change scenario of SSP5-8.5 than that of SSP2-4.5 except 2100s. Besides, Figure 6.8 demonstrated that the largest area difference between two scenarios will in the 2040s, the very high flood hazard area under SSP5-8.5 would reach three times that under the SSP2-4.5 scenario. Zou and Zhou (2022) confirmed that the larger fractions of land and population would be affected by the larger rainfall under the SSP5-8.5 scenario both in China and the global scale.

The very high flood vulnerability areas in the MLYRB were projected to experience a slightly reduction from 2040s to 2100s (Figure 6.9). There will be a shrinkage of 3,300 km^2 of very highly vulnerable area under the SSP2-4.5 scenario and a shrinkage of 9,500 km^2 under the SSP5-8.5 scenario (Table 6.5). According to the wetland and drainage prediction results in the MLYRB from 2040s to 2100s (Appendix 6.1), the areas of wetlands were projected to decline— more rapidly under the SSP5-8.5 scenario (Ma et al., 2023), thus reducing the flood vulnerability. The runoff and vegetation cover factor (Appendix 6.2) was another significant contributor to the flood vulnerability, showing the conversion from the low to the very low level over the study period in the MLYRB. According to the LULC prediction data, the areas converted from grasslands to forests and shrub would expand until 2100, the areas of other land cover categories would generally keep constantly (Luo et al., 2022). Therefore, the vegetation coverage growth brought by forests and shrubs would enhance the infiltration rate

of precipitation and slowdown flood runoff, thus reducing the flood vulnerability (Zhang et al., 2020).

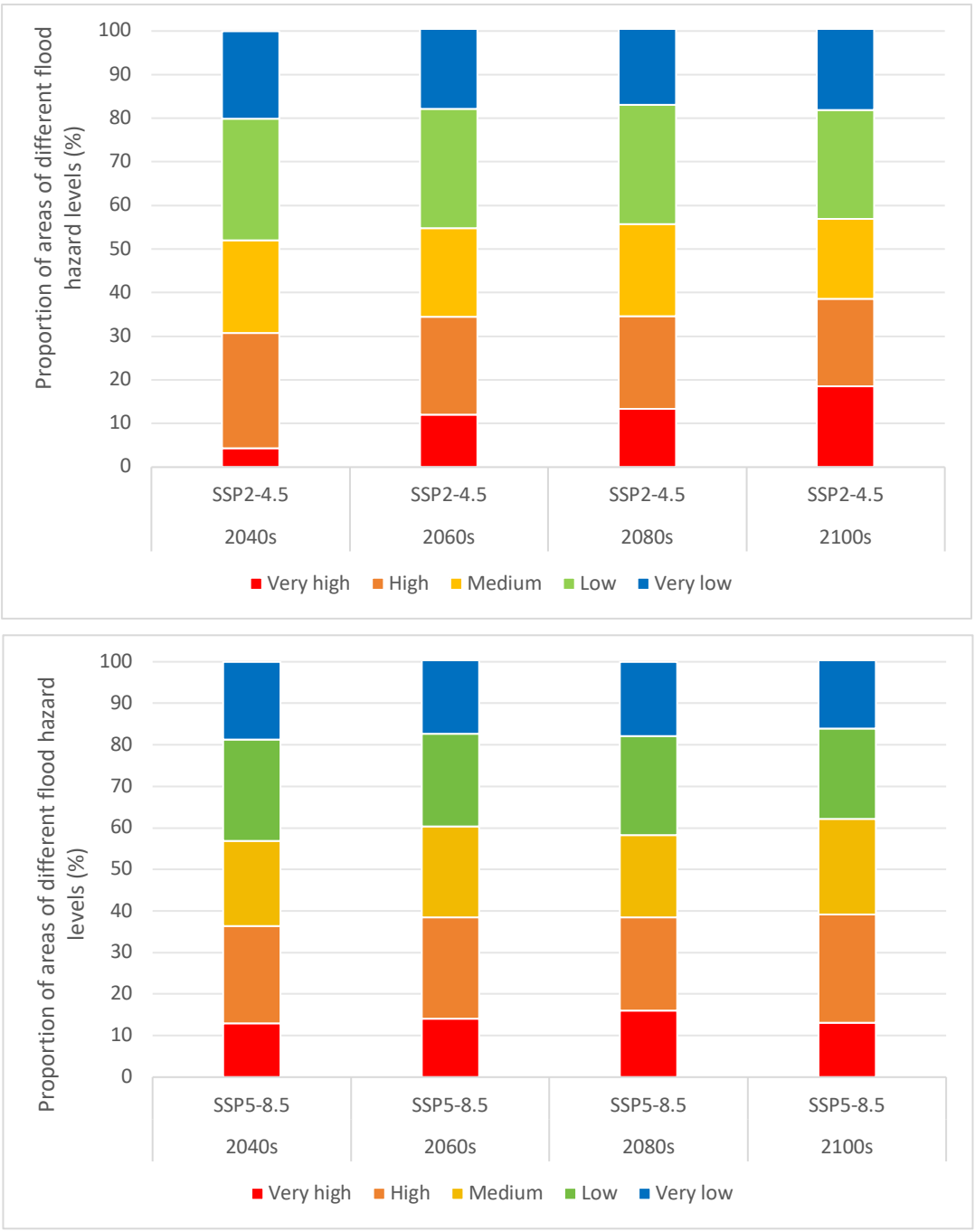

Figure 6.8: Changes in areas of different flood hazard levels of the MLYRB under SSP2-4.5 and SSP5-8.5 scenarios from 2040s to 2100s.

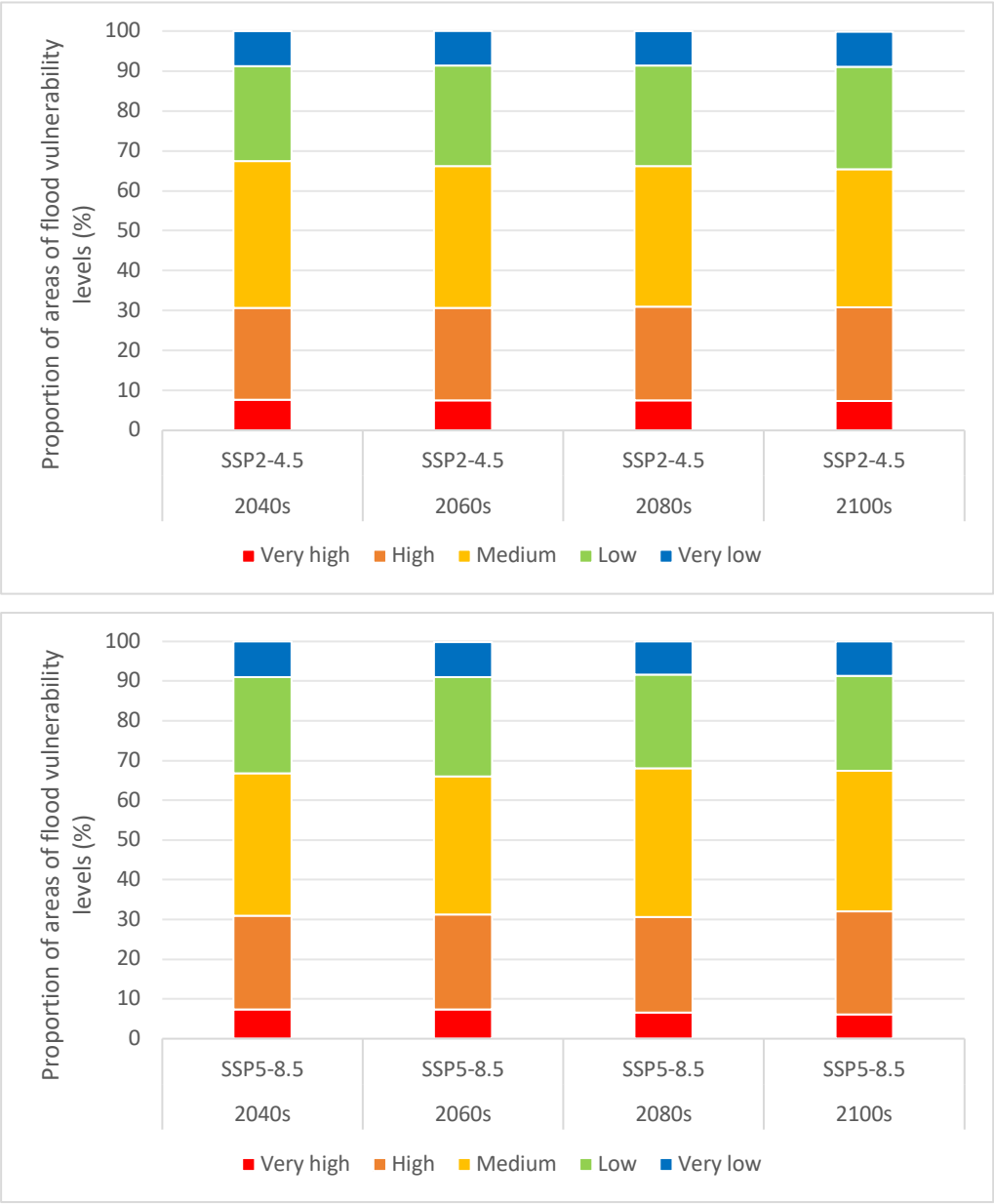

Figure 6.9: Changes in areas of different flood vulnerability levels of the MLYRB under SSP2-4.5 and SSP5-8.5 scenarios from 2040s to 2100s.

The very high flood exposure areas from 2040s to 2100s were predicted to increase totally 100 km^2 under the SSP2-4.5 scenario and 500 km^2 under the SSP5-8.5 scenario in Table 6.6. For the high flood exposure regions, the area showed the prominent decreasing trend (Figure 6.10), which would shrink 47,800 km^2 under the SSP2-4.5 scenario and 38,500 km^2 under the SSP5-8.5 scenario. Appendix 6.3 showed that the areas of the high and very high level GDP were projected to increase under both scenarios of SSP2-4.5 and SSP5-8.5 in the MLYRB,

with the more rapid expansion under the SSP5-8.5 scenario (Wang and Sun, 2022). For the population prediction in Appendix 6.4, population density would decrease rapidly from 2040s to 2100s, typically under the SSP5-8.5 scenario. The result has been confirmed by Chen et al. (2020), indicating that the population of China has been shrinking since 2022, marking the first population decline in decades. Besides, the high level of the site contamination risk areas in the MLYRB, calculated from the LULC data, would expand due to the increase in the forest and shrub coverage — LULC categories with the high contamination index (Luo et al., 2022). Overall, the predicted results of flood exposure indicated that the decline in population density would be greater than the expansion of GDP and contamination risk from 2040s to 2100s under both scenarios. Consequently, it may lead to a slight increase of the very high flood exposure area, but a more substantial decrease in the high flood exposure area.

Figure 6.11 indicated that the total areas of high and very high flood risk level would increase continuously, while the low and very low flood risk areas both contained the decreasing trend. The total areas of high and very high flood risk under the SSP2-4.5 scenario would increase from 30% to 38% of the total MLYRB from 2040s to 2100s; and the areas under the SSP5-8.5 scenario would expand from 36% to 40% during this period. It means that the overall flood risk of the MLYRB will become severer by the end of the 21st century under both scenarios of SSP2-4.5 and SSP5-8.5. However, similar to the trend in very high flood hazard, the very high flood risk areas were projected to experience a slight shrinkage of 3% from 2080s to 2100s under the SSP5-8.5 scenario.

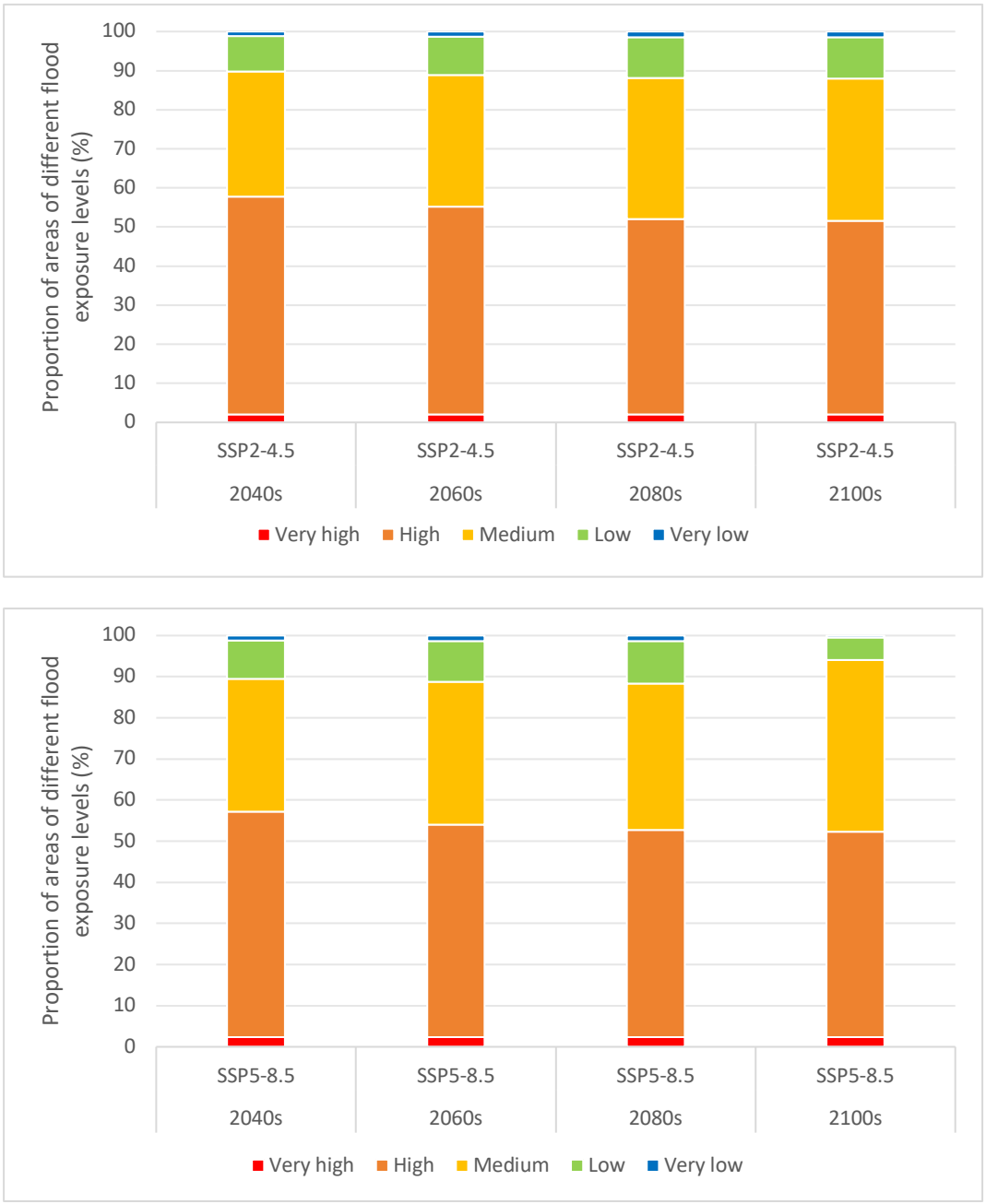

Figure 6.10: Changes in areas of different flood exposure levels of the MLYRB under SSP2-4.5 and SSP5-8.5 scenarios from 2040s to 2100s.

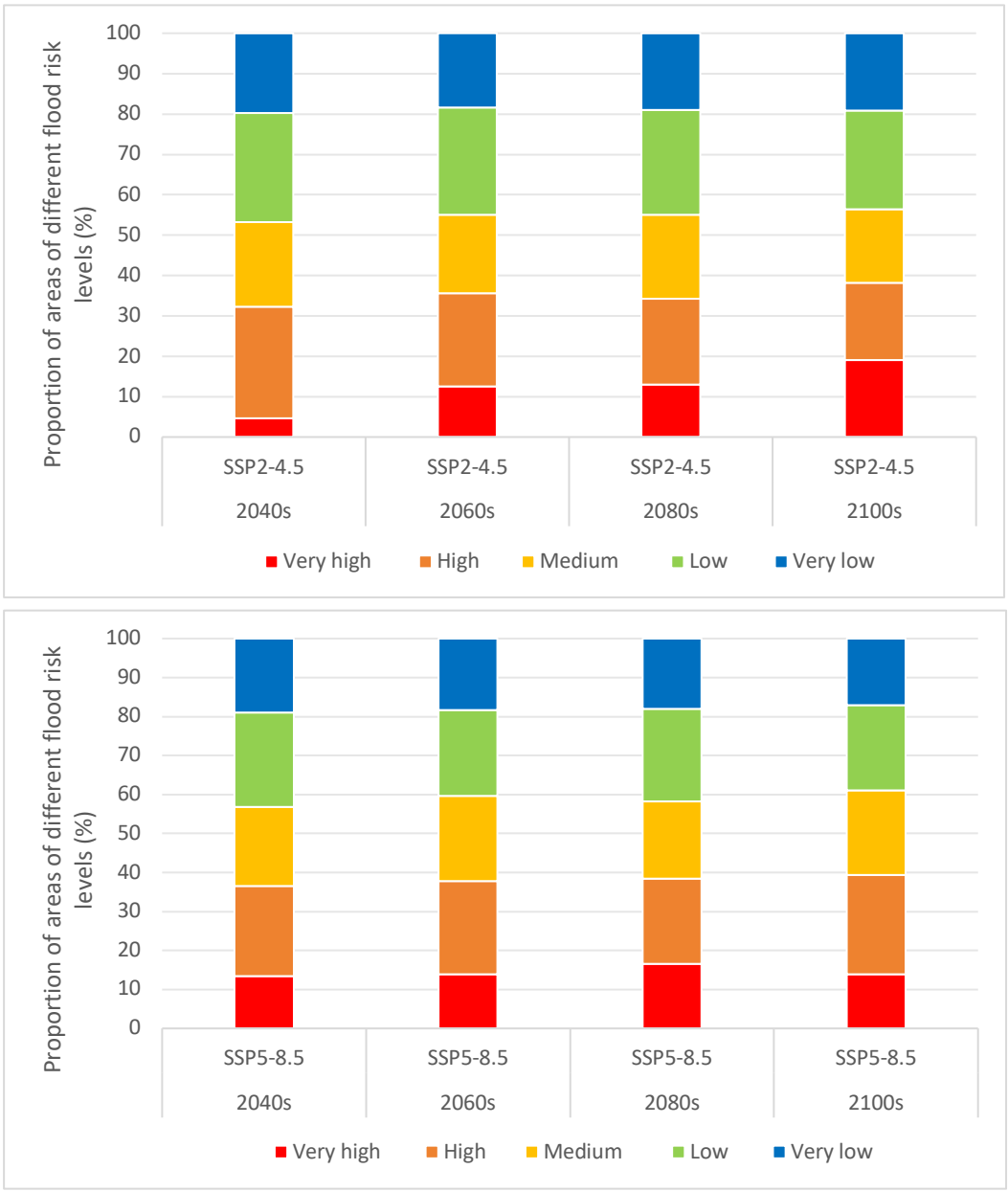

Figure 6.11: Changes in areas of different flood risk levels of the MLYRB under SSP2-4.5 and SSP5-8.5 scenarios from 2040s to 2100s.

Table 6.4: The predicted area of flood hazard level in the MLYRB in 2040s, 2060s, 2080s, and 2100s under the SSP2-4.5 and SSP5-8.5 scenarios.

	Very low (10^4km^2)		Low (10^4km^2)		Medium (10^4km^2)		High (10^4km^2)		Very high (10^4km^2)	
	SSP2-4.5	SSP5-8.5	SSP2-4.5	SSP5-8.5	SSP2-4.5	SSP5-8.5	SSP2-4.5	SSP5-8.5	SSP2-4.5	SSP5-8.5
2040s	16.10	14.99	22.19	19.39	16.95	16.41	21.15	18.64	3.42	10.38
2060s	15.16	14.73	21.86	17.76	16.14	17.48	17.93	19.55	9.61	11.18
2080s	15.29	14.24	21.86	18.99	16.85	15.83	16.92	17.92	10.70	12.75
2100s	15.32	13.74	19.83	17.42	14.66	18.32	15.97	20.85	14.84	10.40

Table 6.5: The predicted area of flood vulnerability level in the MLYRB in 2040s, 2060s, 2080s, and 2100s under the SSP2-4.5 and SSP 5-8.5 scenarios.

	Very low (10^4km^2)		Low (10^4km^2)		Medium (10^4km^2)		High (10^4km^2)		Very high (10^4km^2)	
	SSP2-4.5	SSP5-8.5	SSP2-4.5	SSP5-8.5	SSP2-4.5	SSP5-8.5	SSP2-4.5	SSP5-8.5	SSP2-4.5	SSP5-8.5
2040s	6.76	6.90	18.54	18.86	28.49	27.76	17.72	18.25	6.00	5.74
2060s	6.65	6.85	19.51	19.42	27.55	26.86	18.01	18.57	5.80	5.71
2080s	6.72	6.49	19.46	18.28	27.30	28.95	18.25	18.68	5.78	5.11
2100s	6.79	6.67	19.87	18.52	26.81	27.53	17.67	20.00	5.67	4.79

Table 6.6: The predicted area of flood exposure level in the MLYRB in 2040s, 2060s, 2080s, and 2100s under the SSP2-4.5 and SSP5-8.5 scenarios.

	Very low (10^4km^2)		Low (10^4km^2)		Medium (10^4km^2)		High (10^4km^2)		Very high (10^4km^2)	
	SSP2-4.5	SSP5-8.5	SSP2-4.5	SSP5-8.5	SSP2-4.5	SSP5-8.5	SSP2-4.5	SSP5-8.5	SSP2-4.5	SSP5-8.5
2040s	0.94	0.96	7.04	7.18	24.86	25.14	43.23	42.57	1.59	1.81
2060s	0.99	1.02	7.60	7.74	26.16	26.93	41.32	40.16	1.59	1.81
2080s	1.12	1.09	8.14	7.99	28.04	27.58	38.76	39.19	1.60	1.81
2100s	1.15	0.33	8.24	4.32	28.22	32.43	38.45	38.72	1.60	1.86

Table 6.7: The predicted area of flood risk level in the MLYRB in 2040s, 2060s, 2080s, and 2100s under the SSP2-4.5 and SSP5-8.5 scenarios

	Very low (10^4km^2)		Low (10^4km^2)		Medium (10^4km^2)		High (10^4km^2)		Very high (10^4km^2)	
	SSP2-4.5	SSP5-8.5	SSP2-4.5	SSP5-8.5	SSP2-4.5	SSP5-8.5	SSP2-4.5	SSP5-8.5	SSP2-4.5	SSP5-8.5
2040s	15.03	14.42	20.54	18.41	15.86	15.37	20.94	17.60	3.58	10.15
2060s	13.98	13.95	20.16	16.73	14.81	16.60	17.47	18.14	9.54	10.53
2080s	14.47	13.68	19.66	18.03	15.86	15.03	16.06	16.62	9.90	12.59
2100s	14.56	13.01	18.52	16.51	13.91	16.54	14.49	19.35	14.47	10.54

6.4 Discussion

6.4.1 Validation

In this study, all the projected data for flood risk indicators were derived from the historical data. However, the simulated wetland data (Ma et al., 2023) were not derived from the historical wetland data in the LTWCD_YRB (Guo et al., 2024). Therefore, it is essential to validate the consistency between the historical and simulated wetland data, For the area comparison, Ma et al. (2023) indicated that the difference between historical wetlands and simulated potential wetlands ought to be smaller than 6.3% relative to the total study region, which should be less than 24,970 km^2. The difference between the historical wetland areas and the simulated wetland areas in 2020 is 24,130 km^2. It means the simulated wetland data contains the consistency with the historical LTWCD_YRB dataset. Figure 6.12 demonstrated that the overall wetland spatial distribution in 2020 was generally consistent between the historical and the simulated datasets. However, the dataset from Ma et al. (2023) slightly overestimates the wetland areas compared to historical records from the LTWCD_YRB, particularly in the central MLYRB along the Yangtze River and waterbodies in the eastern region of Taihu Lake. Nevertheless, it is not substantial enough to affect the overall spatial pattern or temporal area changes of the flood risk prediction in this study.

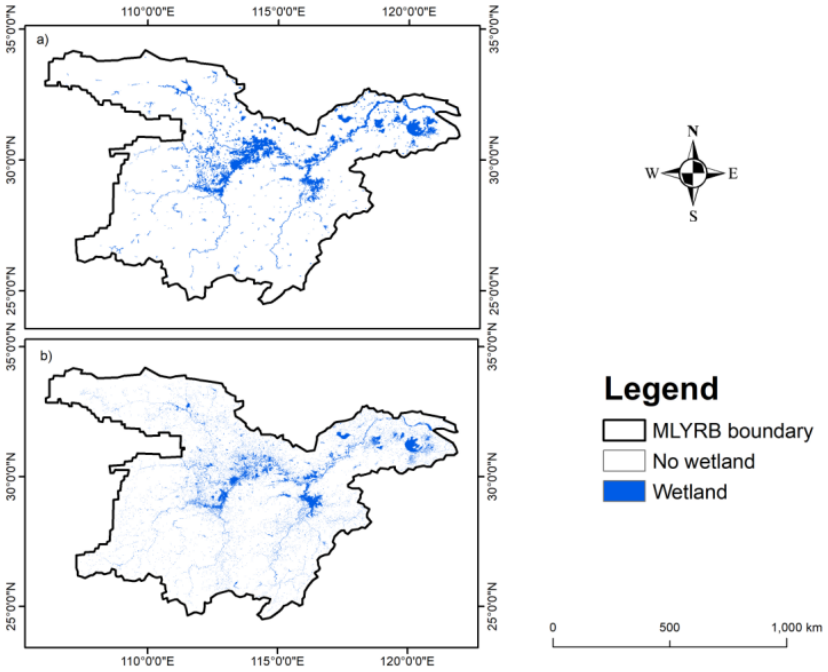

Figure 6.12: The 2020 spatial distribution of a) MLYRB simulated wetlands with 463m resolution; and b) MLYRB existed wetlands with 30m resolution.

The baseline period results of this study can be verified by several studies that assessed the flood risk in the historical period, indicating that flood risks were generally concentrated in the major lake basins of the eastern and central regions of the YRB, typically the Taihu Lake Basin, Wanjiang Plain, Poyang Lake Basin, and Dongting and Honghu Lake Basin (Gao et al., 2021; Guo et al., 2025; Zhang et al., 2020). Wu et al. (2023b) and Xu et al. (2023) confirmed that the extreme precipitation, generally distributed in the southeastern region of the YRB, was projected to contain the significant increasing trend by 2100 under both scenarios of SSP2-4.5 and SSP5-8.5 based on the CMIP6. Peng and Li (2021) verified that the high-middle and high flood risk areas (the top two flood risk levels in the study) were predicted to be generally concentrated in the southeastern of the YRB, covering Jiangsu, Jiangxi, and Hunan from 2020 to 2050 under the SSP2-4.5 and SSP5-8.5 scenarios. Additionally, there existed the northward expansion of the high-middle flood risk area in the predicted period of Peng and Li (2021). For the temporal change of flood risk area under the moderate and high emission scenarios, Bai et al. (2019) predicted that climate change would lead to the increasing flood risk in the future, particularly under the higher emission scenario, The predicted results of this study aligned with these findings, projected the high and very high flood risk areas to be concentrated in Jiangxi, Hunan, and southern Jiangsu, with an overall increasing trend and northward expansion throughout the study period.

6.4.2 Uncertainties

In this study, there were some uncertainties existing in the flood risk indicators when using the CMIP6 data to predict the future flood risk. Uncertainties caused by the overestimation still existed in the precipitation data obtained from the MRI-ESM2-0 model, although it has been confirmed with less relative bias in the YRB than other GCMs and ensemble models (Lu et al., 2022). Besides, the slight overestimation existed in the projected wetland data as well. For the indicators such as GDP, population density, and LULC, future policy uncertainties in China may influence their projections and distributions. The implementation of new towns or

district construction policies to deal with the rapid urbanization in the future could be an example (Chen et al., 2020). In this study, certain indicators such as relative elevation, absolute elevation, and monitoring and early warning capacity were assumed to remain unchanged based on the historical data. Although the topography and the meteorological station distributions in the MLYRB changed slightly over the historical period, this assumption may still introduce some uncertainties into the future flood risk assessment.

Additionally, the use of fixed weights for some indicators across the entire MLYRB over the long term may introduce uncertainties to the flood risk prediction results. The weights of indicators related to the economic development, such as GDP and population density, may carry the greater importance in the regions experiencing rapid economic growth. For example, the study regions covering Henan, Jiangsu and Shanghai, were projected to contain the larger population density and economic development in the future (Peng and Li, 2021; Sang et al., 2024), may require the higher weights for the relevant flood risk indicators than other regions. Therefore, incorporating indicator weight dynamics should be considered in the future AHP process for the flood risk prediction in large-scale study regions.

6.4.3 Suggestions to mitigate future flood risks

The flood risk assessment prediction results of this study indicated that Jiangxi, Hunan, and southern Jiangsu of the MLYRB would be the key area for the future flood risk mitigation. Given the projected increase in the precipitation, along with the rapid economic development and population growth in these regions, both nature-based and socio-economic strategies are essential for the future flood risk mitigation.

For the expansion of the high and very high flood risk areas in the Poyang Lake Basin as well as the Dongting and Honghu Lake Basin, fluvial flood mitigation infrastructures and natural ecosystem developments could be helpful to reduce flood disasters (Peng and Li, 2021). For instance, constructing more reservoirs and drainage systems, controlling lake reclamations, rearranging the local farming and aquacultural development of the flood prone regions, and restoring vegetation-covered wetlands. Besides, the high flood risk areas were projected to

expand in the southern part of Jiangsu around Taihu Lake, an urban region with the extremely high GDP and population density in China (Xu and Chen, 2023). Therefore, the implementation of the 'Sponge City' need to be further developed in the future (Sun et al., 2023). It aims to mitigate the flood risk in the populated and urbanized regions by managing rainwater through the sunken green spaces, permeable ground materials, and extensive drainage systems (Guan et al., 2021). Additionally, the development of satellite technology and meteorological monitoring systems can improve the flood resilience by tracking flood changes and forecasting extreme weather (Jongman, 2021; Tellman et al., 2021).

6.5 Conclusions

This study predicted and analyzed the spatial and temporal changes of flood hazard, vulnerability, exposure, and the integrated flood risk in the MLYRB under the SSP2-4.5 and SSP5-8.5 scenarios from 2040s to 2100s with a 20-year interval. The spatial distribution of the flood risk is projected to be higher in Jiangxi, Hunan, and southern Jiangsu, but lower in Shaanxi and Henan provinces, closely aligning the similar spatial distribution of flood hazard and flood exposure. The areas surrounding Poyang Lake and Dongting Lake were expected to be more vulnerable to floods. There will be a northward expansion of the high flood risk area in the southern part of the Taihu Lake Basin. The expansion will be more prominent under the SSP5-8.5 scenario. The three major basins of the MLYRB, including the Taihu Lake Basin, Poyang Lake Basin, Dongting and Honghu Lake Basin, along with the surrounding provinces including Jiangxi, Hunan, and the southern part of Jiangsu, were projected to experience the larger areas of the high and very high flood risk level over the next 80 years. For the temporal perspective, the highest weight of the increasing high and very high flood hazard led to the overall increasing trend in the high and very high flood risk areas by the end of this century (except the shrinkage of the very high flood risk in 2100s under the SSP5-8.5 scenario). Results illustrated that the total areas of high and very high flood risk level would comprise 38% and 40% of the total MLYRB by 2100 under the SSP2-4.5 and SSP5-8.5 scenarios, respectively.

In the future, it is crucial for local governments to enhance the stormwater storage capacity of water bodies, to effectively manage the urban drainage systems and wetland distributions, and to develop more advanced monitoring and early warning systems for the local meteorology in the predicted flood prone regions. Overall, the flood risk assessment prediction under the climate change and socio-economic scenarios will help with the future flood risk control and management in the MLYRB.

Chapter 7 Discussion

7.1 Major contributions

The LTWCD_YRB dataset established in Chapter 4 is available on the Figshare website (https://doi.org/10.6084/m9.figshare.21859920.v1). It includes 30m resolution wetland classification maps from 1984 to 2021, along with JavaScript code for data processing and machine learning on the GEE platform (Guo et al., 2024). This dataset addresses the lack of a long-term time series wetland dataset with comprehensive wetland categories in the YRB. Compared with other existing wetland datasets covering the YRB, the CAS_Wetland dataset only offers a single year (2015) of national wetland classification map (Mao et al., 2020). The LTWCD_YRB spans a much longer period (1984-2021). Another major advantage of the LTWCD_YRB is that it includes more comprehensive wetland categories than other wetland-related datasets in China, such as the Inland Surface Water Dataset (ISWDC) (Lu et al., 2019), the High Spatial-Temporal Water Body Dataset (HSWDC) (Li et al., 2020), and the China Land Cover Dataset (CLCD) (Yang and Huang, 2021). These non-wetland-focused datasets only provide general water or wetland classes without detailed subcategories. In addition, unlike several existing wetland datasets that focus primarily on the middle or lower reaches of the YRB, such as the long-term Water Middle Reaches of the Yangtze River (Water-MRYR) dataset (Ma et al., 2025), the LTWCD_YRB covers the entire YRB, thus providing the more comprehensive representation of the spatio-temporal dynamics of wetlands across the basin. Therefore, the LTWCD_YRB is the first wetland classification dataset for the YRB to combine the long-term time series, the detailed wetland categorization, and the basin-wide spatial coverage. Besides, the LTWCD_YRB is extendable when recent source datasets are available and could be applied to the larger spatial extent in the future depending on the data availability of sufficient data sources. Overall, the LTWCD_YRB provides the clear advantages over the existing datasets, thereby fulfilling the first objective of this thesis. Researchers and policymakers can search and analyze the spatial and temporal dynamics of different wetland categories across seasons, years, and specific areas of interest in the YRB between 1984 and 2021. Moreover, the GEE-based machine learning algorithm

codes for wetland classification and validation can serve as a reference for researchers, allowing them to adapt and apply the methodology to other wetland classification studies with necessary modifications.

Based on the calculations of wetland areas of the LTWCD_YRB, it completed the objective to compare wetland area changes under their corresponding driving forces. It found that anthropogenic driving forces such as urbanization, fish farming development, and sand dredging affected a larger area of wetlands than natural factors such as sea-level rise, soil erosion, flooding, and temperature or precipitation change. This finding confirmed that as the most populated and developed basin in China, human activities are always the main driving factor of the long-term wetland variations in the YRB, such as the shrinkage of tidal flats in the YRB estuary region, large expansion of aquaculture ponds and shrinkage of lakes in the TLB, PLB, and DLB. However, wetlands in the YRB source region, all of which belong to natural wetland categories, are typically vulnerable to the natural driving force of climate change. Hence, it provides the data support and references for the policymaking of wetland conservation and management to deal with the vulnerable wetland categories in different regions of the YRB. Additionally, the monthly wetland variation data in the PLB and DLB can provide insights into the hydrological process of seasonal floodplains and can support the research on the local flood mitigation (Acreman and Holden, 2013; Li et al., 2019).

The long-term flood risk assessment with effects of wetlands dynamics in Chapter 5 fills the research gap of incorporating the long-term comprehensive wetland data as an indicator in the flood risk assessment. Wetlands in different regions and categories have complex effects on flood risks within a basin. The current flood risk in the YRB is particularly severe in densely populated areas with the high precipitation, exacerbated by climate change (Acreman and Holden, 2013; Cheng et al., 2001; Kundzewicz et al., 2019). Consequently, conducting a long-term, multi-index flood risk assessment that incorporates the effects of wetlands is crucial. Such an assessment can analyze how wetland categories influence the spatial distribution and extent of different flood risk levels in flood-prone regions of the YRB. The future flood risk prediction until the end of this century in Chapter 6, along with wetland

variations, makes the general prediction of the flood hazard, vulnerability, exposure, and the integrated risk at a 20-year interval under different climate change scenarios. The prediction can provide the data support and guidance for the future flood risk prevention in the MLYRB, helping to reduce the flood losses to some extent. Additionally, it has been confirmed that flood risk mitigation approaches in the YRB are primarily rely on the large-scale water conservancy projects. Therefore, the wetland-related strategies in Chapters 5 and 6 to mitigate flood risks based on the flood risk assessment results and the dominant flood risk indicators can serve as a valuable reference for the wetland-related flood risk management in the YRB. These strategies can help to fill the gap in applying nature-based approaches to improve the flood risk resilience in developing countries, where such methods are less common compared to basins in developed countries. (Fournier et al., 2016; Jia et al., 2022).

7.2 Wider implications

To reach the goal of the ecological civilization development, the Chinese government has taken actions to solve pollution and ecological degradation in the continuous economic growth (Hansen et al., 2019; Sheng et al., 2022). The national strategy for the Great Yangtze River Protection Program (GYRPP) launched in 2016 is one of the most representative actions, with aims to make the conservation and restoration of the YRB ecology under the rapid economic growth, and to achieve the long-term sustainable development by balancing conservation and development nexus (Han and Sheng, 2024). The research of this thesis regarding the long-term variations of wetlands and their effects on the YRB flood risk, as well as the future flood risk predictions under the climate change and socio-economic pathways, aligns with the goal of GYRPP. The LTWCD_YRB dataset provides the valuable monitoring data to the long-term wetland conservation of the YRB, typically the wetland variation data in regions experiencing the rapid economic growth. The GYRPP has established 265 key Ecological Function Zones (EFZ) to conserve nature in the YREB (Wei et al., 2024). Industrial development within these EFZs is restricted and requires state approval (Sheng et al., 2022). Among the EFZ types, flood regulation zones are particularly important, aiming to enhance the flood regulation and storage capacity by preserving lake and wetland ecosystems, including the TLB, PLB, and DLB (Sheng et al., 2022). Hence, the long-term flood risk

assessment considering wetland effects on flood regulation zones can provide valuable insights for research on floods and wetlands within the EFZs of the GYRPP. Furthermore, flood risk predictions under climate change scenarios, incorporating wetland dynamics, will support the YRB large-scale ecological restoration projects, which are planned for future implementation (Sheng et al., 2022).

As one of the most representative basins in in the world, characterized by the abundant wetland resources, severe flood disasters, and complex socio-economic conditions, the YRB serves as a key focus for the wetland conservation and flood risk mitigation efforts under climate change. These efforts, as presented in this thesis, are directly aligned with the United Nations SDGs. This thesis makes implications for seven SDGs: Promoting health and well-being for all (SDG 3); ensuring the availability and sustainable management of water and sanitation (SDG 6); making cities inclusive, safe, resilient, and sustainable (SDG 11); promoting sustainable consumption and production (SDG 12); taking urgent action to combat climate change (SDG 13); conserving marine and coastal resources (SDG 14); and protecting, restoring, and sustainably using terrestrial ecosystems (SDG 15). (Mohanty et al., 2024; Molinari et al., 2023).

7.3 Research limitations

The research process to establish the LTWCD_YRB in Chapter 4 was based on the remote-sensed satellite imagery of the GEE platform. Although the GEE-based sample collection is more efficient for collecting a large number of samples in the extensive study region with a long-term time series for this thesis, the lack of fieldwork for ground truth data collection still limits the accuracy of the dataset, especially for the validation purposes. The classification accuracy of certain wetland categories with smaller areas, such as canals and aquaculture ponds, was lower than that of other categories due to challenges in collecting precise samples from Landsat imagery, caused by unclear wetland boundaries and size limitations. Mao et al. (2020) illustrates that the field survey is an effective way to obtain training and validation samples for land cover classifications similar to those used in this

thesis. For example, UAVs equipped with a real-time kinematic GPS were used to identify the categories of those small and inaccessible wetlands (Mao et al., 2020).

Hydrologically, wetlands provide the temporary storage that reduces and delays flood peaks. This additional storage increases lag time and attenuates the flood wave as it travels downstream. Wu et al. (2020) showed that the existing wetlands reduced peak flow by about 24%, flood duration by 1 day, and the total event runoff volume by 17% in the Nenjiang River Basin, demonstrating that extensive wetland complexes can substantially reduce downstream flood risk at the basin scale. The similar hydrological model of the North Carolina Coastal Plain indicated that the vegetation coverage of floodplain wetlands slow the flood wave propagation through the enhanced roughness (Hovis et al., 2021). Tull and Passalacqua (2025) emphasize that the wider and well-connected floodplains generate the stronger attenuation of downstream flood peaks than the narrow or disconnected wetlands. However, the influence of wetlands on the downstream flood risk is not universally mitigating. Some studies observed the increased flooding downstream where wetlands were highly saturated, located lowly in the catchment, or the drawing down storage was too late (Gupta et al., 2024; Lane et al., 2018). Overall, wetlands play the important role in regulating downstream flood risk, although their effectiveness depends on the location, extent, hydrological connectivity, and storage condition of wetlands.

In Chapters 5 and 6, the flood risk was assessed based on three components: hazard, vulnerability, and exposure. The maximum cumulative three-day precipitation serves as the sole hazard indicator and is assigned a substantially higher weight than the vulnerability and exposure indicators. Consequently, the flood risk assessment results are largely dominated by precipitation. As this study adopts a GIS-based multi-index spatial assessment approach that emphasizes the spatial distribution of relative flood risk levels, it does not explicitly simulate the hydrological processes from precipitation to runoff. The potential time lag and routing effects of precipitation on downstream discharge are not accounted for, which may lead to an underestimation of flood hazards in the lower river reaches under the current assessment approach. Additionally, although this study compared the spatial distribution of flood risk

before and after incorporating wetland inputs in the representative flood-prone regions (Section 5.3.1), it does not fully demonstrate how upstream wetlands influence the downstream flood risk and the detailed processes involved. Therefore, more sensitivity tests could be conducted in the future research to quantify how variations in wetland characteristics, such as the location, extent, hydrological connectivity, storage capacity of various wetlands, influence the flood risk downstream. For example, model scenarios may be set up by adjusting different wetland storage capacities while keeping other parameters constant to evaluate how the increased or decreased water retention of wetlands alters the downstream peak flow."

The GIS-based multi-index flood risk assessment methodology applied in Chapters 5 and 6 focuses on the spatial distribution of flood risk by integrating a large number of spatial indicators. In contrast, flood modelling approaches (e.g., HEC-HMS, MIKE-FLOOD, SWAT, and LISFLOOD-FP) (Rajib et al., 2020; Sahu et al., 2023; Tansar et al., 2020) primarily emphasize the simulation of hydrological and hydraulic processes (Grimaldi et al., 2019). Compared with the model-based methods, the GIS-based multi-index approach has the notable advantage of incorporating not only hydrological risks, but also flood vulnerability and exposure, rather than focusing solely on flow dynamics, flood depth, and velocity (Nkwunonwo et al., 2020), thereby providing a more holistic representation of flood risk. In addition, GIS enables detailed spatial analysis and intuitive visualization of flood risk indices and outputs across multiple scales, which enhances the interpretability of results for policymakers in different regions, whereas such interpretability is often more limited in flood modelling approaches. Furthermore, in terms of data accessibility, the GIS-based method relies primarily on remote sensing products and existing spatial datasets, which are increasingly available and cost-effective.

However, the GIS-based multi-index flood risk assessment method has several limitations when compared with the model-based approaches. First, it does not explicitly simulate physical flood processes, such as rainfall–runoff dynamics, flow routing, or inundation depth, which are commonly represented in hydrological and hydraulic models (Bates et al., 2005).

As a result, the downstream impacts of upstream wetlands and precipitation events cannot be directly represented in the resulting flood risk maps. In addition, unlike physics-based hydrological and hydraulic models that rely on the measurable physical parameters, the GIS-based multi-index approach depends heavily on the indicator selection and weighting. Consequently, the generated flood risk results may be sensitive to the quality, spatial resolution, and subjectivity associated with the chosen indicators."

7.4 Uncertainties

7.4.1 Wetland classifier selection

As shown in Chapter 4, RF is selected as the primary classifier of the wetland classification dataset after taking the classification accuracy, robustness, and computational efficiency for the large-scale study region into the consideration. Firstly, RF achieves the better classification results compared to other machine learning classifiers, particularly when using the hyper-spectral or multi-source data (Belgiu and Drăgut, 2016). In the selected representative regions among the YRB, the comparison results of classification accuracy for RF, SVM, CART, ANN, and AdaBoost were shown in Table 7.1, demonstrating that RF achieved the highest classification accuracy. Besides, RF is less sensitive to feature selection, which makes it relatively user-friendly (Li et al., 2015; Vetrivel et al., 2015). Moreover, RF is computationally more efficient and more stable than SVM and other ensemble classifiers such as AdaBoost when handling high-dimensional and multicollinear data at large spatial scales such as the YRB. For ANN, it requires the extensive training cycles and parameter tuning, making it to be less efficient for the large multispectral datasets unless implemented with the Graphics Processing Unit (GPU) acceleration (Chen and Tsou, 2022; Xu et al., 2018). Additionally, SVM and AdaBoost are both sensitive to noise and overfitting, while ANN is vulnerable to overfitting and requires the substantial training samples to generalize effectively. RF reduces the risk of overfitting and ensures robust classification results, even the training data is noise and the class is imbalanced. (Hemmerling et al., 2021; Mei et al., 2016; Rodriguez-Galiano et al., 2012).

Table 7.1: The classification accuracy of different machine learning classifiers in the YRB.

Machine learning classifier	Accuracy				
	Estuary	TLB	PLB	DHB	Source
RF	95.8%	90.5%	90.3%	92.9%	93.7%
SVM	92.3%	89.8%	85.4%	92.7%	81.8%
CART	92.8%	86.3%	88.0%	90.1%	89.5%
ANN	84.1%	78.6%	77.5%	79.8%	80.5%
AdaBoost	93.5%	88.6%	86.8%	91.5%	89.8%

7.4.2 Data sources of the wetland classification

Over the recent decades, multi-source satellite images with different spatial resolutions been widely used for the waterbody extraction and classification, including Landsat, Sentinel-2, and MODIS (Jakovljević et al., 2019). In this study, Landsat image collections were selected as the primary data source because they provide an irreplaceable long-term time series. MODIS was excluded due to its much lower spatial resolution (250m) compared with Landsat (30m) and Sentinel-2 (10m). For Sentinel-2, the atmospherically corrected surface reflectance products are only available from 2017 and contain data gaps in 2017 and 2018 for several regions in the YRB. As a result, Sentinel-2 can only provide the usable data for three years (2019-2021) within the long-term time series (1984-2021) wetland classification of the YRB. As Landsat and Sentinel-2 differ in several fundamental sensor and data characteristics, such as the different spectral band configurations, central wavelengths, spatial resolutions, temporal sampling frequencies, and atmospheric correction algorithms, that can introduce inconsistencies when they are jointly used in the long-term time series wetland classification (Miura et al., 2025; Pahlevan et al., 2019). These inconsistencies may introduce artificial discontinuities in long-term time-series analyses. Therefore, to avoid these uncertainties in the wetland classification results, Landsat image collections were selected as the sole data source in this study. A comparison of wetland classification results for the period 2019–2021 based

on Landsat and Sentinel-2 data (Table 7.2) indicates that classifications derived from Sentinel-2, with its higher spatial and temporal resolution, generally achieve the slightly higher accuracy than those based on Landsat 8. This difference is particularly evident in the YRB estuary and the TLB, which are characterized by small wetland features such as canals and aquaculture ponds that are difficult to distinguish at the coarser spatial resolution.

Table 7.2: The wetland classification accuracy from Landsat and Sentinel-2 between 2019 and 2021.

	2019		2020		2021	
	Landsat	Sentinel-2	Landsat	Sentinel-2	Landsat	Sentinel-2
Estuary	95.7%	98.8%	98.9%	99.7%	99.0%	99.4%
TLB	86.1%	88.6%	89.2%	90.2%	90.8%	91.1%
PLB	91.5%	95.6%	87.4%	90.4%	91.8%	90.8%
DHB	94.7%	95.1%	90.0%	87.2%	93.7%	93.6%
SR	94.5%	96.6%	93.5%	95.5%	92.7%	93.0%

For the future study, given the abundance of wetland resources in the YRB and the relatively limited resolution of Landsat imagery, it would be feasible to integrate higher-resolution data sources in specific regions, particularly for more diverse wetland categories that are difficult to distinguish. For example, PlanetScope imagery, with its higher spatial resolution of 3m and the daily global coverage including the entire YRB after 2017, it could be applied at the local to regional scales to provide the more detailed insights into the rapidly changing lake and vegetation dynamics in wetland monitoring studies (Frazier & Hemingway, 2021; Li et al., 2025; Roy et al., 2021b).

7.4.3 Uncertainties of the flood risk maps

The uncertainties of the flood risk maps presented in Chapters 5 and 6 arise from several aspects. Firstly, uncertainties may occur during data collection and preprocessing. These

include the limited selection of indicators, the potential overestimation of projected precipitation data, and the inconsistencies between the actual spatial resolution of the flood risk patterns and the 1km socio-economic data resolution. Besides, uncertainties associated with the model structure and parameters may be introduced due to the absence of updated weight evaluation in the indicator substitution, as well as the use of fixed weights for certain socio-economic indicators for the long-term flood risk prediction.

The YRB is a macro study region for the flood risk assessment, making the data collection for flood risk indicators complex. Detailed topographical information, diverse characteristics of flood disasters, and direct and indirect socio-economic losses are all necessary to obtain the accurate flood risk assessment results (De Moel et al., 2015; Zhang et al., 2020). As a result, indicators in the flood risk assessments in Chapters 5 and 6 may not comprehensively cover all the flood risk driving factors due to the complexities in modeling the large and dynamic region.

Another uncertainty during the data collection is the overestimation of projected precipitation data obtained from the CMIP6 MRI-ESM2-0 model, though it has been confirmed to have a lower relative bias than other GCMs and ensemble models in the YRB (Lu et al., 2022). Besides, for indicators such as GDP per capita, population density, and LULC, uncertainties may exist in the predicted data collection process caused by the future policy change in China, such as the implementation of new town and district construction policies to deal with the future urbanization (Chen et al., 2020). A part of the indicators, such as relative elevation, absolute elevation, and monitoring and early warning capacity, are assumed to remain unchanged based on the historical data. It may introduce uncertainties into the flood risk prediction results, although the topography and meteorological station distributions in the MLYRB have been confirmed to change slightly over the historical period.

In addition, all the indicator data were converted into spatial layers with a 1 km × 1 km spatial resolution to ensure the consistency and to facilitate the data processing in GIS. However, this process may cause the uncertainties of the flood risk outputs due to the differences in the

original formats and spatial scales of different data sources. For example, several socio-economic flood risk indicators, such as local financial revenue, per capita resident savings, medical service level, were obtained from the China City Statistical Yearbook. These indicators were converted into the raster layers by assigning the city-level statistical values to each 1km × 1 km grid cell. Given that the source data of these indicators were originally complied at administrative unit scales, the conversion to the 1km resolution implied the level of the spatial detail that the original data do not actually contain. As a result, the nominal resolution of the integrated flood risk map may be inconsistent with the true spatial resolution of these socio-economic indicators, and the mapped patterns may reflect grid cell size rather than real spatial variability. In future study, the socio-economic data can be spatially redistributed based on the land use, nighttime lights, or built-up area datasets instead of the unform rasterization, to provide a more realistic spatial representation of the flood risk maps.

In the flood risk assessments in Chapters 5 and 6, substituting the original drainage density indicator with the wetland density from the LTWCD_YRB dataset, without developing a new AHP weight evaluation of indicators, may introduce uncertainties associated with the model's assumptions. However, a sensitivity analysis of the drainage density weight changes, detailed in Section 5.4.1, confirmed that variations in the drainage density weight had minor impacts on the flood risk assessment results.

Using fixed weights for certain indicators in the long-term flood risk assessment and prediction in the large-scale study region, without considering their spatial and temporal dynamics, may also lead to uncertainties of the model assumption in Chapters 5 and 6. The GDP per capita, population density, and other socio-economic indicators in the economic developed and populated regions such as Henan, Shanghai, and a part of Jiangsu located in the TLB, need to be assigned higher weights than other regions (Peng and Li, 2021; Sang et al., 2024; Xu and Chen, 2023). For the temporal perspective, the weight of precipitation for the years with severe flood disasters should be greater than that in other years to improve the accuracy of flood risk assessment results. Therefore, future long-term and large-scale flood risk assessments need to consider the weight dynamics of specific indicators.

Chapter 8 Conclusion

8.1 Summary of the thesis

The YRB is a flood-prone region with the abundant wetland resources. Challenges of wetland conservation and flood risk mitigation still existed under the rapid socio-economic development and climate change. The existing research did not contain the comprehensive analysis regarding the long-term wetland dynamics and flood risks incorporating wetland effects in the YRB. The overall objective of this thesis is to fill in this research gap by establishing a long-term wetland classification dataset with the comprehensive wetland categories for the YRB and assessing flood risks incorporating wetland effects for both historical and future periods. All the research questions mentioned in Chapter 1 have been solved through the research of Chapters 4, 5, and 6.

Chapter 4 produces the LTWCD_YRB dataset by using the RF machine learning classifier on the GEE platform with 30m resolution Landsat 5, 7, and 8 multi-spectral images. The dataset reveals that the total wetland area of the YRB in 2021 was larger than that in 1984. Natural wetlands fluctuated but human-made wetlands increased consistently during these 37 years. Among all the wetland categories, aquaculture ponds exhibited the most significant long-term expansion, particularly in the YRB estuary, TLB, and DHB. In contrast, the inland marsh in the YRB SR experienced the greatest fluctuations. Seasonal wetland dynamics were typically prominent in the PLB, DHB, and SR between May and September. Anthropogenic driving forces had a greater impact on the long-term wetland dynamics in the YRB than natural drivers.

Chapter 5 analyzes the long-term wetland effects on the flood risk in the YRB from 1985 to 2021 by developing an improved GIS-based multi-index flood risk assessment model. The long-term wetland expansions in the TLB, WP, PLB, and DHB all played the significant role in the flood risk mitigation, except during certain years with extreme precipitation events. In contrast, wetland expansions in the SB aggravated the flood risk, although the impact was

limited. For the spatial distribution of flood risk dynamics influenced by wetlands in these flood-prone regions, the eastern TLB demonstrated the stormwater storage potential to mitigate the flood risk. Chaohu Lake and its surrounding areas were regions with high and very high flood risk under wetland effects. In the PLB, high and very high flood risk areas covered more than half of the region, and the weak stormwater storage capacity of seasonal lakes surrounding Poyang Lake increased flood risks during years of heavy precipitation. The northeastern and southwestern regions of the DHB are highly flood-prone regions with the significant wetland effects. Precipitation in the TLB and PLB, runoff and vegetation cover in the WP, GDP in the TLB, and population density in the TLB, the DHB, and the SB are identified as dominant flood risk indicators under the effects of wetlands by using the PCMCI causal inference algorithm. This chapter provides wetland-related suggestions for addressing flood risk changes, such as maximizing stormwater storage capacity, controlling lake reclamation, and increasing vegetation coverage, typically in areas with the high precipitation and dense populations.

Chapter 6 predicts the spatial and temporal dynamics of flood hazard, vulnerability, exposure, and the integrated flood risk in the MLYRB under the SSP2-4.5 and SSP5-8.5 scenarios from 2021 to 2100. The overall flood hazard and the integrated flood risk of the MLYRB are predicted to become more severe by 2100 under both scenarios. In contrast, flood vulnerability and exposure areas are expected to decrease. The high and very high flood risk areas are expected to continue increasing, reaching 38% and 40% of the MLYRB under the SSP2-4.5 and SSP5-8.5 scenarios, respectively. Generally, the spatial distribution of the flood risk is projected to be higher in the south-eastern region (Jiangxi, Hunan, and Jiangsu) and lower in the western region (Shaanxi and Henan) of the MLYRB. The high and very high flood risk areas will expand northward in Jiangxi, Hunan, and the southern part of Jiangsu, typically in the southern TLB over the next 80 years. This expansion is more prominent under the SSP5-8.5 scenario.

The findings of this thesis not only investigate the complex long-term spatial-temporal dynamics of wetlands and flood risks, but also demonstrate the significant effects of wetland

dynamics on flood risks and highlight the importance of sustainable wetland management for mitigating flood risks in the YRB, both now and in the future. The overall framework of this thesis can serve as a reference for investigating the hydrological responses of wetland variations in the large-scale basins. This thesis hopes to contribute to the GYRPP under China's ecological civilization initiatives and align with the United Nations SDGs.

8.2 Future work

8.2.1 Applications in other regions of the world

From a global perspective, wetland conservation and flood risk mitigation in other regions also face emerging challenges, such as the Intermountain West of the United States (Henry et al., 2024), San Francisco Bay and the Mississippi River Delta in the United States (Li et al., 2018), Sanjiang Plain in China (NRSCC, 2014), Lake Urmia in Iran (NRSCC, 2014), the Mekong River Basin in South Asia (Abbas et al., 2016), Kakadu National Park in Australia (NRSCC, 2014), the Danube Delta and the Volga Delta in Europe (NRSCC, 2014). All of these flood-prone regions contain the significant wetland resources listed under the Ramsar Convention, which spans both developed and developing countries. Challenges in wetland conservation and flood risk mitigation vary globally due to differing ecological and socio-economic factors across countries and regions. Therefore, the research on the YRB only serves as one of the case studies. In the future, similar or more advanced methodologies can be applied to establish the long-term wetland classification datasets and to assess long-term flood risks influenced by wetlands in other basins worldwide. These basins, often characterized by abundant but threatened wetland resources, high flood risk, and complex socio-economic factors, could benefit from such analyses. Comparing results from other basins around the world with those from the YRB may offer more inspiration and possibilities for the sustainable wetland conservation and wetland-related flood risk mitigation management.

8.2.2 Managing wetlands as multipurpose nature-based solutions

The awareness of wetlands as nature-based solutions (NbS) for addressing social and environmental challenges and enhancing resilience to climate change has increased over the

recent years (Gupta et al., 2025; Rizzo, 2025). Future wetland planning needs to consider multipurpose NbS, rather than just the single NbS of flood risk mitigation or water pollution control (Rizzo, 2025). The influence of the green infrastructure planning on the wetland conservation and restoration has been evident worldwide (Moreno et al., 2024). The Minghu Wetland Park and the Yanweizhou Wetland Park in China, as well as the South Los Angeles Wetland Park in the United States are notable examples of the green infrastructure planning (Ganapathi et al., 2024; Moreno et al., 2024). In these cases, the wetland design process considered multiple NbS, including the articulation of ecosystems, ecological restoration, urban flood resilience management, and the conversion of degraded riverbanks and marsh habitats into constructed wetland parks with the high social value (Ganapathi et al., 2024; Moreno et al., 2024). In addition to Wetland Parks, the 'Sponge City' project in China is another effective green infrastructure planning in the multipurpose wetland management (Ganapathi et al., 2024). The 'Sponge City' manages wetlands as NbS to improve the stormwater drainage for flood control and to prevent the degradation of surface water quality through the sunken green spaces, permeable ground materials, and extensive drainage systems (Guan et al., 2021). For the coastal wetland management, the Houston Coastal Roulette Planning for Galveston Bay in Mexico planned and designed the green infrastructure for the disaster impact mitigation in coastal regions based on wetland systems. It combined riparian vegetation and coastal forests with agricultural areas. Additionally, it established infrastructures to implement the NbS of regulating the occupation of risk zones and stimulating the conservation of coastal ecosystems (Moreno et al., 2024). As a large basin with the complex socio-economic and ecological environment, the YRB encompasses the densely populated urban and coastal regions as well as the less developed plateau and woodland regions. Therefore, the future work on wetlands in the YRB can focus on designing and managing multipurpose wetlands as NbS across different regions based on the results of wetland variations and their effects on flood risks of this thesis, as well as other environmental impact assessments incorporating wetland effects in the future research.

Supplementary materials

Chapter 5 Section 5.3.3

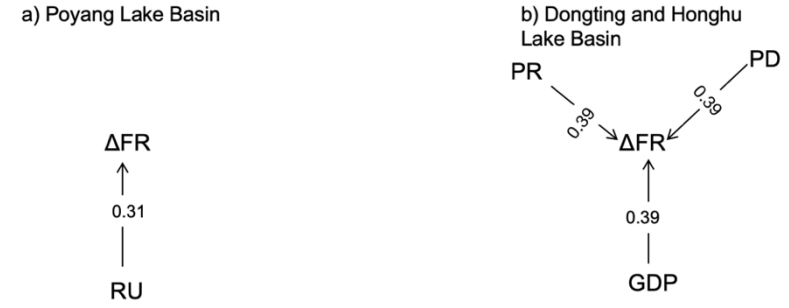

Appendix 5.1: The causal relationships between the ΔFR_{low} and indicators in the a) Poyang Lake Basin; and b) Dongting and Honghu Lake Basin. No indicator exhibits a causal relationship with ΔFR_{low} in the Taihu Lake Basin, Wanjiang Plain, and Sichuan Basin.

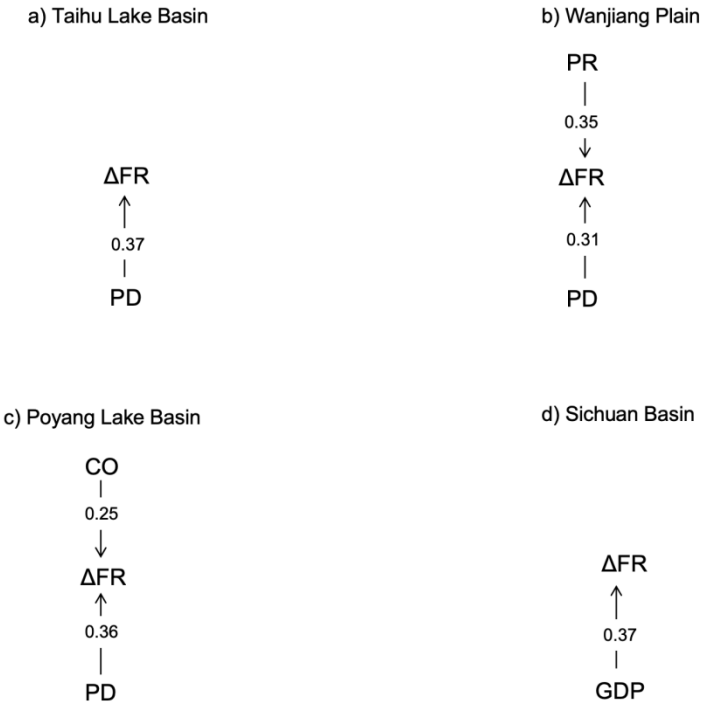

Appendix 5.2: The causal relationship between ΔFR_{medium} and indicators in the a) Taihu Lake Basin; b) Wanjiang Plain; c) Poyang Lake Basin; and d) Sichuan Basin. No indicator exhibits a causal relationship with ΔFR_{medium} in the Dongting and Honghu Lake Basin.

Chapter 6 Section 6.3.2

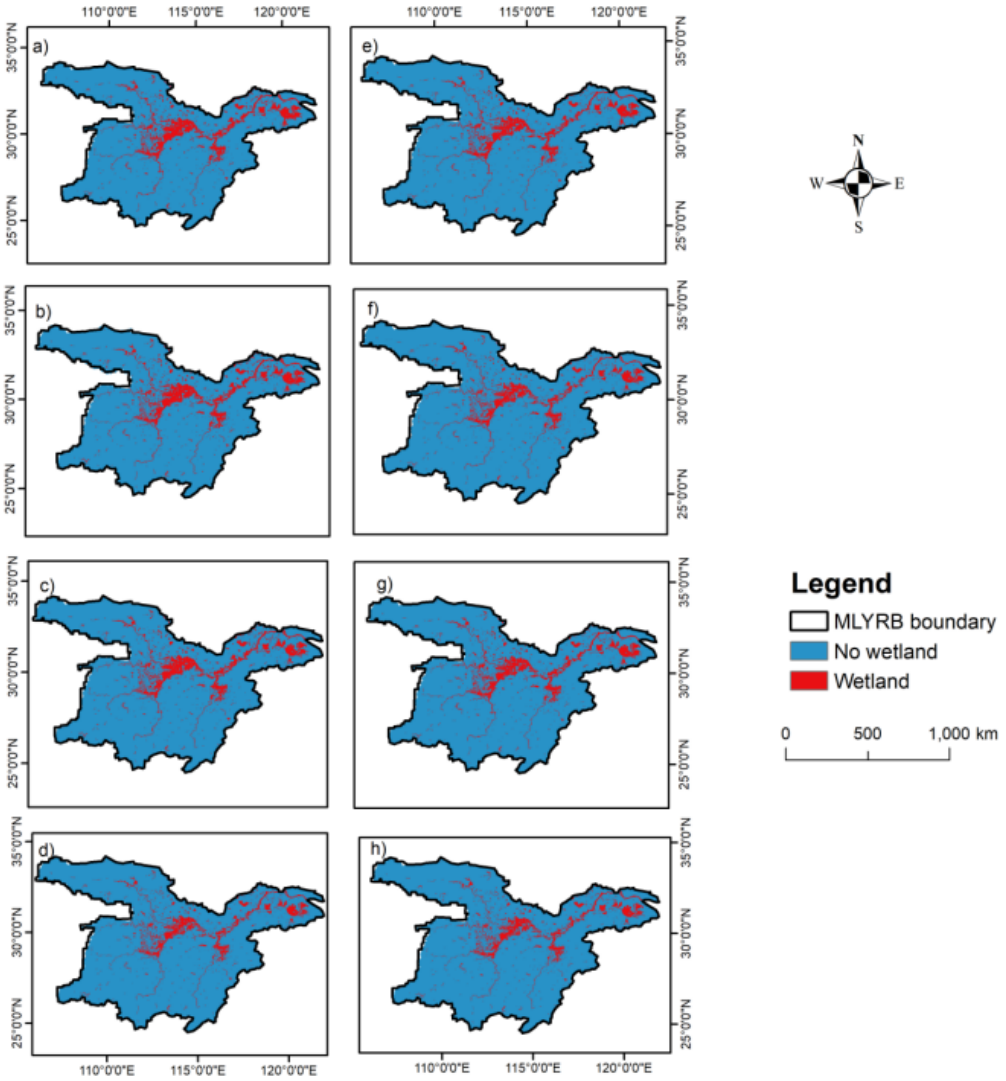

Appendix 6.1: The spatial distribution maps of wetlands in the MLYRB under the SSP2-4.5 scenario in a) 2040s; b) 2060s; c) 2080s; and d) 2100s, under the SSP5-8.5 scenario in e) 2040s; f) 2060s; g) 2080s; and h) 2100s.

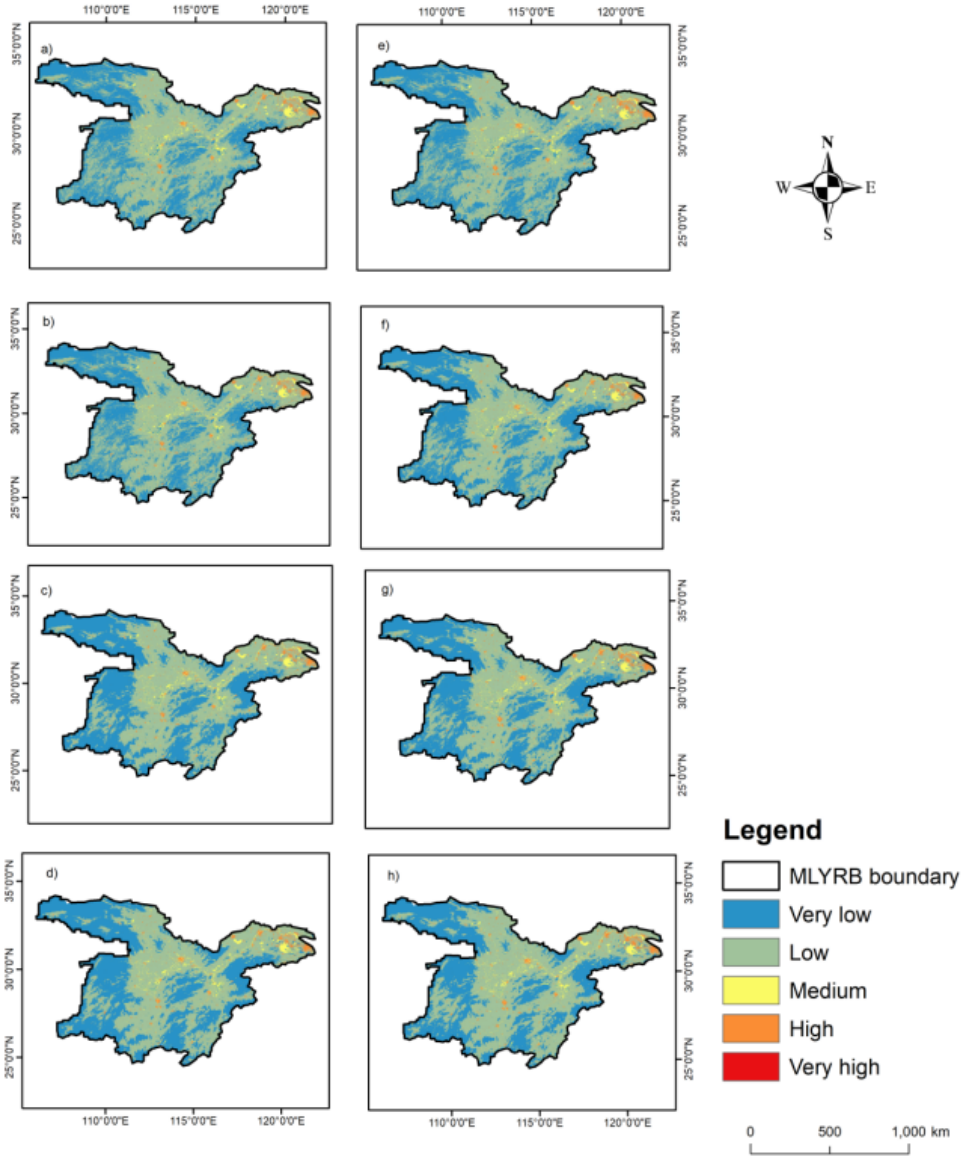

Appendix 6.2: The spatial distribution maps of runoff and vegetation cover factor in the MLYRB under the SSP2-4.5 scenario in a) 2040s; b) 2060s; c) 2080s; and d) 2100s, under the SSP5-8.5 scenario in e) 2040s; f) 2060s; g) 2080s; and h) 2100s.

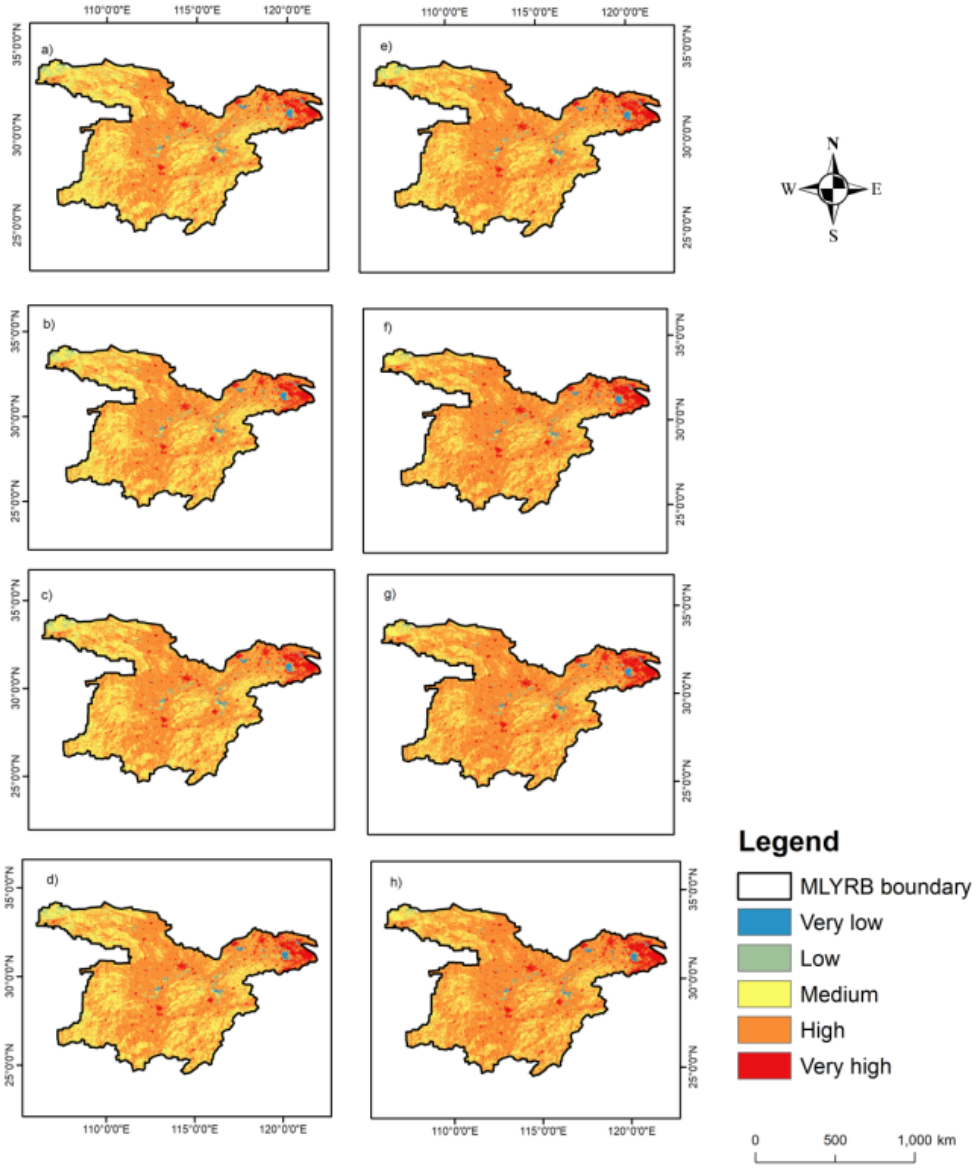

Appendix 6.3: The spatial distribution maps of GDP per capita in the MLYRB under the SSP2-4.5 scenario in a) 2040s; b) 2060s; c) 2080s; and d) 2100s, under the SSP5-8.5 scenario in e) 2040s; f) 2060s; g) 2080s; and h) 2100s.

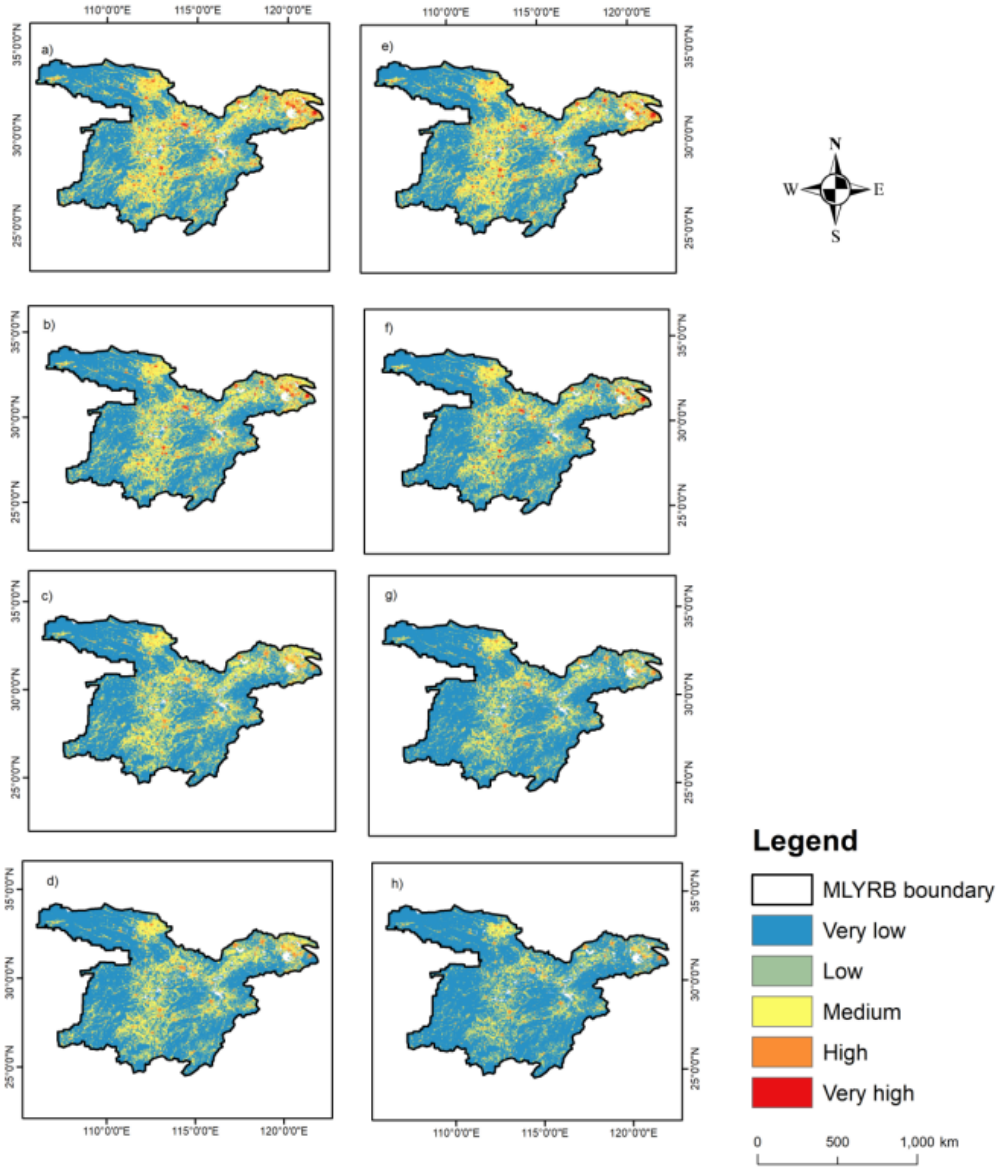

Appendix 6.4: The spatial distribution maps of population density in the MLYRB under the SSP2-4.5 scenario in a) 2040s; b) 2060s; c) 2080s; and d) 2100s, under the SSP5-8.5 scenario in e) 2040s; f) 2060s; g) 2080s; and h) 2100s.

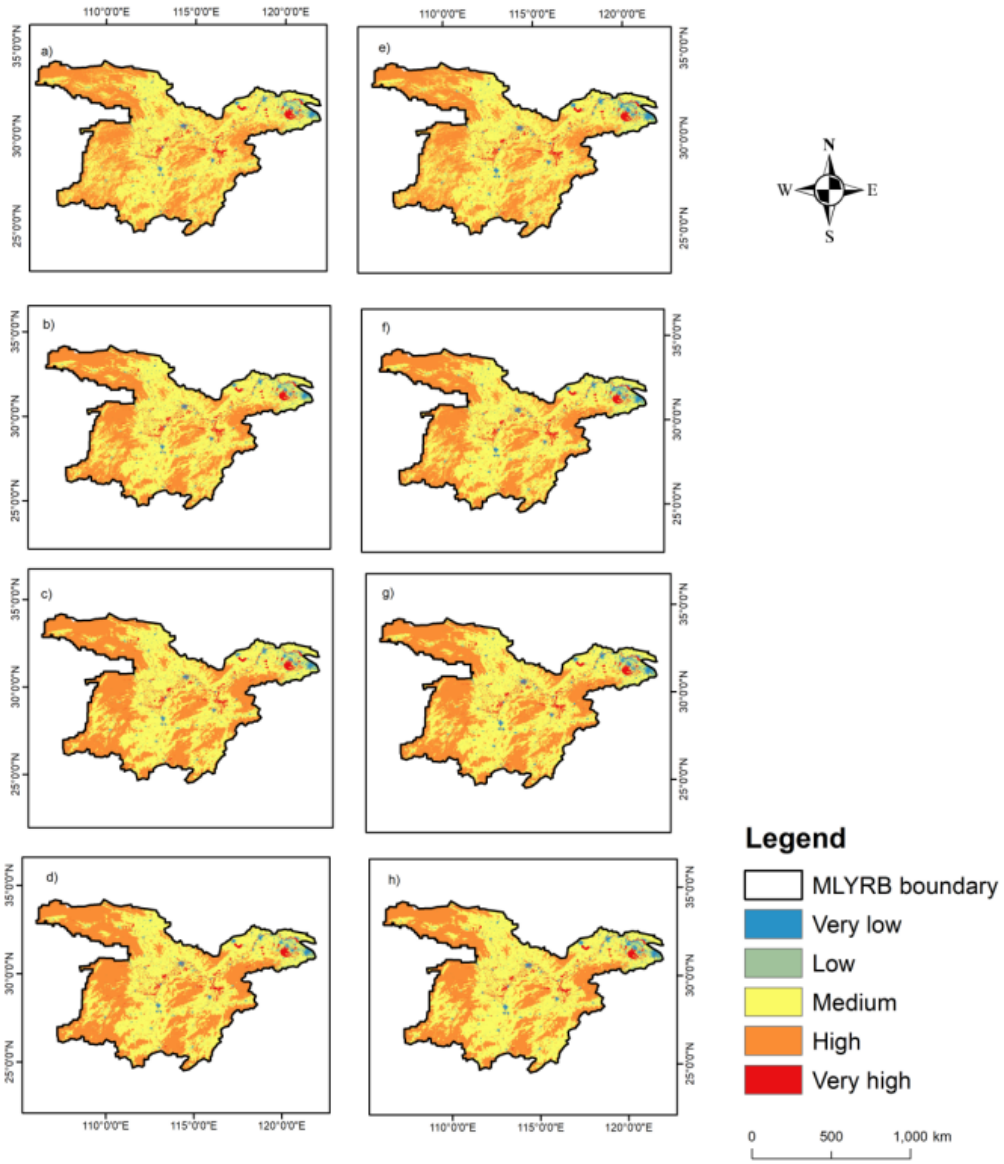

Appendix 6.5: The spatial distribution maps of site contamination risk in the MLYRB under the SSP2-4.5 scenario in a) 2040s; b) 2060s; c) 2080s; and d) 2100s, under the SSP5-8.5 scenario in e) 2040s; f) 2060s; g) 2080s; and h) 2100s.

References

Abbas, A., Amjath-Babu, T. S., Kächele, H., Usman, M., & Müller, K. (2016). An overview of flood mitigation strategy and research support in South Asia: implications for sustainable flood risk management. *International Journal of Sustainable Development & World Ecology*, *23*(1), 98–111. https://doi.org/10.1080/13504509.2015.1111954

Abdelkarim, A., & Gaber, A. F. D. (2019). Flood Risk Assessment of the Wadi Nu'man Basin, Mecca, Saudi Arabia (During the Period, 1988–2019) Based on the Integration of Geomatics and Hydraulic Modeling: A Case Study. *Water*, *11*(9), 1887. https://doi.org/10.3390/w11091887

Abuzwidah, M., Elawady, A., Ashour, A. G., Yilmaz, A. G., Shanableh, A., & Zeiada, W. (2024). Flood Risk Assessment for Sustainable Transportation Planning and Development under Climate Change: A GIS-Based Comparative Analysis of CMIP6 Scenarios. *Sustainability*, *16*(14), 5939. https://doi.org/10.3390/s

Acreman, M., & Holden, J. (2013). How Wetlands Affect Floods. *Wetlands*, *33*(5), 773–786. https://doi.org/10.1007/s13157-013-0473-2

Acreman, M. C., Riddington, R., & Booker, D. J. (2003). Hydrological impacts of floodplain restoration: a case study of the River Cherwell, UK. *Hydrology and Earth System Sciences*, *7*(1), 75–85. https://doi.org/10.5194/hess-7-75-2003

Adhya, T., & Banerjee, S. (2022). Impact of Wetland Development and Degradation on the Livelihoods of Wetland-dependent Communities: a Case Study from the Lower Gangetic Floodplains. *Wetlands*, *42*(7), 65. https://doi.org/10.1007/s13157-022-01588-w

Ahmed, N., Hoque ,Muhammad Al-Amin, Howlader ,Newton, & and Pradhan, B. (2022). Flood risk assessment: role of mitigation capacity in spatial flood risk mapping. *Geocarto International*, *37*(25), 8394–8416. https://doi.org/10.1080/10106049.2021.2002422

Aires, F., Prigent, C., Fluet-Chouinard, E., Yamazaki, D., Papa, F., & Lehner, B. (2018). Comparison of visible and multi-satellite global inundation datasets at high-spatial resolution. *Remote Sensing of Environment*, *216*, 427–441. https://doi.org/10.1016/j.rse.2018.06.015

Alexander, M., S. Priest, A. P. Micou, S. Tapsell, C. Green, D. Parker, and S. Homewood. (2016). Analyzing and evaluating flood risk governance in England - enhancing societal

resilience through comprehensive and aligned flood risk governance. STAR-FLOOD Consortium, Flood Hazard Research Centre, Middlesex
University, London, UK. Available online: http://www.preventionweb.net/publications/view/48467. (accessed on 12 Oct 2024).

Alderman, K., Turner, L. R., & Tong, S. (2012). Floods and human health: A systematic review. *Environment International*, *47*, 37–47. https://doi.org/10.1016/j.envint.2012.06.003

Alfieri, L., Feyen, L., Dottori, F., & Bianchi, A. (2015). Ensemble flood risk assessment in Europe under high end climate scenarios. *Global Environmental Change,* 35, 199–212. https://doi.org/10.1016/j.gloenvcha.2015.09.004

Almar, R., Stieglitz, T., Addo, K. A., Ba, K., Ondoa, G. A., Bergsma, E. W. J., Bonou, F., Dada, O., Angnuureng, D., & Arino, O. (2023). Coastal Zone Changes in West Africa: Challenges and Opportunities for Satellite Earth Observations. *Surveys in Geophysics*, *44*(1), 249–275. https://doi.org/10.1007/s10712-022-09721-4

Alshari, E. A., Abdulkareem, M. B., & Gawali, B. W. (2023). Classification of land use/land cover using artificial intelligence (ANN-RF). *Frontiers in Artificial Intelligence*, *5*. https://doi.org/10.3389/frai.2022.964279

Amani, M., Mahdavi, S., Afshar, M., Brisco, B., Huang, W., Mohammad Javad Mirzadeh, S., White, L., Banks, S., Montgomery, J., & Hopkinson, C. (2019). Canadian Wetland Inventory using Google Earth Engine: The First Map and Preliminary Results. *Remote Sensing*, *11*(7), 842. https://doi.org/10.3390/rs11070842

Armstrong, A., Holden, J., Kay, P., Francis, B., Foulger, M., Gledhill, S., McDonald, A. T., & Walker, A. (2010). The impact of peatland drain-blocking on dissolved organic carbon loss and discolouration of water, results from a national survey. *Journal of Hydrology*, *381*(1), 112–120. https://doi.org/10.1016/j.jhydrol.2009.11.031

Asselen, S. van, Verburg, P. H., Vermaat, J. E., & Janse, J. H. (2013). Drivers of Wetland Conversion: a Global Meta-Analysis. *PLOS ONE*, *8*(11), e81292. https://doi.org/10.1371/journal.pone.0081292

Ayalew, L., & Yamagishi, H. (2005). The application of GIS-based logistic regression for landslide susceptibility mapping in the Kakuda-Yahiko Mountains, Central Japan. *Geomorphology*, *65*(1), 15–31. https://doi.org/10.1016/j.geomorph.2004.06.010

Babayan, G., & Adamovich, B. (2023). Water Quality Assessment of Large Alpine Sevan Lake. *Environmental Processes*, *10*(4), 52. https://doi.org/10.1007/s40710-023-00668-1

Bai, Y., Zhang, Z., & Zhao, W. (2019). Assessing the Impact of Climate Change on Flood Events Using HEC-HMS and CMIP5. *Water, Air, & Soil Pollution*, *230*(6), 119. https://doi.org/10.1007/s11270-019-4159-0

Balica, S., & Wright, N. G. (2010). Reducing the complexity of the flood vulnerability index. *Environmental Hazards*, *9*(4), 321–339. https://doi.org/10.3763/ehaz.2010.0043

Banjara, M., Bhusal, A., Ghimire, A. B., & Kalra, A. (2024). Impact of Land Use and Land Cover Change on Hydrological Processes in Urban Watersheds: Analysis and Forecasting for Flood Risk Management. *Geosciences*, *14*(2), 40. https://doi.org/10.3390/geosciences14020040

Ballard, C. E., McIntyre, N., Wheater, H. S., Holden, J., & Wallage, Z. E. (2011). Hydrological modelling of drained blanket peatland. *Journal of Hydrology*, *407*(1), 81–93. https://doi.org/10.1016/j.jhydrol.2011.07.005

Ballut-Dajud, G. A., Sandoval Herazo, L. C., Fernández-Lambert, G., Marín-Muñiz, J. L., López Méndez, M. C., & Betanzo-Torres, E. A. (2022). Factors Affecting Wetland Loss: A Review. *Land*, *11*(3), 434. https://doi.org/10.3390/land11030434

Bangalang, N., Nadji, J., Nayinggul, A., Nadji, S., Nayinggul, A., Dempsey, S., Mangiru, K., Dempsey, J., McCartney, S., Mairi Macdonald, J., & Robinson, C. J. (2022). Understanding Indigenous values and priorities for wetlands to guide weed management actions: Lessons from the Nardab floodplain in northern Australia's Kakadu National Park. *Ecological Management & Restoration*, *23*(S1), 105–116. https://doi.org/10.1111/emr.12542

Barbier, E.B., 2019. The value of coastal wetland ecosystem services. In *Coastal wetlands* (pp. 947-964). Elsevier. https://doi.org/10.1016/B978-0-444-63893-9.00027-7

Barbier, E. B., Hacker, S. D., Kennedy, C., Koch, E. W., Stier, A. C., & Silliman, B. R. (2011). The value of estuarine and coastal ecosystem services. *Ecological Monographs*, *81*(2), 169–193. https://doi.org/10.1890/10-1510.1

Barredo, J. I. (2009). Normalised flood losses in Europe: 1970–2006. *Natural Hazards and Earth System Sciences*, *9*(1), 97–104. https://doi.org/10.5194/nhess-9-97-2009

Bartsch, A., Wagner, W., Scipal, K., Pathe, C., Sabel, D., & Wolski, P. (2009). Global monitoring of wetlands – the value of ENVISAT ASAR Global mode. *Journal of Environmental Management*, *90*(7), 2226–2233. https://doi.org/10.1016/j.jenvman.2007.06.023

Baral, H. (2013). An assessment of the impact of Koshi floods to birds and mammals. *Nepalese Journal of Biosciences*, *2*. https://doi.org/10.3126/njbs.v2i0.7482

Bathrellos, G. D., Gaki-Papanastassiou, K., Skilodimou, H. D., Papanastassiou, D., & Chousianitis, K. G. (2012). Potential suitability for urban planning and industry development using natural hazard maps and geological–geomorphological parameters. *Environmental Earth Sciences*, *66*(2), 537–548. https://doi.org/10.1007/s12665-011-1263-x

Bates, P. D., Dawson, R. J., Hall, J. W., Horritt, M. S., Nicholls, R. J., Wicks, J., & Mohamed Ahmed Ali Mohamed Hassan. (2005). Simplified two-dimensional numerical modelling of coastal flooding and example applications. *Coastal Engineering*, *52*(9), 793–810. https://doi.org/10.1016/j.coastaleng.2005.06.001

Belgiu, M., & Drăguţ, L. (2016). Random forest in remote sensing: A review of applications and future directions. ISPRS Journal of Photogrammetry and Remote Sensing, 114, 24–31. https://doi.org/10.1016/j.isprsjprs.2016.01.011

Bhere, S., & Reddy, M. J. (2025). Flood risk assessment of suburban region in India by incorporating flood hazard, vulnerability and exposure. *Natural Hazards*, *121*(6), 6625–6649. https://doi.org/10.1007/s11069-024-07062-6

Bhuiyan, Md. J. A. N., & Dutta, D. (2012). Analysis of flood vulnerability and assessment of the impacts in coastal zones of Bangladesh due to potential sea-level rise. *Natural Hazards*, *61*(2), 729–743. https://doi.org/10.1007/s11069-011-0059-3

Bhuiyan, S.R. and Al Baky, A., (2014). Digital elevation based flood hazard and vulnerability study at various return periods in Sirajganj Sadar Upazila, Bangladesh. *International journal of disaster risk reduction*, *10*, 48-58. https://doi.org/10.1016/j.ijdrr.2014.06.001

Blankespoor, B., Dasgupta, S., & Laplante, B. (2014). Sea-Level Rise and Coastal Wetlands. *AMBIO*, *43*(8), 996–1005. https://doi.org/10.1007/s13280-014-0500-4

Blackwell, M. S. A., & Pilgrim, E. S. (2011). Ecosystem services delivered by small-scale wetlands. *Hydrological Sciences Journal*, *56*(8), 1467–1484. https://doi.org/10.1080/02626667.2011.630317

BMTPC, 2010. Guidelines: improving flood resistance of housing [Internet]. New Delhi (India): Building Materials and Technology Promotion Council, Ministry of Housing and Urban Poverty Alleviation, Government of India. Available online: http://www.bmtpc.org/DataFiles/CMS/file/flood-guidelines.pdf. (accessed on 10 Oct 2024).

Boin, M. N., Martins, P. C. S., da Silva, C. A., & Salgado, A. A. R. (2019). Pantanal: The Brazilian Wetlands. In A. A. R. Salgado, L. J. C. Santos, & J. C. Paisani (Eds.), *The Physical Geography of Brazil : Environment, Vegetation and Landscape* (pp. 75–91). Springer International Publishing. https://doi.org/10.1007/978-3-030-04333-9_5

Brammer, H. (2014). Bangladesh's dynamic coastal regions and sea-level rise. *Climate Risk Management*, *1*, 51–62. https://doi.org/10.1016/j.crm.2013.10.001

Bouwer, L. M. (2011). *Have Disaster Losses Increased Due to Anthropogenic Climate Change?* https://doi.org/10.1175/2010BAMS3092.1

Brown, C. F., Brumby, S. P., Guzder-Williams, B., Birch, T., Hyde, S. B., Mazzariello, J., Czerwinski, W., Pasquarella, V. J., Haertel, R., Ilyushchenko, S., Schwehr, K., Weisse, M., Stolle, F., Hanson, C., Guinan, O., Moore, R., & Tait, A. M. (2022). Dynamic World, Near real-time global 10 m land use land cover mapping. *Scientific Data*, *9*(1), 251. https://doi.org/10.1038/s41597-022-01307-4

Bubeck, P., Otto, A., & Weichselgartner, J. (2017). Societal Impacts of Flood Hazards. In *Oxford Research Encyclopedia of Natural Hazard Science*. https://doi.org/10.1093/acrefore/9780199389407.013.281

Bullock, A., & Acreman, M. (2003). The role of wetlands in the hydrological cycle. *Hydrology and Earth System Sciences*, *7*(3), 358–389. https://doi.org/10.5194/hess-7-358-2003

Cai, C., Gu, X., Ye, Y., Yang, C., Dai, X., Chen, D., & Yang, C. (2013). Assessment of pollutant loads discharged from aquaculture ponds around Taihu Lake, China. Aquaculture Research, 44(5), 795–806. https://doi.org/10.1111/j.1365-2109.2011.03088.x

Cai, S., Fan, J., & Yang, W. (2021). Flooding Risk Assessment and Analysis Based on GIS and the TFN-AHP Method: A Case Study of Chongqing, China. *Atmosphere*, *12*(5), 623. https://doi.org/10.3390/atmos12050623

Cai, T., Li, X., Ding, X., Wang, J., & Zhan, J. (2019). Flood risk assessment based on hydrodynamic model and fuzzy comprehensive evaluation with GIS technique. *International Journal of Disaster Risk Reduction*, *35*, 101077. https://doi.org/10.1016/j.ijdrr.2019.101077

Cai, X., Feng, L., Hou, X., & Chen, X. (2016). Remote Sensing of the Water Storage Dynamics of Large Lakes and Reservoirs in the Yangtze River Basin from 2000 to 2014. *Scientific Reports*, *6*(1), 36405. https://doi.org/10.1038/srep36405

Carrivick, J. L., Jones, R., & Keevil, G. (2011). Experimental insights on geomorphological processes within dam break outburst floods. *Journal of Hydrology*, *408*(1), 153–163. https://doi.org/10.1016/j.jhydrol.2011.07.037

Castillo, C., Chollett, I. & Klein, E. (2008). Enhanced duckweed detection using bootstrapped SVM classification on medium resolution RGB MODIS imagery. *International Journal of Remote Sensing*, *29*(19), 5595-5604. https://doi.org/10.1080/01431160801961375

Chaikumbung, M., Doucouliagos, H., & Scarborough, H. (2016). The economic value of wetlands in developing countries: A meta-regression analysis. *Ecological Economics*, *124*, 164–174. https://doi.org/10.1016/j.ecolecon.2016.01.022

Chamberlain, D. A., Phinn, S. R., & Possingham, H. P. (2021). Mangrove Forest Cover and Phenology with Landsat Dense Time Series in Central Queensland, Australia. *Remote Sensing*, *13*(15), 3032. https://doi.org/10.3390/rs13153032

Chan, F.K.S., Griffiths, J.A., Higgitt, D., Xu, S., Zhu, F., Tang, Y.T., Xu, Y. & Thorne, C.R. (2018). "Sponge City" in China—a breakthrough of planning and flood risk management in the urban context. *Land use policy*, *76,* 772-778. https://doi.org/10.1016/j.landusepol.2018.03.005

Chan, F.K.S., Yang, L.E., Scheffran, J., Mitchell, G., Adekola, O., Griffiths, J., Chen, Y., Li, G., Lu, X., Qi, Y. & Li, L. (2021). Urban flood risks and emerging challenges in a Chinese delta: The case of the Pearl River Delta. *Environmental Science & Policy*, *122*, 101-115. https://doi.org/10.1016/j.envsci.2021.04.009

Chan, J. C.-W., & Paelinckx, D. (2008). Evaluation of Random Forest and Adaboost tree-based ensemble classification and spectral band selection for ecotope mapping using airborne hyperspectral imagery. Remote Sensing of Environment, 112(6), 2999–3011. https://doi.org/10.1016/j.rse.2008.02.011

Chatterjee, A., Phillips, B., Stroud, D., Alberts, F., Hails, S., Minaeva, T., Pittock, J., Prietto, C. and Tunde, O. (2008). Wetland management: Planning a guide for site managers. Available online: https://www.ramsar.org/sites/default/files/documents/library/wurc_mgt_planning2008.pdf. (accessed on 01 Oct 2024).

Chen, F., & Tsou, J. Y. (2022). Assessing the effects of convolutional neural network architectural factors on model performance for remote sensing image classification: An in-depth investigation. *International Journal of Applied Earth Observation and Geoinformation*, *112*, 102865. https://doi.org/10.1016/j.jag.2022.102865

Chen, L., Ren, C., Zhang, B., Li, L., Wang, Z., & Song, K. (2018). Spatiotemporal Dynamics of Coastal Wetlands and Reclamation in the Yangtze Estuary During Past 50 Years (1960s–2015). Chinese Geographical Science, 28(3), 386–399. https://doi.org/10.1007/s11769-017-0925-3

Chen, J., Chen, J., Liao, A., Cao, X., Chen, L., Chen, X., He, C., Han, G., Peng, S., Lu, M. and Zhang, W. (2015). Global land cover mapping at 30 m resolution: A POK-based operational approach. *ISPRS Journal of Photogrammetry and Remote Sensing*, *103*, 7-27. https://doi.org/10.1016/j.isprsjprs.2014.09.002

Chen, J., Huang, G., & Chen, W. (2021b). Towards better flood risk management: Assessing flood risk and investigating the potential mechanism based on machine learning models. *Journal of Environmental Management*, *293*, 112810. https://doi.org/10.1016/j.jenvman.2021.112810

Chen, X., Huang, Q., & Zhou, Y. (2024). *Transmission Line Outage Probability Prediction Under Extreme Events Using Peter-Clark Bayesian Structural Learning* (No. arXiv:2411.11980). arXiv. https://doi.org/10.48550/arXiv.2411.11980

Chen, X., Zhang, H., Chen, W., & Huang, G. (2021a). Urbanization and climate change impacts on future flood risk in the Pearl River Delta under shared socioeconomic pathways.

Science of The Total Environment, 762, 143144. https://doi.org/10.1016/j.scitotenv.2020.143144

Chen, Y., Guo, F., Wang, J., Cai, W., Wang, C., & Wang, K. (2020). Provincial and gridded population projection for China under shared socioeconomic pathways from 2010 to 2100. *Scientific Data*, 7(1), 83. https://doi.org/10.1038/s41597-020-0421-y

Chen, Y., Niu, Z., Hu, S. & Zhang, H. (2016). Dynamic monitoring of dongting lake wetland using time-series MODIS imagery. *Journal of Hydraulic Engineering*, 47(9), 1093-1104.

Chen, Y., Yu, J., & Khan, S. (2013). The spatial framework for weight sensitivity analysis in AHP-based multi-criteria decision making. *Environmental modelling & software*, *48*, 129-140. https://doi.org/10.1016/j.envsoft.2013.06.010

Chen, Y., Zhou, H., Zhang, H., Du, G. & Zhou, J. (2015). Urban flood risk warning under rapid urbanization. *Environmental research*, *139*, 3-10. https://doi.org/10.1016/j.envres.2015.02.028

Chen, Z., Yu, L., & Gupta, A. (2001). The Yangtze River: an introduction. *Geomorphology*, *2–3*(41), 73–75. https://www.infona.pl//resource/bwmeta1.element.elsevier-64b02f7c-a3bc-365f-b0be-a5cd124149ba

Chen, Z., Yu, L., & Gupta, A. (2001). The Yangtze River: an introduction. *Geomorphology*, *2–3*(41), 73–75. https://www.infona.pl//resource/bwmeta1.element.elsevier-64b02f7c-a3bc-365f-b0be-a5cd124149ba

Chowdhury, M.S. (2024). Comparison of accuracy and reliability of random forest, support vector machine, artificial neural network, and maximum likelihood method in land use/cover classification of urban setting. *Environmental Challenges*, 14, 100800. https://doi.org/10.1016/j.envc.2023.100800

Christovam, L. E., Pessoa, G. G., Shimabukuro, M. H., & Galo, M. L. B. T. (2019). LAND USE AND LAND COVER CLASSIFICATION USING HYPERSPECTRAL IMAGERY: EVALUATING THE PERFORMANCE OF SPECTRAL ANGLE MAPPER, SUPPORT VECTOR MACHINE AND RANDOM FOREST. *The International Archives of the*

Photogrammetry, Remote Sensing and Spatial Information Sciences, *XLII-2-W13*, 1841–1847. https://doi.org/10.5194/isprs-archives-XLII-2-W13-1841-2019

Christie, E. K., Spencer, T., Owen, D., McIvor, A. L., Möller, I., & Viavattene, C. (2018). Regional coastal flood risk assessment for a tidally dominant, natural coastal setting: North Norfolk, southern North Sea. *Coastal Engineering*, *134*, 177–190. https://doi.org/10.1016/j.coastaleng.2017.05.003

Coleman, J. M., Huh, O. K., & Jr, D. B. (2008). Wetland Loss in World Deltas. *Journal of Coastal Research*, *24*(sp1), 1–14. https://doi.org/10.2112/05-0607.1

Corcoran, J. M., Knight, J. F., & Gallant, A. L. (2013). Influence of Multi-Source and Multi-Temporal Remotely Sensed and Ancillary Data on the Accuracy of Random Forest Classification of Wetlands in Northern Minnesota. Remote Sensing, 5(7), 3212–3238. https://doi.org/10.3390/rs5073212

Cui, L., Gao, C., Zhao, X., Ma, Q., Zhang, M., Li, W., Song, H., Wang, Y., Li, S., & Zhang, Y. (2013). Dynamics of the lakes in the middle and lower reaches of the Yangtze River basin, China, since the late nineteenth century. *Environmental Monitoring and Assessment*, *185*(5), 4005–4018. https://doi.org/10.1007/s10661-012-2845-0

Cui, L., Ge, Z., Yuan, L., & Zhang, L. (2015). Vulnerability assessment of the coastal wetlands in the Yangtze Estuary, China to sea-level rise. Estuarine, Coastal and Shelf Science, 156, 42–51. https://doi.org/10.1016/j.ecss.2014.06.015

Cunillera-Montcusí, D., Beklioğlu, M., Cañedo-Argüelles, M., Jeppesen, E., Ptacnik, R., Amorim, C. A., Arnott, S. E., Berger, S. A., Brucet, S., Dugan, H. A., Gerhard, M., Horváth, Z., Langenheder, S., Nejstgaard, J. C., Reinikainen, M., Striebel, M., Urrutia-Cordero, P., Vad, C. F., Zadereev, E., & Matias, M. (2022). Freshwater salinisation: a research agenda for a saltier world. *Trends in Ecology & Evolution*, *37*(5), 440–453. https://doi.org/10.1016/j.tree.2021.12.005

Dai, X., Yu, Z., Yang, G., & Wan, R. (2020). Role of Flooding Patterns in the Biomass Production of Vegetation in a Typical Herbaceous Wetland, Poyang Lake Wetland, China. *Frontiers in Plant Science*, *11*. https://doi.org/10.3389/fpls.2020.521358

Davidson, N. C. (2014). How much wetland has the world lost? Long-term and recent trends in global wetland area. *Marine and Freshwater Research*, *65*(10), 934–941. https://doi.org/10.1071/MF14173

Dang, K. B., Nguyen, M. H., Nguyen, D. A., Phan, T. T. H., Giang, T. L., Pham, H. H., Nguyen, T. N., Tran, T. T. V., & Bui, D. T. (2020). Coastal Wetland Classification with Deep U-Net Convolutional Networks and Sentinel-2 Imagery: A Case Study at the Tien Yen Estuary of Vietnam. Remote Sensing, 12(19), 3270. https://doi.org/10.3390/rs12193270

Davidson, N. C., Fluet-Chouinard, E., & Finlayson, C. M. (2018). Global extent and distribution of wetlands: trends and issues. *Marine and Freshwater Research*, *69*(4), 620–627. https://doi.org/10.1071/MF17019

Demarquet, Q., Rapinel, S., Dufour, S. and Hubert-Moy, L. (2023). Long-term wetland monitoring using the landsat archive: A review. *Remote Sensing*, *15*(3), 820. https://doi.org/10.3390/rs15030820

De Moel, H., Jongman, B., Kreibich, H., Merz, B., Penning-Rowsell, E., & Ward, P. J. (2015). Flood risk assessments at different spatial scales. *Mitigation and Adaptation Strategies for Global Change*, *20*(6), 865–890. https://doi.org/10.1007/s11027-015-9654-z

Delang, C.O. & Yuan, Z. (2015). China's Grain for Green Program: A review of the largest ecological restoration and rural development program in the world. Switzerland: *Springer International Publishing.* https://doi.org/10.1007/978-3-319-11505-4

Deng, X., Zhong, L., Xie, G., Wan, L., & Song, W. (2019). Spatial and temporal changes of land ecosystem service value in Dongting Lake area in 1995–2015. *Geographical. Research*, **38,** 844-855. https://doi.org/10.11821/dlyj020170999

De Oliveira, M., Morrison, T., O'Brien, K.R. & Lovelock, C.E. (2024). Governance of coastal wetlands: Beyond the community conservation paradigm. *Ocean & Coastal Management*, 255, 107253. https://doi.org/10.1016/j.ocecoaman.2024.107253

Development Assistance Committee Organization for Economic Co-operation and Development (OECD). (1996). *Guidelines for aid agencies for improved conservation and sustainable use of tropical and sub-tropical wetlands*. OECD.

Díaz-Pinzón, L., Sierra, L., & Trillas, F. (2022). The Economic Value of Wetlands in Urban Areas: The Benefits in a Developing Country. *Sustainability*, *14*(14), 8302. https://doi.org/10.3390/su14148302

Ding, W., Wu, J., Tang, R., Chen, X., & Xu, Y. (2022). A Review of Flood Risk in China during 1950–2019: Urbanization, Socioeconomic Impact Trends and Flood Risk Management. *Water*, *14*(20), 3246. https://doi.org/10.3390/w14203246

Disse, M., Johnson, T.G., Leandro, J. and Hartmann, T. (2020). Exploring the relation between flood risk management and flood resilience. *Water Security*, *9*, 100059. https://doi.org/10.1016/j.wasec.2020.100059

Dong, L., Wan, R., Li, B., Tan, Z., Yang, S., & Zhang, T. (2022). Spatiotemporal dynamics of lake wetland in the Wanjiang Plain of the Yangtze River basin, China during the recent century. *Ecological Indicators,* 142, 109295. https://doi.org/10.1016/j.ecolind.2022.109295

Dottori, F., Mentaschi, L., Bianchi, A., Alfieri, L. & Feyen, L. (2020). *Adapting to rising river flood risk in the EU under climate change*. EUR 29955 EN. Luxembourg: Publications Office of the European Union. Available at: https://doi.org/10.2760/14505 [Accessed 28 Mar. 2025].

Dortch, M. S., Zakikhani, M., Kim, S.-C., & Steevens, J. A. (2008). Modeling water and sediment contamination of Lake Pontchartrain following pump-out of Hurricane Katrina floodwater. *Journal of Environmental Management*, *87*(3), 429–442. https://doi.org/10.1016/j.jenvman.2007.01.035

Douglas, I. (2009). Climate change, flooding and food security in south Asia. *Food Security*, *1*(2), 127–136. https://doi.org/10.1007/s12571-009-0015-1

Dou, Y., Xue, X., Zhao, Z., Luo, X., Ji, A., & Luo, T. (2018). Multi-Index Evaluation for Flood Disaster from Sustainable Perspective: A Case Study of Xinjiang in China. *International Journal of Environmental Research and Public Health*, *15*(9), 1983. https://doi.org/10.3390/ijerph15091983

Duan, W., He, B., Nover, D., Fan, J., Yang, G., Chen, W., Meng, H., & Liu, C. (2016). Floods and associated socioeconomic damages in China over the last century. *Natural Hazards*, *82*(1), 401–413. https://doi.org/10.1007/s11069-016-2207-2

Duan, Y., Li, X., Zhang, L., Liu, W., Liu, S., Chen, D., & Ji, H. (2020). Detecting spatiotemporal changes of large-scale aquaculture ponds regions over 1988–2018 in Jiangsu Province, China using Google Earth Engine. Ocean & Coastal Management, 188, 105144. https://doi.org/10.1016/j.ocecoaman.2020.105144

Dugan, P. (1993). *Wetlands in Danger—A World Conservation Atlas*; Oxford University Press: New York, NY, USA.

Du, S., Van Rompaey, A., Shi, P., & Wang, J. (2015). A dual effect of urban expansion on flood risk in the Pearl River Delta (China) revealed by land-use scenarios and direct runoff simulation. *Natural Hazards*, *77*(1), 111–128. https://doi.org/10.1007/s11069-014-1583-8

Du, Y., Xue, H., Wu, S., Ling, F., Xiao, F., & Wei, X. (2011). Lake area changes in the middle Yangtze region of China over the 20th century. *Journal of Environmental Management*, *92*(4), 1248–1255. https://doi.org/10.1016/j.jenvman.2010.12.007

El Naqa, I., & Murphy, M. J. (2015). What Is Machine Learning? In I. El Naqa, R. Li, & M. J. Murphy (Eds.), *Machine Learning in Radiation Oncology: Theory and Applications* (pp. 3–11). Springer International Publishing. https://doi.org/10.1007/978-3-319-18305-3_1

Elshorbagy, A., Bharath, R., Lakhanpal, A., Ceola, S., Montanari, A., & Lindenschmidt, K.-E. (2017). Topography- and nightlight-based national flood risk assessment in Canada. *Hydrology and Earth System Sciences*, *21*(4), 2219–2232. https://doi.org/10.5194/hess-21-2219-2017

Euripidou, E., & Murray, V. (2004). Public health impacts of floods and chemical contamination. *Journal of Public Health*, *26*(4), 376–383. https://doi.org/10.1093/pubmed/fdh163

Eyring, V., Bony, S., Meehl, G. A., Senior, C. A., Stevens, B., Stouffer, R. J., & Taylor, K. E. (2016). Overview of the Coupled Model Intercomparison Project Phase 6 (CMIP6) experimental design and organization. *Geoscientific Model Development,* 9(5), 1937–1958. https://doi.org/10.5194/gmd-9-1937-2016

Eyring, V., Cox, P. M., Flato, G. M., Gleckler, P. J., Abramowitz, G., Caldwell, P., Collins, W. D., Gier, B. K., Hall, A. D., Hoffman, F. M., Hurtt, G. C., Jahn, A., Jones, C. D., Klein, S. A., Krasting, J. P., Kwiatkowski, L., Lorenz, R., Maloney, E., Meehl, G. A., … Williamson,

M. S. (2019). Taking climate model evaluation to the next level. *Nature Climate Change,* 9(2), 102–110. https://doi.org/10.1038/s41558-018-0355-y

Fang, J., Hu, J., Shi, X., & Zhao, L. (2019). Assessing disaster impacts and response using social media data in China: A case study of 2016 Wuhan rainstorm. *International Journal of Disaster Risk Reduction*, *34*, 275–282. https://doi.org/10.1016/j.ijdrr.2018.11.027

Feng, J., Qin, T., Yan, D., Lv, X., Yan, D., Zhang, X. & Li, W. (2024). The role of large reservoirs in drought and flood disaster risk mitigation: A case of the Yellow River Basin. *Science of The Total Environment*, *949*, 175255. https://doi.org/10.1016/j.scitotenv.2024.175255

Feng, L., Hu, C., Chen, X., Cai, X., Tian, L., & Gan, W. (2012). Assessment of inundation changes of Poyang Lake using MODIS observations between 2000 and 2010. *Remote Sensing of Environment*, *121*, 80–92. https://doi.org/10.1016/j.rse.2012.01.014

Feng, S., Li, W., Xu, J., Liang, T., Ma, X., Wang, W., & Yu, H. (2022). Land Use/Land Cover Mapping Based on GEE for the Monitoring of Changes in Ecosystem Types in the Upper Yellow River Basin over the Tibetan Plateau. Remote Sensing, 14(21), 5361. https://doi.org/10.3390/rs14215361

Ferreira, C. S. S., Kašanin-Grubin, M., Solomun, M. K., Sushkova, S., Minkina, T., Zhao, W., & Kalantari, Z. (2023). Wetlands as nature-based solutions for water management in different environments. *Current Opinion in Environmental Science & Health*, *33*, 100476. https://doi.org/10.1016/j.coesh.2023.100476

Finlayson, C.M. and Davidson, N.C. (1999). Global review of wetland resources and priorities for wetland inventory. *Preface iv Summary Report*, *15*.

Finlayson, M., Milton, G., Prentice, C., & Davidson, N. (2018). The Wetland Book: II: Distribution, Description, and Conservation. https://doi.org/10.1007/978-94-007-4001-3

Fluet-Chouinard, E., Stocker, B. D., Zhang, Z., Malhotra, A., Melton, J. R., Poulter, B., Kaplan, J. O., Goldewijk, K. K., Siebert, S., Minayeva, T., Hugelius, G., Joosten, H., Barthelmes, A., Prigent, C., Aires, F., Hoyt, A. M., Davidson, N., Finlayson, C. M., Lehner, B., … McIntyre, P. B. (2023). Extensive global wetland loss over the past three centuries. *Nature*, *614*(7947), 281–286. https://doi.org/10.1038/s41586-022-05572-6

Foulds, S. A., Brewer, P. A., Macklin, M. G., Haresign, W., Betson, R. E., & Rassner, S. M. E. (2014). Flood-related contamination in catchments affected by historical metal mining: An unexpected and emerging hazard of climate change. *Science of The Total Environment*, *476–477*, 165–180. https://doi.org/10.1016/j.scitotenv.2013.12.079

Fournier, M., Larrue, C., Alexander, M., Hegger, D., Bakker, M., Pettersson, M., Crabbé, A., Mees, H., & Chorynski, A. (2016). Flood risk mitigation in Europe: how far away are we from the aspired forms of adaptive governance? *Ecology and Society*, *21*(4). https://www.jstor.org/stable/26270027

Frazier, A. E., & Hemingway, B. L. (2021). A Technical Review of Planet Smallsat Data: Practical Considerations for Processing and Using PlanetScope Imagery. *Remote Sensing*, *13*(19), 3930. https://doi.org/10.3390/rs13193930

Fu, B., Wang, Y. K., Xu, P., & Yan, K. (2013). Mapping the flood mitigation services of ecosystems – A case study in the Upper Yangtze River Basin. Ecological Engineering, 52, 238–246. https://doi.org/10.1016/j.ecoleng.2012.11.008

Gallant, A. L. (2015). The Challenges of Remote Monitoring of Wetlands. *Remote Sensing*, *7*(8), 10938–10950. https://doi.org/10.3390/rs70810938

Gallego-Sala, A. V., Charman, D. J., Brewer, S., Page, S. E., Prentice, I. C., Friedlingstein, P., Moreton, S., Amesbury, M. J., Beilman, D. W., Björck, S., Blyakharchuk, T., Bochicchio, C., Booth, R. K., Bunbury, J., Camill, P., Carless, D., Chimner, R. A., Clifford, M., Cressey, E., … Zhao, Y. (2018). Latitudinal limits to the predicted increase of the peatland carbon sink with warming. *Nature Climate Change*, *8*(10), 907–913. https://doi.org/10.1038/s41558-018-0271-1

Gall, M., Borden, K. A., & Cutter, S. L. (2009). *When Do Losses Count?* https://doi.org/10.1175/2008BAMS2721.1

Gangrade, S., Kao, S.-C., Dullo, T. T., Kalyanapu, A. J., & Preston, B. L. (2019). Ensemble-based flood vulnerability assessment for probable maximum flood in a changing environment. *Journal of Hydrology*, *576*, 342–355. https://doi.org/10.1016/j.jhydrol.2019.06.027

Ganapathi, H., Awasthi, S., & Vasudevan, P. (2024). Wetlands as a Nature-based Solution for Urban Water Management. In A. Stefanakis, H. V. Oral, C. Calheiros, & P. Carvalho (Eds.),

Nature-based Solutions for Circular Management of Urban Water (pp. 259–275). Springer International Publishing. https://doi.org/10.1007/978-3-031-50725-0_15

Gao, Y., Cao, G., Ni, P., Tang, Y., Liu, Y., Bi, J., & Ma, Z. (2021). Natural hazard triggered technological risks in the Yangtze River Economic Belt, China. *Scientific Reports*, *11*(1), 13842. https://doi.org/10.1038/s41598-021-93353-y

Gardner, R. C., Barchiesi, S., Beltrame, C., Finlayson, C., Galewski, T., Harrison, I., Paganini, M., Perennou, C., Pritchard, D., Rosenqvist, A., & Walpole, M. (2015). *State of the World's Wetlands and Their Services to People: A Compilation of Recent Analyses* (SSRN Scholarly Paper No. 2589447). https://doi.org/10.2139/ssrn.2589447

Gardner, R. C., & Finlayson, C. (2018). *Global Wetland Outlook: State of the World's Wetlands and Their Services to People* (SSRN Scholarly Paper No. 3261606). https://papers.ssrn.com/abstract=3261606

Ge, G., Shi, Z., Zhu, Y., Yang, X. & Hao, Y. (2020). Land use/cover classification in an arid desert-oasis mosaic landscape of China using remote sensed imagery: Performance assessment of four machine learning algorithms. *Global Ecology and Conservation*, *22*, e00971. https://doi.org/10.1016/j.gecco.2020.e00971

Ghosh, A., & Joshi, P. K. (2014). A comparison of selected classification algorithms for mapping bamboo patches in lower Gangetic plains using very high resolution WorldView 2 imagery. International Journal of Applied Earth Observation and Geoinformation, 26, 298–311. https://doi.org/10.1016/j.jag.2013.08.011

Gigović, L., Pamučar, D., Bajić, Z., & Drobnjak, S. (2017a). Application of GIS-Interval Rough AHP Methodology for Flood Hazard Mapping in Urban Areas. *Water*, *9*(6), 360. https://doi.org/10.3390/w9060360

Gigović, L., Pamučar, D., Božanić, D. and Ljubojević, S. (2017b). Application of the GIS-DANP-MABAC multi-criteria model for selecting the location of wind farms: A case study of Vojvodina, Serbia. *Renewable energy*, *103*, 501-521.

Gorelick, N., Hancher, M., Dixon, M., Ilyushchenko, S., Thau, D., & Moore, R. (2017). Google Earth Engine: Planetary-scale geospatial analysis for everyone. *Remote Sensing of Environment*, *202*, 18–27. https://doi.org/10.1016/j.rse.2017.06.031

Gislason, P. O., Benediktsson, J. A., & Sveinsson, J. R. (2006). Random Forests for land cover classification. Pattern Recognition Letters, 27(4), 294–300. https://doi.org/10.1016/j.patrec.2005.08.011

Gong, P., Liu, H., Zhang, M., Li, C., Wang, J., Huang, H., Clinton, N., Ji, L., Li, W., Bai, Y. and Chen, B. (2019). Stable classification with limited sample: Transferring a 30-m resolution sample set collected in 2015 to mapping 10-m resolution global land cover in 2017. *Sci. Bull*, *64*(6), 370-373. https://doi.org/10.1016/j.scib.2019.03.002

Gong, P., Niu, Z., Cheng, X., Zhao, K., Zhou, D., Guo, J., Liang, L., Wang, X., Li, D., Huang, H., Wang, Y., Wang, K., Li, W., Wang, X., Ying, Q., Yang, Z., Ye, Y., Li, Z., Zhuang, D., … Yan, J. (2010). China's wetland change (1990–2000) determined by remote sensing. *Science China Earth Sciences*, *53*(7), 1036–1042. https://doi.org/10.1007/s11430-010-4002-3

Goodwell, A. E., Zhu, Z., Dutta, D., Greenberg, J. A., Kumar, P., Garcia, M. H., Rhoads, B. L., Holmes, R. R., Parker, G., Berretta, D. P., & Jacobson, R. B. (2014). Assessment of Floodplain Vulnerability during Extreme Mississippi River Flood 2011. *Environmental Science & Technology*, *48*(5), 2619–2625. https://doi.org/10.1021/es404760t

Gorelick, N., Hancher, M., Dixon, M., Ilyushchenko, S., Thau, D., & Moore, R. (2017). Google Earth Engine: Planetary-scale geospatial analysis for everyone. Remote Sensing of Environment, 202, 18–27. https://doi.org/10.1016/j.rse.2017.06.031

Greb, S. F., DiMichele, W. A., & Gastaldo, R. A. (2006). Evolution and importance of wetlands in earth history. In S. F. Greb & W. A. DiMichele (Eds.), *Wetlands through Time* (p. 0). Geological Society of America. https://doi.org/10.1130/2006.2399(01)

Grimaldi, S., Schumann, G. J.-P., Shokri, A., Walker, J. P., & Pauwels, V. R. N. (2019). Challenges, Opportunities, and Pitfalls for Global Coupled Hydrologic-Hydraulic Modeling of Floods. *Water Resources Research*, *55*(7), 5277–5300. https://doi.org/10.1029/2018WR024289

Guan, B., Chen, S., Liu, X., Gong, X., & Ge, G. (2019). Evolutionary hotspots in the middle and lower reaches of the Yangtze River Basin. *Ecological Informatics,* 52, 1–6. https://doi.org/10.1016/j.ecoinf.2019.03.008

Guan, X., Wang, J., & Xiao, F. (2021). Sponge city strategy and application of pavement materials in sponge city. *Journal of Cleaner Production*, *303*, 127022. https://doi.org/10.1016/j.jclepro.2021.127022

Gulbin, S., Kirilenko, A. P., Kharel, G., & Zhang, X. (2019). Wetland loss impact on long-term flood risks in a closed watershed. *Environmental Science & Policy*, 94, 112–122. https://doi.org/10.1016/j.envsci.2018.12.032

Gupta, A., Bilskie, M. V., & Woodson, C. B. (2025). The potential of wetlands and barrier islands as a coastal defense in mitigating the storm surge. *Frontiers in Ecology and Evolution*, *13*, 1524570. https://doi.org/10.3389/fevo.2025.1524570

GoI. 2009. National Policy on Disaster Management 2009. New Delhi: Ministry of Home Affairs, Government of India.

GoI. 2011. Report of working group on flood management and region specific issues. New Delhi: Planning Commission, Government of India.

Gopal, B. (2013). Future of wetlands in tropical and subtropical Asia, especially in the face of climate change. *Aquatic Sciences*, *75*(1), 39–61. https://doi.org/10.1007/s00027-011-0247-y

Grau-Andrés, R., Gray, A., & Davies, G. M. (2017). Sphagnum abundance and photosynthetic capacity show rapid short-term recovery following managed burning. *Plant Ecology & Diversity*, *10*(4), 353–359. https://doi.org/10.1080/17550874.2017.1394394

Guha-Sapir, D., & Below, R. (2002). *The quality and accuracy of disaster data: A comparative analysis of three global data sets*. Geneva, Switzerland: Provention Consortium.

Gulbin, S., Kirilenko, A. P., Kharel, G., & Zhang, X. (2019). Wetland loss impact on long term flood risks in a closed watershed. *Environmental Science & Policy*, *94*, 112–122. https://doi.org/10.1016/j.envsci.2018.12.032

Guo, D., Shi, W., Qian, F., Wang, S., & Cai, C. (2022). Monitoring the spatiotemporal change of Dongting Lake wetland by integrating Landsat and MODIS images, from 2001 to 2020. *Ecological Informatics*, *72*, 101848. https://doi.org/10.1016/j.ecoinf.2022.101848

Guo, D., Yu, E., & Wang, H. (2016). Will the Tibetan Plateau warming depend on elevation in the future? Journal of Geophysical Research: Atmospheres, 121(8), 3969–3978. https://doi.org/10.1002/2016JD024871

Guo, H. (2017). Big data drives the development of Earth science. *Big Earth Data*, *1*(1–2), 1–3. https://doi.org/10.1080/20964471.2017.1405925

Guo, H., Hu, Q., Zhang, Q., & Feng, S. (2012). Effects of the Three Gorges Dam on Yangtze River flow and river interaction with Poyang Lake, China: 2003–2008. *Journal of Hydrology*, *416–417*, 19–27. https://doi.org/10.1016/j.jhydrol.2011.11.027

Guo, J., Wang, J., & Zhao, X. (2023). Risk Assessment of Flood Disaster in Sichuan Province Based on GIS. *E3S Web of Conferences*, 406, 04008. https://doi.org/10.1051/e3sconf/202340604008

Guo, R., Cheng, L., Li, J., Hahn, P. R., & Liu, H. (2020). A Survey of Learning Causality with Data: Problems and Methods. *ACM Comput. Surv.*, *53*(4), 75:1-75:37. https://doi.org/10.1145/3397269

Guoyi, L.I., Liu, J. & Shao, W. (2023). Urban flood risk assessment under rapid urbanization in Zhengzhou City, China. *Regional Sustainability*, *4*(3), 332-348. https://doi.org/10.1016/j.regsus.2023.08.004

Guo, Z., Zhao, Q., & Shi, X. (2024). A long-term (1984–2021) wetland classification dataset for the Yangtze River Basin from continuous Landsat image collections. *Total Environment Advances,* 11, 200111. https://doi.org/10.1016/j.teadva.2024.200111

Guo, Z., Shi, X., Zhang, D & Zhao, Q. (2025). Effects of Long-Term Wetland Variations on Flood Risk Assessments in the Yangtze River Basin. *Environmental Impact Assessment Review.* 116, 108123. https://doi.org/10.1016/j.eiar.2025.108123.

Gupta, R., Chembolu, V., Marjoribanks, T. I., & Dutta, S. (2024). Assessing the efficacy of hydro-ecological based wetland management approach for flood resilience of a large river catchment. *Journal of Hydrology*, *641*, 131761. https://doi.org/10.1016/j.jhydrol.2024.131761

Ham, J., Chen, Y., Crawford, M. M., & Ghosh, J. (2005). Investigation of the random forest framework for classification of hyperspectral data. IEEE Transactions on Geoscience and Remote Sensing, 43(3), 492–501. https://doi.org/10.1109/TGRS.2004.842481

Han, X., & Sheng, J. (2024). Governing the Future through 'Ecological civilization': Anticipatory Politics and China's Great Yangtze River Protection Programme. *Journal of Contemporary China*. https://www.tandfonline.com/doi/abs/10.1080/10670564.2023.2232747

Hao, B., Ma, M., Li, S., Li, Q., Hao, D., Huang, J., Ge, Z., Yang, H., & Han, X. (2019). Land Use Change and Climate Variation in the Three Gorges Reservoir Catchment from 2000 to 2015 Based on the Google Earth Engine. *Sensors*, *19*(9), 2118. https://doi.org/10.3390/s19092118

Halgamuge, M. N., & Nirmalathas, A. (2017). Analysis of large flood events: Based on flood data during 1985–2016 in Australia and India. *International Journal of Disaster Risk Reduction*, *24*, 1–11. https://doi.org/10.1016/j.ijdrr.2017.05.011

Han, Y., Huang, J., Ling, F., Qiu, J., Liu, Z., Li, X., Chang, C., & Chi, H. (2023). Dynamic Mapping of Inland Freshwater Aquaculture Areas in Jianghan Plain, China. *IEEE Journal of Selected Topics in Applied Earth Observations and Remote Sensing*, *16*, 4349–4361. https://doi.org/10.1109/JSTARS.2023.3269430

Haraguchi, M., & Lall, U. (2015). Flood risks and impacts: A case study of Thailand's floods in 2011 and research questions for supply chain decision making. *International Journal of Disaster Risk Reduction*, *14*, 256–272. https://doi.org/10.1016/j.ijdrr.2014.09.005

Harvey, J. W., Schaffranek, R. W., Noe, G. B., Larsen, L. G., Nowacki, D. J., & O'Connor, B. L. (2009). Hydroecological factors governing surface water flow on a low-gradient floodplain. *Water Resources Research*, *45*(3). https://doi.org/10.1029/2008WR007129

Hegger, D., Driessen, P. P. J., Bakker, M., Alexander, M., Beyers, J.-C., Buijze, A., Bruzzone, S., Choryński, A., Crabbé, A., Deketelaere, K., Delvaux, B., Dieperink, C., van Doorn-Hoekveld, W., Ek, K., Fournier, M., Ganzevoort, W., Gilissen, H. K., Goytia, S., Gralepois, M., & Wiering, M. (2016). *A view on more resilient flood risk governance: key conclusions of the STAR-FLOOD project*. https://doi.org/10.13140/RG.2.1.4402.6001

Hemmerling, J., Pflugmacher, D., & Hostert, P. (2021). Mapping temperate forest tree species using dense Sentinel-2 time series. Remote Sensing of Environment, 267, 112743. https://doi.org/10.1016/j.rse.2021.112743

Henry, A. L., Robinson, R., Sinnott, K., Tarsa, E., Brunson, M. W., & Kettenring, K. M. (2024). Lay of the (wet)land: manager practices and challenges in wetland revegetation. *Restoration Ecology*, *32*(5), e14167. https://doi.org/10.1111/rec.14167

He, Y., Li, X., Guo, W., & Ma, Z. (2012). Division of labor in rhizomatous species: Comparative performance of native and invasive species in the tidal marshes of the Yangtze

River estuary, China. *Journal of Experimental Marine Biology and Ecology*, *422–423*, 122–128. https://doi.org/10.1016/j.jembe.2012.04.010

Holden, J., Chapman, P. J., & Labadz, J. C. (2004). Artificial drainage of peatlands: hydrological and hydrochemical process and wetland restoration. *Progress in Physical Geography: Earth and Environment*, *28*(1), 95–123. https://doi.org/10.1191/0309133304pp403ra

Holden, J., Evans, M. G., Burt, T. P., & Horton, M. (2006). Impact of Land Drainage on Peatland Hydrology. *Journal of Environmental Quality*, *35*(5), 1764–1778. https://doi.org/10.2134/jeq2005.0477

Holden, J., Gascoign, M., & Bosanko, N. R. (2007). Erosion and natural revegetation associated with surface land drains in upland peatlands. *Earth Surface Processes and Landforms*, *32*(10), 1547–1557. https://doi.org/10.1002/esp.1476

Hou, X., Feng, L., Tang, J., Song, X.-P., Liu, J., Zhang, Y., Wang, J., Xu, Y., Dai, Y., Zheng, Y., Zheng, C., & Bryan, B. A. (2020). Anthropogenic transformation of Yangtze Plain freshwater lakes: patterns, drivers and impacts. *Remote Sensing of Environment*, *248*, 111998. https://doi.org/10.1016/j.rse.2020.111998

Hovis, M., Hollinger, J. C., Cubbage, F., Shear, T., Doll, B., Kurki-Fox, J. J., Line, D., Fox, A., Baldwin, M., Klondike, T., Lovejoy, M., Evans, B., West, J., & Potter, T. (2021). Natural Infrastructure Practices as Potential Flood Storage and Reduction for Farms and Rural Communities in the North Carolina Coastal Plain. *Sustainability*, *13*(16), 9309. https://doi.org/10.3390/su13169309

Howie, S. A., Whitfield, P. H., Hebda, R. J., Munson, T. G., Dakin, R. A., & Jeglum, J. K. (2009). Water Table and Vegetation Response to Ditch Blocking: Restoration of a Raised Bog in Southwestern British Columbia. *Canadian Water Resources Journal / Revue Canadienne Des Ressources Hydriques*, *34*(4), 381–392. https://doi.org/10.4296/cwrj3404381

Hrdinka, T., Novický, O., Hanslík, E., & Rieder, M. (2012). Possible impacts of floods and droughts on water quality. *Journal of Hydro-Environment Research*, *6*(2), 145–150. https://doi.org/10.1016/j.jher.2012.01.008

Huang, B., Ouyang, Z., Zheng, H., Zhang, H., & Wang, X. (2008). Construction of an eco-island: A case study of Chongming Island, China. *Ocean & Coastal Management*, *51*(8), 575–588. https://doi.org/10.1016/j.ocecoaman.2008.06.007

Huang, H., Cui, H., & Ge, Q. (2021). Assessment of potential risks induced by increasing extreme precipitation under climate change. *Natural Hazards,* 108(2), 2059–2079. https://doi.org/10.1007/s11069-021-04768-9

Huang, X., & Zhang, L. (2010). Comparison of Vector Stacking, Multi-SVMs Fuzzy Output, and Multi-SVMs Voting Methods for Multiscale VHR Urban Mapping. *IEEE Geoscience and Remote Sensing Letters*, *7*(2), 261–265. https://doi.org/10.1109/LGRS.2009.2032563

Huang, Y., Wang, H., Xiao, W., Chen, L., & Yang, H. (2019). Spatiotemporal characteristics of precipitation concentration and the possible links of precipitation to monsoons in China from 1960 to 2015. *Theoretical and Applied Climatology,* 138(1), 135–152. https://doi.org/10.1007/s00704-019-02814-y

Huang, X., Wang, Y., Li, J., Chang, X., Cao, Y., Xie, J. and Gong, J. (2020). High-resolution urban land-cover mapping and landscape analysis of the 42 major cities in China using ZY-3 satellite images. *Science Bulletin*, *65*(12), 1039-1048. https://doi.org/10.1016/j.scib.2020.03.003

Huabin, W., Gangjun, L., Weiya, X., & Gonghui, W. (2005). GIS-based landslide hazard assessment: an overview. *Progress in Physical Geography*, *29*(4), 548–567. https://doi.org/10.1191/0309133305pp462ra

Huang, Y., Chen, X.S., Zou, Y.A., Zhang, P.Y., Li, F., Hou, Z.Y., Li, X., Zeng, J., Deng, Z.M., Zhong, J.R. and Xie, Y.H. (2022). Exploring the relative contribution of flood regimes and climatic factors to Carex phenology in a Yangtze River-connected floodplain wetland. *Science of The Total Environment*, *847*, 157568. https://doi.org/10.1016/j.scitotenv.2022.157568.

Huo, X., & Niu, Z. (2024). Fine-Resolution Wetland Mapping in the Yellow River Basin Using Sentinel-1/2 Data via Zoning-Based Random Forest with Remote Sensing Feature Preferences. *Water*, *16*(17), 2415. https://doi.org/10.3390/w16172415

Hupp, C. R., Pierce, A. R., & Noe, G. B. (2009). Floodplain geomorphic processes and environmental impacts of human alteration along Coastal Plain rivers, USA. *Wetlands*, *29*(2), 413–429. https://doi.org/10.1672/08-169.1

Hu, Q., Feng, S., Guo, H., Chen, G., & Jiang, T. (2007). Interactions of the Yangtze river flow and hydrologic processes of the Poyang Lake, China. *Journal of Hydrology*, *347*(1), 90–100. https://doi.org/10.1016/j.jhydrol.2007.09.005

Hu, S., Cheng, X., Zhou, D., & Zhang, H. (2017). GIS-based flood risk assessment in suburban areas: a case study of the Fangshan District, Beijing. *Natural Hazards*, *87*(3), 1525–1543. https://doi.org/10.1007/s11069-017-2828-0

Huth, J., Gessner, U., Klein, I., Yesou, H., Lai, X., Oppelt, N., & Kuenzer, C. (2020). Analyzing Water Dynamics Based on Sentinel-1 Time Series—a Study for Dongting Lake Wetlands in China. *Remote Sensing*, *12*(11), 1761. https://doi.org/10.3390/rs12111761

Ifrah, G. (2000). *The universal history of computing: From the abacus to quantum computing*. John Wiley & Sons, Inc.

IPCC (2006). *2006 IPCC Guidelines for National Greenhouse Gas Inventories*. Prepared by the National Greenhouse Gas Inventories Programme, Eggleston, H.S., Buendia, L., Miwa, K., Ngara, T., and Tanabe, K. (eds). IGES, Japan.

IPCC (2012). *Managing the Risks of Extreme Events and Disasters to Advance Climate Change Adaptation: Special Report of the Intergovernmental Panel on Climate Change.* Cambridge University Press, Cambridge, UK.

IPCC (2014). Climate Change 2014: *Synthesis Report.* Cambridge University Press, Cambridge, UK.

IPCC (2021). 'Weather and Climate Extreme Events in a Changing Climate', in *Climate Change 2021 – The Physical Science Basis: Working Group I Contribution to the Sixth Assessment Report of the Intergovernmental Panel on Climate Change*. Cambridge University Press, Cambridge, UK. 1513–1766.

Islam, M. F., Bhattacharya, B., & Popescu, I. (2019). Flood risk assessment due to cyclone-induced dike breaching in coastal areas of Bangladesh. *Natural Hazards and Earth System Sciences*, *19*(2), 353–368. https://doi.org/10.5194/nhess-19-353-2019

Jafari, N., Shahsanai, A., Memarzadeh, M., & Loghmani, A. (2011). Prevention of communicable diseases after disaster: A review. *Journal of Research in Medical Sciences : The Official Journal of Isfahan University of Medical Sciences*, *16*(7), 956–962. https://www.ncbi.nlm.nih.gov/pmc/articles/PMC3263111/

Jakovljević, G., Govedarica, M., & Álvarez-Taboada, F. (2019). Waterbody mapping: a comparison of remotely sensed and GIS open data sources. *International Journal of Remote Sensing*, 40(8), 2936-2964. https://doi.org/10.1080/01431161.2018.1538584

Jamali, A., Mahdianpari, M., Brisco, B., Granger, J., Mohammadimanesh, F., & Salehi, B. (2021). Wetland Mapping Using Multi-Spectral Satellite Imagery and Deep Convolutional Neural Networks: A Case Study in Newfoundland and Labrador, Canada. Canadian Journal of Remote Sensing, 47(2), 243–260. https://doi.org/10.1080/07038992.2021.1901562

Jarvis, A., Reuter, H.I., Nelson, A. & Guevara, E. (2008). Hole-filled SRTM for the globe, Version 4. CGIAR-CSI SRTM 90m Database. Available online: http://srtm.csi.cgiar.org [Accessed 10 Apr. 2025].

Jia, H., Chen, F., Pan, D., Du, E., Wang, L., Wang, N., & Yang, A. (2022). Flood risk management in the Yangtze River basin —Comparison of 1998 and 2020 events. *International Journal of Disaster Risk Reduction*, *68*, 102724. https://doi.org/10.1016/j.ijdrr.2021.102724

Jiang, F., Wen, S., Gao, M., & Zhu, A. (2023). Assessment of NEX-GDDP-CMIP6 Downscale Data in Simulating Extreme Precipitation over the Huai River Basin. *Atmosphere*, *14*(10), 1497. https://doi.org/10.3390/atmos14101497

Jin, G., Li, Z., Deng, X., Yang, J., Chen, D. and Li, W. (2019). An analysis of spatiotemporal patterns in Chinese agricultural productivity between 2004 and 2014. *Ecological Indicators*, *105*, 591-600. https://doi.org/10.1016/j.ecolind.2018.05.073

Jiping, Z., Yili, Z., Linshan, L., Mingjun, D., & Xueru, Z. (2011). Identifying Alpine Wetlands in the Damqu River Basin in the Source Area of the Yangtze River using Object-Based Classification Method. *Journal of Resources and Ecology*, *2*(2), 186–192. https://doi.org/10.3969/j.issn.1674-764x.2011.02.013

Jisha, K. C., & Puthur, J. T. (2021). Ecological Importance of Wetland Systems. In *Wetlands Conservation* (pp. 40–54). John Wiley & Sons, Ltd. https://doi.org/10.1002/9781119692621.ch3

Ji, Z., Li, N., Xie, W., Wu, J., & Zhou, Y. (2013). Comprehensive assessment of flood risk using the classification and regression tree method. *Stochastic Environmental Research and Risk Assessment*, 27(8), 1815–1828. https://doi.org/10.1007/s00477-013-0716-z

Johnson, J.A, & Havranek, A.J. (2013). Effectiveness of Temporary Carp Barriers for Restoring Wild Rice Beds in Upper Clam Lake: 2010 to 2013. Report to St. Croix Tribal Environmental Services. Natural Resources Department/Freshwater Scientific Services LLC, Webster/Maple Grove. http://freshwatersci.com/ Downloads/UpperClamSouthBayWR2013.pdf.

Jongman, B. (2021). The fraction of the global population at risk of floods is growing. *Nature*, *596*(7870), 37–38. https://doi.org/10.1038/d41586-021-01974-0

Jonkman, S. N. (2005). Global Perspectives on Loss of Human Life Caused by Floods. *Natural Hazards*, *34*(2), 151–175. https://doi.org/10.1007/s11069-004-8891-3

Junk, W.J, & de Cunha, C.N. (2005). Pantanal: a large South American wetland at a crossroads. *Ecological Engineering*, *24*(4), 391-401.

Kakuru, W., Turyahabwe, N., & Mugisha, J. (2013). Total Economic Value of Wetlands Products and Services in Uganda. *The Scientific World Journal*, *2013*(1), 192656. https://doi.org/10.1155/2013/192656

Kamal, A. S. M. M., Shamsudduha, M., Ahmed, B., Hassan, S. M. K., Islam, Md. S., Kelman, I., & Fordham, M. (2018). Resilience to flash floods in wetland communities of northeastern Bangladesh. International Journal of Disaster Risk Reduction, 31, 478–488. https://doi.org/10.1016/j.ijdrr.2018.06.011

Karmakar, S., Islam, S. S., Sen, K., Ghosh, S., & Midya, S. (2023). Climate Crisis and Wetland Ecosystem Sustainability. In U. Chatterjee, R. Shaw, S. Kumar, A. D. Raj, & S. Das (Eds.), *Climate Crisis: Adaptive Approaches and Sustainability* (pp. 529–549). Springer Nature Switzerland. https://doi.org/10.1007/978-3-031-44397-8_27

Kaplan, G., & Avdan, U. (2018). Monthly Analysis of Wetlands Dynamics Using Remote Sensing Data. *ISPRS International Journal of Geo-Information*, *7*(10), 411. https://doi.org/10.3390/ijgi7100411

Karra, K., Kontgis, C., Statman-Weil, Z., Mazzariello, J. C., Mathis, M., & Brumby, S. P. (2021). Global land use / land cover with Sentinel 2 and deep learning. *2021 IEEE International Geoscience and Remote Sensing Symposium IGARSS*, 4704–4707. https://doi.org/10.1109/IGARSS47720.2021.9553499

Katzenberger, A., & Levermann, A. (2024). Consistent increase in East Asian Summer Monsoon rainfall and its variability under climate change over China in CMIP6. *Earth System Dynamics*, *15*(4), 1137–1151. https://doi.org/10.5194/esd-15-1137-2024

Kayranli, B., Scholz, M., Mustafa, A., & Hedmark, Å. (2010). Carbon Storage and Fluxes within Freshwater Wetlands: a Critical Review. *Wetlands*, *30*(1), 111–124. https://doi.org/10.1007/s13157-009-0003-4

Kebede, M. M., Kumar, M., Mekonnen, M. M., & Clement, T. P. (2024). Enhancing Groundwater Recharge Through Nature-Based Solutions: Benefits and Barriers. *Hydrology*, *11*(11), 195. https://doi.org/10.3390/hydrology11110195

Khosravi, K., Pourghasemi, H. R., Chapi, K., & Bahri, M. (2016). Flash flood susceptibility analysis and its mapping using different bivariate models in Iran: a comparison between Shannon's entropy, statistical index, and weighting factor models. *Environmental Monitoring and Assessment*, *188*(12), 656. https://doi.org/10.1007/s10661-016-5665-9

Kim, S. G. (2010). The evolution of coastal wetland policy in developed countries and Korea. *Ocean & Coastal Management*, *53*(9), 562–569. https://doi.org/10.1016/j.ocecoaman.2010.06.017

Krich, C., Runge, J., Miralles, D. G., Migliavacca, M., Perez-Priego, O., El-Madany, T., Carrara, A., & Mahecha, M. D. (2020). Estimating causal networks in biosphere-atmosphere interaction with the PCMCI approach. *Biogeosciences,* 17(4), 1033–1061. https://doi.org/10.5194/bg-17-1033-2020

Kingsford, R. t. (2000). Ecological impacts of dams, water diversions and river management on floodplain wetlands in Australia. *Austral Ecology*, *25*(2), 109–127. https://doi.org/10.1046/j.1442-9993.2000.01036.x

Kritikos, T.R., & Davies, T.R. (2011). GIS-based multi-criteria decision analysis for landslide susceptibility mapping at northern Evia, Greece. *Zeitschrift der Deutschen Gesellschaft für Geowissenschaften*, pp.421-434.

Kron, W., Eichner, J., & Kundzewicz, Z. W. (2019). Reduction of flood risk in Europe – Reflections from a reinsurance perspective. *Journal of Hydrology*, *576*, 197–209. https://doi.org/10.1016/j.jhydrol.2019.06.050

Kui, Z., Yan, L. U. O., Jin, U., De, Z., & Xiao, Z. (2008). A Study of Current Status and Conservation of Threatened Wetland Ecological Environment in Sanjiang Plain. *JOURNAL OF NATURAL RESOURCES*, *23*(5), 790–796. https://doi.org/10.11849/zrzyxb.2008.05.006

Kundu, S., Kundu, B., Rana, N.K. & Mahato, S. (2024). Wetland degradation and its impacts on livelihoods and sustainable development goals: An overview. *Sustainable Production and Consumption*. https://doi.org/10.1016/j.spc.2024.05.024

Kundzewicz, Z., Su, B., Wang, Y., Xia, J., Huang, J., & Jiang, T. (2019). Flood risk and its reduction in China. *Advances in Water Resources*, *130*, 37–45. https://doi.org/10.1016/j.advwatres.2019.05.020

Lai, C., Wang, Z., & Song, H. (2011). Risk assessment of flood hazard in Beijing River Basin based on BP neural network. *Water Resource Power*, *29*(3), pp.57-59.

Lai, X., Jiang, J., Liang, Q. & Huang, Q. (2013). Large-scale hydrodynamic modeling of the middle Yangtze River Basin with complex river–lake interactions. *Journal of hydrology*, *492*, 228-243. https://doi.org/10.1016/j.jhydrol.2013.03.049

Lane, C. R., Leibowitz, S. G., Autrey, B. C., LeDuc, S. D., & Alexander, L. C. (2018). Hydrological, Physical, and Chemical Functions and Connectivity of Non-Floodplain Wetlands to Downstream Waters: A Review. *JAWRA Journal of the American Water Resources Association*, *54*(2), 346–371. https://doi.org/10.1111/1752-1688.12633

Lane, S. N., & Milledge, D. G. (2013). Impacts of upland open drains upon runoff generation: a numerical assessment of catchment-scale impacts. *Hydrological Processes*, *27*(12), 1701–1726. https://doi.org/10.1002/hyp.9285

Lewis, M., Moftakhari, H., & Passalacqua, P. (2024). Challenges for compound coastal flood risk management in a warming climate: a case study of the Gulf Coast of the United States. *Frontiers in Water*, *6*. https://doi.org/10.3389/frwa.2024.1405603

Liang, D., Lu, J., Chen, X., Liu, C., & Lin, J. (2020). An investigation of the hydrological influence on the distribution and transition of wetland cover in a complex lake–floodplain system using time-series remote sensing and hydrodynamic simulation. Journal of Hydrology, 587, 125038. https://doi.org/10.1016/j.jhydrol.2020.125038

Liang, W., Yongli, C., Hongquan, C., Daler, D., Jingmin, Z., & Juan, Y. (2011). Flood disaster in Taihu Basin, China: causal chain and policy option analyses. *Environmental Earth Sciences*, *63*(5), 1119–1124. https://doi.org/10.1007/s12665-010-0786-x

Li, C., Sun, N., Lu, Y., Guo, B., Wang, Y., Sun, X., & Yao, Y. (2023). Review on Urban Flood Risk Assessment. *Sustainability*, *15*(1), 765. https://doi.org/10.3390/su15010765

Li, F., Phoon, K. K., Du, X., & Zhang, M. (2013). Improved AHP Method and Its Application in Risk Identification. *Journal of Construction Engineering and Management*, *139*(3), 312–320. https://doi.org/10.1061/(ASCE)CO.1943-7862.0000605

Li, G.-F., Xiang, X.-Y., Tong, Y.-Y., & Wang, H.-M. (2013). Impact assessment of urbanization on flood risk in the Yangtze River Delta. *Stochastic Environmental Research and Risk Assessment*, *27*(7), 1683–1693. https://doi.org/10.1007/s00477-013-0706-1

Li, S., Yu, P. & Sun, S. (2008). Fuzzy risk assessment of flood hazard based on artificial neural network for Detention Basin. *China Rural Water Hydropower*, *6*, pp.60-64.

Li, X., Bellerby, R., Craft, C., & Widney, S. E. (2018). Coastal wetland loss, consequences, and challenges for restoration. *Anthropocene Coasts*, *1*(1), 1–15. https://doi.org/10.1139/anc-2017-0001

Li, X., Yu, X., Jiang, L., Li, W., Liu, Y., & Hou, X. (2014). How important are the wetlands in the middle-lower Yangtze River region: An ecosystem service valuation approach. *Ecosystem Services*, *10*, 54–60. https://doi.org/10.1016/j.ecoser.2014.09.004

Li, X., Yu, X., Hou, X., Liu, Y., Li, H., Zhou, Y., Xia, S., Liu, Y., Duan, H., Wang, Y., Dou, Y., Yang, M., & Zhang, L. (2020). Valuation of Wetland Ecosystem Services in National Nature Reserves in China's Coastal Zones. *Sustainability*, *12*(8), 3131. https://doi.org/10.3390/su12083131

Li, X., Zhang, Q., Xu, C.-Y., & Ye, X. (2015). The changing patterns of floods in Poyang Lake, China: characteristics and explanations. Natural Hazards, 76(1), 651–666. https://doi.org/10.1007/s11069-014-1509-5

Li, Y., Dang, B., Li, W., & Zhang, Y. (2024). GLH-Water: A Large-Scale Dataset for Global Surface Water Detection in Large-Size Very-High-Resolution Satellite Imagery. *Proceedings of the AAAI Conference on Artificial Intelligence*, *38*(20), 22213-22221. https://doi.org/10.1609/aaai.v38i20.30226

Li, Y., Gao, J., Yin, J., Liu, L., Zhang, C., & Wu, S. (2024). Flood Risk Assessment of Areas under Urbanization in Chongqing, China, by Integrating Multi-Models. *Remote Sensing*, *16*(2), 219. https://doi.org/10.3390/rs16020219

Li, Y., Niu, Z., Xu, Z., & Yan, X. (2020). Construction of High Spatial-Temporal Water Body Dataset in China Based on Sentinel-1 Archives and GEE. *Remote Sensing,* 12(15), 2413. https://doi.org/10.3390/rs12152413

Li, Y., Zhou, P., Wang, Y., Li, X., Zhang, Y., & Li, X. (2025). Deep Learning Small Water Body Mapping by Transfer Learning from Sentinel-2 to PlanetScope. *Remote Sensing*, *17*(15), 2738. https://doi.org/10.3390/rs17152738

Li, Y., Zhang, Q., Liu, X., Tan, Z., & Yao, J. (2019). The role of a seasonal lake groups in the complex Poyang Lake-floodplain system (China): Insights into hydrological behaviors. *Journal of Hydrology,* 578, 124055. https://doi.org/10.1016/j.jhydrol.2019.124055

Li, Z., He, W., Cheng, M., Hu, J., Yang, G., & Zhang, H. (2023). SinoLC-1: the first 1 m resolution national-scale land-cover map of China created with a deep learning framework and open-access data. *Earth System Science Data*, *15*(11), 4749–4780. https://doi.org/10.5194/essd-15-4749-2023

Lin, W., Sun, Y., Nijhuis, S., & Wang, Z. (2020). Scenario-based flood risk assessment for urbanizing deltas using future land-use simulation (FLUS): Guangzhou Metropolitan Area as a case study. *Science of The Total Environment,* 739, 139899. https://doi.org/10.1016/j.scitotenv.2020.139899

Liu H., Jiang, D., & Yang, X. (2005). Spatialization Approach to 1km Grid GDP Supported by Remote Sensing[J]. *Geo-information Science.* 7(2), 120-123. https://www.dqxxkx.cn/EN/Y2005/V7/I2/120

Liu, J., Kuang, W., Zhang, Z., Xu, X., Qin, Y., Ning, J., Zhou, W., Zhang, S., Li, R., Yan, C., Wu, S., Shi, X., Jiang, N., Yu, D., Pan, X., & Chi, W. (2014). Spatiotemporal characteristics,

patterns, and causes of land-use changes in China since the late 1980s. *Journal of Geographical Sciences, 24*(2), 195–210. https://doi.org/10.1007/s11442-014-1082-6

Liu, J., & Zhang, C. (2017). Identification of Risks and Estimation of Flood Storage in Ponds. *Mathematical Problems in Engineering*, 2017, e7348384. https://doi.org/10.1155/2017/7348384

Liu, K.-Q., Liang, Y.-T., Zhou, J.-L., & Liu, M. (2013). Drought and Flood Variations and Rationality of Land Use in Honghu Lake During the Last 50 Years. *2013 Third International Conference on Intelligent System Design and Engineering Applications*, 612–617. https://doi.org/10.1109/ISDEA.2012.148

Liu, K., Shi, W., & Zhang, H. (2011). A fuzzy topology-based maximum likelihood classification. ISPRS Journal of Photogrammetry and Remote Sensing, 66(1), 103–114. https://doi.org/10.1016/j.isprsjprs.2010.09.007

Liu, L., Sun, W., & Liu, J. (2023a). Spatio-Temporal Analysis of Simulated Summer Extreme Precipitation Events under RCP4.5 Scenario in the Middle and Lower Reaches of the Yangtze River Basin. *Sustainability,* 15(12), 9218. https://doi.org/10.3390/su15129218

Liu, L., Wang, H., & Yue, Q. (2020). China's coastal wetlands: Ecological challenges, restoration, and management suggestions. *Regional Studies in Marine Science*, *37*, 101337. https://doi.org/10.1016/j.rsma.2020.101337

Liu, R., Dong, J., Jiang, L., Ge, Y., Fan, C., Yang, T., & Zhang, G. (2024). Agricultural flood resistance enhanced after returning farmlands to lakes. *Proceedings of the National Academy of Sciences*, *121*(39), e2410967121. https://doi.org/10.1073/pnas.2410967121

Liu, W., Feng, Q., Engel, B. A., Yu, T., Zhang, X., & Qian, Y. (2023b). A probabilistic assessment of urban flood risk and impacts of future climate change. *Journal of Hydrology*, 618, 129267. https://doi.org/10.1016/j.jhydrol.2023.129267

Liu, W., Zhang, X., Feng, Q., & Engel, B. A. (2025a). City-scale integrated flood risk prediction under future climate change and urbanization based on the shared socioeconomic pathways (SSP) scenarios. *Journal of Hydrology*, *655*, 132971. https://doi.org/10.1016/j.jhydrol.2025.132971

Liu, Y., Tian, T., Zeng, P., Zhang, X.-Y., & Che, Y. (2020). Surface water change characteristics of Taihu Lake from 1984-2018 based on Google Earth Engine. Ying Yong

Sheng Tai Xue Bao = The Journal of Applied Ecology / Zhongguo Sheng Tai Xue Hui, Zhongguo Ke Xue Yuan Shenyang Ying Yong Sheng Tai Yan Jiu Suo Zhu Ban, 31, 3163–3172. https://doi.org/10.13287/j.1001-9332.202009.011

Liu, Y., Yang, P., Zhang, S., & Wang, W. (2022). Dynamic identification and health assessment of wetlands in the middle reaches of the Yangtze River basin under changing environment. Journal of Cleaner Production, 345, 131105. https://doi.org/10.1016/j.jclepro.2022.131105

Liu, Y., Yuan, X., Guo, L., Huang, Y., & Zhang, X. (2017). Driving Force Analysis of the Temporal and Spatial Distribution of Flash Floods in Sichuan Province. *Sustainability,* 9(9), 1527. https://doi.org/10.3390/su9091527

Liu, Z., Coleman, N., Patrascu, F. I., Yin, K., Li, X., & Mostafavi, A. (2025b). Artificial intelligence for flood risk management: A comprehensive state-of-the-art review and future directions. *International Journal of Disaster Risk Reduction*, *117*, 105110. https://doi.org/10.1016/j.ijdrr.2024.105110

Liu, Z., Lu, J., Huang, J., Chen, X., & Zhang, L. (2021). Projection of Reference Crop Evapotranspiration under Future Climate Change in Poyang Lake Watershed, China. *Journal of Hydrologic Engineering*, *26*(1), 05020042. https://doi.org/10.1061/(ASCE)HE.1943-5584.0002020

Lotze, H. K., Reise, K., Worm, B., van Beusekom, J., Busch, M., Ehlers, A., Heinrich, D., Hoffmann, R. C., Holm, P., Jensen, C., Knottnerus, O. S., Langhanki, N., Prummel, W., Vollmer, M., & Wolff, W. J. (2005). Human transformations of the Wadden Sea ecosystem through time: a synthesis. *Helgoland Marine Research*, *59*(1), 84–95. https://doi.org/10.1007/s10152-004-0209-z

Luo, M., Hu, G., Chen, G., Liu, X., Hou, H., & Li, X. (2022). 1 km land use/land cover change of China under comprehensive socioeconomic and climate scenarios for 2020–2100. *Scientific Data,* 9(1), 110. https://doi.org/10.1038/s41597-022-01204-w

Luo, P., Wang, X., Zhang, L., Mohd Arif Zainol, M. R. R., Duan, W., Hu, M., Guo, B., Zhang, Y., Wang, Y., & Nover, D. (2023). Future Land Use and Flood Risk Assessment in the Guanzhong Plain, China: Scenario Analysis and the Impact of Climate Change. *Remote Sensing*, *15*(24), 5778. https://doi.org/10.3390/rs15245778

Luo, K. & Zhang, X. (2022). Increasing urban flood risk in China over recent 40 years induced by LUCC. *Landscape and Urban Planning*, *219*, 104317. https://doi.org/10.1016/j.landurbplan.2021.104317

Lu, K., Arshad, M., Ma, X., Ullah, I., Wang, J., & Shao, W. (2022). Evaluating observed and future spatiotemporal changes in precipitation and temperature across China based on CMIP6-GCMs. *International Journal of Climatology,* 42(15), 7703–7729. https://doi.org/10.1002/joc.7673

Lu, S., Ma, J., Ma, X., Tang, H., Zhao, H., & Hasan Ali Baig, M. (2019). Time series of the Inland Surface Water Dataset in China (ISWDC) for 2000–2016 derived from MODIS archives. Earth System Science Data, 11(3), 1099–1108. https://doi.org/https://doi.org/10.5194/essd-11-1099-2019

Lyu, H.-M., Shen, J. S., & Arulrajah, A. (2018). Assessment of Geohazards and Preventative Countermeasures Using AHP Incorporated with GIS in Lanzhou, China. *Sustainability*, *10*(2), 304. https://doi.org/10.3390/su10020304

Lyu, H.-M., Shen, S.-L., Zhou, A., & Yang, J. (2019). Perspectives for flood risk assessment and management for mega-city metro system. *Tunnelling and Underground Space Technology*, *84*, 31–44. https://doi.org/10.1016/j.tust.2018.10.019

Lyu, H.-M., Yin, Z.-Y., Zhou, A., & Shen, S.-L. (2023). MCDM-based flood risk assessment of metro systems in smart city development: A review. *Environmental Impact Assessment Review*, *101*, 107154. https://doi.org/10.1016/j.eiar.2023.107154

Ma, H., Yang, X., Fan, R., He, K., & Wang, L. (2025). Prolonged water body types dataset of urban agglomeration in central China from 1990 to 2021. *Scientific Data*, *12*(1), 480. https://doi.org/10.1038/s41597-025-04794-3

Ma, S., Qiao, Y.P., Jiang, J., Wang, L.J. & Zhang, J.C. (2021). Incorporating the implementation intensity of returning farmland to lakes into policymaking and ecosystem management: A case study of the Jianghuai Ecological Economic Zone, China. *Journal of Cleaner Production*, 306, 127284. https://doi.org/10.1016/j.jclepro.2021.127284

Ma, Z., Chen, W., Xiao, A., & Zhang, R. (2023). The Susceptibility of Wetland Areas in the Yangtze River Basin to Temperature and Vegetation Changes. *Remote Sensing*, *15*(18), 4534. https://doi.org/10.3390/rs15184534

Mahmoodi, E., Azari, M., & Dastorani, M. T. (2023). Comparison of different objective weighting methods in a multi-criteria model for watershed prioritization for flood risk assessment using morphometric analysis. *Journal of Flood Risk Management,* 16(2), e12894. https://doi.org/10.1111/jfr3.12894

Malczewski, J. (2006). GIS-based multicriteria decision analysis: a survey of the literature. *International Journal of Geographical Information Science*, *20*(7), 703–726. https://doi.org/10.1080/13658810600661508

Mander M, Wolski P, Nkuna K, Warchol J, Trollope W (2015) A review of the hydrology of the South African wetland biome, WRC report no. TT 640/15. Water Research Commission, Pretoria

Mao, D., Wang, Z., Du, B., Li, L., Tian, Y., Jia, M., Zeng, Y., Song, K., Jiang, M., & Wang, Y. (2020). National wetland mapping in China: A new product resulting from object-based and hierarchical classification of Landsat 8 OLI images. ISPRS Journal of Photogrammetry and Remote Sensing, 164, 11–25. https://doi.org/10.1016/j.isprsjprs.2020.03.020

Mao, D., Wang, Z., Wu, J., Wu, B., Zeng, Y., Song, K., Yi, K., & Luo, L. (2018). China's wetlands loss to urban expansion. *Land Degradation & Development*, *29*(8), 2644–2657. https://doi.org/10.1002/ldr.2939

Martínez Prentice, R., Villoslada Peciña, M., Ward, R. D., Bergamo, T. F., Joyce, C. B., & Sepp, K. (2021). Machine Learning Classification and Accuracy Assessment from High-Resolution Images of Coastal Wetlands. *Remote Sensing*, *13*(18), 3669. https://doi.org/10.3390/rs13183669

Mas, J. F., & Flores, J. J. (2008). The application of artificial neural networks to the analysis of remotely sensed data. International Journal of Remote Sensing, 29(3), 617–663. https://doi.org/10.1080/01431160701352154

Massmann, A., Gentine, P., & Runge, J. (2021). *Causal inference for process understanding in Earth sciences* (No. arXiv:2105.00912). arXiv. https://doi.org/10.48550/arXiv.2105.00912

Mayer, T., Poortinga, A., Bhandari, B., Nicolau, A. P., Markert, K., Thwal, N. S., Markert, A., Haag, A., Kilbride, J., Chishtie, F., Wadhwa, A., Clinton, N., & Saah, D. (2021). Deep learning approach for Sentinel-1 surface water mapping leveraging Google Earth Engine. ISPRS Open Journal of Photogrammetry and Remote Sensing, 2, 100005. https://doi.org/10.1016/j.ophoto.2021.100005

Mei, X., Dai, Z., Fagherazzi, S., & Chen, J. (2016). Dramatic variations in emergent wetland area in China's largest freshwater lake, Poyang Lake. Advances in Water Resources, 96, 1–10. https://doi.org/10.1016/j.advwatres.2016.06.003

Meshram, S. G., Alvandi, E., Meshram, C., Kahya, E., & Fadhil Al-Quraishi, A. M. (2020). Application of SAW and TOPSIS in Prioritizing Watersheds. *Water Resources Management*, *34*(2), 715–732. https://doi.org/10.1007/s11269-019-02470-x

McCauley, L. A., Anteau, M. J., van der Burg, M. P., & Wiltermuth, M. T. (2015). Land use and wetland drainage affect water levels and dynamics of remaining wetlands. *Ecosphere*, *6*(6), art92. https://doi.org/10.1890/ES14-00494.1

McCartney, M. P., Rebelo, L.-M., & Sellamuttu, S. S. (2015). Wetlands, Livelihoods and Human Health. In C. M. Finlayson, P. Horwitz, & P. Weinstein (Eds.), *Wetlands and Human Health* (pp. 123–148). Springer Netherlands. https://doi.org/10.1007/978-94-017-9609-5_7

McGlade, J., Bankoff, G., Abrahams, J., Cooper-Knock, S.J., Cotecchia, F., Desanker, P., Erian, W., Gencer, E., Gibson, L., Girgin, S. and Hirsch, F. (2019). *Global assessment report on disaster risk reduction 2019.*

Mcleod, E., Chmura, G. L., Bouillon, S., Salm, R., Björk, M., Duarte, C. M., Lovelock, C. E., Schlesinger, W. H., & Silliman, B. R. (2011). A blueprint for blue carbon: toward an improved understanding of the role of vegetated coastal habitats in sequestering CO2. *Frontiers in Ecology and the Environment*, *9*(10), 552–560. https://doi.org/10.1890/110004

Milani, G., Kneubühler, M., Tonolla, D., Doering, M., & E. Schaepman, M. (2020). Characterizing Flood Impact on Swiss Floodplains Using Interannual Time Series of Satellite Imagery. *IEEE Journal of Selected Topics in Applied Earth Observations and Remote Sensing*, *13*, 1479–1493. https://doi.org/10.1109/JSTARS.2020.2980381

Millennium Ecosystem Assessment (2005) *Ecosystems and Human Well-Being: Wetlands and Water Synthesis*. World Resources Institute, Washington, DC.

Mitsch, W.J. and Gosselink, J.G. (2015) Wetlands. 5th Edition, John Wiley & Sons, Inc., Hoboken.

Miyamoto, H., & Kimura, R. (2016). Tree population dynamics on a floodplain: A tradeoff between tree mortality and seedling recruitment induced by stochastic floods. *Water Resources Research*, *52*(9), 7226–7243. https://doi.org/10.1002/2015WR018528

Miura, Y., Shamsudduha, M., Suppasri, A., & Sano, D. (2025). A Global Multi-Sensor Dataset of Surface Water Indices from Landsat-8 and Sentinel-2 Satellite Measurements. *Scientific Data*, *12*(1), 1253. https://doi.org/10.1038/s41597-025-05562-z

Mohanty, S., Pandey, P. C., Pandey, M., Srivastava, P. K., & Dwivedi, C. S. (2024). Wetlands contribution and linkage to support SDGs, its indicators and targets- A critical review. *Sustainable Development*, *n/a*(n/a). https://doi.org/10.1002/sd.2948

Mondal, S. K., Tao, H., Huang, J., Wang, Y., Su, B., Zhai, J., Jing, C., Wen, S., Jiang, S., Chen, Z., & Jiang, T. (2021). Projected changes in temperature, precipitation and potential evapotranspiration across Indus River Basin at 1.5–3.0 °C warming levels using CMIP6-GCMs. *Science of The Total Environment,* 789, 147867. https://doi.org/10.1016/j.scitotenv.2021.147867

Moreno, O. (2024). Urban Wetlands as Resilient Landscape Infrastructure—The Case of Llanquihue Green Infrastructure Plan, Chile. In C. Rojas Quezada (Ed.), *Urban Wetlands in Latin America: Protection, Conservation, Innovation, Restoration, and Community for Sustainable and Water Sensitive Cities* (pp. 105–117). Springer Nature Switzerland. https://doi.org/10.1007/978-3-031-69590-2_8

Morris, J., Hess, T. M., Gowing, D. J., Leeds-Harrison, P. B., Bannister, N., Wade, M., & Vivash, R. M. (2004). *Integrated washland management for flood defence and biodiversity*. https://publications.naturalengland.org.uk/publication/63017

Mountrakis, G., Im, J. & Ogole, C. (2011). Support vector machines in remote sensing: A review. *ISPRS journal of photogrammetry and remote sensing*, *66*(3), 247-259. https://doi.org/10.1016/j.isprsjprs.2010.11.001

Meng, Y., Zhang, J., Yang, X., & Wang, Z. (2023). Spatial–Temporal Mapping and Landscape Influence of Aquaculture Ponds in the Yangtze River Economic Belt from 1985 to 2020. *Remote Sensing*, *15*(23), 5477. https://doi.org/10.3390/rs15235477

Nasiri, H., Mohd Yusof, M. J., & Mohammad Ali, T. A. (2016). An overview to flood vulnerability assessment methods. *Sustainable Water Resources Management*, *2*(3), 331–336. https://doi.org/10.1007/s40899-016-0051-x

National Bureau of Statistics. Available online: https://data.stats.gov.cn/easyquery.htm?cn=C01, (accessed on 12 Oct 2024).

National, M. (2019). Daily meteorological dataset of basic meteorological elements of China National Surface Weather Station (V3.0). National Tibetan Plateau / Third Pole Environment Data Center.

Nandi, A., Mandal, A., Wilson, M., & Smith, D. (2016). Flood hazard mapping in Jamaica using principal component analysis and logistic regression. *Environmental Earth Sciences*, *75*(6), 465. https://doi.org/10.1007/s12665-016-5323-0

Nayak, A., & Bhushan, B. (2022). Wetland Ecosystems and Their Relevance to the Environment: Importance of Wetlands. In *Handbook of Research on Monitoring and Evaluating the Ecological Health of Wetlands* (pp. 1–16). IGI Global. https://doi.org/10.4018/978-1-7998-9498-8.ch001

Nayak, A., & Bhushan, B. (2022). Wetland Ecosystems and Their Relevance to the Environment: Importance of Wetlands. In *Handbook of Research on Monitoring and Evaluating the Ecological Health of Wetlands* (pp. 1–16). IGI Global Scientific Publishing. https://doi.org/10.4018/978-1-7998-9498-8.ch001

Nehzak, K., Aghaei, M., Mostafazadeh, R. & Rabiei-Dastjerdi, H. (2022). Assessment of machine learning algorithms in land use classification. In *Computers in Earth and Environmental Sciences* 97-104. https://doi.org/10.1016/j.gecco.2020.e00971

Nguyen, H. D., Dang, D. K., Nguyen, Q.-H., Bui, Q.-T., & Petrisor, A.-I. (2022). Evaluating the effects of climate and land use change on the future flood susceptibility in the central region of Vietnam by integrating land change modeler, machine learning methods. *Geocarto International,* 37(26), 12810–12845. https://doi.org/10.1080/10106049.2022.2071477

Nguyen, H. D., Fox, D., Dang, D. K., Pham, L. T., Viet Du, Q. V., Nguyen, T. H. T., Dang, T. N., Tran, V. T., Vu, P. L., Nguyen, Q.-H., Nguyen, T. G., Bui, Q.-T., & Petrisor, A.-I. (2021). Predicting Future Urban Flood Risk Using Land Change and Hydraulic Modeling in a River

Watershed in the Central Province of Vietnam. *Remote Sensing,* 13(2), 262. https://doi.org/10.3390/rs13020262

Nguyen, H. D., Nguyen, Q.-H., Dang, D. K., Van, C. P., Truong, Q. H., Pham, S. D., Bui, Q.-T., & Petrisor, A.-I. (2024). A novel flood risk management approach based on future climate and land use change scenarios. *Science of The Total Environment,* 921, 171204. https://doi.org/10.1016/j.scitotenv.2024.171204

Niu, Z., Gong, P., Cheng, X., Guo, J., Wang, L., Huang, H., Shen, S., Wu, Y., Wang, X., Wang, X., Ying, Q., Liang, L., Zhang, L., Wang, L., Yao, Q., Yang, Z., Guo, Z., & Dai, Y. (2009). Geographical characteristics of China's wetlands derived from remotely sensed data. *Science in China Series D: Earth Sciences*, *52*(6), 723–738. https://doi.org/10.1007/s11430-009-0075-2

Niu, Z., Zhang, H., Wang, X., Yao, W., Zhou, D., Zhao, K., Zhao, H., Li, N., Huang, H., Li, C., Yang, J., Liu, C., Liu, S., Wang, L., Li, Z., Yang, Z., Qiao, F., Zheng, Y., Chen, Y., … Gong, P. (2012). Mapping wetland changes in China between 1978 and 2008. *Chinese Science Bulletin*, *57*(22), 2813–2823. https://doi.org/10.1007/s11434-012-5093-3

Niu, Z., Zhang, H., & Gong, P. (2011). More protection for China's wetlands. *Nature*, *471*(7338), 305–305. https://doi.org/10.1038/471305c

Nkwunonwo, U. C., Whitworth, M., & Baily, B. (2020). A review of the current status of flood modelling for urban flood risk management in the developing countries. *Scientific African*, *7*, e00269. https://doi.org/10.1016/j.sciaf.2020.e00269

Nogueira, A. R., Pugnana, A., Ruggieri, S., Pedreschi, D., & Gama, J. (2022). Methods and tools for causal discovery and causal inference. *WIREs Data Mining and Knowledge Discovery*, *12*(2), e1449. https://doi.org/10.1002/widm.1449

NRSCC. (2014). *Annual Report on Remote Sensing Monitoring of Global Ecosystem and Environment (Large Area Wetlands of International Importance)*; National Remote Sensing Center of China: Beijing, China.

Olofsson, P., Foody, G. M., Herold, M., Stehman, S. V., Woodcock, C. E., & Wulder, M. A. (2014). Good practices for estimating area and assessing accuracy of land change. Remote Sensing of Environment, 148, 42–57. https://doi.org/10.1016/j.rse.2014.02.015

O'Neill, B. C., Tebaldi, C., van Vuuren, D. P., Eyring, V., Friedlingstein, P., Hurtt, G., Knutti, R., Kriegler, E., Lamarque, J.-F., Lowe, J., Meehl, G. A., Moss, R., Riahi, K., & Sanderson, B. M. (2016). The Scenario Model Intercomparison Project (ScenarioMIP) for CMIP6. *Geoscientific Model Development,* 9(9), 3461–3482. https://doi.org/10.5194/gmd-9-3461-2016

O'Neill, B. C., Kriegler, E., Ebi, K. L., Kemp-Benedict, E., Riahi, K., Rothman, D. S., van Ruijven, B. J., van Vuuren, D. P., Birkmann, J., Kok, K., Levy, M., & Solecki, W. (2017). The roads ahead: Narratives for shared socioeconomic pathways describing world futures in the 21st century. *Global Environmental Change,* 42, 169–180. https://doi.org/10.1016/j.gloenvcha.2015.01.004

Oubennaceur, K., Chokmani, K., Gauthier, Y., Ratte-Fortin, C., Homayouni, S., & Toussaint, J.-P. (2021). Flood Risk Assessment under Climate Change: The Petite Nation River Watershed. *Climate*, *9*(8), 125. https://doi.org/10.3390/cli9080125

Pahlevan, N., Chittimalli, S. K., Balasubramanian, S. V., & Vellucci, V. (2019). Sentinel-2/Landsat-8 product consistency and implications for monitoring aquatic systems. *Remote Sensing of Environment*, *220*, 19–29. https://doi.org/10.1016/j.rse.2018.10.027

Pal, S. K., Adeloye, A. J., Babel, M. S., & Das Gupta, A. (2011). Evaluation of the Effectiveness of Water Management Policies in Bangladesh. *International Journal of Water Resources Development*, *27*(2), 401–417. https://doi.org/10.1080/07900627.2011.564973

Parker, V. T., Callaway, J. C., Schile, L. M., Vasey, M. C., & Herbert, E. R. (2011). Climate Change and San Francisco Bay-Delta Tidal Wetlands. *San Francisco Estuary and Watershed Science*, *9*(3). https://doi.org/10.15447/sfews.2011v9iss3art3

Pathan, A. I., Girish Agnihotri, P., Said, S., & Patel, D. (2022). AHP and TOPSIS based flood risk assessment- a case study of the Navsari City, Gujarat, India. *Environmental Monitoring and Assessment*, *194*(7), 509. https://doi.org/10.1007/s10661-022-10111-x

Pearl, J. (2010). Causal inference. *Causality: objectives and assessment*. 39-58.

Pelletier, C., Valero, S., Inglada, J., Champion, N., & Dedieu, G. (2016). Assessing the robustness of Random Forests to map land cover with high resolution satellite image time series over large areas. Remote Sensing of Environment, 187, 156–168. https://doi.org/10.1016/j.rse.2016.10.010

Pei, F., Wu, C., Qu, A., Xia, Y., Wang, K., & Zhou, Y. (2017). Changes in Extreme Precipitation: A Case Study in the Middle and Lower Reaches of the Yangtze River in China. *Water,* 9(12), 943. https://doi.org/10.3390/w9120943

Pekel, J.-F., Cottam, A., Gorelick, N., & Belward, A. S. (2016). High-resolution mapping of global surface water and its long-term changes. Nature, 540(7633), 418–422. https://doi.org/10.1038/nature20584

Peng, J.-T., Zhu, X.-D., Sun, X., & Song, X.-W. (2018). Identifying external nutrient reduction requirements and potential in the hypereutrophic Lake Taihu Basin, China. *Environmental Science and Pollution Research,* 25. https://doi.org/10.1007/s11356-018-1250-9

Peng, L., & Li, Z. (2021). Ensemble Flood Risk Assessment in the Yangtze River Economic Belt under CMIP6 SSP-RCP Scenarios. *Sustainability*, *13*(21), 12097. https://doi.org/10.3390/su132112097

Peng, L., Wang, Y., Yang, L., Garchagen, M., & Deng, X. (2024). A comparative analysis on flood risk assessment and management performances between Beijing and Munich. *Environmental Impact Assessment Review*, *104*, 107319. https://doi.org/10.1016/j.eiar.2023.107319

Peng, L., Xia, J., Li, Z., Fang, C. and Deng, X. (2020). Spatio-temporal dynamics of water-related disaster risk in the Yangtze River Economic Belt from 2000 to 2015. *Resources, Conservation and Recycling*, *161*, 104851. https://doi.org/10.1016/j.resconrec.2020.104851

Peng, L., Wang, Y., Yang, L., Garchagen, M., & Deng, X. (2024). A comparative analysis on flood risk assessment and management performances between Beijing and Munich. *Environmental Impact Assessment Review*, *104*, 107319. https://doi.org/10.1016/j.eiar.2023.107319

Peng, W., Wang, D., & Cai, Y. (2021). Assessing Ecological Vulnerability under Climate Change and Anthropogenic Influence in the Yangtze River Estuarine Island-Chongming Island, China. *International Journal of Environmental Research and Public Health*, *18*(21), 11642. https://doi.org/10.3390/ijerph182111642

Peng, X., Heng, X., Li, Q., Li, J., & Yu, K. (2022). From Sponge Cities to Sponge Watersheds: Enhancing Flood Resilience in the Sishui River Basin in Zhengzhou, China. *Water*, *14*(19), 3084. https://doi.org/10.3390/w14193084

Perry, L. G., Reynolds, L. V., Beechie, T. J., Collins, M. J., & Shafroth, P. B. (2015). Incorporating climate change projections into riparian restoration planning and design. *Ecohydrology*, *8*(5), 863–879. https://doi.org/10.1002/eco.1645

Petit-Boix, A., Arahuetes, A., Josa, A., Rieradevall, J., & Gabarrell, X. (2017). Are we preventing flood damage eco-efficiently? An integrated method applied to post-disaster emergency actions. Science of The Total Environment, 580, 873–881. https://doi.org/10.1016/j.scitotenv.2016.12.034

Pokhariya, H. S., Singh, D. P., & Prakash, R. (2023). Evaluation of different machine learning algorithms for LULC classification in heterogeneous landscape by using remote sensing and GIS techniques. *Engineering Research Express*, *5*(4), 045052. https://doi.org/10.1088/2631-8695/acfa64

Poulter, B., Fluet-Chouinard, E., Hugelius, G., Koven, C., Fatoyinbo, L., Page, S. E., Rosentreter, J. A., Smart, L. S., Taillie, P. J., Thomas, N., Zhang, Z., & Wijedasa, L. S. (2021). A Review of Global Wetland Carbon Stocks and Management Challenges. In *Wetland Carbon and Environmental Management* (pp. 1–20). American Geophysical Union (AGU). https://doi.org/10.1002/9781119639305.ch1

Pronger, J., Schipper, L. A., Hill, R. B., Campbell, D. I., & McLeod, M. (2014). Subsidence Rates of Drained Agricultural Peatlands in New Zealand and the Relationship with Time since Drainage. *Journal of Environmental Quality*, *43*(4), 1442–1449. https://doi.org/10.2134/jeq2013.12.0505

Qin, X., Wang, S., & Meng, M. (2024). SEA for better climate adaptation in the face of the flood risk: Multi-scenario, strategic forecasting, nature-based solutions. *Environmental Impact Assessment Review*, *106*, 107495. https://doi.org/10.1016/j.eiar.2024.107495

Quan, N. H., Toan, T. Q., Dang, P. D., Phuong, N. L., Anh, T. T. H., Quang, N. X., Quoc, D. P., Quoi, L. P., Hanington, P., & Sea, W. B. (2018). Conservation of the Mekong Delta wetlands through hydrological management. *Ecological Research*, *33*(1), 87–103. https://doi.org/10.1007/s11284-017-1545-1

Rajkhowa, S., & Sarma, J. (2021). 14 - Climate change and flood risk, global climate change. In S. Singh, P. Singh, S. Rangabhashiyam, & K. K. Srivastava (Eds.), *Global Climate Change* (pp. 321–339). Elsevier. https://doi.org/10.1016/B978-0-12-822928-6.00012-5

Ramkar, P., & Yadav, S. M. (2021). Flood risk index in data-scarce river basins using the AHP and GIS approach. *Natural Hazards*, *109*(1), 1119–1140. https://doi.org/10.1007/s11069-021-04871-x

Ran, Q., Wang, J., Chen, X., Liu, L., Li, J., & Ye, S. (2022). The relative importance of antecedent soil moisture and precipitation in flood generation in the middle and lower Yangtze River basin. *Hydrology and Earth System Sciences*, *26*(19), 4919–4931. https://doi.org/10.5194/hess-26-4919-2022

Riahi, K., van Vuuren, D. P., Kriegler, E., Edmonds, J., O'Neill, B. C., Fujimori, S., Bauer, N., Calvin, K., Dellink, R., Fricko, O., Lutz, W., Popp, A., Cuaresma, J. C., Kc, S., Leimbach, M., Jiang, L., Kram, T., Rao, S., Emmerling, J., … Tavoni, M. (2017). The Shared Socioeconomic Pathways and their energy, land use, and greenhouse gas emissions implications: An overview. *Global Environmental Change*, *42*, 153–168. https://doi.org/10.1016/j.gloenvcha.2016.05.009

Rizzo, A. (2025). Wetland community expertise in the new nature-based solutions and circular economy vision. *Emerging Developments in Constructed Wetlands.* 681-694. https://doi.org/10.1016/B978-0-443-14078-5.00028-3

Rahmati, O., Zeinivand ,Hossein, & and Besharat, M. (2016). Flood hazard zoning in Yasooj region, Iran, using GIS and multi-criteria decision analysis. *Geomatics, Natural Hazards and Risk*, *7*(3), 1000–1017. https://doi.org/10.1080/19475705.2015.1045043

Rajkhowa, S., & Sarma, J. (2021). 14 - Climate change and flood risk, global climate change. In S. Singh, P. Singh, S. Rangabhashiyam, & K. K. Srivastava (Eds.), *Global Climate Change,* 321–339. Elsevier. https://doi.org/10.1016/B978-0-12-822928-6.00012-5

Ramkar, P., & Yadav, S. M. (2021). Flood risk index in data-scarce river basins using the AHP and GIS approach. *Natural Hazards*, *109*(1), 1119–1140. https://doi.org/10.1007/s11069-021-04871-x

Ramsar Convention Bureau. (2001). Wetlands values and functions. Ramsar Convention Bureau, Gland, Switzerland.

https://www.ramsar.org/sites/default/files/documents/library/handbook1_5ed_introductiontoconvention_e.pdf

Rajkhowa, S., & Sarma, J. (2021). 14 - Climate change and flood risk, global climate change. In S. Singh, P. Singh, S. Rangabhashiyam, & K. K. Srivastava (Eds.), Global Climate Change (pp. 321–339). Elsevier. https://doi.org/10.1016/B978-0-12-822928-6.00012-5

Rajib, A., Liu, Z., Merwade, V., Tavakoly, A. A., & Follum, M. L. (2020). Towards a large-scale locally relevant flood inundation modeling framework using SWAT and LISFLOOD-FP. *Journal of Hydrology*, *581*, 124406. https://doi.org/10.1016/j.jhydrol.2019.124406

Razi, M.A. & Athappilly, K. (2005). A comparative predictive analysis of neural networks (NNs), nonlinear regression and classification and regression tree (CART) models. *Expert systems with applications*, *29*(1), 65-74. https://doi.org/10.1016/j.eswa.2005.01.006

Reed, D., van Wesenbeeck, B., Herman, P. M. J., & Meselhe, E. (2018). Tidal flat-wetland systems as flood defenses: Understanding biogeomorphic controls. *Estuarine, Coastal and Shelf Science*, *213*, 269–282. https://doi.org/10.1016/j.ecss.2018.08.017

Rodriguez-Galiano, V. F., Ghimire, B., Rogan, J., Chica-Olmo, M., & Rigol-Sanchez, J. P. (2012). An assessment of the effectiveness of a random forest classifier for land-cover classification. ISPRS Journal of Photogrammetry and Remote Sensing, 67, 93–104. https://doi.org/10.1016/j.isprsjprs.2011.11.002

Rogers, K., Kelleway, J. J., Saintilan, N., Megonigal, J. P., Adams, J. B., Holmquist, J. R., Lu, M., Schile-Beers, L., Zawadzki, A., Mazumder, D., & Woodroffe, C. D. (2019). Wetland carbon storage controlled by millennial-scale variation in relative sea-level rise. *Nature*, *567*(7746), 91–95. https://doi.org/10.1038/s41586-019-0951-7

Rojas, O., Soto, E., Rojas, C., & López, J. J. (2022). Assessment of the flood mitigation ecosystem service in a coastal wetland and potential impact of future urban development in Chile. Habitat International, 123, 102554. https://doi.org/10.1016/j.habitatint.2022.102554

Ronco, F., Büscher, H. H., Indermaur, A., & Salzburger, W. (2020). The taxonomic diversity of the cichlid fish fauna of ancient Lake Tanganyika, East Africa. *Journal of Great Lakes Research*, *46*(5), 1067–1078. https://doi.org/10.1016/j.jglr.2019.05.009

Rouillard, J. J., Benson, D., & Gain, A. K. (2014). Evaluating IWRM implementation success: are water policies in Bangladesh enhancing adaptive capacity to climate change impacts? *International Journal of Water Resources Development*, *30*(3), 515–527. https://doi.org/10.1080/07900627.2014.910756

Roy, D. P., Huang, H., Houborg, R., & Martins, V. S. (2021b). A global analysis of the temporal availability of PlanetScope high spatial resolution multi-spectral imagery. *Remote Sensing of Environment*, *264*, 112586. https://doi.org/10.1016/j.rse.2021.112586

Roy, S., Bose, A., & Chowdhury, I. R. (2021a). Flood risk assessment using geospatial data and multi-criteria decision approach: a study from historically active flood-prone region of Himalayan foothill, India. *Arabian Journal of Geosciences*, *14*(11), 999. https://doi.org/10.1007/s12517-021-07324-8

Rubin, D. B. (2005). Causal Inference Using Potential Outcomes. *Journal of the American Statistical Association*, *100*(469), 322–331. https://doi.org/10.1198/016214504000001880

Runge, J. (2018). Causal network reconstruction from time series: From theoretical assumptions to practical estimation. Chaos: *An Interdisciplinary Journal of Nonlinear Science*, 28(7), 075310. https://doi.org/10.1063/1.5025050

Runge, J., Bathiany, S., Bollt, E., Camps-Valls, G., Coumou, D., Deyle, E., Glymour, C., Kretschmer, M., Mahecha, M. D., Muñoz-Marí, J., van Nes, E. H., Peters, J., Quax, R., Reichstein, M., Scheffer, M., Schölkopf, B., Spirtes, P., Sugihara, G., Sun, J., … Zscheischler, J. (2019a). Inferring causation from time series in Earth system sciences. *Nature Communications*, *10*(1), 2553. https://doi.org/10.1038/s41467-019-10105-3

Runge, J., Gerhardus, A., Varando, G., Eyring, V., & Camps-Valls, G. (2023). Causal inference for time series. *Nat Rev Earth Environ* 4, 487–505. https://doi.org/10.1038/s43017-023-00431-y

Runge, J., Nowack, P., Kretschmer, M., Flaxman, S., & Sejdinovic, D. (2019b). Detecting and quantifying causal associations in large nonlinear time series datasets. *Science Advances*, 5(11), eaau4996. https://doi.org/10.1126/sciadv.aau4996

Saaty, T. L. (1977). A scaling method for priorities in hierarchical structures. *Journal of Mathematical Psychology*, *15*(3), 234–281. https://doi.org/10.1016/0022-2496(77)90033-5

Sahu, M. K., Shwetha, H. R., & Dwarakish, G. S. (2023). State-of-the-art hydrological models and application of the HEC-HMS model: a review. *Modeling Earth Systems and Environment*, *9*(3), 3029–3051. https://doi.org/10.1007/s40808-023-01704-7

Sajjad, M., Chan, J. C. L., & Kanwal, S. (2020). Integrating spatial statistics tools for coastal risk management: A case-study of typhoon risk in mainland China. *Ocean & Coastal Management*, *184*, 105018. https://doi.org/10.1016/j.ocecoaman.2019.105018

Samuels, P., Klijn, F., & Dijkman, J. (2006). An analysis of the current practice of policies on river flood risk management in different countries. *Irrigation and Drainage*, *55*(S1), S141–S150. https://doi.org/10.1002/ird.257

Sang, M., Jiang, J., Huang, X., Zhu, F., & Wang, Q. (2024). Spatial and temporal changes in population distribution and population projection at county level in China. *Humanities and Social Sciences Communications*, *11*(1), 1–13. https://doi.org/10.1057/s41599-024-02784-1

Santoro, M., & Wegmüller, U. (2014). Multi-temporal Synthetic Aperture Radar Metrics Applied to Map Open Water Bodies. *IEEE Journal of Selected Topics in Applied Earth Observations and Remote Sensing*, *7*(8), 3225–3238. https://doi.org/10.1109/JSTARS.2013.2289301

Sax, M. S., Bassuk, N., van Es, H., & Rakow, D. (2017). Long-term remediation of compacted urban soils by physical fracturing and incorporation of compost. *Urban Forestry & Urban Greening*, *24*, 149–156. https://doi.org/10.1016/j.ufug.2017.03.023

Secretariat, R.C. (2010). Designating ramsar sites: strategic framework and guidelines for the future development of the list of wetland for international importance. *Gland, Switzerland*.

Shang, X., & Chisholm, L. A. (2014). Classification of Australian Native Forest Species Using Hyperspectral Remote Sensing and Machine-Learning Classification Algorithms. IEEE Journal of Selected Topics in Applied Earth Observations and Remote Sensing, 7(6), 2481–2489. https://doi.org/10.1109/JSTARS.2013.2282166

Shankman, D., Davis, L., & de Leeuw, J. (2009). River management, land use change, and future flood risk in China's Poyang Lake region. *International Journal of River Basin Management*, 7(4), 423–431. https://doi.org/10.1080/15715124.2009.9635400

Shao, M., Zhao, G., Kao, S.C., Cuo, L., Rankin, C. and Gao, H. (2020). Quantifying the effects of urbanization on floods in a changing environment to promote water security—A

case study of two adjacent basins in Texas. *Journal of Hydrology*, *589*, 125154. https://doi.org/10.1016/j.jhydrol.2020.125154

Sharma, L. K., & Naik, R. (2024). Wetland Ecosystems. In L. K. Sharma & R. Naik (Eds.), *Conservation of Saline Wetland Ecosystems: An Initiative towards UN Decade of Ecological Restoration* (pp. 3–32). Springer Nature. https://doi.org/10.1007/978-981-97-5069-6_1

Sharma, S., Phartiyal, M., Madhav, S., & Singh, P. (2021). Global Wetlands. In *Wetlands Conservation* (pp. 1–16). John Wiley & Sons, Ltd. https://doi.org/10.1002/9781119692621.ch1

Sheng, J., Rui, D., & Han, X. (2022). Governmentality and sociotechnical imaginary within the conservation-development nexus: China's Great Yangtze River Protection Programme. *Environmental Science & Policy*, *136*, 56–66. https://doi.org/10.1016/j.envsci.2022.05.018

Shen, J., Li, J., Ma, Q., Wang, D., & Du, S. (2023). Response of flood regulation service to land use changes and dam construction—A case study in the Yangtze River Basin. *Ecological Indicators*, *154*, 110715. https://doi.org/10.1016/j.ecolind.2023.110715

Shimizu, S., Hoyer, P.O., Hyvärinen, A., Kerminen, A. and Jordan, M., 2006. A linear non-Gaussian acyclic model for causal discovery. *Journal of Machine Learning Research*, *7*(10). https://dl.acm.org/doi/abs/10.5555/1248547.1248619

Santoro, M., & Wegmüller, U. (2014). Multi-temporal Synthetic Aperture Radar Metrics Applied to Map Open Water Bodies. *IEEE Journal of Selected Topics in Applied Earth Observations and Remote Sensing*, *7*(8), 3225–3238. https://doi.org/10.1109/JSTARS.2013.2289301

Shiru, M. S., Kim, J. H., & Chung, E.-S. (2022). Variations in Projections of Precipitations of CMIP6 Global Climate Models under SSP 2–45 and SSP 5–85. *KSCE Journal of Civil Engineering*, *26*(12), 5404–5416. https://doi.org/10.1007/s12205-022-0149-7

Slinski, K. M., Hogue, T. S., & McCray, J. E. (2019). Active-Passive Surface Water Classification: A New Method for High-Resolution Monitoring of Surface Water Dynamics. *Geophysical Research Letters*, *46*(9), 4694–4704. https://doi.org/10.1029/2019GL082562

Shen, J., Li, J., Ma, Q., Wang, D., & Du, S. (2023). Response of flood regulation service to land use changes and dam construction—A case study in the Yangtze River Basin. *Ecological Indicators*, *154*, 110715. https://doi.org/10.1016/j.ecolind.2023.110715

Sheng, J., Rui, D., & Han, X. (2022). Governmentality and sociotechnical imaginary within the conservation-development nexus: China's Great Yangtze River Protection Programme. *Environmental Science & Policy*, *136*, 56–66. https://doi.org/10.1016/j.envsci.2022.05.018

Shinn, J.E. (2016). Adaptive environmental governance of changing social-ecological systems: Empirical insights from the Okavango Delta, Botswana. *Global Environmental Change*, *40*, 50-59. https://doi.org/10.1016/j.gloenvcha.2016.06.011

Sidike, P., Asari, V.K. & Sagan, V. (2018). Progressively Expanded Neural Network (PEN Net) for hyperspectral image classification: A new neural network paradigm for remote sensing image analysis. *ISPRS Journal of Photogrammetry and Remote Sensing*, *146*, 161-181. https://doi.org/10.1016/j.isprsjprs.2018.09.007

Simon, S., Déri-Takács, J., Szijártó, M., Szél, L., & Mádl-Szőnyi, J. (2023). Wetland Management in Recharge Regions of Regional Groundwater Flow Systems with Water Shortage, Nyírség Region, Hungary. *Water*, *15*(20), 3589. https://doi.org/10.3390/w15203589

Singh, A., Thakur, N., & Sharma, A. (2016). A review of supervised machine learning algorithms. *2016 3rd International Conference on Computing for Sustainable Global Development (INDIACom)*, 1310–1315. https://ieeexplore.ieee.org/abstract/document/7724478

Smardon, R.C. (2009). *Sustaining the Worlds Wetlands: Setting Policy and Resolving Conflicts*; Springer: New York, NY, USA.

Smardon, R. C., & Faust, B. B. (2006). Introduction: international policy in the biosphere reserves of Mexico's Yucatan peninsula. *Landscape and Urban Planning*, *74*(3), 160–192. https://doi.org/10.1016/j.landurbplan.2004.09.002

Smith, K., Lawrence, G., MacMahon, A., Muller, J., & Brady, M. (2016). The resilience of long and short food chains: a case study of flooding in Queensland, Australia. *Agriculture and Human Values*, *33*(1), 45–60. https://doi.org/10.1007/s10460-015-9603-1

Song, C., & Wang, J. (2014). Erosion-accretion changes and controlled factors of the submerged delta in the Yangtze Estuary in 1982–2010. *Acta Geogr. Sin*, 69, 1683-1696. http://www.geog.com.cn/EN/10.11821/dlxb201411009

Song, S., Zhang, X., Gao, Z., & Yan, X. (2023). Evaluation of atmospheric circulations for dynamic downscaling in CMIP6 models over East Asia. *Climate Dynamics*, *60*(7), 2437–2458. https://doi.org/10.1007/s00382-022-06465-0

Spirtes, P. and Glymour, C. (1991). An algorithm for fast recovery of sparse causal graphs. *Social science computer review*, *9*(1), 62-72. https://doi.org/10.1177/089443939100900106

Sugihara, G., May, R., Ye, H., Hsieh, C. H., Deyle, E., Fogarty, M., & Munch, S. (2012). Detecting causality in complex ecosystems. *Science*, *338*(6106), 496–500. https://doi.org/10.1126/science.1227079

Sugianto, S., Deli, A., Miswar, E., Rusdi, M., & Irham, M. (2022). The Effect of Land Use and Land Cover Changes on Flood Occurrence in Teunom Watershed, Aceh Jaya. *Land*, *11*(8), 1271. https://doi.org/10.3390/land11081271

Sun, D., Wang, X., Yu, M., Ouyang, Z., & Liu, G. (2023). Dynamic evolution and decoupling analysis of agricultural nonpoint source pollution in Taihu Lake Basin during the urbanization process. *Environmental Impact Assessment Review*, *100*, 107048. https://doi.org/10.1016/j.eiar.2023.107048

Sun, G., Lei, G., Qu, Y., Zhang, C., & He, K. (2020). The Operation of the Three Gorges Dam Alters Wetlands in the Middle and Lower Reaches of the Yangtze River. *Frontiers in Environmental Science*, *8*. https://doi.org/10.3389/fenvs.2020.576307

Sun, H., Cheng, X., & Dai, M. (2016). Regional flood disaster resilience evaluation based on analytic network process: a case study of the Chaohu Lake Basin, Anhui Province, China. *Natural Hazards,* 82(1), 39–58. https://doi.org/10.1007/s11069-016-2178-3

Sun, S., & Mao, R. (2008). An introduction to lake Taihu. In *Lake Taihu, China: Dynamics and Environmental Change* (pp. 1-67). Dordrecht: Springer Netherlands.

Sun, D., Wang, X., Yu, M., Ouyang, Z., & Liu, G. (2023). Dynamic evolution and decoupling analysis of agricultural nonpoint source pollution in Taihu Lake Basin during the urbanization process. *Environmental Impact Assessment Review*, *100*, 107048. https://doi.org/10.1016/j.eiar.2023.107048

Sun, Y., Zhang, Q., & Singh, V. P. (2024). Flooding in the Yellow River Basin, China: Spatiotemporal patterns, drivers and future tendency. *Journal of Hydrology: Regional Studies*, *52*, 101706. https://doi.org/10.1016/j.ejrh.2024.101706

Sunderland, T., Achdiawan, R., Angelsen, A., Babigumira, R., Ickowitz, A., Paumgarten, F., Reyes-García, V., & Shively, G. (2014). Challenging Perceptions about Men, Women, and Forest Product Use: A Global Comparative Study. *World Development*, *64*, S56–S66. https://doi.org/10.1016/j.worlddev.2014.03.003

Su, S., Chen, X., DeGloria, S. D., & Wu, J. (2010). Integrative fuzzy set pair model for land ecological security assessment: a case study of Xiaolangdi Reservoir Region, China. *Stochastic Environmental Research and Risk Assessment*, *24*(5), 639–647. https://doi.org/10.1007/s00477-009-0351-x

Talukdar, S., Singha, P., Mahato, S., Shahfahad, Pal, S., Liou, Y.-A., & Rahman, A. (2020). Land-Use Land-Cover Classification by Machine Learning Classifiers for Satellite Observations—A Review. *Remote Sensing*, *12*(7), 1135. https://doi.org/10.3390/rs12071135

Tang, H., Cao, H., Yuan, S., Xiao, Y., Jiang, C., & Gualtieri, C. (2020a). A Numerical Study of Hydrodynamic Processes and Flood Mitigation in a Large River-lake System. *Water Resources Management*, *34*(12), 3739–3760. https://doi.org/10.1007/s11269-020-02628-y

Tang, Y., Leon, A. S., & Kavvas, M. L. (2020b). Impact of Dynamic Storage Management of Wetlands and Shallow Ponds on Watershed-scale Flood Control. *Water Resources Management*, *34*(4), 1305–1318. https://doi.org/10.1007/s11269-020-02502-x

Tanoue, M., Taguchi, R., Nakata, S., Watanabe, S., Fujimori, S., & Hirabayashi, Y. (2020). Estimation of Direct and Indirect Economic Losses Caused by a Flood With Long-Lasting Inundation: Application to the 2011 Thailand Flood. *Water Resources Research*, *56*(5), e2019WR026092. https://doi.org/10.1029/2019WR026092

Tansar, H., Babur, M., & Karnchanapaiboon, S. L. (2020). Flood inundation modeling and hazard assessment in Lower Ping River Basin using MIKE FLOOD. *Arabian Journal of Geosciences*, *13*(18), 934. https://doi.org/10.1007/s12517-020-05891-w

Tassi, A., & Vizzari, M. (2020). Object-Oriented LULC Classification in Google Earth Engine Combining SNIC, GLCM, and Machine Learning Algorithms. *Remote Sensing*, *12*(22), 3776. https://doi.org/10.3390/rs12223776

Tellman, B., Sullivan, J. A., Kuhn, C., Kettner, A. J., Doyle, C. S., Brakenridge, G. R., Erickson, T. A., & Slayback, D. A. (2021). Satellite imaging reveals increased proportion of population exposed to floods. *Nature*, *596*(7870), 80–86. https://doi.org/10.1038/s41586-021-03695-w

Temmerman, S., Meire, P., Bouma, T. J., Herman, P. M. J., Ysebaert, T., & De Vriend, H. J. (2013). Ecosystem-based coastal defence in the face of global change. *Nature*, *504*(7478), 79–83. https://doi.org/10.1038/nature12859

Thaler, T., & Hartmann, T. (2016). Justice and flood risk management: reflecting on different approaches to distribute and allocate flood risk management in Europe. *Natural Hazards*, *83*(1), 129–147. https://doi.org/10.1007/s11069-016-2305-1

Thieken, A. H., Kienzler, S., Kreibich, H., Kuhlicke, C., Kunz, M., Mühr, B., Müller, M., Otto, A., Petrow, T., Pisi, S., & Schröter, K. (2016). Review of the flood risk management system in Germany after the major flood in 2013. *Ecology and Society*, *21*(2). https://www.jstor.org/stable/26270411

Thomas, H., & Nisbet, T. R. (2007). An assessment of the impact of floodplain woodland on flood flows. *Water and Environment Journal*, *21*(2), 114–126. https://doi.org/10.1111/j.1747-6593.2006.00056.x

Thorslund, J., Jarsjo, J., Jaramillo, F., Jawitz, J. W., Manzoni, S., Basu, N. B., Chalov, S. R., Cohen, M. J., Creed, I. F., Goldenberg, R., Hylin, A., Kalantari, Z., Koussis, A. D., Lyon, S. W., Mazi, K., Mard, J., Persson, K., Pietro, J., Prieto, C., … Destouni, G. (2017). Wetlands as large-scale nature-based solutions: Status and challenges for research, engineering and management. *Ecological Engineering*, *108*, 489–497. https://doi.org/10.1016/j.ecoleng.2017.07.012

Tull, N., & Passalacqua, P. (2025). Flood Wave Attenuation as a Function of Floodplain Storage, Secondary Channel Conveyance, and Discharge. *Water Resources Research*, *61*(5), e2024WR038582. https://doi.org/10.1029/2024WR038582

Tselka, I., Detsikas, S.E., Petropoulos, G.P. & Demertzi, I.I. (2023). Google Earth Engine and machine learning classifiers for obtaining burnt area cartography: A case study from a Mediterranean setting. In *Geoinformatics for geosciences*, 131-148. Elsevier. https://doi.org/10.1016/B978-0-323-98983-1.00008-9

UNDP (2004). Reducing disaster risk. A challenge for development. Bureau for Crisis Prevention and Recovery (BRCP), New York.

UNISDR. (2011). Revealing risk, redefining development. Global assessment report on disaster risk reduction 2011. Geneva, Switzerland: United Nations International Strategy for Disaster Risk Reduction.

Van, R., & Temmerman, S. (2019). A global exploration of tidal wetland creation for nature-based flood risk mitigation in coastal cities. Estuarine, *Coastal and Shelf Science,* 226, 106262. https://doi.org/10.1016/j.ecss.2019.106262

Vegad, U., Pokhrel, Y., & Mishra, V. (2024). Flood risk assessment for Indian sub-continental river basins. *Hydrology and Earth System Sciences*, *28*(5), 1107–1126. https://doi.org/10.5194/hess-28-1107-2024

Vetrivel, A., Gerke, M., Kerle, N., & Vosselman, G. (2015). Identification of damage in buildings based on gaps in 3D point clouds from very high resolution oblique airborne images. ISPRS Journal of Photogrammetry and Remote Sensing, 105, 61–78. https://doi.org/10.1016/j.isprsjprs.2015.03.016

Vörösmarty, C. J., McIntyre, P. B., Gessner, M. O., Dudgeon, D., Prusevich, A., Green, P., Glidden, S., Bunn, S. E., Sullivan, C. A., Liermann, C. R., & Davies, P. M. (2010). Global threats to human water security and river biodiversity. *Nature*, *467*(7315), 555–561. https://doi.org/10.1038/nature09440

Wang, H., Huang, L., Guo, W., Zhu, Y., Yang, H., Jiao, X., & Zhou, H. (2022). Evaluation of ecohydrological regime and its driving forces in the Dongting Lake, China. *Journal of Hydrology: Regional Studies*, *41*, 101067. https://doi.org/10.1016/j.ejrh.2022.101067

Wang, H., Liu, X. & Wang, H. (2016). The Yangtze River floodplain: threats and rehabilitation. *American Fisheries Society Symposium,* 84, 263-291. Bethesda, MD, USA: American Fisheries Society.

Wang, Q., Chen, J., Liu, F., & Li, W. (2014). Morphological changes and resource allocation of *Zizania latifolia* (Griseb.) Stapf in response to different submergence depth and duration. *Flora - Morphology, Distribution, Functional Ecology of Plants*, *209*(5), 279–284. https://doi.org/10.1016/j.flora.2014.03.006

Wang, T., & Sun, F. (2022). Global gridded GDP data set consistent with the shared socioeconomic pathways. *Scientific Data*, *9*(1), 221. https://doi.org/10.1038/s41597-022-01300-x

Wang, X., Xia, J., Dong, B., Zhou, M., & Deng, S. (2021). Spatiotemporal distribution of flood disasters in Asia and influencing factors in 1980–2019. *Natural Hazards*, *108*(3), 2721–2738. https://doi.org/10.1007/s11069-021-04798-3

Wang, X., Xie, S., Zhang, X., Chen, C., Guo, H., Du, J., & Duan, Z. (2018). A robust Multi-Band Water Index (MBWI) for automated extraction of surface water from Landsat 8 OLI imagery. *International Journal of Applied Earth Observation and Geoinformation*, *68*, 73–91. https://doi.org/10.1016/j.jag.2018.01.018

Wang, X., Zhao, X., Zhang, Z., Yi, L., Zuo, L., Wen, Q., Liu, F., Xu, J., Hu, S., & Liu, B. (2016). Assessment of soil erosion change and its relationships with land use/cover change in China from the end of the 1980s to 2010. *CATENA*, *137*, 256–268. https://doi.org/10.1016/j.catena.2015.10.004

Wang, Y., Li, Z., Tang, Z., & Zeng, G. (2011). A GIS-Based Spatial Multi-Criteria Approach for Flood Risk Assessment in the Dongting Lake Region, Hunan, Central China. *Water Resources Management*, *25*(13), 3465–3484. https://doi.org/10.1007/s11269-011-9866-2

Waqas, U., Ahmed, M. F., Rashid, H. M. A., & Al-Atroush, M. E. (2023). Optimization of neural-network model using a meta-heuristic algorithm for the estimation of dynamic Poisson's ratio of selected rock types. *Scientific Reports*, *13*(1), 11089. https://doi.org/10.1038/s41598-023-38163-0

Weerasinghe, K. M., Gehrels, H., Arambepola, N. M. S. I., Vajja, H. P., Herath, J. M. K., & Atapattu, K. B. (2018). Qualitative Flood Risk assessment for the Western Province of Sri Lanka. *Procedia Engineering*, *212*, 503–510. https://doi.org/10.1016/j.proeng.2018.01.065

Wei, J., He, X., & Bao, Y. (2011). Anthropogenic impacts on suspended sediment load in the Upper Yangtze river. Regional Environmental Change, 11(4), 857–868. https://doi.org/10.1007/s10113-011-0222-0

Wei, M., Chen, W., & Wang, Y. (2024). Assessment of the Implementation Effects of Main Functional Area Planning in the Yangtze River Economic Belt. *Land*, *13*(7), 940. https://doi.org/10.3390/land13070940

Wieczorek, G. F., Larsen, M. C., Eaton, L. S., Morgan, B. A., & Blair, J. L. (2001). *Debris-flow and flooding hazards associated with the December 1999 storm in coastal Venezuela and strategies for mitigation*. Reston, VA: U.S. Geological Survey. https://doi.org/10.3133/ofr01144

Willner, S. N., Otto, C., & Levermann, A. (2018). Global economic response to river floods. *Nature Climate Change*, *8*(7), 594–598. https://doi.org/10.1038/s41558-018-0173-2

Wing, O. E. J., Lehman, W., Bates, P. D., Sampson, C. C., Quinn, N., Smith, A. M., Neal, J. C., Porter, J. R., & Kousky, C. (2022). Inequitable patterns of US flood risk in the Anthropocene. *Nature Climate Change*, *12*(2), 156–162. https://doi.org/10.1038/s41558-021-01265-6

World Meteorological Organization (WMO). (1999). Comprehensive Risk Management for Natural Hazards – Technical Document 955. Available online: https:// 10.1002/9781118281116. [accessed 06 Mar 2025].

World Meteorological Organization (WMO). (2021). Weather-related disasters increase over past 50 years, causing more damage but fewer deaths. Available online: https://wmo.int/media/news/weather-related-disasters-increase-over-past-50-years-causing-more-damage-fewer-deaths. (accessed on 11 Dec 2024).

Wu, J., Chen, X., & Lu, J. (2022). Assessment of long and short-term flood risk using the multi-criteria analysis model with the AHP-Entropy method in the Poyang Lake basin. *International Journal of Disaster Risk Reduction,* 75, 102968. https://doi.org/10.1016/j.ijdrr.2022.102968

Wu, X., Wang, L., Niu, Z., Jiang, W., & Cao, Q. (2023b). More extreme precipitation over the Yangtze River Basin, China: Insights from historical and projected perspectives. *Atmospheric Research*, *292*, 106883. https://doi.org/10.1016/j.atmosres.2023.106883

Wu, Y., Sun, J., Hu, B., Zhang, G., & Rousseau, A. N. (2023a). Wetland-based solutions against extreme flood and severe drought: Efficiency evaluation of risk mitigation. *Climate Risk Management*, *40*, 100505. https://doi.org/10.1016/j.crm.2023.100505

Wu, Y., Zhang, G., Rousseau, A. N., Xu, Y. J., & Foulon, É. (2020). On how wetlands can provide flood resilience in a large river basin: A case study in Nenjiang River Basin, China. Journal of Hydrology, 587, 125012. https://doi.org/10.1016/j.jhydrol.2020.125012

Xia, J., & Chen, J. (2021). A new era of flood control strategies from the perspective of managing the 2020 Yangtze River flood. *Science China Earth Sciences*, *64*(1), 1–9. https://doi.org/10.1007/s11430-020-9699-8

Xie, C., Huang, X., Mu, H., & Yin, W. (2017). Impacts of Land-Use Changes on the Lakes across the Yangtze Floodplain in China. *Environmental Science & Technology*, *51*(7), 3669–3677. https://doi.org/10.1021/acs.est.6b04260

Xing, L., Tang, X., Wang, H., Fan, W., & Wang, G. (2018). Monitoring monthly surface water dynamics of Dongting Lake using Sentinel-1 data at 10 m. *PeerJ*, *6*, e4992. https://doi.org/10.7717/peerj.4992

Xing, W., Bao, K., Gallego-Sala, A. V., Charman, D. J., Zhang, Z., Gao, C., Lu, X., & Wang, G. (2015). Climate controls on carbon accumulation in peatlands of Northeast China. *Quaternary Science Reviews,* 115, 78–88. https://doi.org/10.1016/j.quascirev.2015.03.005

Xiong, J., Wang, X., Zhao, D., & Zhao, Y. (2022). Spatiotemporal pattern and driving forces of ecological carrying capacity during urbanization process in the Dongting Lake area, China. *Ecological Indicators*, *144*, 109486. https://doi.org/10.1016/j.ecolind.2022.109486

Xue, Z., Lyu, X., Chen, Z., Zhang, Z., Jiang, M., Zhang, K., & Lyu, Y. (2018). Spatial and Temporal Changes of Wetlands on the Qinghai-Tibetan Plateau from the 1970s to 2010s. *Chinese Geographical Science*, *28*(6), 935–945. https://doi.org/10.1007/s11769-018-1003-1

Xu, C., Yuan, C., Li, X., Lin, Y., & Fan, H. (2023). Projection of disaster-causing risk of extreme precipitation in the Yangtze River Basin based on CMIP6. *Hydrology Research*, *54*(3), 401–417. https://doi.org/10.2166/nh.2023.141

Xu, D., Ivanov, V. Y., Kim, J., & Fatichi, S. (2019). On the use of observations in assessment of multi-model climate ensemble. *Stochastic Environmental Research and Risk Assessment,* 33(11), 1923–1937. https://doi.org/10.1007/s00477-018-1621-2

Xu, H., Hou, X., Pan, S., Bray, M., & Wang, C. (2024). Socioeconomic impacts from coastal flooding in the 21st century China's coastal zone: A coupling analysis between coastal flood risk and socioeconomic development. *Science of The Total Environment,* 917, 170187. https://doi.org/10.1016/j.scitotenv.2024.170187

Xu, J., Jing, Y., & Yan, W. (2025). Divergent Responses of Ecological Quality Under Various Periods of Urbanization in the Yangtze River Basin of China. *Sustainability*, *17*(6), 2756. https://doi.org/10.3390/su17062756

Xu, J., Yang, D., Yi, Y., Lei, Z., Chen, J., & Yang, W. (2008). Spatial and temporal variation of runoff in the Yangtze River basin during the past 40 years. Quaternary International, 186(1), 32–42. https://doi.org/10.1016/j.quaint.2007.10.014

Xu, L., & Chen, S. S. (2023). Coupling coordination degree between social-economic development and water environment: A case study of Taihu lake basin, China. *Ecological Indicators*, *148*, 110118. https://doi.org/10.1016/j.ecolind.2023.110118

Xu, R., Tao, Y., Lu, Z., & Zhong, Y. (2018). Attention-Mechanism-Containing Neural Networks for High-Resolution Remote Sensing Image Classification. *Remote Sensing*, *10*(10), 1602. https://doi.org/10.3390/rs10101602

Xu, T., Weng, B., Yan, D., Wang, K., Li, X., Bi, W., Li, M., Cheng, X., & Liu, Y. (2019a). Wetlands of International Importance: Status, Threats, and Future Protection. *International Journal of Environmental Research and Public Health*, *16*(10), 1818. https://doi.org/10.3390/ijerph16101818

Xu, W., Fan, X., Ma, J., Pimm, S. L., Kong, L., Zeng, Y., Li, X., Xiao, Y., Zheng, H., Liu, J., Wu, B., An, L., Zhang, L., Wang, X., & Ouyang, Z. (2019b). Hidden Loss of Wetlands in China. Current Biology, 29(18), 3065-3071.e2. https://doi.org/10.1016/j.cub.2019.07.053

Xu, X. (2017). China population spatial distribution kilometer grid dataset. *Resource and Environment Science Data Registration and Publishing System.* https://doi.org/10.12078/2017121101

Xu, X. (2020). China Population Spatial Distribution Kilometre Grid Dataset. Resource and environmental science data registration and publishing system. https://doi. 10.12078/2017121101

Xu, X., Yang, G., Tan, Y., Liu, J. and Hu, H. (2018). Ecosystem services trade-offs and determinants in China's Yangtze River Economic Belt from 2000 to 2015. *Science of the Total Environment*, *634*, 1601-1614. https://doi.org/10.1016/j.scitotenv.2018.04.046

Xu, Z., Dong, B., Gao, X., Wang, P., Ren, C., Li, S., Xu, H., Lei, F., Wei, Z., Lu, Z., & Liu, X. (2023). Land-Use Change and Driving Force Analysis of Wetland in Poyang Lake Based on

Remote Sensing. *Journal of the Indian Society of Remote Sensing*, *51*(10), 2077–2093. https://doi.org/10.1007/s12524-023-01749-2

Yang, J., & Huang, X. (2021). The 30m annual land cover dataset and its dynamics in China from 1990 to 2019. Earth System Science Data, 13(8), 3907–3925. https://doi.org/10.5194/essd-13-3907-2021

Yang, W.-C., Lin, K.-H., Wu, C.-W., Chang, Y.-J., & Chang, Y.-S. (2020). Effects of Waterlogging with Different Water Resources on Plant Growth and Tolerance Capacity of Four Herbaceous Flowers in a Bioretention Basin. *Water*, *12*(6), 1619. https://doi.org/10.3390/w12061619

Yang, X., Ding, J., & Hou, H. (2013). Application of a triangular fuzzy AHP approach for flood risk evaluation and response measures analysis. *Natural Hazards*, *68*(2), 657–674. https://doi.org/10.1007/s11069-013-0642-x

Yan, R., Cai, X., Wang, X., Li, E., Deng, F., Li, H., Jiang, L & Zhao, S. (2013). Distribution status of wetland nature reserves and the problems in Yangtze River watershed. *Wetland Science*, **11**(01), 136-144. https://caod.oriprobe.com/articles/32082763/Distribution_Status_of_Wetland_Nature_Reserves_and.htm

Yazdandoost, F., Moradian, S., Izadi, A., & Aghakouchak, A. (2021). Evaluation of CMIP6 precipitation simulations across different climatic zones: Uncertainty and model intercomparison. *Atmospheric Research*, *250*, 105369. https://doi.org/10.1016/j.atmosres.2020.105369

Yin, D., Chen, Y., Jia, H., Wang, Q., Chen, Z., Xu, C., Li, Q., Wang, W., Yang, Y., Fu, G., & Chen, A. S. (2021). Sponge city practice in China: A review of construction, assessment, operational and maintenance. *Journal of Cleaner Production*, *280*, 124963. https://doi.org/10.1016/j.jclepro.2020.124963

Yin, J., Ye, M., Yin, Z., & Xu, S. (2015). A review of advances in urban flood risk analysis over China. *Stochastic Environmental Research and Risk Assessment*, *29*(3), 1063–1070. https://doi.org/10.1007/s00477-014-0939-7

Yosri, A., Ghaith, M., & El-Dakhakhni, W. (2024). Deep learning rapid flood risk predictions for climate resilience planning. *Journal of Hydrology*, *631*, 130817. https://doi.org/10.1016/j.jhydrol.2024.130817

Youssef, A. M., Pradhan, B., & Sefry, S. A. (2015). Flash flood susceptibility assessment in Jeddah city (Kingdom of Saudi Arabia) using bivariate and multivariate statistical models. *Environmental Earth Sciences*, *75*(1), 12. https://doi.org/10.1007/s12665-015-4830-8

Yuan, Z., Yin, J., Wei, M., & Yuan, Y. (2021). Spatio-Temporal Variations in the Temperature and Precipitation Extremes in Yangtze River Basin, China during 1961–2020. *Atmosphere*, *12*(11), 1423. https://doi.org/10.3390/atmos12111423

Yue, Y., Yan, D., Yue, Q., Ji, G., & Wang, Z. (2021). Future changes in precipitation and temperature over the Yangtze River Basin in China based on CMIP6 GCMs. *Atmospheric Research,* 264, 105828. https://doi.org/10.1016/j.atmosres.2021.105828

Yu, C., Cheng, X., Hall, J., Evans, E. P., Wang, Y., Hu, C., Wu, H., Wicks, J., Scott, M., Sun, H., Wang, J., Ren, M., & Xu, Z. (2012). A GIS-supported impact assessment of the hierarchical flood-defense systems on the plain areas of the Taihu Basin, China. *International Journal of Geographical Information Science*, *26*(4), 643–665. https://doi.org/10.1080/13658816.2011.609486

Yu, F., Chen, Z., Ren, X., & Yang, G. (2009). Analysis of historical floods on the Yangtze River, China: Characteristics and explanations. *Geomorphology*, *113*(3), 210–216. https://doi.org/10.1016/j.geomorph.2009.03.008

Yu, J., Zou, L., Xia, J., Chen, X., Wang, F. and Zuo, L. (2023). A multi-dimensional framework for improving flood risk assessment: Application in the Han River Basin, China. *Journal of Hydrology: Regional Studies*, *47*, 101434. https://doi.org/10.1016/j.ejrh.2023.101434

Yu, J., Zou, L., Xia, J., Zhang, Y., Zuo, L. & Li, X. (2023). Investigating the spatial–temporal changes of flood events across the Yangtze River Basin, China: Identification, spatial heterogeneity, and dominant impact factors. *Journal of Hydrology*, *621*, 129503. https://doi.org/10.1016/j.jhydrol.2023.129503

Zhang, C., Sun, F., Sharma, S., Zeng, P., Mejia, A., Lyu, Y., Gao, J., Zhou, R., & Che, Y. (2023). Projecting multi-attribute flood regime changes for the Yangtze River basin. *Journal of Hydrology*, *617*, 128846. https://doi.org/10.1016/j.jhydrol.2022.128846

Zhang, D., Shi, X., Xu, H., Jing, Q., Pan, X., Liu, T., Wang, H., & Hou, H. (2020a). A GIS-based spatial multi-index model for flood risk assessment in the Yangtze River Basin, China. *Environmental Impact Assessment Review*, *83*, 106397. https://doi.org/10.1016/j.eiar.2020.106397

Zhang, D., Wang, G., & Zhou, H. (2011). Assessment on agricultural drought risk based on variable fuzzy sets model. *Chinese Geographical Science*, *21*(2), 167–175. https://doi.org/10.1007/s11769-011-0456-2

Zhang, F., Chen, T., Zhang, F., Shen, X., Lan, Y. (2020b). Extreme features of severe precipitation in Meiyu period over the middle and lower reaches of Yangtze River Basin in June–July 2020 Meteorol. Mon., 46 (11), 1405-1414. https://doi.org/10.7519/j.issn.1000-0526.2020.11.002

Zhang, H., Liu, S., & Fang, Q. (2019). Study on Flood Risk Characteristics and Disaster Prevention Countermeasures in the Taihu Basin. *IOP Conference Series: Earth and Environmental Science*, *401*(1), 012021. https://doi.org/10.1088/1755-1315/401/1/012021

Zhang, J., Li, J., Zhu, C., Bao, A., Frankl, A., De Maeyer, P. & Van de Voorde, T., (2025). A comprehensive environmental index for monitoring ecological quality of typical alpine wetlands in Central Asia. *Ecological Indicators*, *171*, 113216. https://doi.org/10.1016/j.ecolind.2025.113216

Zhang, X., Hu, Y., Zhao, L., Fu, S., Cui, Y., Fulati, G., Wang, X., & Zhou, J. (2024b). Dynamic monitoring and restorability evaluation of alpine wetland in the eastern edge of Qinghai–Tibet Plateau. *Global Ecology and Conservation*, *51*, e02948. https://doi.org/10.1016/j.gecco.2024.e02948

Zhang, X., Liu, L., Chen, X., Gao, Y., Xie, S., & Mi, J. (2021). GLC_FCS30: global land-cover product with fine classification system at 30 m using time-series Landsat imagery. *Earth System Science Data*, *13*(6), 2753–2776. https://doi.org/10.5194/essd-13-2753-2021

Zhang, Y., Li, Z., Xu, H., Ge, W., Qian, H., Li, J., Sun, H., Zhang, H., & Jiao, Y. (2024). Impact of floods on the environment: A review of indicators, influencing factors, and evaluation methods. *Science of The Total Environment*, *951*, 175683. https://doi.org/10.1016/j.scitotenv.2024.175683

Zhang, Y., Wang, G., & Wang, Y. (2011). Changes in alpine wetland ecosystems of the Qinghai–Tibetan plateau from 1967 to 2004. Environmental Monitoring and Assessment, 180(1), 189–199. https://doi.org/10.1007/s10661-010-1781-0

Zhang, Y., Zhou, D., Niu, Z., & Xu, F. (2014). Valuation of lake and marsh wetlands ecosystem services in China. *Chinese Geographical Science*, *24*(3), 269–278. https://doi.org/10.1007/s11769-013-0648-z

Zhao, R., Wang, J., Li, L., Zhang, L., Lu, H., Jiang, X., Chen, X., Han, Z., Dang-zhi, C., Wang, H. & Yang-jian, L. (2024). Evaluation of alpine wetland ecological degradation based on alpine wetland degradation index: A case study in the first meander of the yellow river. *Ecological Indicators*, *158*, 111414. https://doi.org/10.1016/j.ecolind.2023.111414

Zhao, Z., Liu, L., Wang, Z., Zhang, Y., Li, L., & Liu, F. (2020). Dynamic Changes of Plateau Wetlands in the Damqu River Basin, Yangtze River Source Region, China, 1988–2015. *Wetlands*, *40*. https://doi.org/10.1007/s13157-020-01271-y

Zheng, S., Zhong, Z., Zou, Q., Ding, Y., Yang, L., & Luo, X. (2021). Overall Situation of Yangtze River Basin. In S. Zheng, Z. Zhong, Q. Zou, Y. Ding, L. Yang, & X. Luo (Eds.), *Flood Resources Utilization in the Yangtze River Basin* (pp. 19–69). Springer. https://doi.org/10.1007/978-981-15-8108-3_2

Zheng, L., Liu, H., Huang, Y., Yin, S., & Jin, G. (2020). Assessment and analysis of ecosystem services value along the Yangtze River under the background of the Yangtze River protection strategy. Journal of Geographical Sciences, 30(4), 553–568. https://doi.org/10.1007/s11442-020-1742-7

Zheng, S., Zhong, Z., Zou, Q., Ding, Y., Yang, L., & Luo, X. (2021). Overall Situation of Yangtze River Basin. In S. Zheng, Z. Zhong, Q. Zou, Y. Ding, L. Yang, & X. Luo (Eds.), *Flood Resources Utilization in the Yangtze River Basin* (pp. 19–69). Springer. https://doi.org/10.1007/978-981-15-8108-3_2

Zheng, Y., Niu, Z., Gong, P., & Wang, J. (2015). A database of global wetland validation samples for wetland mapping. *Science Bulletin*, *60*(4), 428–434. https://doi.org/10.1007/s11434-014-0717-4

Zheng, Y., Niu, Z., Gong, P., Li, M., Hu, L., Wang, L., Yang, Y., Gu, H., Mu, J., Dou, G., Xue, H., Wang, L., Li, H., Dou, G., & Dang, Z. (2017). A method for alpine wetland delineation and features of border: Zoigê Plateau, China. *Chinese Geographical Science*, *27*(5), 784–799. https://doi.org/10.1007/s11769-017-0897-3

Zheng, Y., Zhang, H., Niu, Z., & Gong, P. (2012). Protection efficacy of national wetland reserves in China. *Chinese Science Bulletin*, *57*(10), 1116–1134.

Zhou, C., & Xia, Q. (2020). Practical Experience in Global Watershed Legislation and Its Enlightenment to the Legislation of Yangtze River Law. 931–937. https://doi.org/10.2991/aebmr.k.191225.178

Zhou, Q., Leng, G., Su, J., & Ren, Y. (2019). Comparison of urbanization and climate change impacts on urban flood volumes: Importance of urban planning and drainage adaptation. *Science of The Total Environment,* 658, 24–33. https://doi.org/10.1016/j.scitotenv.2018.12.184

Zhu, Y., Ye, A. & Zhang, Y. (2022). Changes of total and artificial water bodies in inland China over the past three decades. *Journal of Hydrology*, *613*, 128344. https://doi.org/10.1016/j.jhydrol.2022.128344

Zhu, Z., Zhang, S., Zhang, Y., Lu, H., Feng, X., Jin, H., & Gao, Y. (2024). Flood risk transfer analysis based on the "Source-Sink" theory and its impact on ecological environment: A case study of the Poyang Lake Basin, China. *Science of The Total Environment*, *921*, 171064. https://doi.org/10.1016/j.scitotenv.2024.171064

Ziwei, L., Xiangling, T., Liju, L., Yanqi, C., Xingming, W., & Dishan, Y. (2023). GIS-based risk assessment of flood disaster in the Lijiang River Basin. *Scientific Reports*, *13*(1), 6160. https://doi.org/10.1038/s41598-023-32829-5

Zou, L., & Zhou, T. (2022). Mean and extreme precipitation changes over China under SSP scenarios: results from high-resolution dynamical downscaling for CORDEX East Asia. *Climate Dynamics*, *58*(3), 1015–1031. https://doi.org/10.1007/s00382-021-05947-x

Zou, Q., Zhou, J., Zhou, C., Song, L., & Guo, J. (2013). Comprehensive flood risk assessment based on set pair analysis-variable fuzzy sets model and fuzzy AHP. *Stochastic Environmental Research and Risk Assessment*, *27*(2), 525–546. https://doi.org/10.1007/s00477-012-0598-5